WIND TUNNEL TEST FOR GUYED MAST DYNAMIC CHARACTERISTICS UNDER WIND LOADS

A Thesis Submitted to the College of

Graduate Studies and Research

in Partial Fulfillment of the Requirements

for the Degree of Master of Science

in the Department of Civil and Geological Engineering

University of Saskatchewan

Saskatoon

By

Ningli Zhu

PERMISSION TO USE

In presenting this thesis in partial fulfillment of the requirements for a Postgraduate degree from the University of Saskatchewan, I agree that the Libraries of this University may make it freely available for inspection. I further agree that permission for copying of this thesis in any manner, in whole or in part, for scholarly purposes may be granted by the professors who supervised my thesis work or, in their absence, by the Head of the Department or the Dean of the College in which my thesis work was done. It is understood that any copying, publication, or use of this thesis or parts thereof for financial gain shall not be allowed without my written permission. It is also understood that due recognition shall be given to me and to the University of Saskatchewan in any scholarly use which may be made of any material in my thesis.

Requests for permission to copy or to make other use of material in this thesis in whole or part should be addressed to:

Head of the Department of Civil and Geological Engineering

University of Saskatchewan

Saskatoon, Saskatchewan

Canada S7N 5A9

ABSTRACT

An experimental wind tunnel study on the dynamic response of a 300 m tall guyed telecommunication mast under various wind loads was undertaken at the Boundary Layer Wind Tunnel Laboratory (BLWTL) in the University of Western Ontario, London, Canada. Although the dynamic response of guyed masts subjected to turbulent wind loads has been routinely analyzed using a number of numerical models, typically in the frequency domain, limited experimental verification of the dynamic analysis results has been performed. Full-scale measurements, where available, have proven to be difficult to correlate with analytical models due to the tremendous uncertainty inherent in field measurements. As a result, the need for systematic validation of existing analytical models remains.

In this investigation, a representative 300 m tall guyed telecommunication mast has been designed and modeled to an appropriate scale. Based on Canadian Standard CSA S37-01, and an empirical study on 41 existing guyed masts, the 300 m tall guyed mast was designed using wind load conforming to representative Canadian climate data obtained from National Building Code of Canada (NBCC 1995). Appropriate properties for the dynamically scaled full aeroelastic model were derived from the 300 m tall prototype guyed mast, which was intended to represent a realistic guyed mast for broadcasting applications in Canada.

The wind tunnel test of the guyed mast model was carried out in both open country and over water exposures, simulating medium and low turbulence flow conditions, respectively. Dynamic response characteristics measured during the wind

tunnel tests have been analysed and summarized, including dynamic displacements, bending moments, response spectra and peak factors, as well as natural frequencies, mode shapes and structural damping. Comparisons have been made with predictions obtained from an existing frequency domain analysis model.

The wind tunnel test results show that good agreement was generally achieved between the frequency domain analytical model and the wind tunnel model with respect to both the magnitude and distribution of the monitored responses. It was found that measured dynamic bending moments were distributed in a fairly uniform manner over the mast height, and that mean (static) bending moments exhibit large variations, along with near-zero response zones at points of contraflexure. It was also found that nonlinear damping effects, associated with vibrations of the highly slackened leeward guys on the upper levels of the mast, may be beneficial in reducing dynamic mast displacements.

The spectrum studies indicated that lowest modes were dominated by large guy movements at top guy level and small mast movements, the middle modes were characterized by coupled effects between the guyed cables and mast, meanwhile the highest modes involved significant mast movements with little guy vibration. It is evident that the top of the mast displacement are dominated by the first and second modes.

ACKNOWLEDGEMENTS

First, I am deeply grateful to my supervisor, Dr. Bruce F. Sparling, who had led me to the guyed mast field and enriched my life through my gradate courses. As a guyed mast expert, with his outstanding guidance and encouragement, not to mention his incredible patience, these have meant much to me throughout the course of this research work and completion of this thesis document. Without his expertise and insight, I would never have made it this far. In addition, I would like to extend my great appreciation to Dr. Sparling's wife, Nancy, and their lovely children for their warm hospitality I received during my stay in Saskatoon.

I would also like to express my sincere gratitude to my co-supervisor, Dr. J. Peter C. King, the Research Director and Chair of the Boundary Layer Wind Tunnel Laboratory (BLWTL) at the University of Western Ontario (UWO). His remarkable ingenuity, passion and hands-on guidance with the modeling and wind tunnel test made this journey go smoothly and ensured the test completed successfully.

Besides my supervisors, I would like to thank my Advisory Committee members: Dr. Jim Kells, Dr. Leon Wegner, Dr. David Sumner, and Dr. Gordon Putz for their invaluable suggestions and advice with regard to this research work.

It is with great gratitude that I acknowledge the staff at the BLWTL, UWO, London. As part of my studies were spent in the BLWTL, I received generous assistance there. In particular, I would like to acknowledge Gerry Dafoe, Lingzhe Kong, and Kevin Barker.

I am indebted to Keith Palibroda and Henry Berg from Engineering Shops who helped me to construct the guyed mast model; Dr. David Sumner and Dave Deutscher from the Department of Mechanical Engineering for their help for the wind drag test of the mast section model conducted in the Wind Tunnel Laboratory at the University of Saskatchewan.

Special thanks are due to Simon Weisman, the President of Weisman Consultants Inc. (Toronto), for his generous donation of the commercial software used—Guyed Mast, and the valuable assistance during the design of the guyed mast prototype.

I would like to send a big "thank-you" to the people in the Department of Civil Engineering and the structural lab. In particular, Dale Pavier, Mazin Alwash, Dr. Mel Hosain and Maureen Limet who offered me encouragement, help and friendship.

Financial support provided by the Natural Sciences and Engineering Research Council of Canada is greatly appreciated.

Last, but not the least, I must thank my husband—Hongliang Zhuang, for his great sacrifice, understanding and support which enabled me to get there, and fulfill my dream to become a reality. I can't thank him enough for his love and support through my academic career. His trust in my ability has carried me forward during the years of my graduate study.

This thesis is dedicated with love to our daughter, Jessica Michelle Zhuang, who came into our lives on July 9, 2007.

TABLE OF CONTENTS

LIST OF TABLES

LIST OF FIGURES

DEFINITION OF SYMBOLS

a_G	Unstrained cross-sectional area of guy
A	Cross-sectional area of structural member
A_d	Projected area
A_g	Projected gross area
A_s	The net projected area of one face of the structure
B	Face width of mast (center to center distance between mast legs)
C_a	Cauchy number; also aerodynamic viscous damping coefficient; and a speed-up factor for structures located on tops of buildings
C_D	Surface drag coefficient
C_e	Wind exposure factor
C_g	Gust factor applied to mean wind pressure
C_s	Structural viscous damping coefficient
$C_D A$	Effective drag area
d	Typical member dimension; also the inside diameter of a spine
d_G	Diameter of guy cable
D	Outside diameter of a spine
D_F	Reduction factor to flat members
E	Modulus of elasticity of material
E_{eff}	Effective modulus of elasticity for structure

E_G	Elastic modulus of guy
f	Frequency in Hz
$\overline{F}$	Mean wind drag force
F_D	Wind drag force
F_r	Froude number
$F_U(t)$	Instantaneous wind drag force
$F_u(t)$	Instantaneous fluctuating component of wind drag force
$\tilde{F}_{PL}$	Equivalent static load used in proposed patch load method
FFT	Fast Fourier Transform
g_a	Gravitational acceleration (9.81 m/s^2)
g_p	Statistical peak factor applied to fluctuating response component
h	Vertical distance between upper and lower ends of guy
H	Horizontal component of guy tension; also a characteristic length of the body
I	Structural moment of inertia
$I_r(z)$	Influence line for response r
$i_u(z)$	Turbulence intensity = $\tilde{u}/\overline{U}(z)$
I_m	Mast bending moment of inertia about a centroidal axis
κ	The von Kármán constant ($\kappa \cong 0.4$);
k	Stiffness of the structure
k_e	Horizontal elastic stiffness of a single guy about its own plane
k_{e_mw}	Axial stiffness of music wire

k_{e_sp}	Elastic stiffness of an extension spring
k_{EQ}	Equivalent horizontal stiffness of a single guy
k_g	Horizontal gravitational stiffness of a single guy in its own plane
k_{TOT}	Total horizontal stiffness of a guy group
k_{xx}	Horizontal stiffness of a single guy in its own plane
K^{G1}	First equivalent spring constant in spring-mass guy model
K^{G2}	Second equivalent spring constant in spring-mass guy model
L	Characteristic length
L_c	Length of straight chord line joining two ends of guy
L_o	Scaling constant for modified Kolmogorov spectrum
L_u	Length scale, $L_u \approx 1200m$
L_{us}	Original unstretched length of guy
m	Mass of the structure
M^G	Equivalent lumped mass in spring-mass guy model
M_x	Bending moment about x-x axis
M_y	Bending moment about y-y axis
n	Number of guys in guy group
n_f	Reduced frequency
N	Factor for determining k_{TOT} ; 1.5 for three guys
P	The effective wind velocity pressure
p_d	Wind dynamic pressure
q	Wind velocity pressure at the reference height

q_H	Mean wind pressure at the top of the mast
r	Response component in global coordinate system
r'	Response component in local coordinate system
$r(t)$	Instantaneous response at time t
$\hat{r}$	Peak value of dynamic response
$\overline{r}$	Mean (time-averaged) value of response
$\widetilde{r}$	Root-mean-square (*rms*) value of dynamic response
$r_B(t)$	Quasi-static background response component
$\widetilde{r}_B$	Quasi-static background component of *rms* dynamic response
$\widetilde{r}_{est}$	Estimated dynamic response
r_n	Normalized response, $r_n = r\overline{U}_{ref} / \overline{U}$
r_{pL_i}	Resultant response for the i^{th} static patch load case
$\hat{r}_{PL}$	Peak dynamic response determined using patch load method
$\widetilde{r}_{PL}$	Resultant response due to patch loads
$r_R(t)$	Resonant response component
$\widetilde{r}_R$	Total *rms* resonant response from all vibration modes
r_x	Response components in x-axis (alongwind) direction
r'_x	Response components in local coordinate system x' axis
r_y	Response components in y-axis (crosswind) direction
r'_y	Response components in local coordinate system y' axis
rms	Root-mean-square value
R	Radius of the mast from its centroid to the centroid of the legs

$\overline{R}$	Static response to the mean wind, with no gust factor ($C_g = 1.0$)
$\hat{R}$	Peak design response to turbulent wind loading;
R_e	Reynolds number
R_s	Ratio of projected area; $R_s = A_s / A_g$
S	Horizontal span between upper and lower ends of guy
S_{GF_i}	Power spectrum of the generalized force for i^{th} vibration mode
$S_r(f)$	Power spectrum for response
$S_u(f)$	Power spectral density function for alongwind turbulence
T	Period of time history sample
$\overline{T}$	Average tension in guy
T_B	Guy tension at bottom end of cable
T_o	Guy tension at lower end of cable
T_T	Guy tension at upper end of cable
$u(t)$	Alongwind fluctuating wind velocity
$\tilde{u}$	Alongwind *rms* fluctuating wind velocity
u_*	Shear velocity of the flow
$U(t)$	Instantaneous alongwind fluctuating wind velocity
$\overline{U}$	Mean wind speed component
$\overline{U}_{10}$	Mean wind speed at an elevation of 10 m above the ground
$\overline{U}_g$	Free-stream gradient wind speed at the top of the boundary layer
$\overline{U}_H$	Mean wind speed at the top of the mast
U_{ref}	Design wind speed at reference height

$v(t)$	Crosswind fluctuating wind velocity
$v(z)$	Alongwind displacement pattern of mast
$\tilde{v}$	Crosswind *rms* fluctuating wind velocity
V	Representative wind velocity
V_B	Vertical component of cable tension at lower end of cable
V_T	Vertical component of cable tension at upper end of cable
w_G	Weight of guy per unit length
$\tilde{w}$	Vertical *rms* fluctuating wind velocity
z	The elevation above ground
z_o	Characteristic roughness length of site
z_G	The elevation at the gradient speed
z_{ref}	The reference elevation
α	The horizontal angle between the mean wind vector and the vertical plane of a single guy, measured in clockwise direction; also an exposure factor related to the surface roughness in power law
α_w	Wind load factor ($\alpha_w = 1.5$)
δ	Boundary layer thickness
Δ	Difference between the measured and predicted response
Δ_G	Maximum sag in a guy measured normal to chord line
λ_B	Background scaling factor for patch load method
λ_{BM}	Bending moment scaling factor
λ_{EA}	Axial stiffness scaling factor
λ_{EI}	Bending moment scaling factor

λ_f	Frequency scaling factor; also drag force per unit length scaling factor
λ_F	Force scaling factor
λ_L	Geometric scale of model (ratio between linear dimensions of the model and the prototype); also span length factor for simpler dynamic analysis method
λ_i	Mass moment of inertia per unit length scaling factor
λ_I	Turbulence intensity factor; also mass moment of inertia scaling factor
λ_m	Mass per unit length scaling factor
λ_M	Mass scaling factor
λ_R	Resonant amplification factor for patch load method
λ_T	Time scaling factor
λ_{TL}	Turbulence length scale factor for patch load method
λ_v	Velocity scaling factor
λ^2	Guy stiffness parameter [after Irvine (1978)]
λ_ρ	Mass density scaling factor
λ_ζ	Damping scaling factor
μ	Coefficient of viscosity of the air
ν	Response cycling rate; also kinematic viscosity of the air ($\nu \approx 14.9\times10^{-6} m^2/s$)
θ	Vertical angle between chord line of guy and a horizontal plane
ρ	Flow mass density

ρ_a	Air density
ρ_s	Structural bulk density
ζ	Damping expressed as a ratio of the critical damping
ξ_s	Structural damping ratio
ξ_a	Aerodynamic damping ratio
ω_o	Fundamental undamped natural frequency of a taut wire
$\omega(t)$	Vertical fluctuating wind velocity
ω_n^{IA}	Undamped natural frequency of the guy's n^{th} in-plane anti-symmetric vibration mode
ω_n^{IS}	Undamped natural frequency of the guy's n^{th} in-plane symmetric vibration mode
ω_n^{IA}	Undamped circular natural frequency of the guy's n^{th} in-plane anti-symmetric vibration mode
ω_n^{IS}	Undamped circular natural frequency of the guy's n^{th} in-plane symmetric vibration mode
ω_o	Fundamental undamped natural circular frequency of a taut wire
φ_{cd}	Normalized effective drag area of mast
φ_u	Normalized dimensional wind speed
Φ	Eigenvector matrix of undamped vibration mode shapes

Coordinate Systems: (defined using right-hand rule)

$x-y-z$	Global coordinate system: origin at base of mast, *x*-axis in direction of mean wind vector, *z*-axis vertical
$x'-y'-z'$	Local mast coordinate system, x'-axis in direction of current alongwind, *z*-axis vertical

1. INTRODUCTION

1.1 INTRODUCTORY REMARKS

Because of their height, slenderness and overall flexibility, guyed telecommunication masts are inherently sensitive to dynamic excitation provided by wind turbulence. The low self weight and the relatively small equipment loads carried also mean that wind action accounts for a disproportionately high portion of critical structural load effects relative to conventional civil engineering structures.

Guyed communication masts play a strategic role in the ever-increasing global communication networks and broadcasting industry, as a means of supporting a variety of antennas and transmission equipment (Figure 1.1). Therefore, the cost to society of a failure or collapse of a guyed mast in terms of the loss of transmission and the associated safety risks typically far outweighs the cost of the structure itself. In particular, problems can arise due to the lack of communication in the case of emergencies. As a result, ensuring the reliability and security of guyed mast performance is of great importance.

A schematic of a typical guyed mast is illustrated in Figure 1.2. A guyed mast usually comprises a slender lattice steel mast that is typically pinned at its base, guyed cables anchored at ground level and, perhaps, a flexible antenna cantilevered on the top of the mast. The mast typically has three or four legs, made from solid round members, galvanized steel angles or tubes, connected by horizontal and diagonal components

Figure 1.1. A typical guyed mast (photo courtesy of Weisman Consultants Inc.).

(web members), assembled in different configurations, which serve to transfer wind induced forces to the foundation. Masts with triangular cross sections (three legs) are

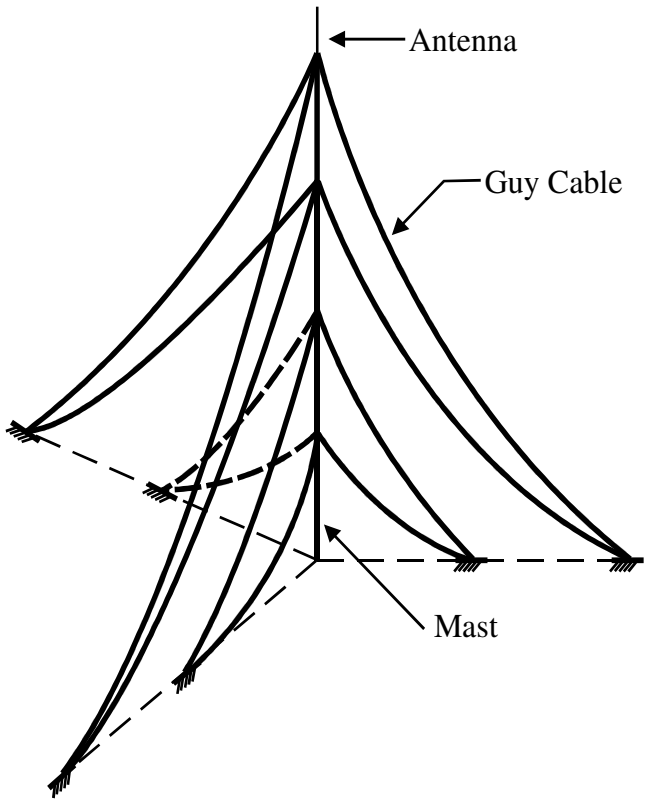

Figure 1.2. Typical guyed mast configuration.

most commonly used in North America, while masts with square cross sections (four legs) are popular in Europe and the other parts of the world (Wahba 1999). The pretensioned guyed cables supply lateral supports to the mast at several levels along the mast height as a means of reducing vibration and increasing the stiffness of the structure; as well, guy cables contribute to internal damping, apply axial prestressing forces to the mast, and help transfer wind loads from the mast to the ground.

Guyed masts account for the tallest man-made structures in the world, with some exceeding 600 m in height. At the same time, they have relatively light self weights, and they are very slender, with typical face width to height ratios ranging from 1/80 to 1/180, making them extremely flexible. The slenderness of the mast, and the inherent

sag in the guys, which introduces non-linearity to the system, as well as the complex interaction between mast and guys, make the structural behaviour very complicated and significantly different from other conventional structures.

The random, dynamic and fluctuating nature of wind also introduces additional complexity to the structural analysis. The dynamic response of guyed masts under gusty wind conditions is known to exhibit significantly different characteristics, as well as being generally larger, than the static response to the steady component of the wind (Sparling et al. 1996). As a result, an accurate assessment of dynamic wind load effects is essential for developing a safe design for guyed masts.

1.2 BACKGROUND

Over the years, the dynamic characteristics of guyed masts under turbulent wind loads have been of great interest for researchers world-wide due to their complexity, the inherent non-linearity of the structure and the complicated nature of wind loads in the boundary layer. The significant differences between the static and dynamic behaviour of guyed masts have been studied by a number of researchers (Kolousek 1947, Davenport 1959, Beitin 1969, Vellozzi 1975, Allsop 1983, Davenport and Loh 1986, Ben Kahla 1993, Sparling 1995, Sparling and Gress 1997, Wahba 1999). Generally, shorter and stiffer structures can be analyzed using a simple static analysis method. For taller and more flexible structures, such as guyed masts, on the other hand, more sophisticated dynamic analysis techniques are required to predict the peak dynamic response. The current Canadian design CSA Standard S37-01 (CSA 2001) cautions that special attention should be paid to the dynamic effects of wind for guyed masts over 250 m in

height. That is, the loads corresponding to the peak dynamic response should be considered carefully in design.

The dynamic response of telecommunication guyed masts, subjected to turbulent wind loads, has been routinely analyzed using a number of numerical models. Static analysis models such as the gust factor method, employed in CSA S37-01 (CSA 2001), determine the peak, or total, response by simply factoring the mean loads by a constant value, a so-called gust factor; pseudo-dynamic analysis models, such as the patch load method (Sparling 1995) and other simplified methods (Sparling and Gress 1997, BS 8100-4 1995), estimate the dynamic portion of the response by manipulating a series of factors based on purely static analysis results. Typically, two general types of dynamic analytical models, frequency domain and time domain methods (Davenport 1959, Vellozzi 1975, IASS 1981, Allsop 1983, Davenport and Loh 1986, Sparling 1995), have been used to perform full dynamic analyses of guyed masts.

While the available numerical models have been developed to a fairly high level of technical sophistication, uncertainty remains regarding some of the key underlying physical processes. Issues requiring clarification include the role and significance of nonlinear guy behaviour, the relative importance of the across wind response, and the effective damping and drag area of guyed mast structures. Furthermore, the question of whether existing normal numerical models account for the inherent non-linearity of guyed masts in an adequate manner requires better understanding of the true dynamic behaviour of the structure. To date, insufficient experimental data are available to adequately answer these questions and, thus, to validate the proposed analytical methods.

Full-scale field measurements provide the most direct indication of guyed mast behaviour (Peil and Nölle 1992, Fahleson 1995); however, this type of testing is usually costly and difficult to carry out. First of all, the size of these structures, coupled with their generally remote locations, makes the required instrumentation both costly and inconvenient to install; second, the complex and random nature of the turbulent wind loading is difficult to characterize to the degree that can be reliably replicated in numerical studies. In addition, the terrain of the site restricts the turbulence conditions that can be studied. Furthermore, extreme loading events, which are of most interest from a design perspective, may not occur over extended periods of time, if ever. Therefore, there remains a need for simpler experiments which are capable of examining the dynamic response of guyed masts subject to realistic wind loads.

Wind tunnel testing, as a convenient alternative to field measurements, provides an opportunity to observe the dynamic response of large-scale structures under realistic wind loading. Among the advantages associated with wind tunnel tests are: the relatively low costs involved; the ability to control, measure and reliably quantify the wind climate; the opportunity to study design level wind storms; and the ability to install intensive levels of instrumentation. Wind tunnel investigations are recognized as an alternative approach to conventional analytical methods in situations where more precise information or where extreme wind conditions are sought.

1.3 SCOPE AND OBJECTIVES

The need to obtain the experimental data relating to the dynamic response of guyed masts under wind loads was the motivating factor for this study. The primary objective of the wind tunnel study was therefore to obtain reliable measurement data

representing the dynamic response of a full scale 300 m tall guyed mast under various wind conditions.

The current project has been designed to use wind tunnel testing, which provides a realistic assessment of the detailed wind load distribution, to determine the nonlinear, wind-induced dynamic response characteristics of guys and guyed telecommunication masts under both open country (moderate turbulence) exposure and over water (low turbulence) exposure.

The specific objectives of this research program are as follows:

- To assess the dynamic response of an aeroelastic wind tunnel model of a realistic 300 m tall guyed mast;
- To perform comparisons between the measured dynamic response of the physical model and that predicted based on a frequency domain analytical model;
- To validate the existing frequency domain model as well as the accepted design standard approach;
- To obtain experimentally measured data relating to the dynamic response of guyed masts under various wind conditions as well as wind azimuths; and
- To evaluate different wind orientation effects on the dynamic response characteristics of both the mast and guy cables.

In this investigation, one open country wind condition and one over water wind condition were considered when performing the wind tunnel test to determine the dynamic characteristics of guyed masts. While the three-dimensional buffeting response due to wind turbulence was measured, the predicted response based on the numerical

model was limited to the two-dimensional response only. In addition, buffeting was the only source of dynamic excitation considered and the mast and the guy cables were assumed to be ice free.

1.4 METHODOLOGY

The current research project made use of wind tunnel testing to determine the wind-induced, nonlinear dynamic response characteristics of guys and guyed telecommunication masts under various wind conditions. The primary focus of the investigation was to obtain experimental measurements of guyed mast dynamic behaviour in order to compare the measured response with predictions obtained from an existing numerical model.

Based on a frequency domain analytical approach, Sparling (1995) developed a numerical model specifically for guyed masts. This model was adopted throughout this study as the basis for comparison with the wind tunnel test results. This numerical model is introduced in detail in Section 2.5.

The current investigation was conducted incorporating the following steps. First of all, a representative 300 m tall guyed mast was designed on the basis of the Canadian design standard S37-01 (CSA 2001) and a parametric study of the typical physical characteristics of 41 existing guyed masts. The design wind load was selected from National Building Code of Canada (NBCC 1995) climatic data, which describe design wind conditions in Canada. The full dynamic response of the 300 m tall guyed mast was analysed using the frequency domain numerical model; as well, the design was checked using the commercially available static analysis software GUYMAST, generously supplied by Weisman Consultants Inc. (Toronto, Canada). In this way, an attempt was

made to produce a design for a realistic guyed mast that could be used for broadcasting applications in Canada.

Second, a full aeroelastic model of the 300 m tall guyed mast was designed based on Froude number scaling. The appropriate properties of the structure, such as stiffness, mass and drag area of the mast and guy cables were derived from the prototype of the 300 m guyed mast described above. Third, the aeroelastic model of the guyed mast was then constructed to a scale of 1:100 at the College of Engineering, University of Saskatchewan, and was instrumented at the Boundary Layer Wind Tunnel Laboratory (BLWTL) of the University of Western Ontario, London, Canada.

After fabrication was completed, wind tunnel testing of the guyed mast model was carried out at the BLWTL. The wind tunnel test was conducted in both open country and over water flow conditions to study the dynamic response of guyed masts to various wind loads. Three different orientations relative to the mean wind direction, including wind parallel to the windward guy lane, wind parallel to one face of the mast, and wind perpendicular to one face of the mast (denoted in subsequent discussions as wind at 0^o, 30^o and 60^o, respectively) were conducted in order to obtain the maximum peak dynamic response to wind loads from any direction. In addition, the properties of the guyed mast model were measured under still wind conditions in order to quantify its fundamental mode shapes, natural frequencies and structural damping.

Finally, the results of the test were analysed to provide estimates of full scale structural dynamic response characteristics such as bending moment, displacement, natural frequencies, mode shapes, damping and response spectra, which were then compared with results from the existing frequency domain analysis model.

1.5 OUTLINE OF THE PROJECT

The primary focus of this study was the experimental measurement of the dynamic characteristics of a representative guyed mast. Comparisons of the dynamic response characteristics of the physical model with those predicted by the numerical model of the guyed mast under wind loads were also made.

Chapter 2 introduces the theory, background and published literature pertinent to guyed mast dynamic response. The characteristics of natural wind, as well as the static and dynamic behaviour of guys and guyed mast systems subjected to wind turbulence are summarized. Existing numerical models for both static and dynamic analysis are presented; in particular, the frequency domain analytical model, used as the basis for comparison with the measured results, is introduced briefly, as well as the previous experimental investigations on guyed masts performed to date.

Chapter 3 describes the techniques used to design and model the guyed mast as well as the model construction. The model design in terms of the selection of appropriate wind characteristics and the physical properties of the structure is described. This chapter also presents the details of the model construction including mast, cladding, guy cables and the base, along with the comparison of the resulting stiffness, mass and other salient properties between the model and the scaled prototype.

Chapter 4 deals with the details of the wind tunnel tests of the guyed mast model. This chapter describes the model instrumentation and calibration, wind tunnel test setup and procedure conducted in the BLWTL, along with the wind climate modelling and determination of the dynamic properties of the model in still air condition. A section

drag test conducted on the mast cladding at the University of Saskatchewan is also presented.

Chapter 5 presents the wind tunnel test results. Data processing procedures applied to the experimental data are introduced. The measured dynamic responses (e.g. bending moment, displacement, natural frequencies, mode shapes, peak factors, structural damping and power spectra characteristics) are compared with those from the numerical model based on the frequency domain method. In addition, the dynamic characteristics at different wind speeds, along with the drag test results of the sectional model, are provided.

Finally, a brief summary of this research, along with the conclusions based on the wind tunnel test results, are given in Chapter 6. Recommendations for future work on wind tunnel testing of the guyed mast model are provided as well.

2. STATIC AND DYNAMIC RESPONSE OF GUYED MASTS TO WIND LOADS—BACKGROUND AND LITERATURE REVIEW

2.1 INTRODUCTION

The dynamic response of guyed masts under wind loads is a complex process, due not only to the three-dimensional dynamic response, but also to the inherently nonlinear nature of guy cables, and the complex interaction between the mast and guys, which substantially complicates the analysis process (Cohen and Perrin 1957; Dean 1961; Nakamoto and Chiu 1985; Sparling and Davenport 1997, 2001). A lot of attention has therefore been focused on the analysis of the dynamic response using various numerical models.

This chapter presents various approaches for studying the static and dynamic characteristics of guys and guyed masts in turbulent wind, as a prelude to the wind tunnel investigation. Both the static and dynamic responses are introduced; however, the emphasis is placed on the dynamic response. The characteristics of natural wind are presented as background for both the wind tunnel and numerical studies. Numerical models for analyzing the static and dynamic response, particularly the dynamic frequency domain analysis model, are dealt with in detail. Finally, previous experimental investigations of guyed masts are presented in this chapter.

Guy cables play a critical role in determining the static and dynamic response of guyed masts. In addition to providing lateral support to the mast, guy cables also

contribute significant axial and shear forces to the mast, as well as a large portion of the total system mass. A detailed discussion of the static and dynamic behaviour of guy cables is therefore included in this chapter.

2.2 CHARACTERISTICS OF THE NATURAL WIND

2.2.1 Description of Wind Speed

Wind in the atmospheric boundary layer close to the earth's surface is invariably turbulent, and thus, by nature, a randomly fluctuating and dynamic process. A typical wind speed time history over a 20-second interval is illustrated in Figure 2.1. As can be seen in this figure, the instantaneous wind speed $U(t)$, where t is time, may be broken into a mean wind velocity component $\overline{U}$, which is assumed to remain constant over a short time period T, and a fluctuating velocity component $u(t)$, which is time dependant.

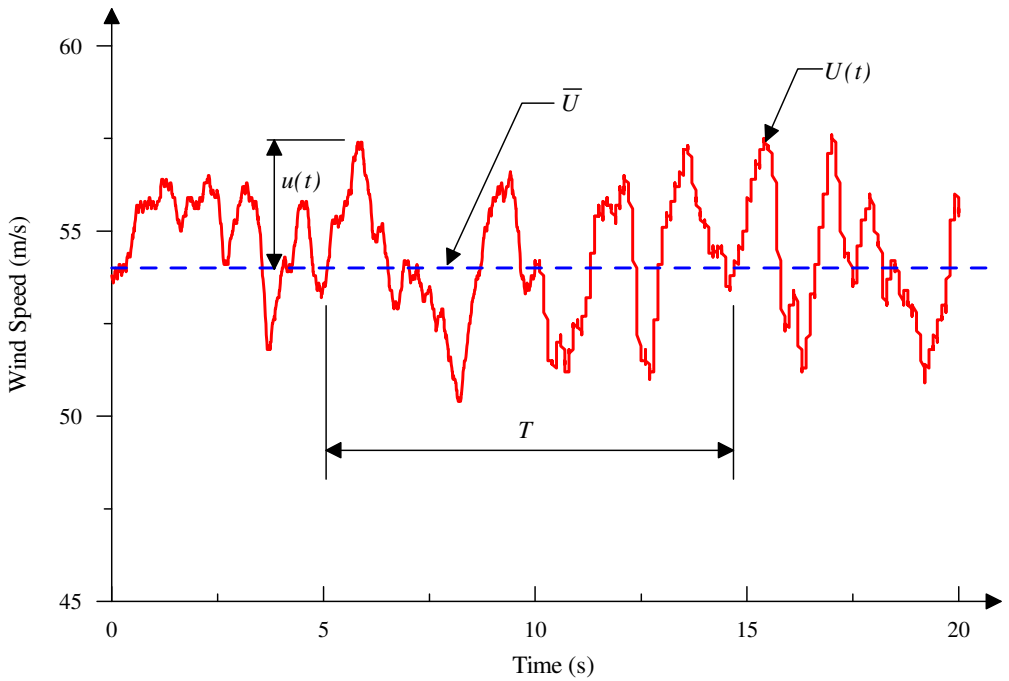

Figure 2.1. Example wind speed time history over a 20 second interval (from the BLWTL measurement).

The mean component $\overline{U}$ is given by:

$$\overline{U} = \frac{1}{T}\int_{T} U(t)dt \,. \tag{2.1}$$

Since the magnitude of $\overline{U}$ is the time-averaged value of $U(t)$, it is dependent on the averaging period, T. For a given wind time history, the computed value of $\overline{U}$ will tend to decrease with an increasing averaging period T and increase for decreasing T. An averaging period T of one hour ($T = 3{,}600\,s$) is adopted in the NBCC (NBCC 1995).

An important characteristic of wind in the atmospheric boundary layer is that the mean wind speed increases with height above the ground surface. An empirical power law approach, taking the effect of ground surface roughness into account, is a common means for relating the variation of mean wind speed with height z above ground, as follows (Simiu and Scanlan 1996):

$$\overline{U}(z) = \overline{U}_g \left(\frac{z}{z_G}\right)^{\alpha} = \overline{U}_{ref}\left(\frac{z}{z_{ref}}\right)^{\alpha} \tag{2.2}$$

where $\overline{U}(z)$ is the mean wind speed, $\overline{U}_g$ is the free-stream gradient wind speed at the top of the boundary layer, z_G is the approximate height at which the gradient speed is attained, z_{ref} is the reference elevation (normally taken as 10 m above the ground surface), $\overline{U}_{ref}$ is mean wind speed at reference height z_{ref} and α is an exponential factor dependent upon roughness of terrain. An alternative method used to define mean wind speed variation with height is the logarithmic law (Simiu and Scanlan 1996):

$$\overline{U}(z) = \frac{1}{\kappa} u_* \ln\frac{z}{z_o} \tag{2.3}$$

where κ is the von Kármán constant ($\kappa \cong 0.4$), z_o is the characteristic roughness

length for the surface terrain, and u_* is the shear velocity of the flow, expressed with relation to a reference mean wind speed $\overline{U}_{ref}$ as

$$u_* = \frac{k\overline{U}_{ref}}{\ln\left(\frac{z_{ref}}{z_o}\right)}. \tag{2.4}$$

Typical values of parameters z_o and α, as well as the corresponding approximate boundary layer depth δ for different types of ground surface roughness conditions are shown in Table 2.1.

Table 2.1 Wind speed profile parameter values (Davenport 1965 and ANSI 1982).

Terrain	z_o (mm)	α	δ (m)
Coastal Areas	5-10	0.10	213
Open Terrain	10-100	0.16	275
Suburban Terrain	300-1,000	0.28	400
Centers of Large Cities	1,000-5,000	0.40	520

The logarithmic and power law can be matched at any elevation z by the relation

$$\alpha = \left\{\ln\left(\frac{z}{z_o}\right)\right\}^{-1}. \tag{2.5}$$

Both the power law and logarithmic law describe the mean wind velocity profile and are strongly influenced by the terrain at the site.

Surface roughness affects the wind speed at all elevations within the boundary layer. The mean wind speed within the boundary layer can also be related to the gradient wind speed $\overline{U}_g$ at the top of the boundary layer by:

$$\overline{U} = \overline{U}_g \left(\frac{z}{\delta} \right)^{\alpha} \tag{2.6}$$

where δ is the boundary layer thickness (see Table 2.1 for typical values). In general, the rougher a surface is, the thicker the boundary layer.

It should be noted that although both logarithmic and power laws are empirical formulas, the power law has been used more often in engineering practice since it is more representative of the entire boundary layer. The logarithmic law is, strictly speaking, limited to the lowest few hundred meters; as well, it produces negative wind speeds at height $z < z_o$.

The instantaneous fluctuating wind speed $u(t)$ is defined by Davenport (1965) as

$$u(t) = U(t) - \overline{U} \,. \tag{2.7}$$

A root-mean-square (*rms*) value, $\tilde{u}$, of the fluctuating component of wind $u(t)$, is defined as

$$\tilde{u} = \sqrt{\tilde{u}^2} \tag{2.8}$$

where $\tilde{u}^2$ is mean-square value, or variance, which can be calculated as

$$\tilde{u}^2 = \frac{1}{T} \int_T u(t)^2 \, dt = \frac{1}{T} \int_T \left[U(t) - \overline{U} \right]^2 dt \,. \tag{2.9}$$

The *rms* fluctuating wind speed $\tilde{u}$ can be related to the wind speed profile parameters $\overline{U}_{10}$ and z_o by the expression

$$\tilde{u} = \frac{\overline{U}_{10}}{\ln\left(\frac{10}{z_o} \right)} \,. \tag{2.10}$$

The magnitude of the wind speed fluctuations is also commonly expressed in terms of the turbulence intensity:

$$i_u(z) = \frac{\tilde{u}}{\overline{U}(z)}. \tag{2.11}$$

The turbulence intensity $i_u(z)$ therefore decreases with height while increasing with ground roughness.

In fact, wind turbulence is a three-dimensional structure. Components of wind turbulence can be divided into three orthogonal directions: alongwind turbulence $u(t)$, acting parallel to the mean wind direction; crosswind turbulence $v(t)$, acting perpendicular to the mean wind direction; and vertical turbulence $w(t)$ (ASCE 2002). The *rms* values for crosswind turbulence component $\tilde{v}$ and vertical turbulence component $\tilde{w}$ can be related to $\tilde{u}$ in an approximate manner as follows (Davenport 1977):

$$\tilde{v} = 0.8\ \tilde{u} \tag{2.12}$$

$$\tilde{w} = 0.5\ \tilde{u}\ . \tag{2.13}$$

2.2.2 Wind Load

The instantaneous alongwind drag force acting on an object at a given elevation may be given as:

$$F_U(t) = p_d(t)\ A_d\ C_D \tag{2.14}$$

where the dynamic wind pressure is:

$$p_d(t) = \frac{1}{2}\rho_a \cdot U(t)^2 \tag{2.15}$$

and A_d is the projected surface area, C_D is the drag coefficient for the object, ρ_a is the

mass density of air, and $U(t)$ is the instantaneous wind velocity at that elevation:

$$U(t) = \overline{U} + u(t). \tag{2.16}$$

Since the mean wind speed $\overline{U}$ is generally much higher than fluctuating wind speed $u(t)$, second-order effects associated with $u(t)$ can be neglected, so that the total drag force $F_U(t)$ may be separated into a mean drag force $\overline{F}$ and a dynamic fluctuating drag force $F_u(t)$ as follows:

$$F_U(t) = \overline{F} + F_u(t). \tag{2.17}$$

Here, $\overline{F}$ represents a nearly static wind force, given by

$$\overline{F} = \left[\frac{1}{2}\rho_a \, \overline{U}^2\right] A_d \, C_D \tag{2.18}$$

and $F_u(t)$ is considered to be the dynamic gust loading component, given by

$$F_u(t) = \rho_a \, \overline{U} \, u(t) \, A_d \, C_D. \tag{2.19}$$

For convenience, and by convention, therefore, the response of structures to gusty winds is typically divided into two components: the mean (static) response due to $\overline{F}$, which is time invariant, and the dynamic, time-varying response component due to $F_u(t)$. Further details regarding the dynamic response are provided in Section 2.5.

2.2.3 Power Spectrum

Power spectral density functions, or power spectra, which represent the rate of change of the mean square value of a parameter with frequency, provide an indication of how the energy of a particular random parameter is distributed with frequency. Figure 2.2 illustrates typical wind turbulence power spectra at three different wind speeds, showing that the wind speed fluctuations contain contributions from a wide

range of different frequencies. An important property of power spectra is that the total area under the spectrum over all frequencies is equal to the mean-square value ($\tilde{u}^2$) of the wind speed fluctuations, or

$$\tilde{u}^2 = \int_0^\infty S_u(f) \cdot df \tag{2.20}$$

where $S_u(f)$ is the power spectrum for the wind speed fluctuations and f is the frequency.

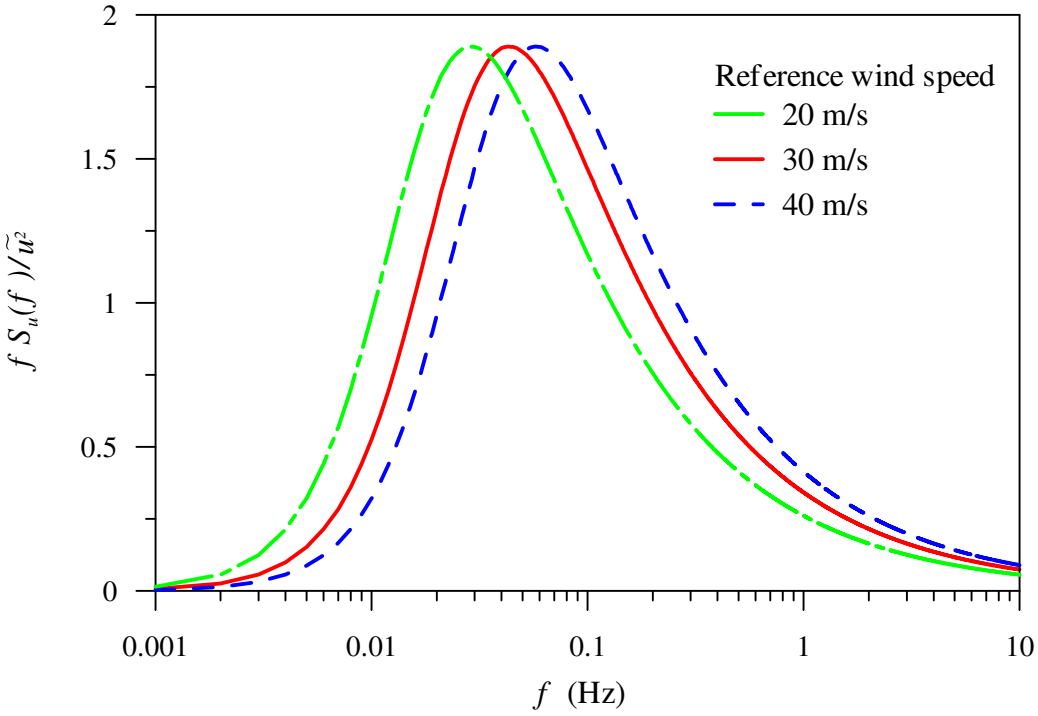

Figure 2.2. Power spectral density function for alongwind turbulence (after Davenport 1964).

A number of analytical expressions have been proposed to describe turbulence spectra, including the so-called Davenport spectrum adopted by the National Building Code of Canada (NBCC 1995):

$$\frac{f \cdot S_u(f)}{\tilde{u}^2} = 4.0 \cdot \frac{n_f^2}{(1+n_f^2)^{4/3}} \tag{2.21}$$

where n_f is a reduced frequency

$$n_f = \frac{L_u \cdot f}{\overline{U}_{10}} \tag{2.22}$$

and L_u is a turbulence length scale ($L_u \approx 1200\, m$).

The Davenport spectrum is plotted in Figure 2.2 for three different mean reference wind speeds: $\overline{U}_{10} = 10\, m/s$, $\overline{U}_{10} = 20\, m/s$ and $\overline{U}_{10} = 30\, m/s$. It is evident that increasing mean wind speeds increase the contribution of high frequency components of turbulence.

2.3 STATIC AND DYNAMIC BEHAVIOUR OF GUY CABLES

2.3.1 Static Behaviour of Guy Cables

A particular feature of a guyed mast is the non-linearity introduced by sag in the guy cables. As illustrated in Figure 2.3, when a guyed cable is supported by its ends, it will deflect in a catenary profile which contains a finite amount of sag due to its self weight, even though it is highly pretensioned. The sag in the cables requires that the cable length be greater than its chord length L_c. A historical summary of analytical expressions for the elastic catenary profile were proposed by Irvine (1981). Generally, the assumption is made that a cable has finite axial stiffness and negligible flexural stiffness; as well, the cable is generally assumed to be hanging in a vertical plane under the influence of its self-weight. The horizontal and vertical spans of the cable between supports were described by relating the horizontal and vertical components of cable tension T_T at its top end:

$$S = \frac{H\,L_{us}}{E_G\,a_G} + \frac{H}{w_G}\left[\sinh^{-1}\left(\frac{V_T}{H}\right) - \sinh^{-1}\left(\frac{V_T - w_G\,L_{us}}{H}\right)\right] \tag{2.23}$$

$$h = \frac{w_G\,L_{us}^{\,2}}{E_G\,a_G}\left(\frac{V_T}{w_G\,L_{us}} - \frac{1}{2}\right) + \frac{H\,L_{us}}{w_G\,L_{us}}\left[\left\{1+\left(\frac{V_T}{H}\right)^2\right\}^{\frac{1}{2}} - \left\{1+\left(\frac{V_T - w_G\,L_{us}}{H}\right)^2\right\}^{\frac{1}{2}}\right] \tag{2.24}$$

where :

S = the horizontal cable span;
H = the horizontal component of tension;
L_{us} = the unstressed length of the guy cable;
E_G = the elastic modulus of the cable;
a_G = unstrained cross-sectional area of the cable;
w_G = weight of cable per unit length;
h = the vertical cable span between the two ends of a guy;
T_B = the cable tension at the bottom end;
V_B = the vertical component of the tension at the bottom end; and
V_T = the vertical component of the tension at the top end.

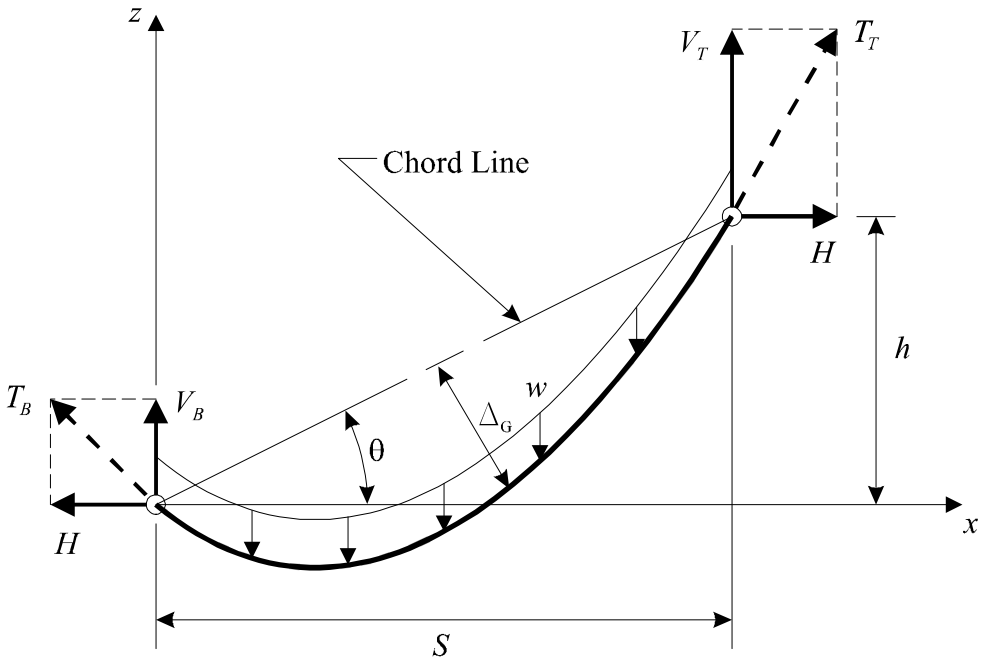

Figure 2.3. Schematic of suspended guy cable defining the important variables (from Sparling 1995).

When guyed masts are subjected to wind loads, the mast deflects laterally in the alongwind direction and, consequently, the attached guy cables are displaced at their upper ends. As shown in Figure 2.3, the resistance from the guy cables is generated by elastic stretching of the cable and changes to the amount of sag in the cable profile, both of which contribute to guy stiffness. The horizontal component of tension H in the guy cable thus changes in such a way as to oppose the mast motion at the attachment levels. The horizontal stiffness of a guy cable, k_{xx}, is given by the change in the horizontal component of tension ΔH per unit horizontal displacement of the mast at the guy attachment point Δx:

$$k_{xx} = \frac{\Delta H}{\Delta x}. \tag{2.25}$$

The sag in the guy profile, however, introduces a nonlinear relationship between the resisting force H and the displacement. To simplify consideration of the sag, guy cables have often been assumed to possess a parabolic, rather than the true catenary profile (Davenport 1959, Davenport and Steels 1965). Irvine (1981) suggested that the guy could be considered as parabolic profile when the cable sag to span ratio (Δ_G / L_c) was less than 1/8. By assuming a parabolic profile in a guy cable, Shears (1968) defined the horizontal stiffness of a guy k_{xx} by the expression

$$k_{xx} = k_e \left[1 + \frac{w_G^2 \cdot L_c^3 \cdot k_e}{12 \overline{T}^3 \cdot \left\{ 1 + \frac{8}{3} \left(\frac{\Delta_G}{L_c} \right)^2 \right\}} \right]^{-1} \tag{2.26}$$

where :

$\overline{T}$ = the average tension in the guy;

k_e = the horizontal stiffness due to the elastic axial strain (defined below); and

Δ_G = the maximum sag of the cable, measured as a perpendicular distance from the chord line (Figure 2.3), calculated as:

$$\Delta_G = \frac{(w_G \cos\theta)}{8\overline{T}} \cdot L_c^2 \tag{2.27}$$

where θ is the vertical angle between the chord line and horizontal. Since the sag Δ_G is very small compared to the chord length L_c for taut wires, the equivalent horizontal stiffness of a guy (Equation 2.26) can be simplified to:

$$k_{EQ} \cong \left[\frac{1}{k_e} + \frac{1}{k_g} \right]^{-1} \tag{2.28}$$

which suggests that guy cables behave as two horizontal springs, k_e and k_g, acting in series: the spring k_e represents the elastic stretch, while the other spring k_g includes all gravitational resistance. The elastic stiffness k_e of a perfectly taut wire is defined by:

$$k_e = \frac{a_G E_G}{L_c} \cdot \cos^2(\theta). \tag{2.29}$$

The stiffness component k_g is often termed the gravitational stiffness of a guy and is determined by:

$$k_g = \frac{12\,(\overline{T})^3}{w_G^2\, L_c^3} \tag{2.30}$$

where the average guy tension $\overline{T}$ is approximately taken at the mid-height of the guy :

$$\overline{T} \cong T_o + \frac{1}{2} w_G\, h \tag{2.31}$$

in which T_o is the guy tension at lower end. Equation 2.30 also strongly suggests the significant influence of guy pre-tension on the guy stiffness.

Special note must be made of the leeward guy cables. The assumption of a parabolic profile is based on a small amount of sag in the guy cables, which provides adequate representation for guys under unloaded (still air) conditions due to the inherently high pre-tension used. In strong wind conditions, however, as the mast deflection increases, the leeward guy will slacken, causing increased sag. Eventually, these guys may reach a stage that the accuracy of the parabolic approximation is no longer acceptable.

At each guy support level, typically three or four guy cables are attached to the mast. When a guyed mast is in an unloaded position, the total horizontal stiffness of all guys is determined from the equivalent guy stiffness k_{EQ} by the expression:

$$k_{TOT} = \sum_{i}^{n} \cos^2 \alpha_i \left[\frac{1}{k_{e_i}} + \frac{1}{k_{g_i}} \right]^{-1} = \sum_{i}^{n} k_{EQ_i} \cos^2 \alpha_i \qquad (2.32)$$

where n is the number of guys attached to the mast at that support level and α is the angle between the guy cable and the wind direction. A definition of wind angle α is shown in Figure 2.4. For guys which radiate symmetrically out from the mast, each guy has approximately the same horizontal stiffness. Equation 2.32 therefore is simplified to:

$$k_{TOT} = N k_{EQ} \qquad (2.33)$$

where $N = 1.5$ for three symmetric guys and $N = 2.0$ for four symmetric guy cables.

A numerical study carried out by Ben Kahla (1993) indicated that the tension on a windward guy increases with increased wind velocity since the wind drag force increases the guy's apparent weight, while the tension in a leeward guy first decreases to its neutral position where it loses its tension as it is lifted up by the wind, then begins

increasing with further increases in the wind velocity. The neutral position of a leeward guy was defined as that where the vertical component of wind drag force acting on the under side of the guy cable effectively cancels its unit weight (w_G).

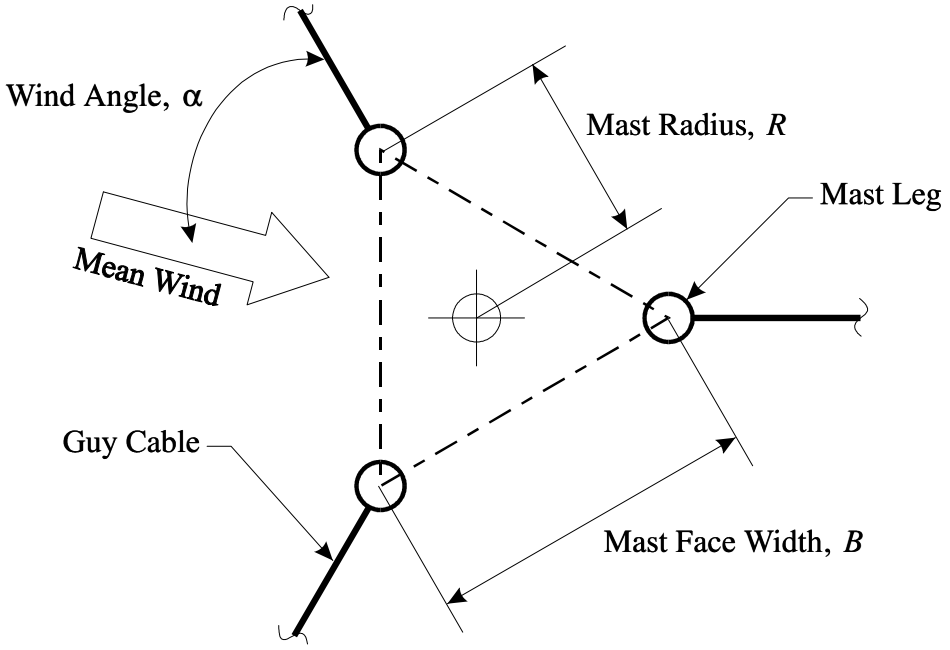

Figure 2.4 Space definition of wind angle α (from Sparling 1995).

2.3.2 Dynamic Behaviour of Guy Cables

2.3.2.1 Overview

The dynamic response of a guyed mast under wind loads is largely dependent on the behaviour of the guyed cables due to their frequency dependent stiffness, relatively large inertia and nonlinearity. The leeward guy cables become slack under wind loads, and therefore contribute little stiffness to the whole structure. At the same time, the tension and stiffness of the windward guys increase as the guys become taut due to the reduced sag.

A numerical study to examine the nonlinear dynamic response of guy cables in turbulent wind loads was undertaken by Sparling and Davenport (2001), using a time domain finite element approach based on nonlinear catenary cable elements. It was reported that nonlinear behaviour of guy cables appears to suppress the resonant response of slackened guys at their fundamental frequency.

2.3.2.2 Natural Frequencies and Mode Shapes

The nonlinear behaviour of guy cables also complicates the evaluation of the natural frequencies and mode shapes of guyed masts, which are important factors in studying the dynamic characteristics of guyed masts. The natural frequencies of guyed masts have been found to be influenced by a number of factors. McCaffrey and Hartmann (1972) compared the natural frequencies and mode shapes of guyed masts using a parabolic guy model and a catenary guy model. It was found that most of the natural frequencies of the guyed mast system in the low frequency range were due to the presence of the guys; as well, the natural frequencies were essentially the same for both parabolic and catenary guy models. An increasing initial tension in the guy cables has been found to result in a significant increase in the natural frequencies of a guyed mast (Madugula et al. 1998, Wang et al. 2003). Wahba (1999) carried out numerical dynamic analysis of a guyed mast and reported that the height of the mast is the most direct factor in determining the lowest natural frequency of guyed masts.

Irvine (1978) proposed analytical expressions for the natural frequencies and mode shapes of taut, inclined elastic guy cables, which were assumed to have parabolic profiles with small sag (the sag-to-span ratio is less than 1/8), small vibration amplitudes and be without coupling effects between the in-plane (vertical) and out-of-

plane (lateral) vibrations. Vibration modes of in-plane vibrations were distinguished as either symmetric or anti-symmetric about the midpoint of the cable. Based on the parabolic assumption of cable profile, only the symmetric modes are extensional (i.e. cause axial stretching), and generate dynamic tension and the resulting reaction force on the mast; thus, they are of importance in the dynamic analysis of guyed masts.

The symmetric in-plane modes can be characterized by a single stiffness parameter λ^2, expressing the relative influence of gravitational and elasticity effects (Irvine 1978). This stiffness parameter λ^2 is expressed as:

$$\lambda^2 = \left(\frac{w_G \, L_c \cos\theta}{\overline{T}} \right)^2 \frac{\left(\frac{a_G \, E_G \, L_c}{\overline{T}} \right)}{L_c \left[1 + 8 \left(\frac{\Delta_G}{L_c} \right)^2 \right]}. \tag{2.34}$$

Since the sag-to-span ratio of a cable is typically small when applying the parabolic profile approximation, Equation. 2.34 thus can be rewritten by relating to the elastic and gravitational force directly:

$$\lambda^2 \approx 12 \cdot \frac{k_e}{k_g}. \tag{2.35}$$

The influence of cable tautness on the natural frequencies of in-plane cable vibration was outlined by Irvine (1981), and illustrated in Figure 2.5, where the natural frequencies have been normalized by the fundamental taut wire natural frequency, ω_o. As shown in this figure, the lowest natural frequency of the cables is the first symmetric in-plane mode (w_1^{IS}) for taut cables with low λ^2, after which the anti-symmetric modes (ω_n^{IA} where $n = 1,2,3$) and symmetric modes (ω_n^{IS} where $n = 1,2,3$) alternate. As the sag of the guys increases, the frequency at the lowest symmetric vibration mode varies with

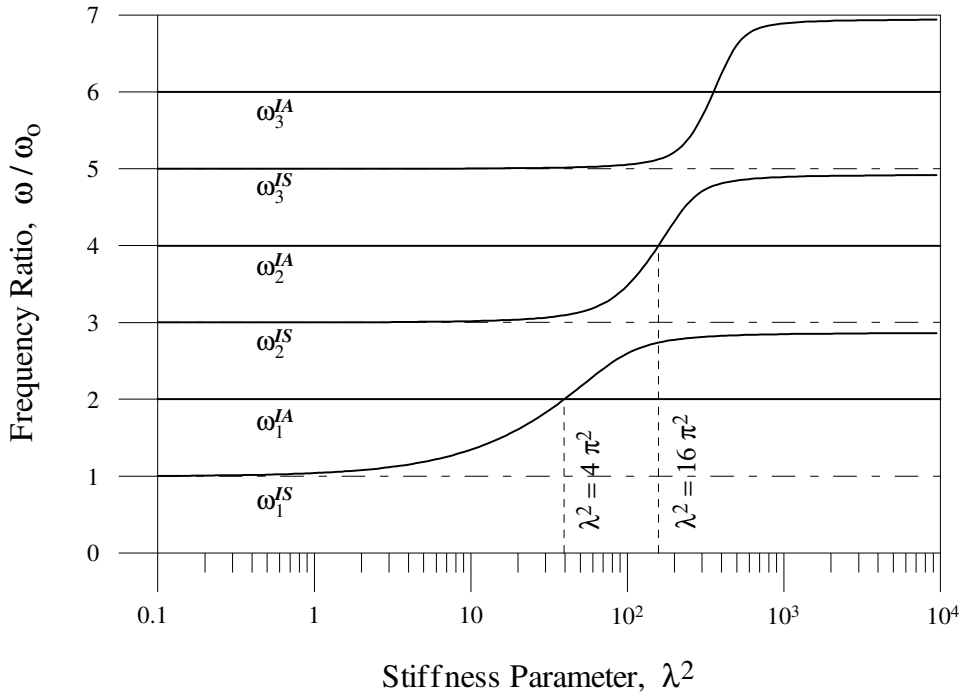

Figure 2.5. Variation in guy-plane natural frequencies with λ^2 (from Sparling 1995).

the stiffness parameter λ^2, while the anti-symmetric mode frequencies (ω_n^{IA}) does not. A potentially dangerous motion of guys could therefore occur if the two vibration mode frequencies coincide at crossover point since energy could then be transferred between the non-extensional anti-symmetric and extensional symmetric modes. For the n^{th} pair of symmetric and anti-symmetric modes, the crossover point occurs at a stiffness parameter value of:

$$\lambda^2 = (n+1)^2 \pi^2 . \tag{2.36}$$

However, this possibility of model crossover can be reduced if guy stiffness satisfies Equation 2.35. Irvine (1978) also presented the shape of first symmetric in-plane mode for different λ^2 , illustrated in Figure 2.6. As can be seen in this figure, the taut cables with low sag where $\lambda^2 \approx 1$ have a mode shape that is approximately sinusoidal; for slack

cables with large sag, on the other hand, the mode shape is more like an inextensible chain, with two internal nodes (points of zero displacement).

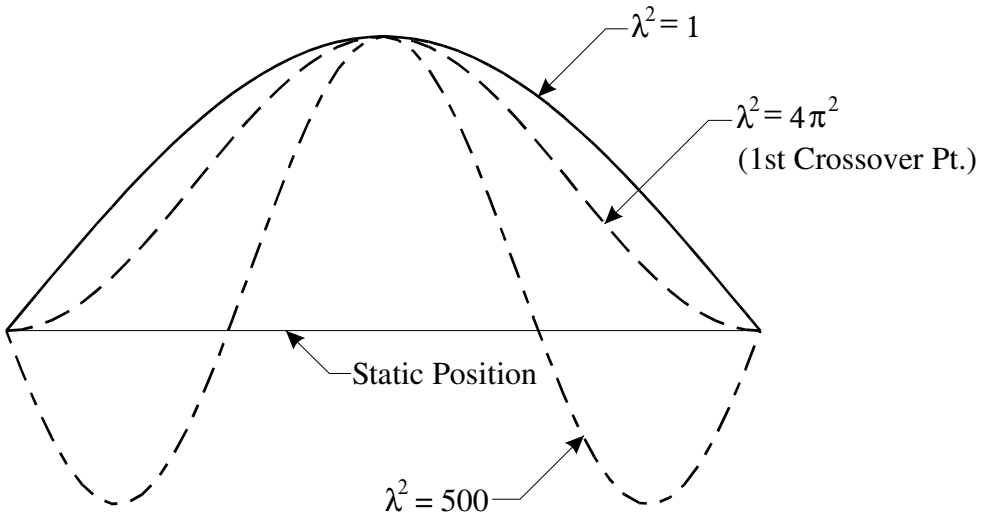

Figure 2.6. Variations in the 1st symmetric in-plane mode shape with cable tautness (from Sparling 1995).

2.3.2.3 Dynamic Cable Stiffness

Historically, linear guy models have been used widely in dynamic analysis due to the complexity that arises from consideration of the geometrically nonlinear behaviour of guy cables. The first dynamic solution for guy cables was proposed by Kolousek (1947) based on the assumption of parabolic profile in cables. Dean (1961) proposed dynamic formulas for guy cables using catenary properties rather than the parabolic approximation. This method, however, neglected the elastic stretch of the guy and that the vibration mode was assumed to be quasi-static. Davenport and Steels (1965) extended the solution by including the effects of viscous damping, and proposed the damped guy modulus, which was examined by experiment for moderate amplitude movements.

A commonly used guy model to analyze the dynamic behaviour of guy cables is a *spring-mass model*, which was first developed by Hartmann and Davenport (1966). This model was later applied to study the dynamic response of CFPL tower in London, Ontario, with a height of 304 m. The guy cables in this model were assumed to be taut, so that its static profile was approximately parabolic; in addition, only the first in-plane mode of vibration was considered. The two springs in the system, one with spring constant K^{G1} and the other with spring constant K^{G2}, represent the elastic stiffness and the gravitational stiffness, respectively. The lumped mass M^G represents the inertial properties of the guy. According to Hartmann and Davenport (1966), the equivalent properties of the spring-mass model for a cable vibrating in its own first in-plane (vertical) symmetric mode, were given by the expression:

$$K^{G1} = k_e \left(1 - \frac{4\, w_G\, L_c \sin\theta}{\pi^2\, \overline{T}} \right) \tag{2.37}$$

$$K^{G2} = \frac{K^{G1}}{\dfrac{4 w_G\, L_c}{\pi^2\, \overline{T}} \left[\dfrac{2\, g_a\, k_e}{\omega_o^2\, \overline{T}} - \sin\theta \left\{ 1 + \dfrac{8}{\pi^2} \left(\dfrac{w_G\, L_c}{\overline{T}} \right) \left(\dfrac{g_a\, k_e}{\omega_o^2\, \overline{T}} \right) \right\} \right]} \tag{2.38}$$

$$M^G = \frac{K^{G2}}{\omega_o^2} \left(1 - \frac{4}{\pi^2} \sin\theta\, \frac{w_G\, L_c}{\overline{T}} \right) \tag{2.39}$$

where g_a is the gravitational acceleration (9.81 m/s^2) .

Based on the simplified *spring-mass* model, Kärnä (1984) proposed a modified *spring-mass* guy model by inserting a viscous dashpot that represents both structural and aerodynamic damping mechanisms. While introducing the damping into the system, Sparling (1995) refined the *spring-mass* guy model by placing two fictitious linear viscous dampers: the structural damping C_s and aerodynamic damping C_a in parallel

with the springs. Figure 2.7 illustrates an example of the structural model for a single level guy cable. The structural damping C_s takes into account the energy lost in the cable due to heat loss caused by stretching, bending and internal friction, while the aerodynamic damping C_a takes into consideration the effects of the wind counteracting the movement of the guy. This *spring-mass* guy model is used in the numerical model throughout this study, in which the structural damping ratio was taken as 0.5% of critical, while the aerodynamic damping was calculated explicitly for each vibration mode.

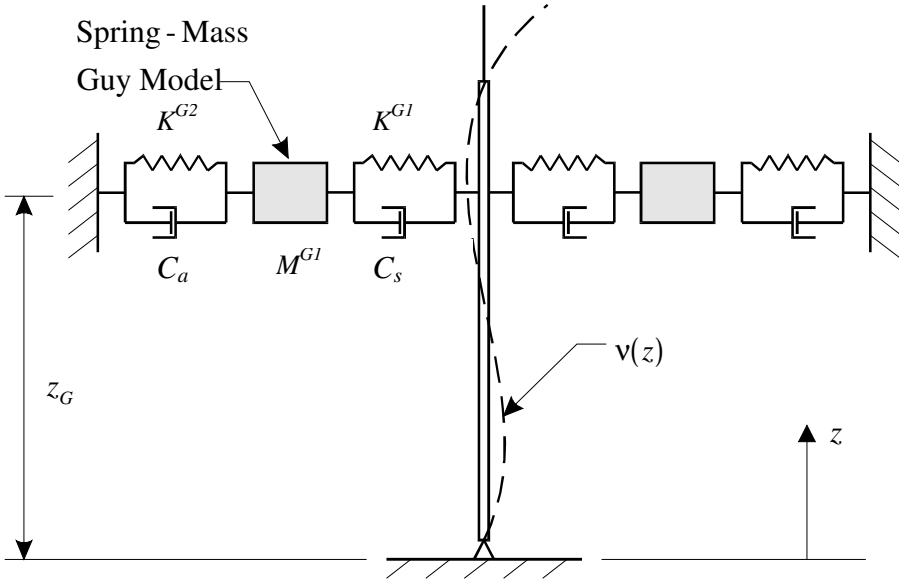

Figure 2.7 Equivalent spring-mass guy model (from Sparling 1995).

2.4 STATIC AND DYNAMIC ANALYSIS MODEL FOR GUYED MASTS SUBJECTED TO TURBULENT WIND

2.4.1 Introduction

Mostly, it has been assumed that guyed masts vibrate linearly about their static equilibrium position to simplify dynamic calculations (Hartmann and Davenport 1966,

Davenport and Vickery 1968, McCaffrey and Hartmann 1972, IASS 1981). Methods for estimating the wind-induced static and dynamic response of guyed masts are discussed in the following sections.

2.4.2 Numerical Models for Static Analysis of Guyed Masts

For static analysis of guyed masts, both beam-column models and three-dimensional truss finite element models have been widely used to represent the lattice mast structure. In the beam-column model, an equivalent elastic beam-column with the appropriate bending and axial stiffness represents the shaft, while nonlinear elastic supports at the guy attachment points have been used to represent the guys. In the space truss approach, on the other hand, each leg, diagonal and horizontal member is modelled individually.

The guyed space truss model and the equivalent beam-column model were compared in the approximate analyses of guyed masts subjected to wind loads (Ben Kahla 1993). In the 3D-truss model (Figure 2.8a), the mast members (legs, diagonals and horizontals) were modelled as three-dimensional, two-node truss elements with three degrees of freedom at each node. Three-dimensional cable elements were modelled using elastic catenary cable elements. The equivalent beam-column model, as shown in Figure 2.8b, used a single flexural element that was capable of reproducing the deformations of the centroidal axis of the mast. It was demonstrated that the beam-column method generally gave the same results as the 3D-truss model.

By taking into account the nonlinear effects of guyed cables, Wahba (1999) also used both the 3D-truss model and beam-column approaches to analyze the response of guyed masts. In the 3D-truss model, the mast was treated as three-dimensional truss

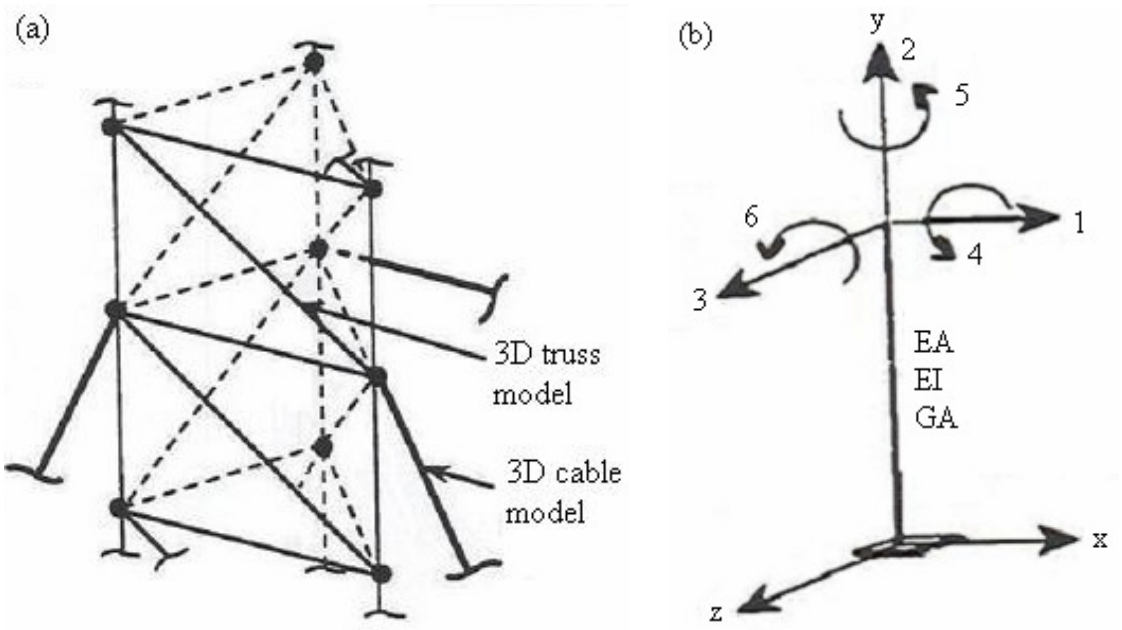

Figure 2.8. (a) Guyed space truss model; (b) beam-column model (from Ben Kahla 1993).

elements on nonlinear elastic supports modelled for the guys; the beam-column model, on the other hand, adopted a more traditional finite element approach, in which the mast was modelled using beam-column elements and guys were explicitly modelled as nonlinear cable elements. It was concluded that no advantages were gained by the use of the 3D-truss model; in addition, more conservative rotations were obtained when using the beam-column model on nonlinear supports.

Based on the equivalent beam-column model, Meshmesha et al. (2003) employed an equivalent thin plate approach that explicitly considered effects such as shear and torsion in defining the bending rigidity, as well as the equivalent axial area of the guyed mast. Again, by comparing this model with the 3D-truss element model of a guyed mast, good agreement was observed between this simple beam-column element and the 3D-truss model.

2.4.3 Numerical Models for Dynamic Analysis of Guyed Masts

Many analysis models have been proposed to evaluate the dynamic response of guyed masts. Investigations of the dynamic response of guyed masts using pseudo-dynamic analytical models typically include the gust factor method, patch load method and other simplified methods. Basically, the common assumption made in these analytical models was that guyed masts vibrate linearly about their static equilibrium position produced by the mean wind load. Also, all represent attempts to develop simplified static analysis methods which simulate a full dynamic analysis.

In the current Canadian standard CSA S37-01 (CSA 2001) for the design of guyed masts and antennae, a purely static analysis is performed using the gust factor approach. In this method, an equivalent static wind pressure *P* is used to approximate dynamic response effects. A uniform gust effect factor C_g, typically taken as 2.0 regardless of the height of the mast, is applied to the mean wind pressure throughout to define an equivalent static load intended to produce the same peak response as would be caused by dynamic effects. The design wind pressure is determined by the following formula:

$$P_{wind}(z) = q\, C_e(z)\, C_g\, C_a \tag{2.40}$$

where $P_{wind}(z)$ is the effective wind pressure at elevation *z*; *q* is the reference velocity pressure ($q = \frac{1}{2}\rho_a\, \overline{U}_{ref}{}^2$), taken as the 30-year return period mean hourly wind pressure at reference height, and C_e is the height factor:

$$C_e(z) = \left(\frac{z}{10}\right)^{0.2}. \tag{2.41}$$

The parameter C_a is a speed-up factor for structures located on tops of buildings, which is taken to be a constant value of 1 for ground-mounted masts. This approach was shown to be approximate for guyed masts due to the contribution of the higher modes of vibrations to the total response (Ben Kahla 1993), and could result in an underestimation of the peak wind loads. The application of a constant gust factor was also questioned by Vellozzi (1975). In addition, it has been found that predictions of peak response based on the static behaviour under steady winds can give misleading and often unconservative results (Davenport and Sparling 1992).

In the gust factor method, because the peak response is predicted based on the static response to a perfectly correlated wind force over the entire mast height, the dynamic portion of the total response is poorly reproduced since the lack of spatial correlation in wind gusts plays a key role in response fluctuations. A comparison between the static and dynamic response of an example guyed mast by using the gust factor method and dynamic analysis method, respectively, is illustrated in Figure 2.9. It is evident that the magnitude of the dynamic response tends to be much higher than static response in both bending moments and shear. The dynamic bending moments are also distributed in a fairly uniform manner along the mast while mean (static) bending moments exhibit large variations as well as zero response at contraflexure points. Similar features can be found in the shear response diagram. The dynamic shear response maintains a more consistent non-zero value in all spans while static shear response inevitably passes through zero near the midspan.

A patch load method, which takes the dynamic response characteristics of guyed masts into account, along with the spatial structure in turbulent winds, has been

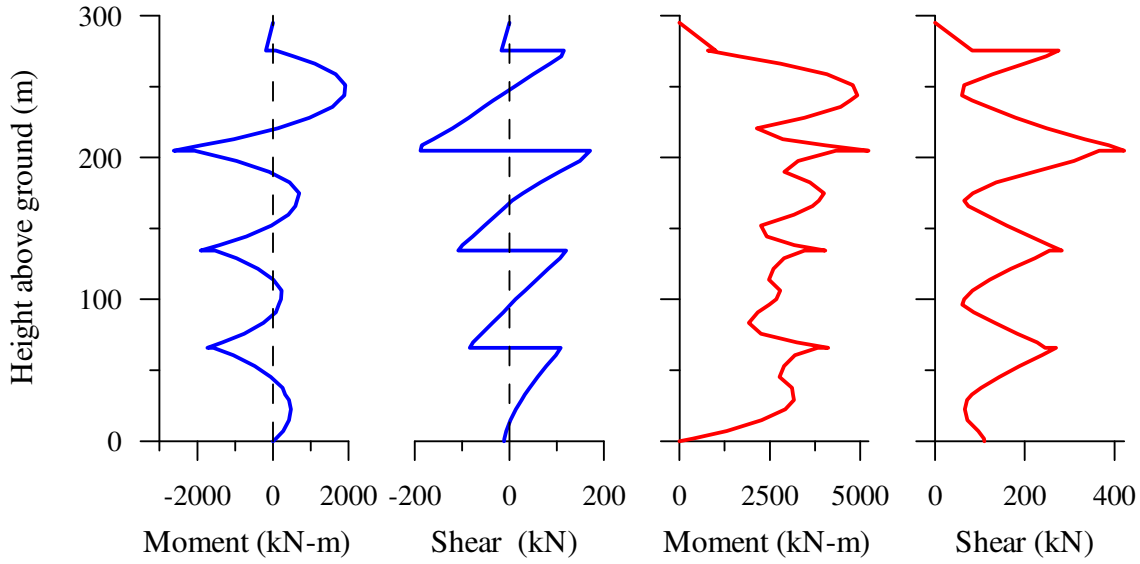

Figure 2.9. Comparison of static and dynamic response of a 300 m guyed mast.

investigated by Davenport and Sparling (1992). The effects of gusty winds were reproduced by using a series of static load patterns as illustrated in Figure 2.10. The patch load method has been adopted in the British Standard BS 8100-Part 4 (BSI 1994) and the European Standard EC3 (CEN 1997) as a mandatory procedure; as well, it has been included in the Canadian design standard CSA-S37-01 (CSA 2001) as an optional method.

Using only static loads and responses, a "patch" loading technique was used in which a number of different load cases were combined in order to generate the peak response of the structure:

$$\hat{r} = \bar{r} \pm \tilde{r}_{PL}\, \lambda_B\, \lambda_R\, \lambda_{TL}\, g_p \tag{2.42}$$

where:

$\hat{r}$ = the design peak response;
$\bar{r}$ = the mean response component;
$\tilde{r}_{PL}$ = the resultant patch load response;
λ_B = the background scaling factor;

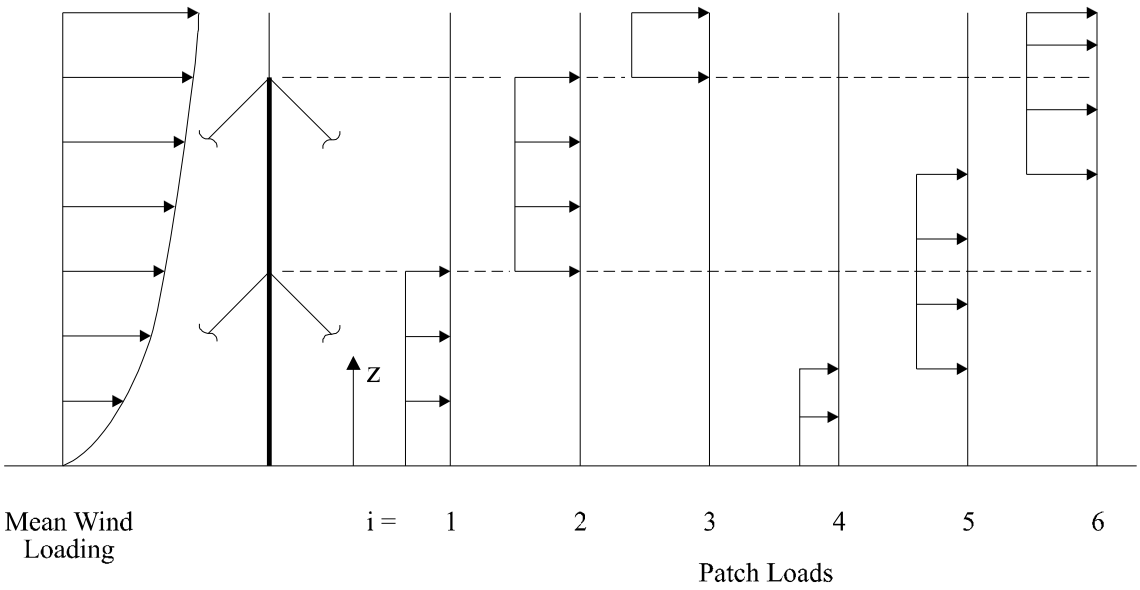

Figure 2.10. Required patch loads for patch load method for a two-level mast with a cantilever antenna (from Sparling 1995).

λ_R = the resonant amplification factor;
λ_{TL} = the turbulence length scale factor; and
g_p = a peak factor which is taken as 4.0.

The resultant patch load response $\tilde{r}_{PL}$ is determined by a series of patch load cases applied to the mast, which is given by

$$\tilde{r}_{PL} = \sqrt{\sum_{i=1}^{n_{LC}} r_{PL_i}^2} \ , \tag{2.43}$$

where r_{pL_i} is the resulting response for the i^{th} static patch load case, and n_{LC} is the total number of patch load cases. Since patch loads are intended to represent the lack of correlation in wind gusts, the patch load method generates reliable results (Nielsen 1991, Sparling et al. 1996).

Sparling and Gress (1997) developed a simpler dynamic analysis method for guyed masts subjected to buffeting due to turbulent winds. Based on a single static load case, the peak dynamic response was generated by adjusting scaling factors according

to the structural geometry and wind conditions. In this method, the peak design response $\hat{R}$ is given by

$$\hat{R} = \overline{R} \pm \tilde{r}_{est}\, \lambda_L \lambda_I \,, \tag{2.44}$$

where:

$\hat{R}$ = the peak design response to turbulent wind loading;
$\overline{R}$ = the static response to the mean wind, with no gust factor ($C_g = 1.0$);
$\tilde{r}_{est}$ = dynamic response estimated from static analysis results;
λ_L = the span length factor; and
λ_I = the turbulence intensity factor.

Commonly used full dynamic analytical methods for predicting dynamic response of guyed masts include both frequency domain models, which make use of statistical descriptions of the wind, and time domain models, which use deterministic definitions of turbulent wind fields. In the frequency domain approach, the gusty winds are characterized in a probabilistic manner using statistically derived descriptions of relevant properties such as frequency content and spatial organization. A detailed description of the frequency domain approach is presented in Section 2.5. Alternatively, the dynamic analysis of guyed masts can be undertaken using a time domain approach, in which the response is determined explicitly at a series of discrete time intervals (Buchholdt et al. 1986; Iannuzzi and Spinelli 1989; Sparling and Davenport 1997). Since the state of the structural system is then known at any given instant, nonlinear structural properties such as guy stiffness and mast axial forces can be updated continuously to reflect current conditions. The velocity and the acceleration of the structure can also be obtained from the first and the second derivatives of displacement, respectively.

Sparling and Davenport (1998) used the time domain method to determine the three-dimensional dynamic response to wind turbulence by doing step-by-step integration. The difficulty of the time domain approach, on the other hand, is that the time history of wind force function must be explicitly defined for all parts of the structure at each time interval. A recent study, though, indicated that both approaches give similar response predictions if the assumed wind characteristics are comparable (Sparling 2001).

2.5 FREQUENCY DOMAIN ANALYTICAL MODEL FOR GUYED MASTS

2.5.1 Introduction

Dynamic response calculations for turbulent buffeting conditions are most commonly performed in the frequency domain method in order to take advantage of the frequency dependent character of both the wind loads and mechanical properties of the structure (Davenport 1961; Vellozzi 1975; IASS 1981). Instead of the time history of the forcing function, only statistical characteristics of the wind have to be known in order to determine the structure response. Based on work done by Davenport (1987) and other researchers (Allsop 1983, Davenport and Loh 1986), Sparling (1995) developed a detailed frequency domain analysis model specifically for guyed masts. In this approach, the nonlinear structural properties were taken into account in the calculation of the static response to mean wind loads, while linear vibration was assumed about the mean equilibrium position.

The time history of a specific response, or load effect, $r(t)$, in gusty wind conditions typically resembles the plot illustrated in Figure 2.11(a). Conceptually, this

response could represent a wide variety of structural actions including the displacement, shear force or bending moment at some locations in the mast, as well as tension in a guy cable. In the frequency domain approach, this response is separated into a time-averaged mean component $\bar{r}$ and a fluctuating dynamic component $\tilde{r}$. As indicated in Figure 2.11(b), the fluctuating component may be further subdivided into large, slowly varying quasi-static background response fluctuations $r_B(t)$ and highly irregular resonant response fluctuations $r_R(t)$ (Allsop 1983).

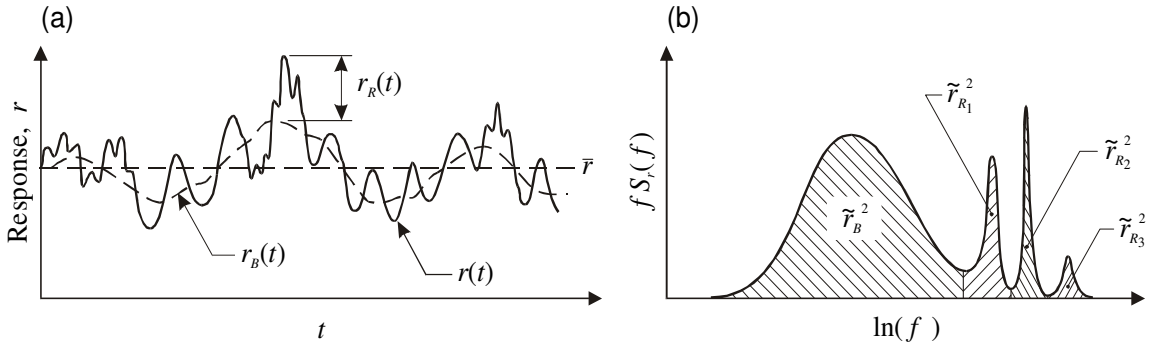

Figure 2.11. Representations of wind-induced response: (a) time history; and (b) power spectrum.

Assumptions made for the frequency domain analysis model were that the guyed mast vibrated linearly about the mean equilibrium position of the system, the guys were modelled using a simplified spring-mass model, and the mast vibrated only in a vertical plane in the alongwind direction. Only some of the key concepts are reviewed in this section; details are provided in Sparling (1995).

2.5.2 Mean Response

The mean and dynamic responses of guyed masts in turbulent winds can be determined by using response influence lines (Davenport 1987, Sparling 1995). In this approach, the influence line for a particular response (bending moment, shear or

deflection) at a specified location on the mast is defined as a function describing the magnitude of the response by applying a unit force at any location on the mast. Using the influence line method, the mean response component $\bar{r}$ of the mast due to the static (mean) component of wind force $\overline{F}(z)$ is given by the expression

$$\bar{r} = \int_H \overline{F}(z)\, I_r(z)\, dz \tag{2.45}$$

where $I_r(z)$ is the influence line for the response and H is the mast height. Example influence lines for various responses on a guyed mast are shown in Figure 2.12.

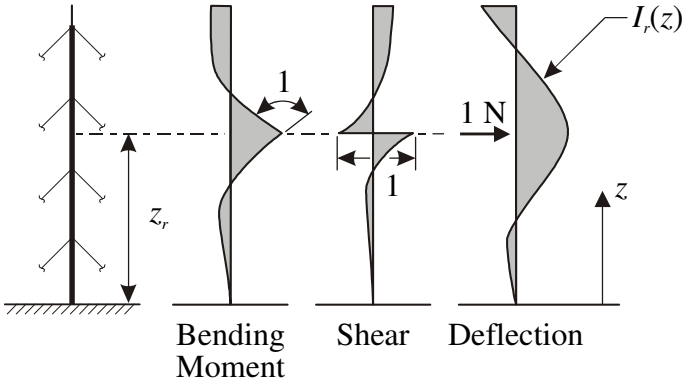

Figure 2.12. Example of influence lines for guyed mast (from Sparling 1995).

2.5.3 Dynamic Response

As suggested in Figure 2.11, the dynamic response $\tilde{r}$ consists of a background response component $\tilde{r}_B$ and a resonant response component $\tilde{r}_R$. The fluctuating response can be characterized in terms of its frequency content using a power spectral density function, or power spectrum $S_r(f)$, the area under which represents the mean-square value of the dynamic response, $\tilde{r}^2$; here, f denotes the frequency in Hz. As suggested in Figure 2.11(b), response spectra for guyed masts in turbulent winds typically feature a wider peak spread over a broad band of frequencies in the low

frequency, quasi-static background range, along with a series of narrow, higher frequency resonant peaks centered on the natural frequencies of the structure. Hence, the background response is also called a quasi-static response since it occurs at frequencies below the natural frequency of the structure, where the dynamic effects are minimal. The resonant response, on the other hand, features one resonant peak representing each significant vibration mode; therefore the total resonant response for a structure with well separated natural frequencies is the sum of all modal responses:

$$\tilde{r}_R^2 = \sum_i \tilde{r}_{R_i}^2 \,. \tag{2.46}$$

The total *rms* value of the wind fluctuations is then determined by

$$\tilde{r} = \sqrt{\tilde{r}_B^2 + \sum_i \tilde{r}_{R_i}^2} \,. \tag{2.47}$$

The peak value $\hat{r}$ of the specific response in question can be estimated from the mean and *rms* components using the expression

$$\hat{r} = \bar{r} \pm g_p \tilde{r} = \bar{r} \pm g_p \sqrt{\tilde{r}_B^2 + \sum_i \tilde{r}_{R_i}^2} \tag{2.48}$$

in which $\tilde{r}_B$ is the *rms* background response, and $\tilde{r}_{R_i}$ is the *rms* resonant response in the i^{th} vibration mode. As demonstrated by Davenport (1964), the statistical peak factor g_p can be estimated by the expression

$$g_p = \sqrt{2\ln(\nu T)} + \frac{0.5772}{\sqrt{2\ln(\nu T)}} \tag{2.49}$$

where T is the period over which the response is considered [s] and the response cycling rate ν is

$$v = \sqrt{\frac{\int f^2 \, S_r(f) \, \mathrm{d}f}{\int S_r(f) \, \mathrm{d}f}} \approx \frac{\sqrt{\sum_i f_i^2 \, \tilde{r}_{R_i}^2}}{\sqrt{\tilde{r}_B^2 + \sum \tilde{r}_{R_i}^2}} \tag{2.50}$$

and f_i is the i^{th} natural frequency. For guyed masts in gusty winds, g_p varies over the limited range of approximately 3.5 to 4.25 (Sparling 1995).

In the frequency domain method used in this study, the background response and resonant response were determined individually, and the total peak response of the guyed mast was then defined by combining them using Equation 2.47. The background response component $\tilde{r}_B$ was determined based on the static properties of the system at the mean equilibrium position while the resonant response component $\tilde{r}_R$ was obtained based on the dynamic properties of guys and mast as represented by the spring-mass model described in Section 2.3.2.3.

As introduced in the previous section, the background and resonant dynamic responses can also be determined by using influence line method. The background response component was determined by using expression (Davenport 1987):

$$\tilde{r}_B^2 = \left[\rho_a \, (C_D \, A)_H \, \overline{U}_H\right]^2 \tilde{u}^2 \int_H \int_H e^{-\frac{|z_2 - z_1|}{L_u}} \left[\varphi_{cd} \, \varphi_u \, I_r\right]_{z_1} \left[\varphi_{cd} \, \varphi_u \, I_r\right]_{z_2} \, dz_1 \, dz_2 \ . \tag{2.51}$$

The normalized effective drag area parameter φ_{cd} and the normalized wind speed parameter φ_u were defined as follows:

$$\varphi_{cd}(z) = \frac{C_D(z) \, A(z)}{(C_D \, A)_H} \tag{2.52}$$

$$\varphi_u(z) = \frac{\overline{U}(z)}{\overline{U}_H} \tag{2.53}$$

where $(C_D \, A)_H$ is effective drag area at the top of the mast and $\overline{U}_H$ is the mean wind

speed at the top of the mast. The resonant response component for the i^{th} vibration mode is:

$$\tilde{r}_{R_i} = \sqrt{\frac{\pi f_i S_{GF_i}(f_i)}{4(\xi_{s_i} + \xi_{a_i})}} \frac{\int_H m(z)\,\Phi_i(z)\,I_r(z)\,dz}{\int_H m(z)\Phi_i(z)^2\,dz} \tag{2.54}$$

where *m(z)* is the mass of the mast per unit length, S_{GF_i} is the spectrum of the generalized force for the i^{th} vibration mode, ξ_{s_i} is the i^{th} structural damping ratio expressed as a fraction of critical damping, ξ_{a_i} is the aerodynamic damping ratio, and Φ_i is the eigenvector of the i^{th} mode shape. Detailed expressions for the dynamic response using the influence line method have been published by Sparling (1995).

In a structure vibrating in response to turbulent winds, energy dissipating forces may arise from two sources: mechanical damping inherent in the structure and aerodynamic damping, which is effective in helping to suppress a resonant response. The aerodynamic damping ratio is equal to

$$\zeta_a = \frac{c_a}{2\sqrt{k\,m}} \tag{2.55}$$

where the aerodynamic damping coefficient is defined as

$$c_a = \rho \overline{U}\, A_d\, C_D\,. \tag{2.56}$$

The structural damping ξ_s was generally taken as 0.5% of critical for all modes.

2.5.4 Computer Program Based on Frequency Domain Analysis Model

Based on the frequency domain analytical model described above, a computer program specifically designed for guyed masts and the wind tunnel model was

developed by Sparling (1995). The salient physical properties of guyed masts such as the mass, stiffness and drag forces, as well as the wind characteristics such as the mean wind speed profile, spatial characteristics, and wind spectra, were taken into account. Also accounted for are the nonlinear static response of guyed masts and the effects of mean wind loads acting on the guys (Sparling 1995). One assumption used in the program was that *rms* values of the wind speed fluctuation $\tilde{u}$ were assumed to be invariant with elevation. In addition, as presented in Chapter 1, only alongwind response was taken into account in the program. Both of these intrinsic assumptions differed somewhat from results observed in the wind tunnel tests, as seen in Chapter 5. This frequency domain analysis program has been used throughout this study as a basis for comparison with the measured wind tunnel results.

2.6 EXPERIMENTAL INVESTIGATIONS ON GUYED MASTS

Although a number of numerical models have been used to estimate the buffeting response of guyed masts, very limited experimental work focused on the dynamic characteristics of guyed masts under wind loads have been conducted to date.

Hartmann and Davenport (1966) carried out a full-scale measurement on a 305 m tall CFPL mast (London, Ontario), guyed at four levels, to examine the dynamic response. The full-scale measurement was limited to wind observations and the acceleration records at a height of 204 m under a mean wind speed of 9.57 m/s at a reference height of 10 m above the ground. The observed results examined the simplified guyed mast model where spring-mass guy model was applied.

Full-scale measurements were also conducted on a 245 m tall guyed mast where the site was fairly flat and lacking any trees (Nakamoto and Chiu 1985). The mean wind

velocity measured was approximately 13.9 m/s at a height of 8.2 m above the ground. The power-law exponent for wind speed velocity profile, as well as the resonant frequencies and representative damping ratios, were determined from the experimental data obtained from anemometers and accelerometers installed at five locations along the mast.

Peil and Nölle (1992) conducted an extensive full-scale study on a 344 m tall guyed mast in winds with maximum speeds up to 50 m/s. The dynamic response of the mast was determined by measured strains obtained at four levels on the mast, as well as acceleration readings measured at five levels. Experimental results were compared with static and dynamic model calculations based on random vibrations. It was found that the static calculation underestimated the bending stress of the mast. It was further suggested that it is important to take into account the non-linearity of guyed cables.

The static and dynamic testing of telecommunication guyed masts by means of a shake table to obtain the natural frequencies and mode shapes was conducted by Wahba (1999). In this study, the linear-scale models of the guyed masts were mounted on a shake table and instrumented with accelerometers. Static wind loads were then applied to the model, in which wind loads were simulated by applying static concentrated loads through horizontal cables attached to the mast at various points along the height; in addition, the applied loads were increased along the height in order to model the increase in wind speed with height.

Wind tunnel investigations on both a full aeroelastic model and a section model of a 260 m tall guyed stack were undertaken by Davenport and Vickery (1968); as well, full-scale measurement was carried out so that comparisons could be made between the

results of full-scale measurements, wind tunnel tests and the theoretical results from an analytical model based on the frequency domain approach. Satisfactory agreement between predicted natural frequencies and mode shapes and those from the experimental full-scale measurements as well as the wind tunnel aeroelastic model was reported. It was found that the lowest vibration modes were dominated by motion of the guys with relatively little participation from the mast; the lowest mode corresponded to large amplitude motion of the top guy while the next few modes had significant vibration of guys at progressively lower guy support levels in turn. The intermediate vibration modes featured coupled guy and mast modes, while the highest modes had significant vibrations within the mast. The experimental results from both wind tunnel tests and full scale measurements showed that the mechanical damping for a guyed stack was approximately 0.6% of critical damping. The drag response of the wind tunnel model results indicated that the frequency domain analytical model was adequate for predicting the dynamic response of the guyed stack.

Wind tunnel tests using a wind speed scale of 1:1.6 (model : prototype) on two guyed mast models were carried out by Wang et al. (2003). Both guyed mast models were built to a geometry scale of 1:100, with a height of 2 m and a constant anchor radius of 1.5 m. One model was constructed as a lattice mast with a face width 15 mm and guyed at three levels, while another model, with a cylinder mast made of a brass tube with diameter ϕ = 12.5 mm and thickness δ = 0.15 mm, was guyed at two levels. The models were tested with different initial tensions of guys. The acceleration and the *rms* values of displacement were compared with a numerical model based on the discrete method of random vibration. It was found that increasing guy initial tensions

could increase the structure stiffness significantly. However, both Froude number and Reynolds number effects were not taken into account in these models, which may have meant that the guy stiffness was not modelled properly with respect to gravity effects on a tall guyed mast (ASCE 1997).

Since few experimental studies have been done to date, more studies need to be conducted to ascertain the actual dynamic behaviour of guyed masts. Wind loads, being random, are hard to model realistically and reliably by other means. Therefore, a wind tunnel study on a properly scaled tall guyed mast, which is capable of modelling the inherent nonlinear effects associated with guyed cables, is needed for a better understanding and as a basis for verifying existing models.

3. DYNAMICALLY SCALED GUYED MAST MODEL

3.1 INTRODUCTION

As reviewed in the previous chapter, guyed masts exhibit complex dynamic behaviour in wind loads for which very few experimental measurements are currently available to allow for detailed comparisons with theoretical solutions. For the proposed wind tunnel investigation, a representative 300 m tall guyed telecommunication mast was designed, modelled, constructed, instrumented and tested in the Boundary Layer Wind Tunnel Laboratory (BLWTL), London, Ontario, to study the wind-induced dynamic response of guyed masts.

This chapter describes three stages of the test program: the design of a 300 m guyed mast prototype, the model scaling technique used to determine required model properties, and the construction of the guyed mast model. The detailed wind tunnel testing, as well as the model instrumentation, are presented in Chapter 4.

Guyed masts are complex structures due to their many special characteristics, as described in Chapter 2. The guyed mast model, therefore, should be able to accurately represent the special characteristics of guyed masts. In particular, the nonlinear effects due to the sag in the guy cables, the mast slenderness and light weight, must be accounted for, all of which complicates the model design and construction.

3.2 300 M GUYED MAST PROTOTYPE

3.2.1 Description of the 300 m Guyed Mast Prototype

A fictitious 300 m tall guyed mast, designed in conformance with the Canadian design standard CSA-S37-01 (CSA 2001), was used as the prototype for the wind tunnel study. Representative properties for the prototype were selected on the basis of a parametric study of 41 existing guyed masts of various sizes. As shown in Figure 3.1 and Figure 3.2, the selected mast featured a triangular steel lattice structure with a constant 3 m face width and a 3 m panel height, solid round legs ranging from 119 mm to 152 mm in diameter, structural angle diagonal and horizontal members, a pinned base, and a 15 m antenna cantilevered above the mast. Four evenly spaced guy support levels, spaced approximately 72 m apart, were used, each of which included three guy cables that radiated symmetrically outward and were anchored at either a 100 m or 200 m radius from the base of the mast. Standard steel galvanized bridge strand was used for the guy cables, ranging in size from 36 mm to 46 mm in diameter. In accordance with provisions of CSA-S37-01 (CSA 2001), initial tensions were kept between 8-15% of the rated breaking strength of the strands. Some linear and discrete structure appurtenances such as ladders, transmission lines and platforms, were considered as additional features of the mast. The design of the prototype was checked using GUYMAST (Weisman Consultants Inc., Toronto, Ontario), commercial software designed specifically for guyed masts, based on the static gust factor analysis method. The member capacity checks were undertaken in accordance with the Canadian Standard CSA S37-01 (CSA 2001), in which a safety factor of 1.67 is used for guy cables.

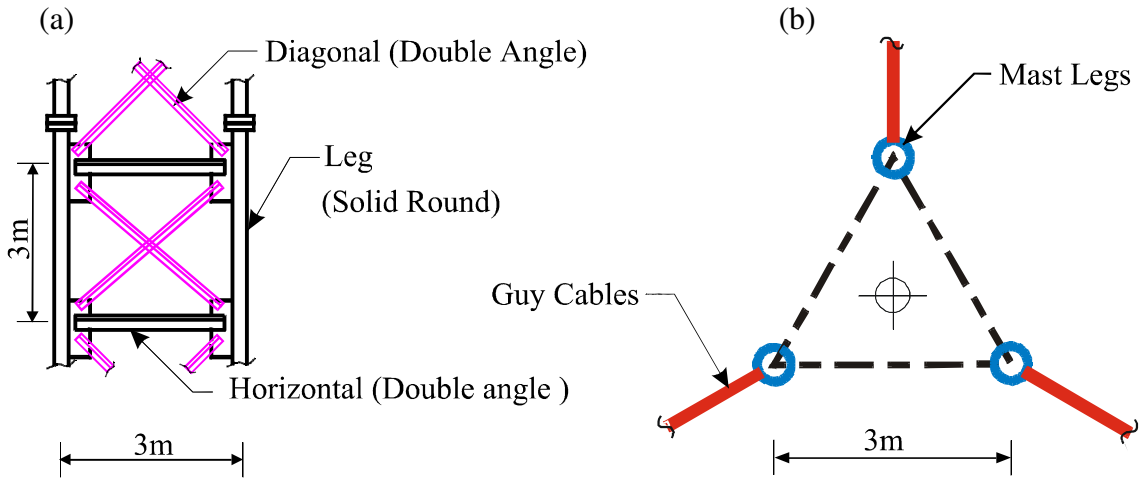

Figure 3.1. Typical guyed mast configuration: (a) elevation of typical mast panel; and (b) horizontal section.

To accommodate model construction requirements, the guyed mast was assumed to be located on a small hill with a height of 11.3 m above the surrounding flat terrain. It was also assumed that there were no large parabolic dishes or any other significant protruding antennae; therefore, no supplemental structural elements (i.e. extra guys) were required to resist torsion. The properties of the cables are listed in Table 3.1.

Table 3.1. Geometry and physical properties of guy cables.

Level	Height [m]	L_c [m]	θ [deg]	a_G [mm^2]	w_G [kN/m]	$\overline{T}$ [kN]	E_G [MPa]
1	68.98	119.97	35.07	1116	0.0873	195.75	165,470
2	140.98	171.72	55.12	1290	0.1	194.08	165,470
3	212.98	290.85	47.05	1290	0.1	197.67	165,470
4	284.98	347.0	55.17	800	0.061	190.57	165,470

3.2.2 Design Wind Load

A mean hourly wind speed of 32 m/s, defined at a reference elevation of 10 m above the ground surface, was assumed for the prototype design. To place this in the

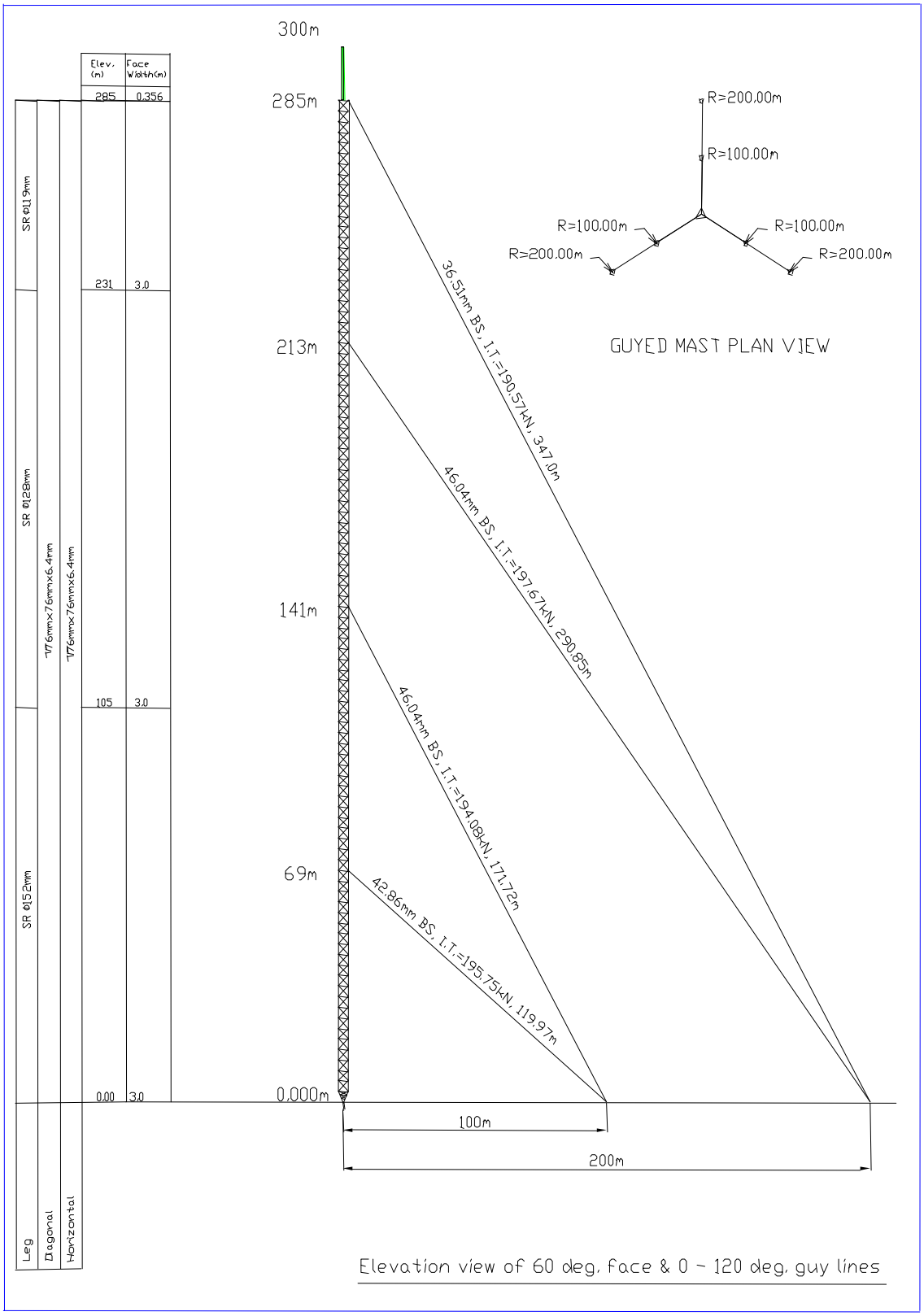

Figure 3.2. Description of the prototype guyed mast design (where SR = solid round; BS = bridge standard; I.T. = Initial tension; and R = guy anchor radius).

context of the Canadian wind climate, a frequency distribution of reference mean hourly wind speeds with a 30-year return period taken in flat open terrain from 640 sites across Canada is shown in Figure 3.3 (NBCC 1995). As can be seen in this figure, the prototype design wind speed of 32 m/s is well above the national average value of 25.5 m/s (1.8 standard deviations above the average), thereby representing a fairly severe wind storm. In addition, smooth, uniform terrain was assumed for the mast site.

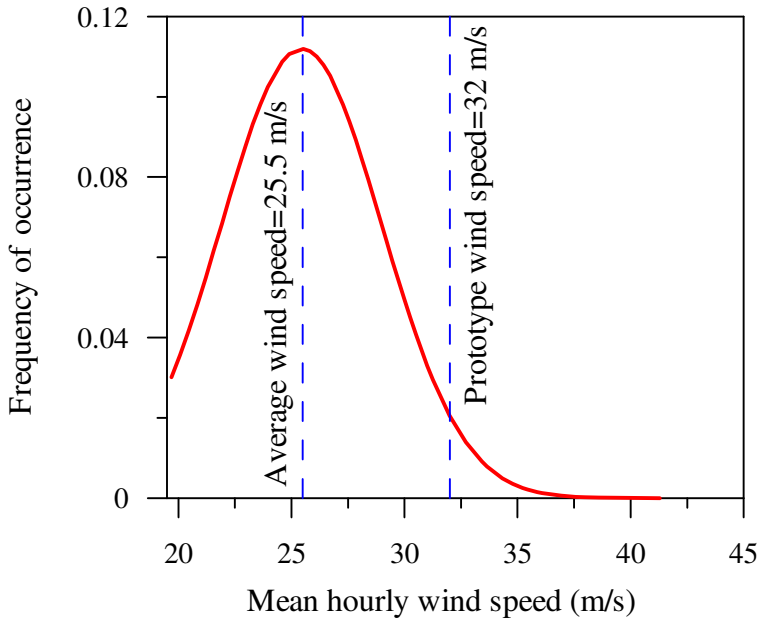

Figure 3.3. Frequency distribution of 1/30 year mean hourly wind speeds in Canada.

In accordance with NBCC (1995), a wind load factor of $\alpha_w = 1.5$ was applied to the design hourly wind pressure, resulting in a design wind speed at the reference height

$$U_{ref} = 32\frac{m}{s}\sqrt{\alpha_w} = 32\frac{m}{s}\sqrt{1.5} = 39.2\frac{m}{s}. \qquad (3.1)$$

Different wind directions acting on the mast will produce different forces in the various members of the structure. Therefore, wind loads oriented at 0^o, 30^o and 60^o (defined in Chapter 2) to any face of the triangular mast were applied in order to obtain the governing member forces in the structure (CSA 2001).

3.3 GUYED MAST MODELLING

3.3.1 Overview

Aeroelastic forces become very important for light weight, slender, flexible and dynamically sensitive structures such as guyed masts. Since these important forces can not be measured with stationary models, a full aeroelastic dynamic model of a guyed mast, with representative stiffness, mass and drag characteristics, was used for this investigation. Froude number (F_r) scaling was adopted in the guyed mast modeling to ensure that gravitational forces were properly accounted for.

A geometric scale (the ratio between linear dimensions of the model and the prototype) of λ_L =1:100 was chosen in order to ensure that the resulting model could be accommodated in the 4 m high x 5 m wide low-speed section of the wind tunnel. The resulting 3 m high model was the tallest ever tested at the BLWTL, as well being as the largest aeroelastic guyed mast model known to the author. In spite of that fact, however, the selected scale still introduced difficulties into the design and construction of the guyed mast model due to limitations in the materials that were readily available.

In addition to similarity requirements for the wind velocity and the exterior geometry, the influence of key physical properties must be properly accounted for in model studies in order to gather realistic information on the static and dynamic response of the prototype structure. A full aeroelastic wind tunnel model is thus required to reproduce the stiffness, mass, drag characteristics as well as the shape of the prototype structure.

In this section, the guyed mast modelling procedure is broken into three parts: (i) velocity scaling; (ii) mast modelling; and (iii) guy modelling. The detailed scaling

relationships that were used to determine the requisite model properties are described below.

3.3.2 Wind Velocity Scaling

Since the vibration of guyed masts is strongly influenced by the action of gravity, the gravity effect must be correctly simulated by making the Froude Number, which represents the ratio of the inertial to the gravitational forces, constant between the model and the prototype. More specifically, the Froude number F_r is defined as:

$$F_r = \frac{V}{\sqrt{gH}} \tag{3.2}$$

in which V is the velocity of the wind (m/s), g is gravitational acceleration (9.81 m/s^2), and H is a characteristic length of the body. The required wind speed for the model was therefore obtained by satisfying the following relationship:

$$\left(\frac{V}{\sqrt{g\,H}}\right)_{\mathrm{mod}\,el} = \left(\frac{V}{\sqrt{g\,H}}\right)_{prototype} . \tag{3.3}$$

Using the geometry scale of $\frac{H_{\mathrm{mod}\,el}}{H_{prototype}} = \lambda_L = 1{:}100$, and noting that the acceleration of gravity g is the same in the model and the prototype, the resulting Froude number scaled velocity ratio λ_v between the model and the prototype is therefore equal to the square root of the length scale, or

$$\lambda_v = \frac{V_{\mathrm{mod}\,el}}{V_{prototype}} = \sqrt{\lambda_L} = 0.1, \tag{3.4}$$

meaning that wind speeds in the wind tunnel were required to be one-tenth of their full-scale values. This fact, however, forced the wind tunnel tests to be conducted at

relatively low wind speeds where independence of force coefficients with wind speed may not have been achieved for some elements.

Faithful modelling of the structure of the wind is of vital importance in the wind tunnel test since the wind turbulence characteristics have a strong effect on the structure. However, strict scaling of the mean wind and the turbulence effects including Reynolds number (R_e) similarity requirements is not possible for a wind tunnel model since wind tunnel tests are performed at wind speeds much smaller than full scale (ASCE 1997). The Reynolds number (R_e) is defined as:

$$R_e = \frac{\rho V D}{\mu} = \frac{V D}{\nu} \tag{3.5}$$

where μ is the coefficient of viscosity of the air, *D* is the outside diameter of the object, and ν is kinematic viscosity of the air ($\nu \approx 14.9 \times 10^{-6} \frac{m^2}{s}$). Therefore, no attempt was made to achieve Reynolds number similarity between the model and prototype; test results, though, were later examined to assess the degree of sensitivity of the model response to Reynolds number effects (see Section 5.9).

3.3.3 Mast Modelling

3.3.3.1 Overview

The mast of the guyed mast model was mainly composed of the spine and the cladding shown in Figure 3.1. The stainless steel spine was used to model the stiffness provided by the three mast legs of the prototype, while the plastic cladding was used to model the drag characteristics of the actual structure. Using this combination of spine

and cladding, the important physical properties of the mast (mass, stiffness and drag force) were represented.

Sketches of the guyed mast model are given in Figure 3.4 and Figure 3.5. As shown in Figure 3.5, the mast model featured a triangular cross section of cladding with a constant face width of 30 mm over its entire height. The non-dimensional similarity requirements for an aeroelastic model of a guyed mast include the following components: mass scaling (m_m), stiffness scaling $(EI)_m$ and effective drag area $(C_D A)_m$ modeling (here subscript *m* denotes the model).

3.3.3.2 Scaling of Structural Stiffness

For free standing structures such as guyed masts, the scaling of stiffness is based on maintaining the equality of the Cauchy Number C_a, while Froude number scaling does not usually play a significant role. The Cauchy number is generally defined as

$$C_a = \frac{E_{eff}}{\rho V^2} \tag{3.6}$$

where ρ is the flow (air) mass density and E_{eff} is the effective modulus of elasticity for the structural section considered. For example, E_{eff} for bending stiffness of the mast spine with length *L* maybe defined as follows:

$$E_{eff} = \frac{EI}{L^4}. \tag{3.7}$$

This stiffness similarity between the model and the prototype therefore requires that

$$\left(\frac{E_{eff}}{\rho V^2}\right)_{\mathrm{mod}\,el} = \left(\frac{E_{eff}}{\rho V^2}\right)_{prototype}. \tag{3.8}$$

As a result, the bending (flexural) stiffness scaling parameter λ_{EI} is thereby 1.00E-10

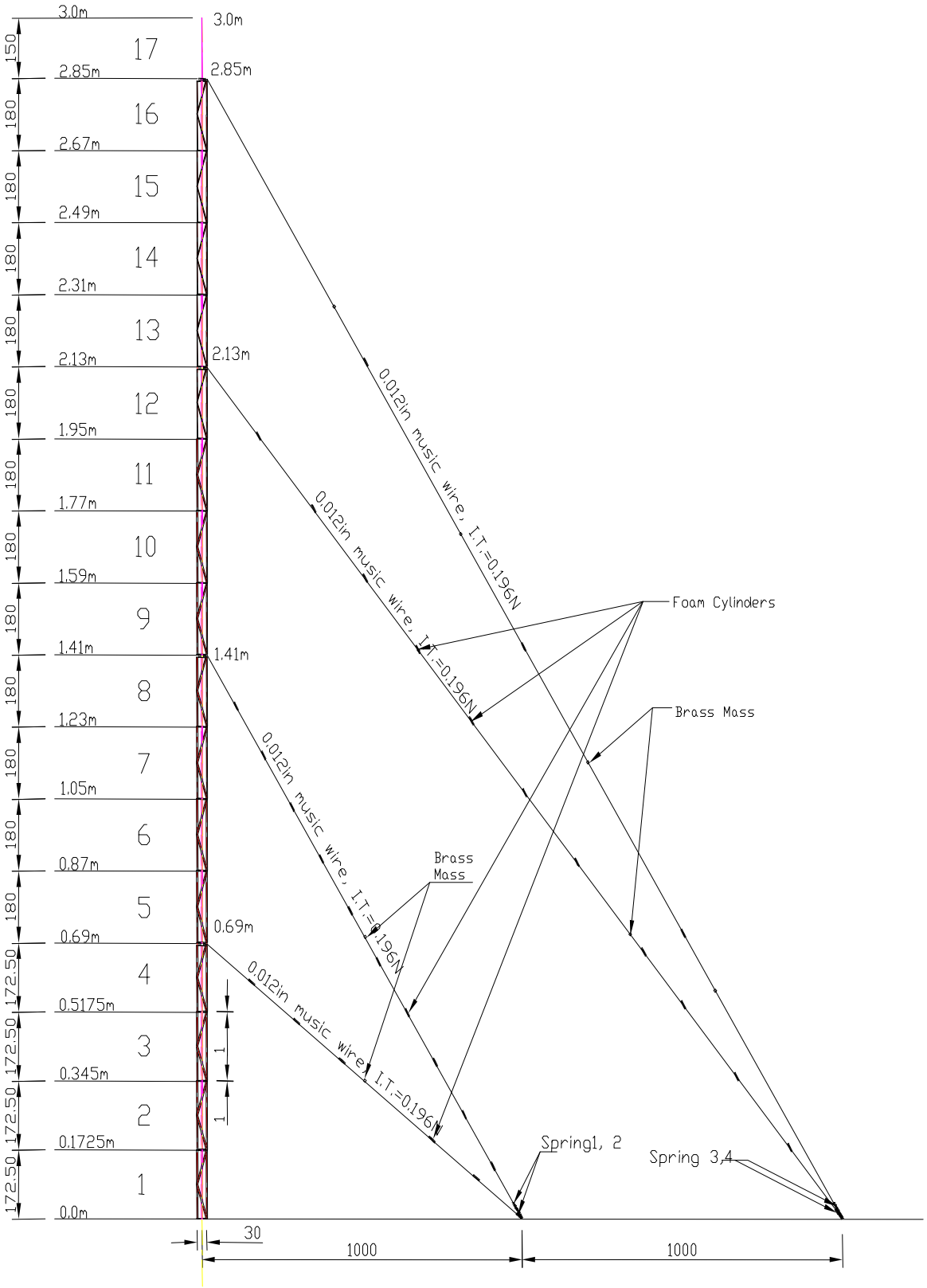

Figure 3.4. Sketch of the 3 m aeroelastic guyed mast model (all dimensions shown in mm; I.T. = initial tension).

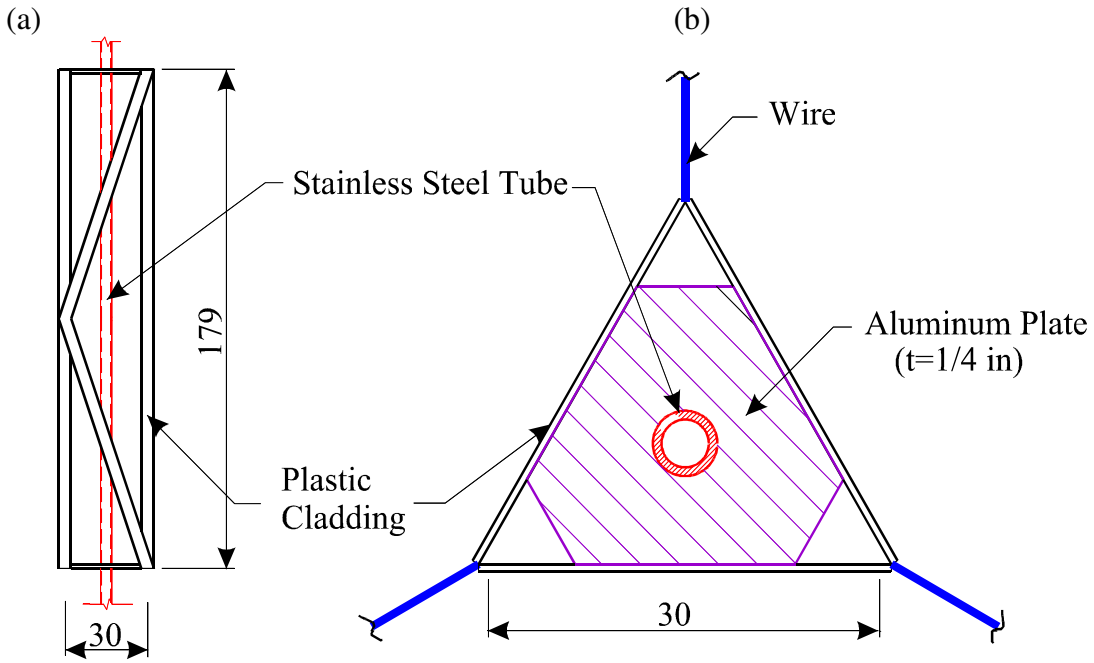

Figure 3.5. Guyed mast model (dimensions in mm): (a) elevation of typical mast section showing the spine and cladding; and (b) horizontal section.

for modelling the stiffness of the mast, or

$$\lambda_{EI} = \frac{(E\,I)_{\mathrm{mod}\,el}}{(E\,I)_{prototype}} = 1.0\times10^{-10}. \qquad (3.9)$$

The bending stiffness of the prototype mast was calculated by using the equivalent beam-column model of a triangular cross-section mast, which takes into account the stiffness of mast legs, as well as that of the horizontal and diagonal struts (Ben Kahla 1993). Due to the low required bending stiffness of the model, the flexural stiffness was provided by a single equivalent spine (stainless steel tube) as shown in Figure 3.5.

3.3.3.3 Mass Scaling

The modelling of the mass was achieved by scaling the inertia forces of the structure to those of the flow consistently, invoking the following ratio relationship of the effective bulk density of the structure to the air density:

$$\left(\frac{\rho_s}{\rho}\right)_{\mathrm{mod}\,el} = \left(\frac{\rho_s}{\rho}\right)_{prototype} \tag{3.10}$$

where ρ_s is the structural bulk density (mass per unit projected volume). In wind tunnel simulations, the air densities are unchanged from prototype condition ($\rho_{\mathrm{mod}\,el} \approx \rho_{\mathrm{Pr}\,ototype}$); consequently,

$$\lambda_\rho = \frac{(\rho_s)_{\mathrm{mod}\,el}}{(\rho_s)_{prototype}} = 1.0\,. \tag{3.11}$$

The resulting mass scaling factor (mass per unit length) was then

$$\lambda_m = \frac{m_{\mathrm{mod}\,el}}{m_{prototype}} = 1.0\times10^{-4}\,. \tag{3.12}$$

The total mass of the prototype mast (including three mast legs, bracing members, the antenna and some attached apparatus) was scaled to the equivalent mass achieved by the spine and the cladding components of the model mast; as well, the model mass included four aluminum plates which were located at the four guy attachment levels for the purpose of connecting the three guys at each level (Figure 3.5b).

3.3.3.4 Effective Drag Area Scaling

The effective drag area scaling was governed by the requirement to scale the product of $C_D \times d$, where d is a typical member dimension and C_D is the drag coefficient. The drag force F_D scaling parameter λ_f (force per unit length) is defined as follows:

$$\frac{(F_D)_{\mathrm{mod}\,el}}{(F_D)_{prototype}} = \lambda_f = \lambda_v^2 \lambda_L \tag{3.13}$$

Substituting Equation 2.18 into F_D, the effective drag area scaling parameter can be expressed from Equation 3.13 :

$$\frac{(C_D d)_{\text{mod el}}}{(C_D d)_{prototype}} = \lambda_L \tag{3.14}$$

The design drag coefficient C_D for the prototype is dependent upon the solidity ratio R_s for latticed masts (CSA 2001), where R_s is defined as the ratio of the net projected area of one face of the structure A_s to the projected gross area A_g :

$$R_s = \frac{A_s}{A_g}. \tag{3.15}$$

For triangular masts, C_D is calculated as follows:

$$C_D = 3.4(R_s)^2 - 4.7(R_s) + 3.4. \tag{3.16}$$

The drag factor C_D also depends on the shape and roughness of the member, as well as the Reynolds number. Since the mast of the model was largely composed of cladding with rectangular cross-sections, Reynolds number effects for mast elements were assumed to be small due to the sharp edges of the cladding components, and thus were not a major consideration.

A reduction factor D_F was also applied to flat members such as cladding when calculating the maximum projected area of the appurtenances attached to one face of the mast (EIA/TIA-222-E, 1996). The total effective drag area was therefore equal to $(C_D d) \times D_F$ where $D_F = 0.8$ for flat members attached to one face of the cladding.

As illustrated in Figure 3.5b, shielding effects had to be considered for drag forces acting on the spine since the distance of the spine behind the windward face of the

structure was less than 1.5 times the face width for triangular mast. Shielding factors for the cladding were obtained from NBCC (1995).

Due to a lack of more precise information, drag factors for the model were estimated using the same relationships as used for the prototype. Since it was suspected that these prototype relationships may not be strictly valid at the model scale, further drag tests for the model cladding were conducted in the wind tunnel laboratory at the University of Saskatchewan, to investigate the effective drag area of the cladding. These drag tests are described in Chapter 4.

3.3.3.5 Conclusions

Scaling parameters for various model properties, based on the relationships presented above, are summarised in Table 3.2. Here, the scaling parameter λ is defined as the ratio between a given property of the model and its corresponding value in the prototype.

Comparisons of key mast properties of the model, as designed, and the scaled prototype guyed mast are shown in Figure 3.6. As can be seen in this figure, good agreement between the model and the scaled prototype values for stiffness, mass and drag area was achieved.

3.3.4 Guy Cable Modelling

3.3.4.1 Overview

The guy cables are important components of guyed masts for the simple reason that the guys supply the lateral stiffness as well as a significant portion of the total mass of the system. The inherently nonlinear behaviour of the guys, as well as the nonlinear

Table 3.2. Aeroelastic model scaling parameters (from ASCE 1997).

Parameter	Similitude Requirement*	Scale Value
Length	$\lambda_L = L_m / L_p$	1.00E-02
Density	$\lambda_\rho = \rho_m / \rho_p$	1.0
Velocity	$\lambda_v = V_m / V_p$	0.1
Mass per Unit Length	$\lambda_m = \lambda_\rho \lambda_L^2$	1.00E-04
Mass	$\lambda_M = \lambda_\rho \lambda_L^3$	1.00E-06
Mass Moment of Inertia per Unit Length	$\lambda_i = \lambda_m \lambda_L^2$	1.00E-08
Mass Moment of Inertia	$\lambda_I = \lambda_M \lambda_L^2$	1.00E-10
Damping	$\lambda_\zeta = \zeta_m / \zeta_p$	1.0
Stiffness	$\lambda_{EI} = \lambda_v^2 \lambda_L^4$	1.00E-10
Elastic stiffness	$\lambda_{EA} = \lambda_v^2 \lambda_L^2$	1.00E-06
Force Per Unit Length	$\lambda_f = \lambda_v^2 \lambda_L$	1.00E-04
Force	$\lambda_F = \lambda_v^2 \lambda_L^2$	1.00E-06
Bending Moment	$\lambda_{BM} = \lambda_v^2 \lambda_L^3$	1.00E-08
Time	$\lambda_T = \lambda_L / \lambda_v$	0.1

*The subscript "*m*" denotes model while "*p*" denotes full scale prototype.

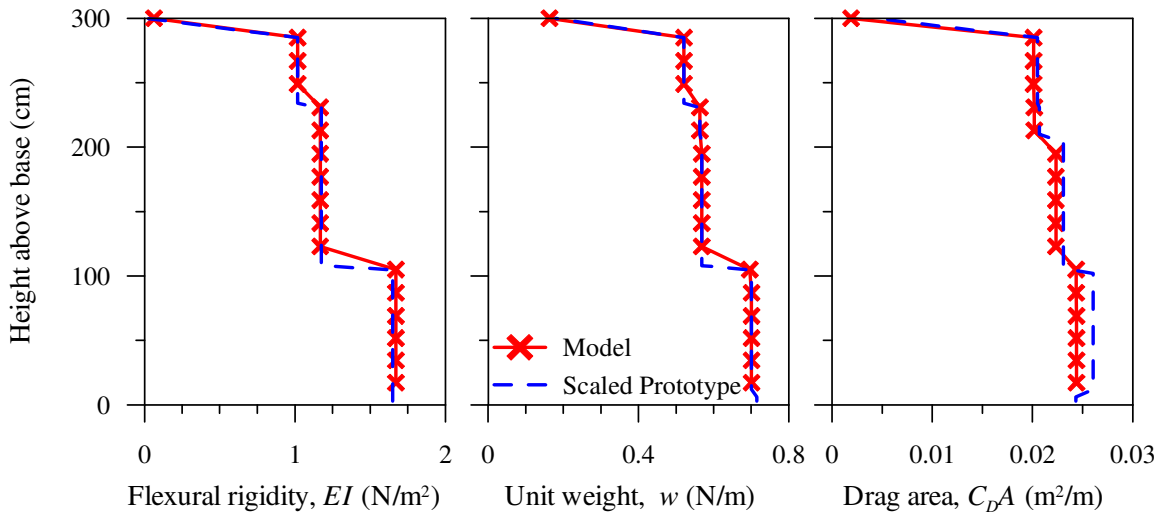

Figure 3.6. Comparison of the key mast properties of the model and scaled prototype.

interaction between guy cables and the mast, makes the cable modelling more challenging. However, accurate modelling of the guy cables, and the guy stiffness in particular, plays a strategic role in producing reliable results from the wind tunnel tests. As with the mast, the physical properties of the guy cables must be scaled properly in terms of similarity with the mass, stiffness and effective drag area of the prototype.

As shown in Figure 3.4, the 3 m tall guyed mast model was guyed at four guy attachment levels along the mast. Because of its suitable size and properties, 1 pound music wire, with a diameter of 0.012 in (0.305 mm), was used for all the guys on the model.

3.3.4.2 Scaling of Guy Stiffness

The equivalent horizontal stiffness k_{EQ} of the guy cables was achieved by enforcing Cauchy Number C_a similarity requirements between the model and prototype, thereby ensuring that the ratio of the elastic to inertia forces was maintained using Equation 3.8, where

$$E_{eff} = \frac{EA}{L^2} \tag{3.17}$$

for the axial guy stiffness. The resulting ratio of axial stiffness λ_{EA} was therefore

$$\lambda_{EA} = \frac{(EA)_{\mathrm{mod}\,el}}{(EA)_{prototype}} = 1.0\times10^{-6}\,. \tag{3.18}$$

Guy stiffness includes contribution from both elastic and gravity forces. It was therefore important to include the effect of cable sag when modeling the axial stiffness of a guy cable. As discussed in Section 2.3, the resistance of a suspended cable to horizontal motion of the mast is generated by two physical mechanisms: elastic

stretching of the cable, represented by the elastic cable stiffness component k_e, and changes due to the amount of sag in the cable profile, represented by the gravitational stiffness component k_g (ASCE 2002). For a relatively taut cable, the resulting equivalent horizontal stiffness may be obtained by considering the elastic and gravitational components as acting in series, as suggested by Equation 2.28.

In order to achieve the correct elastic stiffness for the guy wires, small extension springs were incorporated at the bottom end of each wire. The equivalent axial stiffness k_{e_eq} achieved from the music wire and extension springs is therefore given by

$$k_{e\_eq} = \frac{1}{\frac{1}{k_{e\_sp}} + \frac{1}{k_{e\_mw}}}, \tag{3.19}$$

where k_{e_sp} is the elastic stiffness of the extension springs and k_{e_mw} is the axial stiffness of the music wire obtained using Equation 2.29.

Similarity of gravity stiffness was achieved by adding brass weights to the wire to produce the desired sag. The guy pretension also has a large influence on the gravity stiffness (see Equation 2.30). Since the force scaling parameter λ_F is only 1.0E-06 (see Table 3.2), the model-scale initial tension was found to be as low as 0.196 N (20 g). These low levels of guy pretension required in the model made it very challenging with respect to the choice of the materials available and the model erection procedures to be used.

Furthermore, when modelling the elastic and gravitational stiffness of a guy cable, it was necessary to consider not only the equivalent stiffness of wires (k_{EQ}) comprising the elastic and gravitational stiffness, but also the ratio between the elastic stiffness and

the gravitational stiffness. As outlined in Section 2.3.2.2, the stiffness parameter λ^2 must be considered to ensure that the natural frequencies of the model guys were correct (Irvine 1978).

In summary, the discrepancies and difficulties encountered when imposing similarity requirement on the guy stiffness arose from the following: (i) the wires used to model the guy cables had to produce the same equivalent stiffness as the scaled prototype as well as maintaining the ratio between the elastic and the gravity stiffness; and (ii) the scaling of gravity stiffness. The extremely low pretension of wires was difficult to achieve in practice; also, this scaled pretension value could not produce the desired gravity stiffness, so that extra weights had to be added to the wires in order to model the sag of the prototype. The increased gravity stiffness k_g necessitated an increase of the elastic stiffness k_e, to maintain the stiffness parameter λ^2, resulting in an increased equivalent stiffness k_{EQ}, as well as increased guy mass. A further limitation on the wire size was that it had to be large enough so that its drag coefficient could be approximately Reynolds number independent over the wind speeds used in the tests. As a result of all of these constraints, a number of modifications were made to the prototype design in order to reflect practical limitations in the model construction; however, attempts were made to avoid straying too far from what would be representative of Canadian design practice.

A comparison of the model guy and the scaled prototype guy stiffness is shown in Figure 3.7. From this figure, it is evident that satisfactory similarity of the elastic and gravity stiffness components was achieved; the stiffness parameters also agree well, so

that the natural frequencies of the model and scaled prototypes should have been similar.

It should be noted that scaling of the guy properties was performed on the basis of still air (no wind) conditions. As the model was displaced in response to applied wind loads, the sag and stiffness characteristics changed in a nonlinear manner. No attempt was made to match the model and scaled prototype properties under loaded conditions.

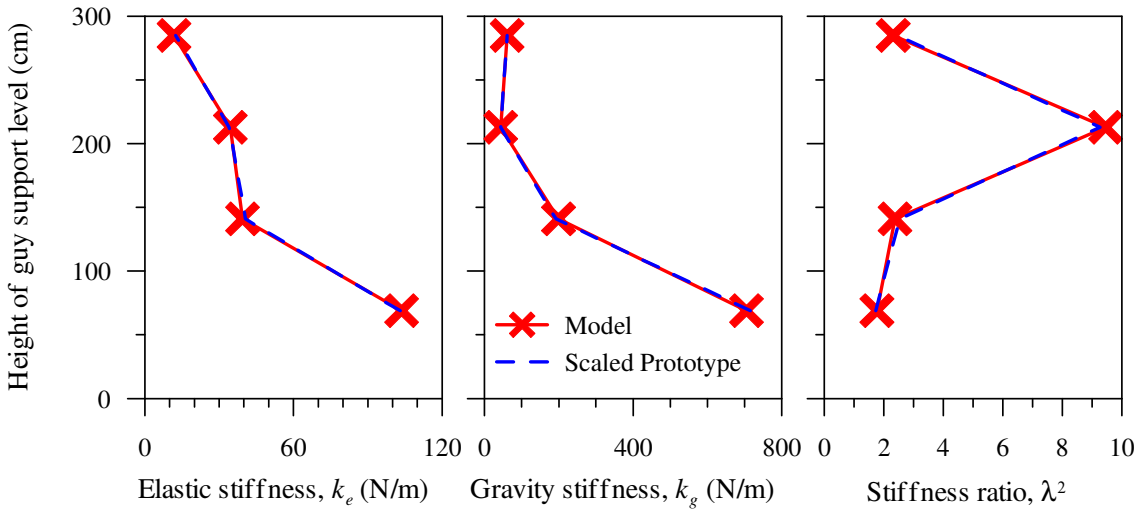

Figure 3.7. Comparison of the model and the prototype guy stiffness components.

3.3.4.3 Mass Scaling

The procedure used for mass scaling of the guy cables was the same as that for the mast scaling described in Section 3.3.3.3. The scaling parameter of mass per unit length λ_m (the ratio between the model and the full-scale) was maintained at 1.0E-04, as required by Equation 3.11. The small brass weights not only provided the model with additional gravity stiffness, but also contributed to the mass in order to achieve desired mass scaling. Thus, the equivalent mass was obtained by the combined effect of the 1

pound music wire, the brass weights, and the foam cylinders which are presented in Section 3.3.4.4.

3.3.4.4 Drag Area Scaling

As presented in Section 3.3.3.4, drag area scaling for the guy cables was governed by the geometric scaling ratio λ_L. The equivalent drag area was achieved by considering the combined effect of the music wire, brass weights, and the foam cylinders incorporated onto the wires.

Because the guy wires had a roughly circular cross sectional shape, attention had to be given to the drag coefficient C_D, which was dependant upon Reynolds number R_e effects over a certain range of wind speeds.

Figure 3.8 illustrates the variation in the drag coefficient with Reynolds number for a smooth circular cross section in smooth flow. As shown in this figure, C_D drops sharply in the critical region ($R_e \approx 10^5 \sim 10^6$) while for lower ranges of R_e (i.e. the subcritical region), C_D exhibits a practically constant value ($C_D \approx 1.2$) over a wide range of R_e values. In addition to the flow velocity, the drag coefficient C_D is also known to depend upon the roughness of the cylinder surface (Simiu and Scanlan 1996).

In the model design, therefore, attempts were made to utilize wire sizes that would result in a drag coefficient that was relatively Reynolds number insensitive. That is, the Reynolds number of the wires in the model was kept in the subcritical range (Figure 3.8.).

A comparison of key guy properties between the model and the scaled prototype is shown in Figure 3.9. It is apparent that satisfactorily agreement was achieved. The

equivalent stiffness plot also shows that the model guys at higher levels exhibit softer properties due to increased sag effects in these wires.

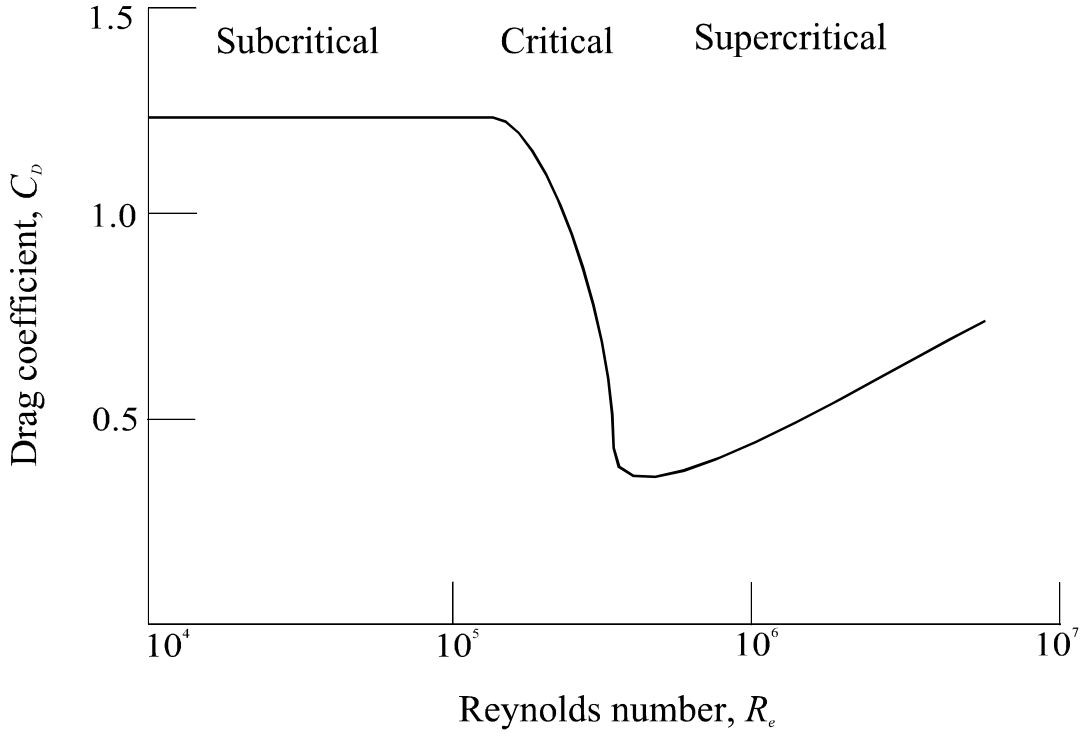

Figure 3.8. Evolution of mean drag coefficient with Reynolds number for a circular cylinder (Simiu and Scanlan 1996).

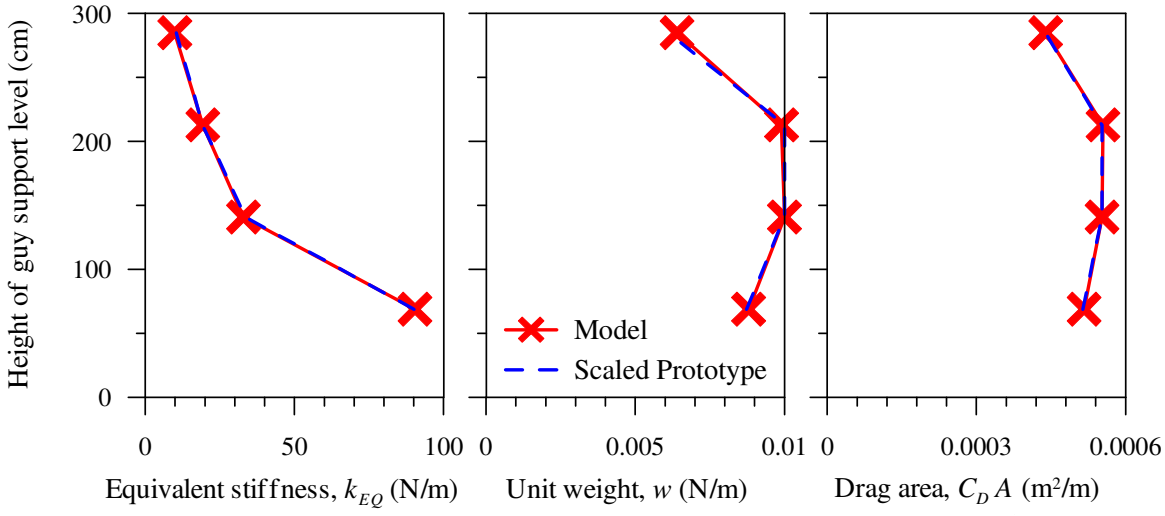

Figure 3.9. Comparison of selected guy properties between the model and the scaled prototype.

3.4 CONSTRUCTION OF THE WIND TUNNEL MODEL

3.4.1 Description of the 300 m Guyed Mast Model

For the wind tunnel investigation, a full aeroelastic model of the 300 m guyed mast was constructed to a 1:100 scale at the University of Saskatchewan and at the BLWTL at the University of Western Ontario. As shown in Figure 3.5, the model featured cladding with a triangular cross-section and a constant face width of 30 mm. The legs of the mast were modelled as a central spine made from stainless steel tubing located at the centroid of the cross-section. The basic mast geometry, including the face width, cladding pattern and panel height, remained constant over the entire height. The mast was guyed at four guy levels with three wires at each level. The guy anchor radius (the distance between the centre of the mast base and the anchor point) was set at 1 m for first and second guy levels, and at 2 m for the top two levels.

Some of the significant challenges encountered during the design and construction of the model included finding components of a sufficiently small size and suitable material, as well as accurately reproducing the low levels of guy pretension (0.196 N) required in the model.

3.4.2 Mast Construction

The model mast was composed of a slender spine and cladding assembly. The spine consisted of three stainless steel tubes used for the main mast sections and a solid brass rod used to represent the 15 m cantilevered top antenna assumed for the prototype. At each connection between mast segments, snug fitting brass inserts were placed inside the tubes; the three stainless steel tubing pieces and brass rod were silver-soldered

together so that relative rotations between the segments were prevented at the connection locations. Table 3.3 provides the physical properties of the spine.

Table 3.3 Physical properties of the model spine[†].

Section	Height [m]	*D* [mm]	*d* [mm]	*E* [MPa]
1	1.05	4.19	3.43	200,000
2	2.31	3.76	3.00	200,000
3	2.85	3.63	2.90	200,000
4	3.0	0.0625	-	103,000

[†] *D* is the outside diameter, *d* is the inside diameter, and *E* is the elastic modulus

The cladding assembly had a triangular cross-section in plan with a constant 30 mm face width, measured from centre to centre of the cladding legs, and a constant panel height of 179 mm. As shown in Figure 3.10, the cladding assembly was constructed with an ABS plastic skeleton, which represented the mast structure, and thin carbon fibre struts to securely attach the cladding to the spine in a symmetric manner without increasing the spine stiffness. Carbon fibre was chosen as the strut material due to its high strength and the extremely light weight. To ensure the correct geometry, the carbon struts were fabricated using a jig consisting of two blocks into which 3 holes were symmetrically drilled (Figure 3.11); thus, the carbon struts were accurately and consistently made to the desired dimensions. To achieve the proper drag area as well as the very light required weight, cladding panels with a thickness as low as 0.51 mm were fabricated at the BLWTL using a rapid-prototyping machine. When attaching cladding sections to the mast, a gap of 1 mm was maintained between adjacent cladding sections to ensure that the cladding was discontinuous and would not increase the rigidity of the mast spine (Figure 3.12b).

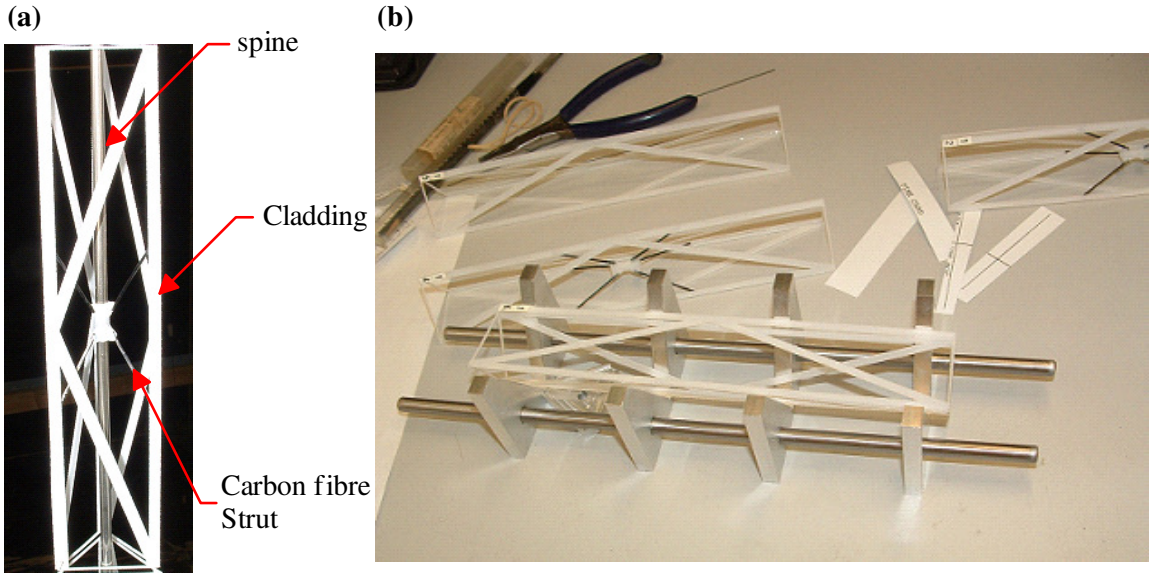

Figure 3.10. Model mast construction: (a) spine and cladding assembly; and (b) fabrication jig.

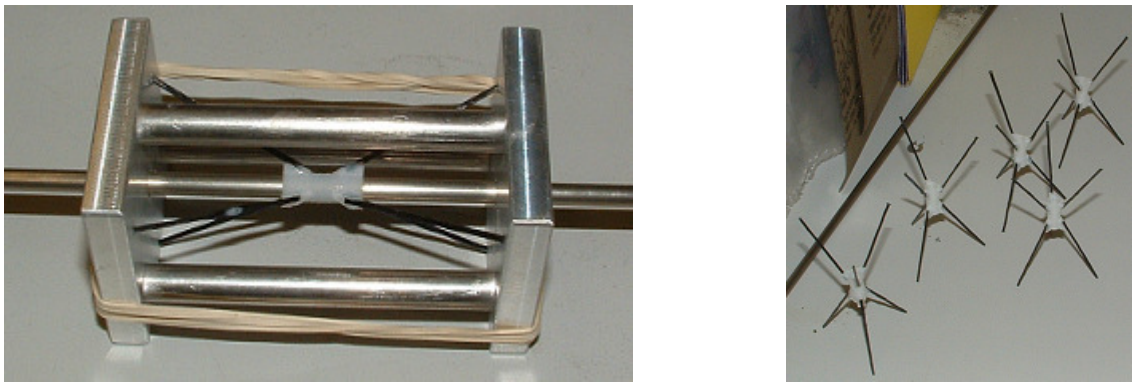

Figure 3.11. Jig for the fabrication of the carbon fibre struts.

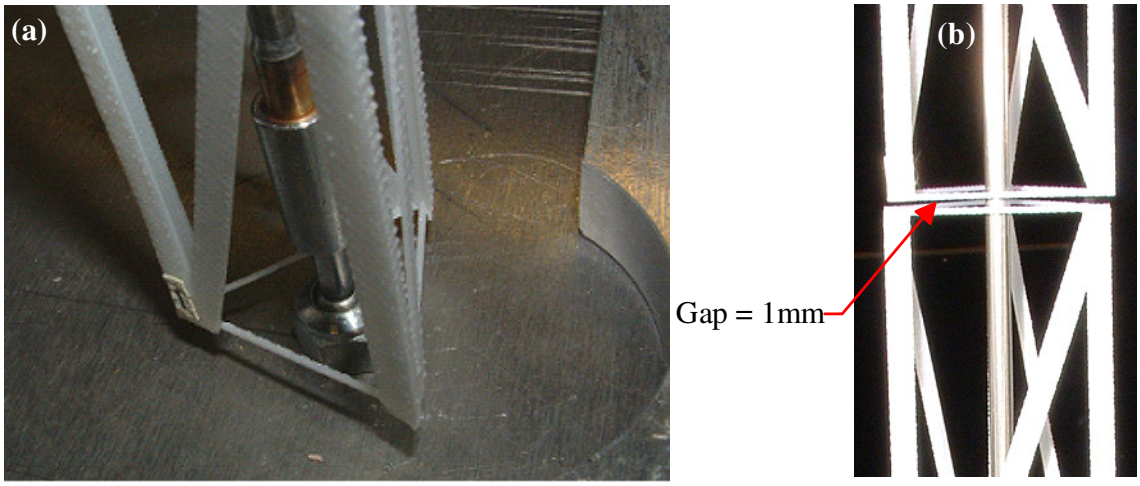

Figure 3.12. Mast model details: (a) pinned mast base; and (b) 1 mm gap between adjacent cladding segments.

A straight, swivel-type ball-bearing connector (Figure 3.12a) was used to connect the bottom spine segment to the base, thus reproducing the pinned base connection of the prototype guyed mast. The pinned base allowed free rotations in all directions while preventing all displacements.

To facilitate the erection of the model and its alignment in the wind tunnel, the guyed mast model was mounted on a rigid base assembly, the top of which was set at an elevation of 113 mm above the floor (Figure 3.13a). The base assembly consisted of a 12.7 mm (1/2 in) thick hexagonal aluminum plate, upon which the mast was mounted, a 1.6 mm (1/16 in) thin hexagonal aluminum plate which rested on the floor, and three 2.2 m long HSS tubular members radiating out symmetrically from the centre, to which the guy anchors were attached (Figure 3.14b). The two plates and the three tubular beams were connected using six 100 mm (4 in) long screws which ensured a rigid base assembly. During erection, the mast was held in a vertical position by guides attached to a temporary support column (Figure 3.13b) that was removed prior to testing.

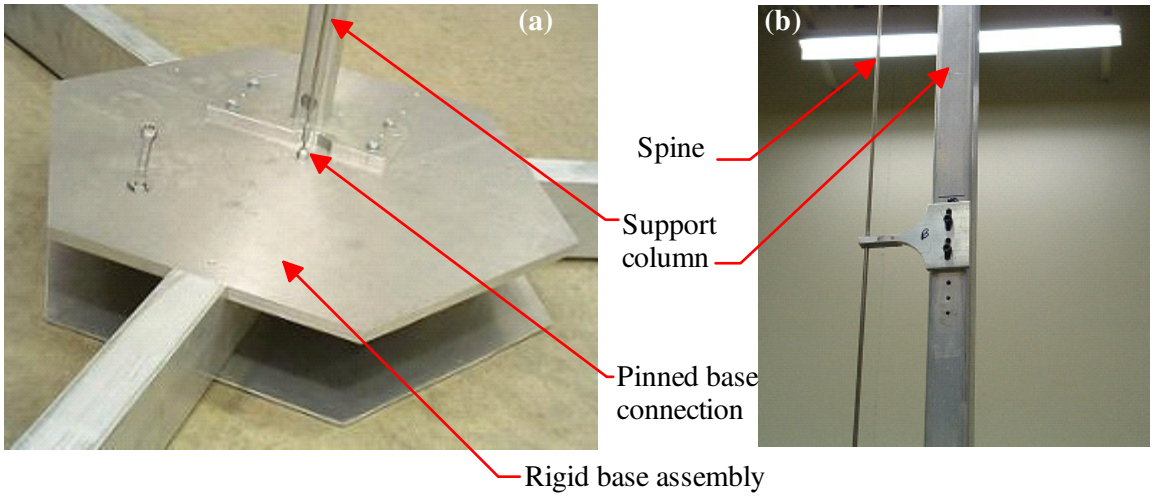

Figure 3.13. Mast base and erection details (shown without cladding attached for clarity): (a) pinned base connection and base assembly; and (b) erection support column.

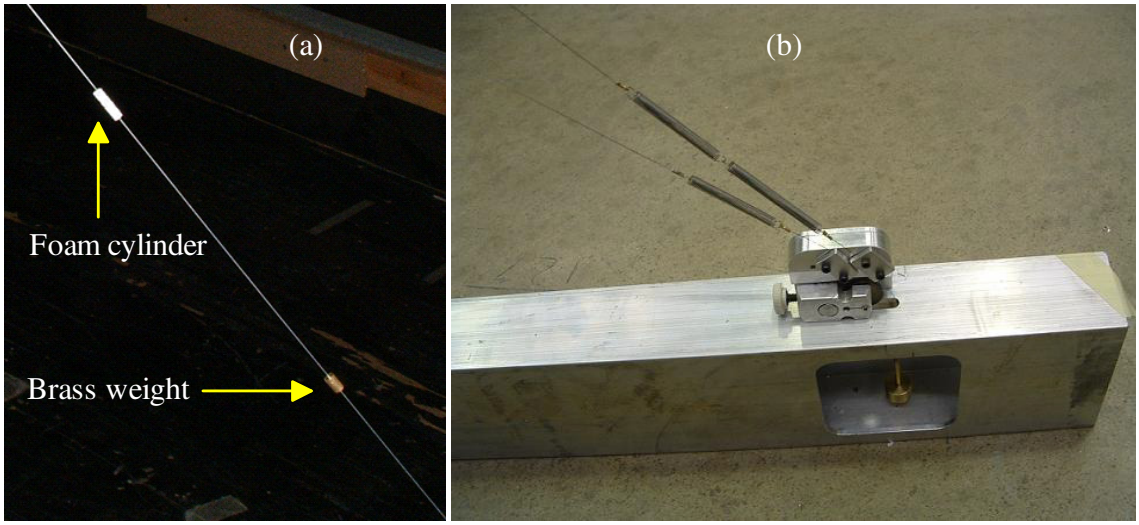

Figure 3.14. Model guy cable components: (a) foam cylinders and brass weights; and (b) springs, anchor and pretensioning system.

3.4.3 Guy Construction

The model guy wires were constructed using 0.305 mm (0.012 in) diameter, one-pound music wire. Brass weights were attached along the wires at prescribed intervals in order to produce an appropriate averaged unit weight, as well as the correct gravity stiffness, k_g. Foam cylinders, 10 mm in length with diameters as low as 2.54 mm, were attached along the wires to generate the necessary averaged drag area (Figure 3.14a). In order to soften the wire response sufficiently to achieve the desired elastic stiffness k_e, small springs were inserted at the bottom end of the guys (Figure 3.14b). The model guy wires were attached to the aluminum plates glued on the spine at the four guy attachment levels. At each level, three guy wires were connected at the desired distance from the mast centroid to the mast using the screws and the small tube spacers (Figure 3.15b); this arrangement simulated connections of the actual guys to the mast legs on the prototype. A photograph of a model guy wire showing its sag under still air conditions is shown in Figure 3.15a.

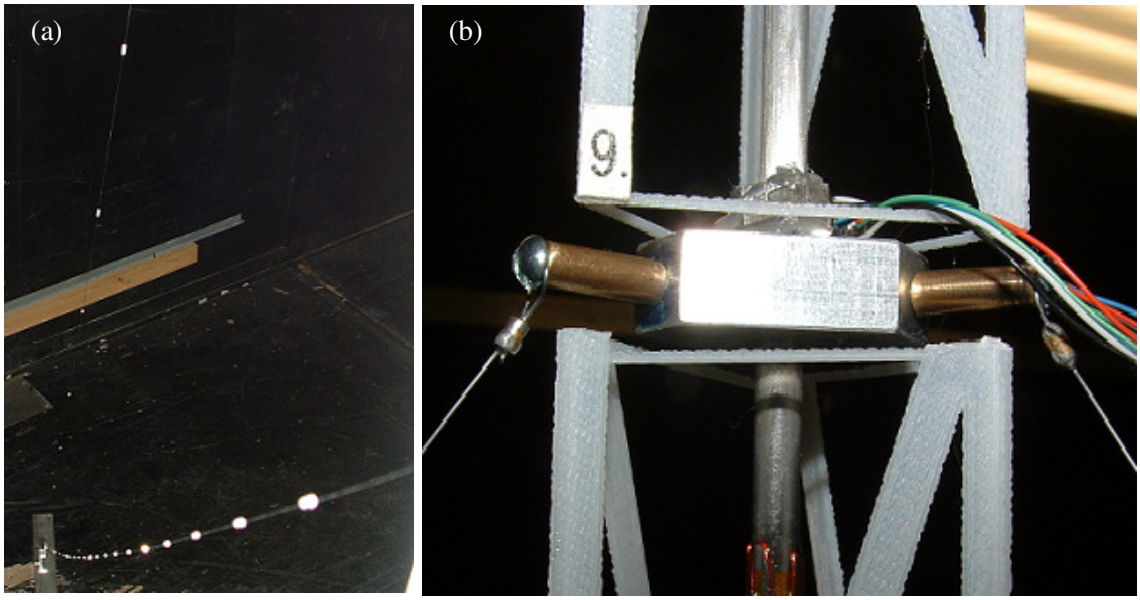

Figure 3.15. (a) Guy showing the sag; (b) guy attachment level.

The geometry and physical properties of the guy wires are summarized in Table 3.4, where L_c is the straight chord length between wire ends, θ is the vertical angle between the chord line and the horizontal line, T_o is the initial tension, and E_G is the elastic modulus of the wires. The properties of the springs used for each guy level are summarized in Table 3.5.

Table 3.4 Geometry and physical properties of the model guys.

Level	Height [m]	L_c [m]	θ [deg]	T_o [N]	E_G [MPa]
1	0.69	1.151	34.60	0.196	200,000
2	1.41	1.682	54.78	0.196	200,000
3	2.13	2.865	46.84	0.196	200,000
4	2.85	3.438	54.93	0.196	200,000

Table 3.5 Extensional spring properties for each guy.

Guy Level	Spring Model	Amount	Spring Stiffness (kN/m)
1	E0180-014-1250-s	1	0.105
2	E0180-014-0750-s	1	0.04
3	E0180-014-1000-s	1	0.035
4	E0180-014-1250-s + E0180-014-1250-s	2	0.0119

The major difficulty encountered in the construction and erection of the model was that of setting the individual guy pretension. The very low required pretension of 20 g (0.196 N) for each guy wire was achieved by passing the bottom end of the wire over a small, low friction nylon pulley with jewel pivots (Figure 3.14b) that was attached to the guy anchor block, and hanging a known mass (20 g) from the end of the wire. Once the prescribed pretension was induced, the wire was securely clamped to the anchor block (Figure 3.14b). The top ends of the wires were clamped to the mast in such a way as to reproduce the eccentric connection of the guys to the mast legs on the prototype (Figure 3.15b).

3.5 NUMERICAL COMPARISONS OF THE MODEL AND THE PROTOTYPE DYNAMIC PROPERTIES

As a check of the model scaling procedures, dynamic analysis results for the guyed mast model were compared with those of the prototype, using the frequency domain analysis model described in Section 2.5 as the basis for this comparison. The results presented herein were generated assuming the following full-scale wind conditions: a reference mean wind speed ($\overline{U}_{ref}$) of 32 m/s, an exponential wind speed

profile with $\alpha = 0.1$ (see Equation 2.5), and a mean wind direction oriented at 60° (wind perpendicular to one face of the mast).

Dynamic response comparisons, including mast bending moments and displacements, for the prototype and model are shown in Figure 3.16. In these plots, the model response has been scaled to a full scale basis using the scaling relationships defined in Table 3.2. ($\lambda_{BM} = 10^{-8}$ for bending moments and $\lambda_L = 0.01$ for displacements). As can be seen in this figure, the responses obtained from the model and the prototype analyses are very similar.

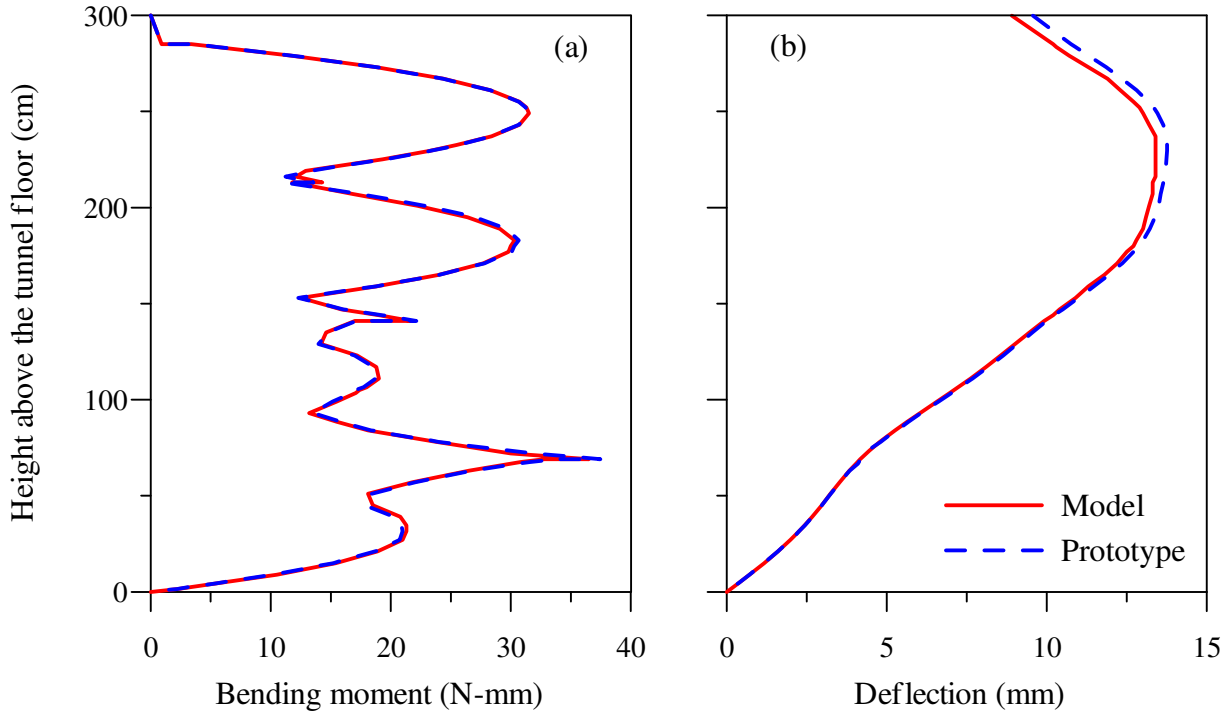

Figure 3.16. Comparisons of dynamic response between the model and scaled prototype: (a) bending moment; (b) deflection.

Similar comparisons of the model and prototype natural frequencies are summarized in Table 3.6 . The corresponding mode shapes are compared in Figure

3.17. Once again, the agreements between the model and the prototype responses are generally excellent.

Table 3.6 Comparison of predicted natural frequencies of the model and prototype.

Modes	f_{model} (Hz)	$f_{prototype} / \lambda_f^{*}$ (Hz)	Error (%)
1	2.2	2.2	0
2	3.05	3	1.6
3	3.11	3.1	0.03
4	3.69	3.7	0
5	4.41	4.4	0
6	5.6	5.6	0
7	5.97	5.9	1.18
8	7.39	6.9	7.1

* $\lambda_f = 0.01$ (natural frequency scaling parameter).

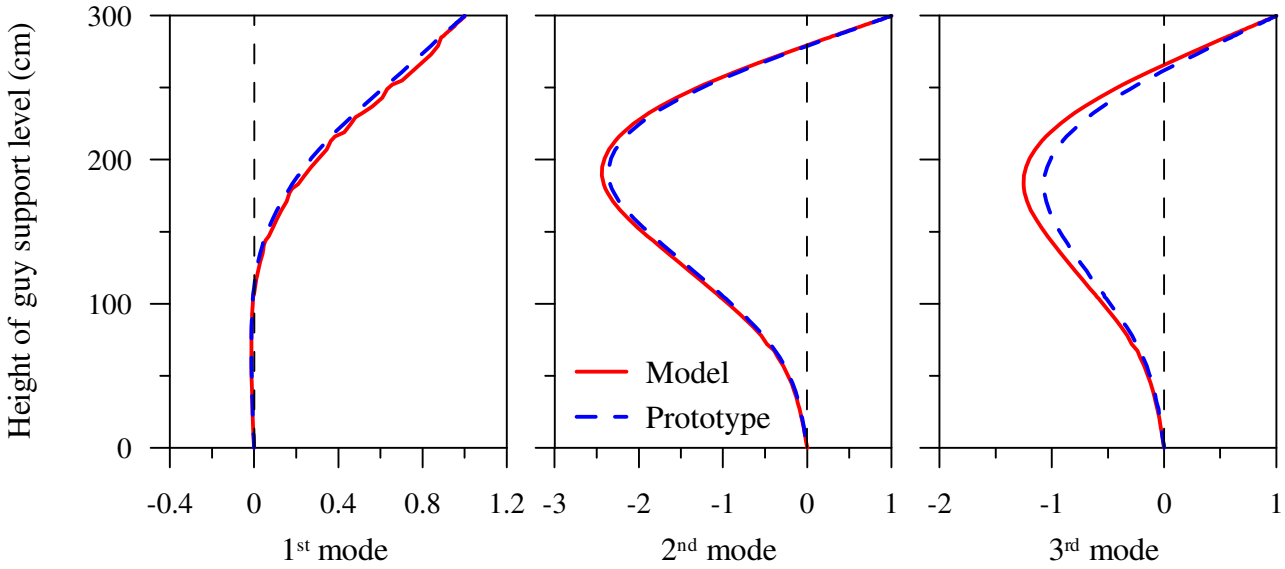

Figure 3.17 Comparisons of predicted mode shapes of the model and scaled prototype.

As indicated by these results, the predicted dynamic response characteristics obtained from the scaled model of the guyed mast and the prototype are consistently

comparable. For the purpose of this study, then, it was concluded that the scaling laws applied in designing the model were compatible with the frequency domain analytical model used. Comparisons between the predicted (numerical) and the measured (wind tunnel) responses are provided in Chapter 5.

4. DESCRIPTION OF WIND TUNNEL TEST PROGRAM

4.1 INTRODUCTION

The wind tunnel model of a 300 m guyed mast was constructed as described in Chapter 3. This chapter presents the experimental program of wind tunnel tests carried out at the Boundary Layer Wind Tunnel Laboratory (BLWTL) at the University of Western Ontario (UWO), London, Canada. The wind tunnel test results are summarized in Chapter 5.

A brief introduction to the BLWTL is presented in Section 4.2, followed by the model instrumentation, including model calibration, described in Sections 4.3 and 4.4. The detailed wind tunnel model studies conducted for the 300 m guyed mast are presented in Section 4.5, considering both open country (moderate turbulence) and over water (low turbulence) exposure, as well as three different wind directions. Section 4.6 is devoted to the wind conditions in the BLWTL, including the mean wind profiles, turbulence intensity and velocity spectra. The mode shape measurements, performed under still wind conditions to measure the natural frequencies, fundamental structural mode shapes, as well as the damping levels in the guyed mast model are reviewed in Section 4.7. In addition, a section drag test of the model mast cladding conducted in the Wind Tunnel Laboratory at the University of Saskatchewan is provided in Section 4.8.

4.2 INTRODUCTION TO WIND TUNNEL TESTING

Although sophisticated computational methods have been well developed, it remains necessary to carry out physical experiments to examine the dynamic characteristics of guyed masts in wind loads. Wind tunnel testing, which provides a realistic assessment of the detailed wind load distribution, makes it possible to model different wind conditions in a rapid, economical and accurate means to generate wind-induced vibration of the structure.

The wind tunnel simulates the atmospheric flows by duplicating the characteristics of natural wind flows, in order to achieve the dynamic behaviour of the model that are similar to those of the prototype on site. An important measure of the practical value of all model test data is their relationship to full-scale experience. Accurately modelling wind is therefore of vital importance in wind tunnel testing. The characteristics of natural wind must be simulated correctly in the wind tunnel to represent those at the site of the prototype. The similarity requirements for the wind tunnel include: (i) the mean wind velocity profile; (ii) the variation of turbulence intensities with height; and (iii) the wind velocity spectra of turbulence in the alongwind, crosswind and vertical directions.

The BLWTL at the University of Western Ontario (Figure 4.1), which has both a high-speed and a low-speed testing section, was used to simulate the turbulent boundary layer of natural wind. The low-speed section, characterized by a 52 m long tunnel with a cross sectional area 5 m wide × 4 m high, and a water tank with a removable cover for wind and wave interaction studies, is capable of developing a maximum wind speed of 36 km/hr (10 m/s). It is particularly well suited for studies involving large models

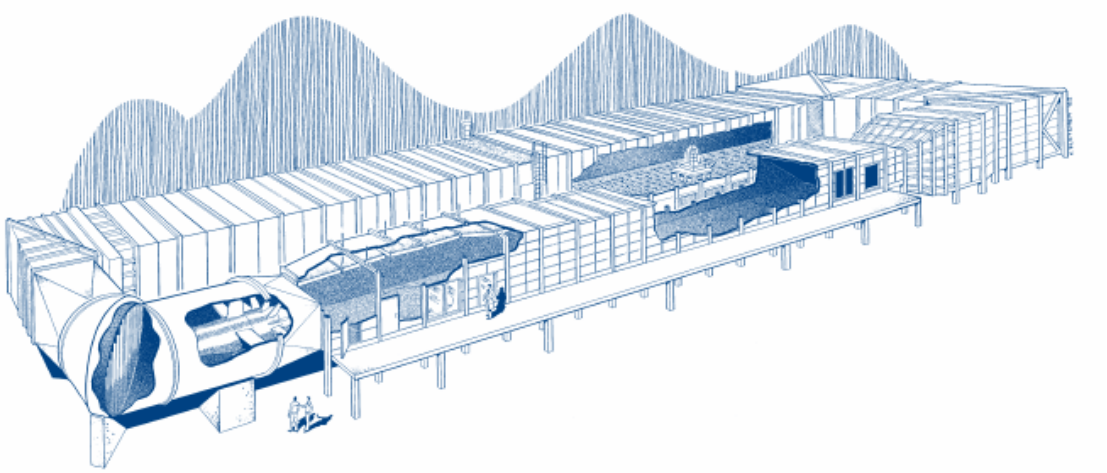

Figure 4.1. Drawing of the BLWTL at UWO, London, Canada (from the BLWTL).

and Froude number scaling, which generally require large scales and relatively low wind speeds. The high-speed section, on the other hand, has a maximum wind speed of about 100 km/hr (28 m/s), which allows higher velocity scales and Reynolds numbers. The dimensions of the wind tunnel test sections in the BLWTL are listed in Table 4.1.

Table 4.1. The dimensions of the test sections in the BLWTL, UWO.

	Length (m)	Width (m)	Height (m)	Maximum Wind Speed (km/hr)
Overall Size	64	15	6	-
High Speed Test Section	39	3.4	2.5	100
Low Speed Test Section	52	5	4	36

In this investigation, the wind tunnel test of the 3 m tall, Froude number scaled guyed mast model was conducted in the low-speed test section. To recreate the prototype design wind conditions, a maximum wind speed of 5.5 m/s was required at a reference height of 2.62 m above the tunnel floor (the elevation of the reference Pitot tube).

4.3 MODEL INSTRUMENTATION

4.3.1 Overview

The instrumentation installed on the aeroelastic guyed mast model at the BLWTL included strain gauges, used to measure wind induced bending moments, high sensitivity miniature accelerometers to monitor mast motion at the four guy support levels, and a laser displacement transducer for measuring alongwind displacements at the top guy support level. Due to the low levels of tension experienced by the guy wires and the large dynamic displacements the wires were likely to undergo, no attempt was made to measure the guy response directly. The instrumentation on the model enabled measurement of the dynamic response, which was compared with that of the numerical analytical model.

4.3.2 Strain Gauges

Precision strain gauges EA-09-031DE-350 (made by Vishay Micro-Measurements), suitable for stainless steel with high transverse sensitivity of $(+0.4 \pm 0.2)\%$ at 24^{o}C, were used to measure the wind induced static and dynamic bending moments of the model (Figure 4.2). The strain gauges were of an open-faced construction with a 0.03 mm (0.001 in) flexible polyimide film backing. The gauges were trimmed to a width of 0.81 mm in order to fit onto the small diameter tubing (mast spine), which ranged from 3.6 mm (0.143 in) to 4.2 mm (0.165 in) in diameter. Attempts were made to mount the gauges to measure strains occurring about two orthogonal axes. Coatings were applied immediately after the strain gauges were installed to protect the open-faced gauges.

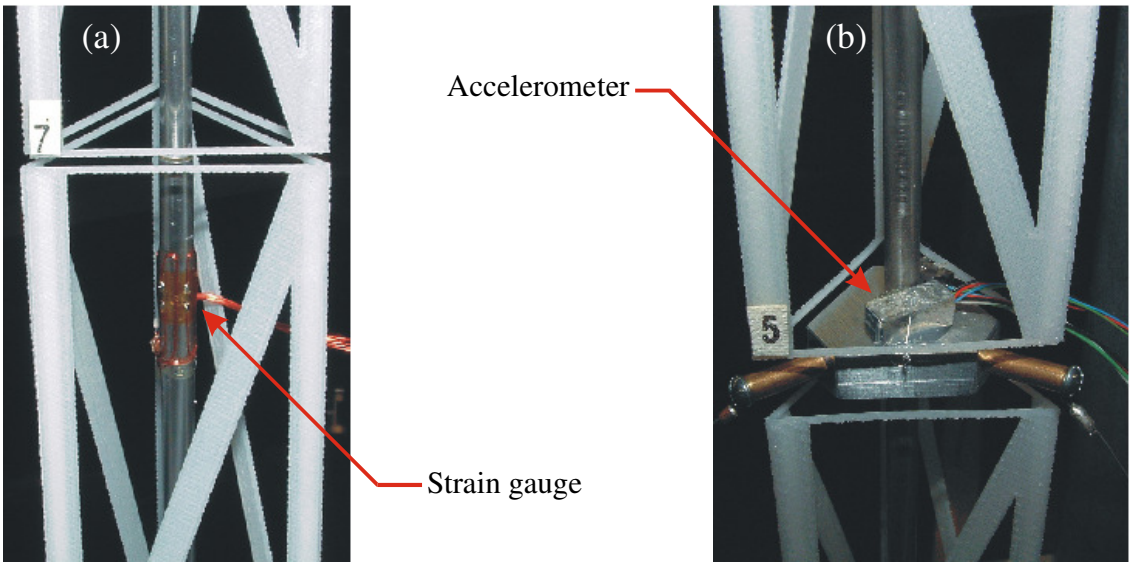

Figure 4.2. Mast instrumentation: (a) strain gauges; and (b) accelerometers.

Figure 4.3 illustrates the locations of the instruments used on the model. A total of 24 strain gauges was installed at six locations along the mast height: four were located at the mid-span between guy levels at approximately the highest bending moment location in these regions, while the other two were placed just below the middle two guy attachment levels of the model. As seen in Figure 4.3, four gauges were attached directly to the mast spine at each of the six strain gauge locations, spaced at 90° to each other around the spine perimeter, so that the mast bending moment response could be monitored in two orthogonal directions (Figure 4.2a). At the location of strain gauge level 2, which was at the joint between tube 1 and tube 2, the strain gauges were mounted about 30 mm away from the joint so that any stress concentrations due to the joint were minimized in the strain gauge readings; the same was true for gauge levels 3 and 5, where the gauges were close to the aluminum plates and the gauge sites were shifted downwards by 30 mm or so to stay away from the stress concentrations caused by the aluminum plate.

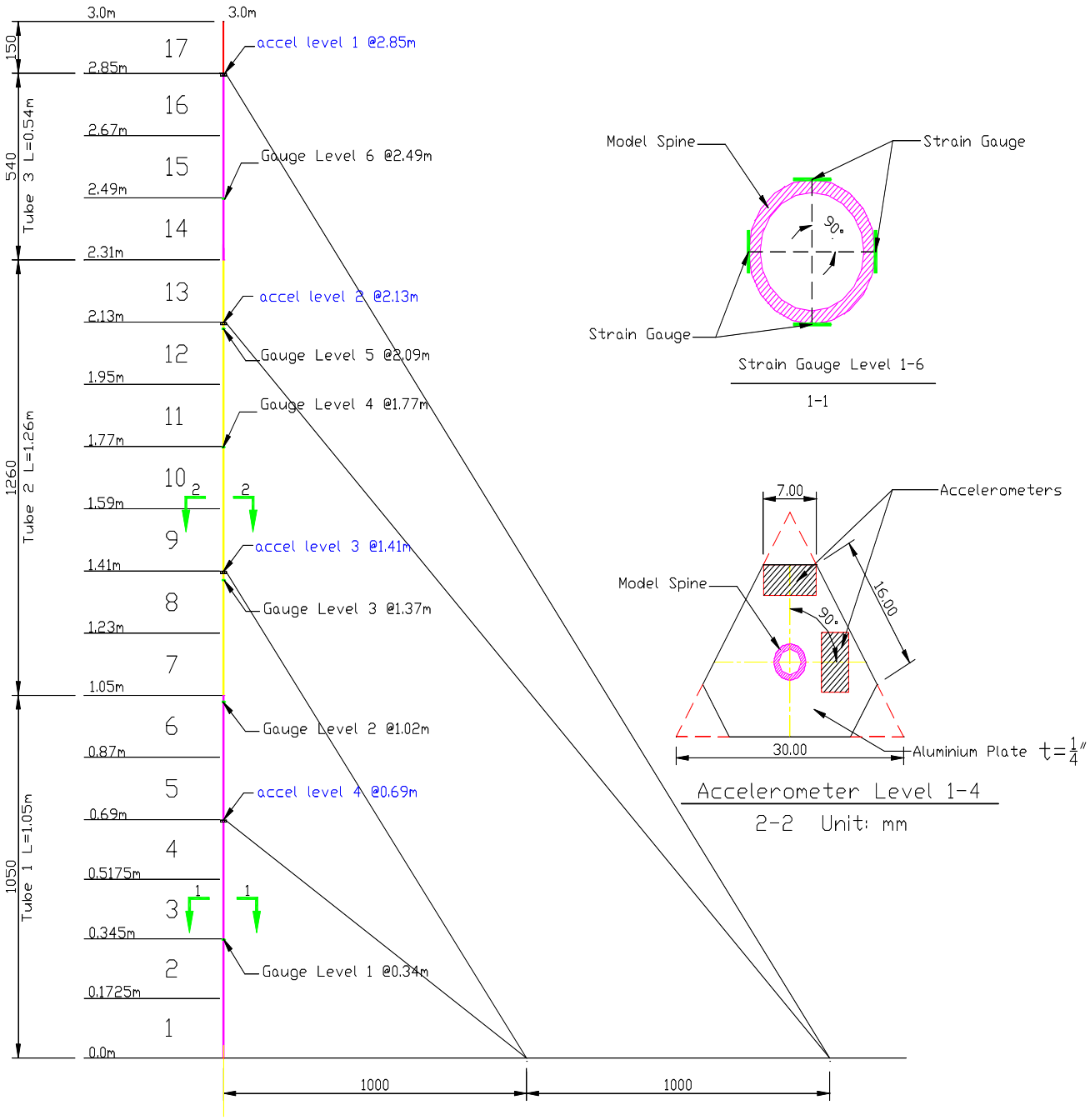

Figure 4.3. The location of the instrumentation.

4.3.3 Accelerometers

Figure 4.3 also shows the location of the accelerometers used on the model. A total of eight Entran EGA miniature accelerometers (Entran Devices, Inc. Fairfield, NJ,

USA) was used to monitor the mast motion at four guy attachment levels on the guyed mast model (Figure 4.3). Figure 4.2(b) shows the accelerometers on the mast. The accelerometers had a sensitivity of 15 mV/g and a frequency response of up to 150 Hz for dynamic measurement. One of the important characteristics of these accelerometers was their extremely light weight (0.5 gram per accelerometer) since both size and mass were of prime importance in the design and construction of the model mast. As can be seen in Figure 4.2(b) and Figure 4.3, two accelerometers at every guy support level were mounted perpendicular to each other, oriented to measure two orthogonal components of the horizontal mast acceleration.

4.4 STRAIN GAUGE CALIBRATION

Strain gauges were calibrated to provide an accurate and reliable measurement of bending moments. Calibration factors for the strain gauges were used to convert the measured value (Volts) obtained from the data acquisition system directly into that of bending moment (kN-m). Rather than the strains in individual gauges, only the difference between readings in corresponding pairs of gauges on opposite faces of the spine were read; therefore, the bending moments in the spine could be determined, but not the net axial forces.

The strain gauges were arranged according to Wheatstone bridge circuit theory (Figure 4.4) at each level, in which two gauges were mounted to form a half-bridge configuration. The dynamic strain-gauge readings could be determined by the change in resistance in the gauges. In this test, the Wheatstone bridge was used as a null-balance system, in which the output voltage "*E*" from the bridge was adjusted to a zero reading

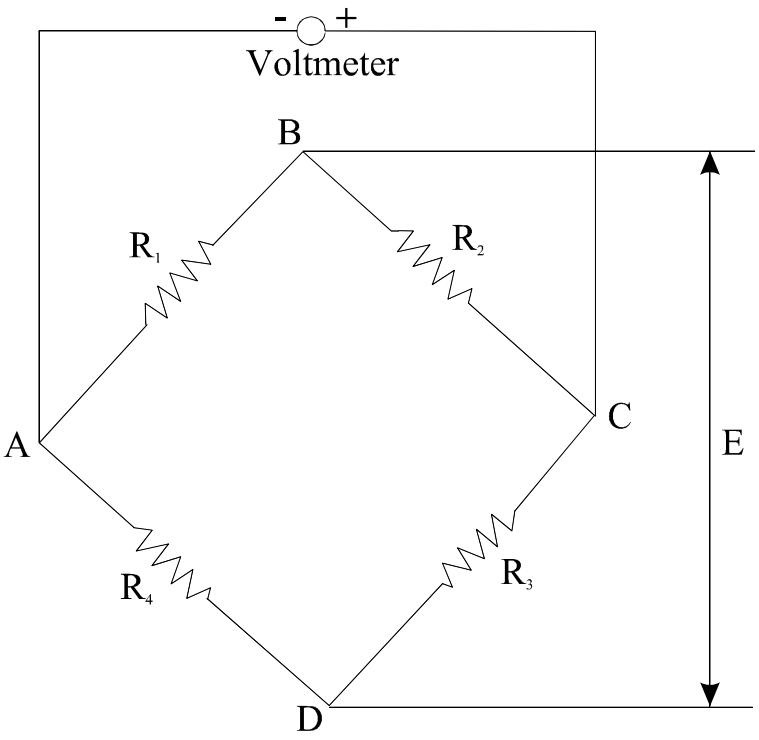

Figure 4.4. The Wheatstone bridge circuit.

to ensure the bridge was balanced prior to each test. The Wheatstone bridge could then be employed for strain measurement.

Calibration at each gauge level was performed with the gauges installed on the model spine prior to application of the mast cladding. The strain gauge calibrations were conducted in two orthogonal directions, denoted as the *X* and *Y* directions, by applying static loads in carefully controlled configurations on the spine which was mounted as either a simply supported or a cantilevered beam. The Wheatstone bridge was initially balanced to zero ($E = 0$, where E is moment-induced voltage, see Figure 4.4) before application of the loads. Loads in the range of 0 to 60 g were added incrementally for the cantilevered beam while loads ranging from 0 to 200 g were used for the simply supported beam. The E was measured and correlated to the known calculated bending moment in the spine at the location of the gauges.

A photograph of calibration procedure conducted with the spine mounted as a cantilever beam is shown in Figure 4.5, while the calibration set-up using a simply supported beam configuration is shown in Figure 4.6. The cantilever mounting arrangement was considered to produce more accurate results since the simply support condition was difficult to achieve in practice because the portions of the spine extending beyond the supports inevitably created some negative moments at supports. However, the cantilever calibration configuration was not feasible for the two gauge levels near the middle of the spine due to the long cantilevered length that would have been required, and the large resulting strains.

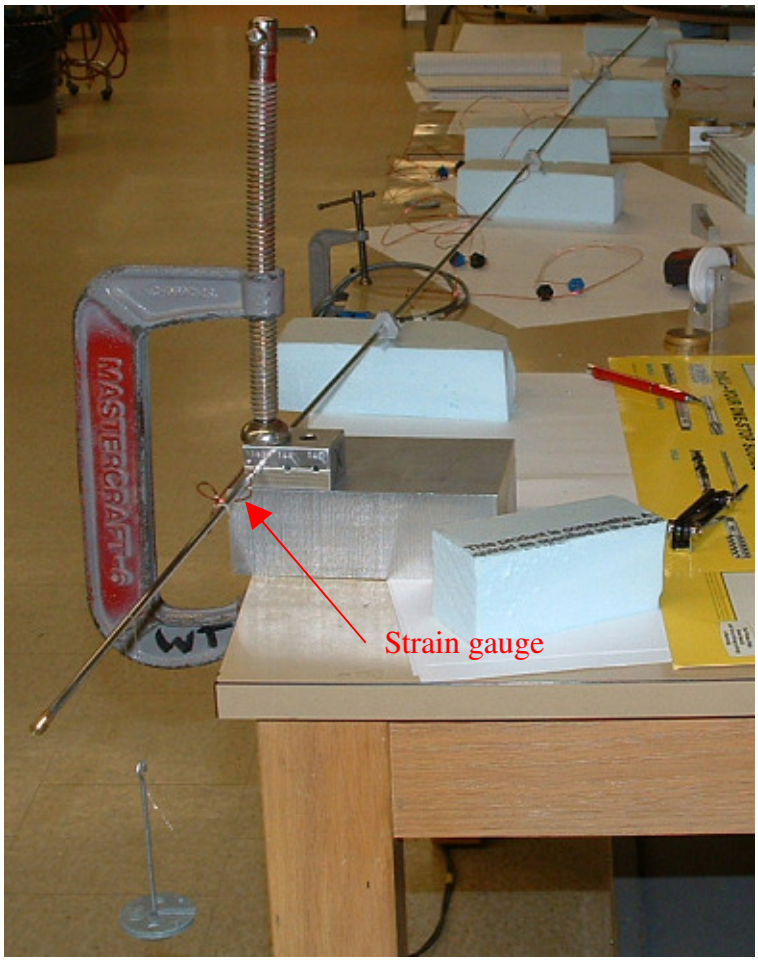

Figure 4.5. Strain gauge calibration under the cantilever beam configuration.

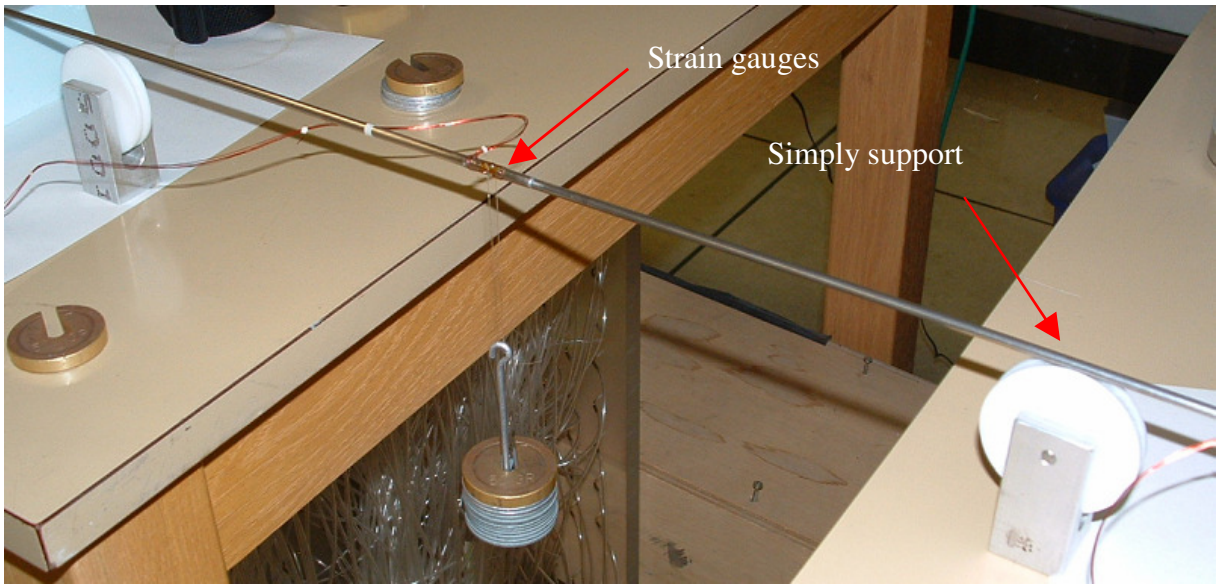

Figure 4.6. Strain gauge calibration under the simply support configuration.

In this calibration process, a voltmeter read the output voltage signal that was proportional to the load applied on the beam. The relationship between the measured voltage and the applied load could therefore be used to convert the voltage into units of bending moment (kN-m) per volt, a parameter called the "calibration factor".

Example plots showing variations of the applied bending moments and the corresponding measured voltage are given in Figure 4.7. A best fit line was then employed to express the relationship between the applied bending moment and the output voltage. Calibration factors could thus be obtained from this figure. The two orthogonal pairs of gauges at each level were calibrated separately. However, both pairs of gauges were read for all calibration trials in case a slight misalignment of the gauges may have induced some coupling between the bending moments measured from the two gauge pairs, as indicated in Figure 4.7. For properly aligned orthogonal gauge pairs, the coupling between the readings was negligible (i.e. for bending about the *X*-axis of the

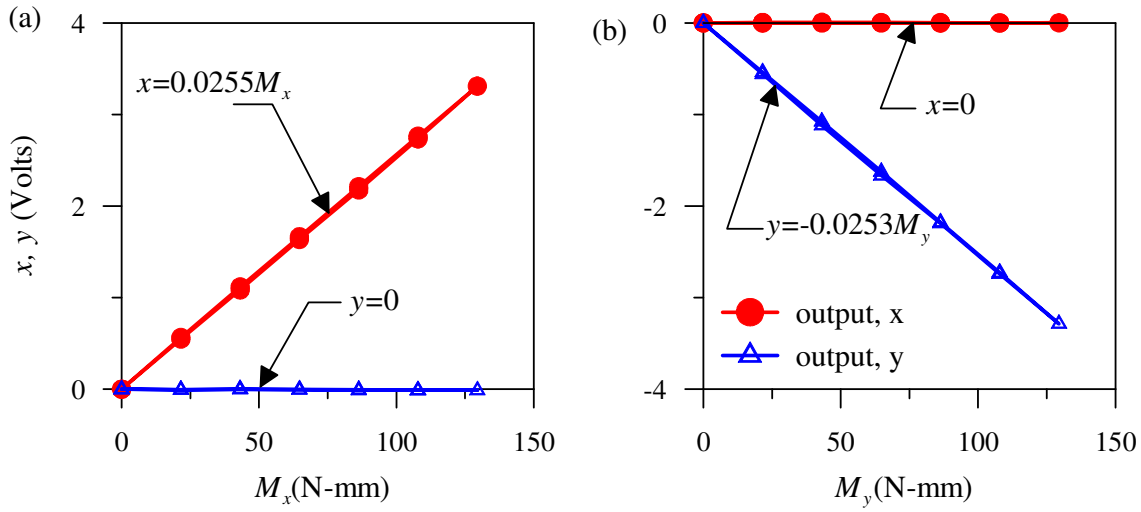

Figure 4.7. Gauge calibration comparison (Gauge level 1): (a) for bending about the *X*-axis of the spine; and (b) for bending about the *Y*-axis of the spine.

spine, readings from the gauge pair mounted in the orthogonal direction (*Y*) were negligible, and vice versa).

Attempts were made to calibrate gauges as cantilever beams in order to obtain accurate calibration factors. However, for the middle two gauge levels, only simply supported beam trials could be conducted due to the excessive length of the cantilever that would have been required. The calibration factors of strain gauges at the six levels are summarized in Table 4.2. Note may be made of the fact that the calibration factors at gauge level 3 and 4, whose calibrations were conducted in the simply supported beam configuration, were higher than those of the remaining gauges, possibly due to the inherent bending moment at the supports that affected the accuracy of the calibration. As a result, various strategies were investigated to adjust those calibration factors in order to produce consistent results with the other gauges.

Table 4.2 Calibration factors for strain gauges

Support	Gauge Level	Elev. (m)	Direction	Calibration Factor (N-mm /Volt)	Direction	Calibration Factor (N-mm/Volt)
Cantilever Beam	1	0.345	*X*	39.216	*Y*	39.526
	2	1.035	*X*	44.137	*Y*	43.561
Simply supported Beam	3	1.385	*X*	53.191	*Y*	50.505
	4	1.765	*X*	55.309	*Y*	55.005
Cantilever Beam	5	2.105	*X*	44.626	*Y*	46.279
	6	2.485	*X*	41.263	*Y*	41.094

4.5 WIND TUNNEL TEST FOR AEROELASTIC GUYED MAST MODEL

4.5.1 Overview

The wind tunnel test program for the full aeroelastic model of the 300 m guyed mast comprised one set of tests in open country exposure and one set of tests in over water exposure, respectively. Three different angles of wind azimuth relative to the structure were investigated in both open country and over water exposure. As illustrated in Figure 4.8, the selected wind directions included wind parallel to the windward guy lane, wind parallel to one face of the mast, and wind perpendicular to one face of the mast (denoted in subsequent discussions as wind at 0^o, 30^o and 60^o, respectively). Thus, a total of six test series was performed, each with simulated full-scale mean wind speeds of up to 55 m/s (198 km/hr) near the top of the prototype. The test series are illustrated in Table 4.3, in which OC denotes open country (moderate turbulent boundary layer flow) and OW denotes over water (low turbulence flow). Within each series, the tests were repeated for mean wind speeds varying from 0 m/s to the maximum values, in the increments shown in Table 4.3.

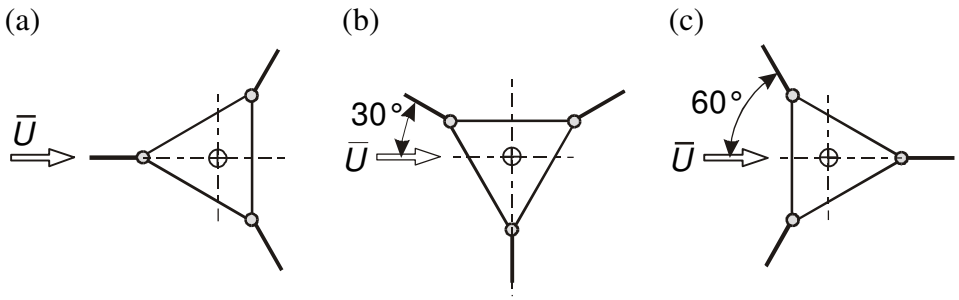

Figure 4.8. Definition of wind directions: (a) wind at 0°; (b) wind at 30° and (c) wind at 60°.

Table 4.3. Wind tunnel test series for the guyed mast model.

Wind Condition	Wind Azimuth (degree)	Maximum Mean Wind Speed* (m/s)	Wind Speed Increment (m/s)	Test Series
Open Country	0	5.428	2.2	OC-0
	30	5.545	2.38	OC-30
	60	5.557	4.7	OC-60
Over Water	0	5.527	4.07	OW-0
	30	5.541	4.07	OW-30
	60	5.563	4.08	OW-60

*The model-scale mean wind speed measured at 2.62 m above the tunnel floor.

4.5.2 Wind Tunnel Instrumentation

In addition to strain gauges and accelerometers mounted on the aeroelastic guyed mast model, other instrumentation, including Pitot tubes and a laser transducer, were also used to measure the properties of the wind and the model dynamic displacement.

Three Pitot tubes attached to the pressure transducers were used for measuring wind speeds in the wind tunnel. One reference Pitot tube (Figure 4.9b) was mounted from the tunnel ceiling and set at 2.616 m high above the tunnel floor; in addition, two auxiliary Pitot tubes were installed at 0.6 m and 1.56 m above the floor of the wind tunnel upstream of the model, as shown on the left side of Figure 4.14.

A single laser transducer (Figure 4.9a) was used to measure alongwind displacements of the mast at the top guy support level. The laser itself was mounted on a rod suspended from the ceiling of the wind tunnel on the leeward side of the guyed mast model. The laser was oriented horizontally, parallel to the mean wind direction, and was aligned on a reflective target glued to the top guy support level on the model.

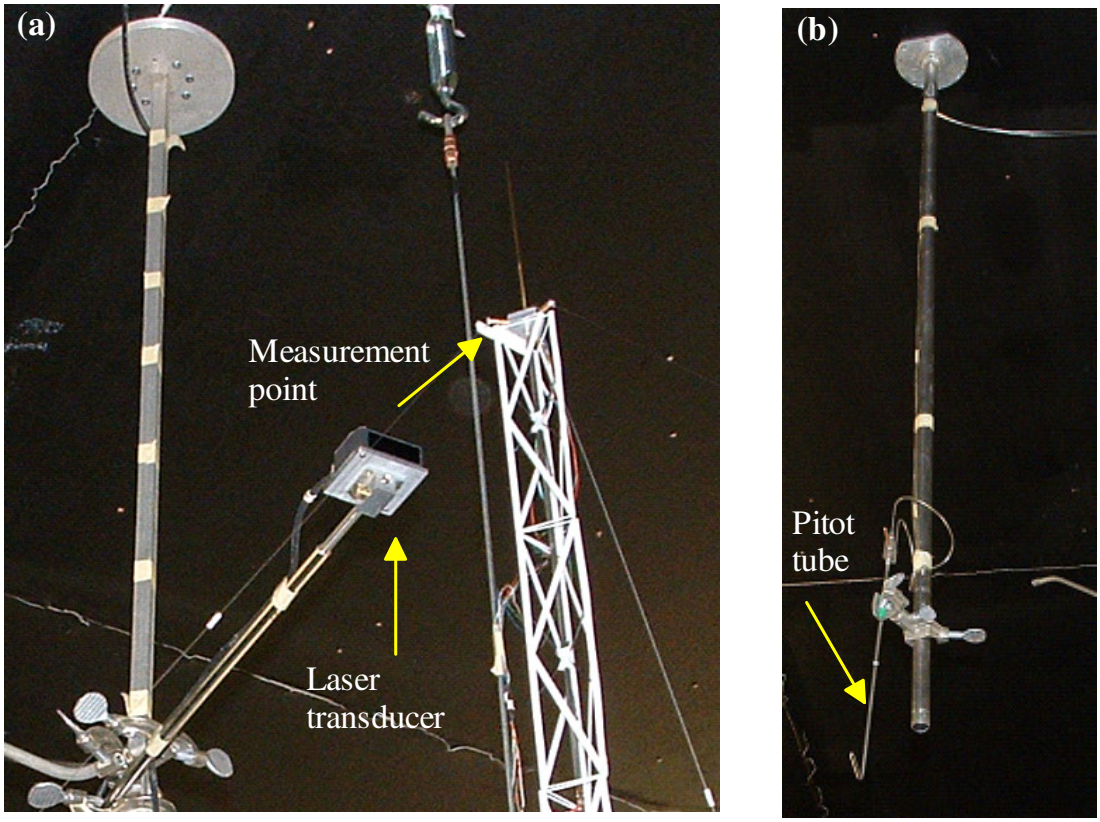

Figure 4.9. Wind tunnel instruments: (a) Laser transducer; (b) Pitot tube.

The data acquisition system (Figure 4.10) for the wind tunnel testing sampled 26 channels of data continuously at a rate of 110 Hz, including 12 channels of strain gauges, 8 channels of accelerometers, a laser transducer and 5 channels of Pitot tubes (3 channels for reference Pitot tubes and the other 2 channels for auxiliary Pitot tubes). This data were filtered (as described in the subsequent sections) and stored electronically as time series data for subsequent analyses.

Figure 4.10. Computer controlled data acquisition system.

4.5.3 Experimental Setup

The aeroelastic guyed mast model was mounted on the floor of the low speed wind tunnel section floor at the BLWTL centered over a fixed dowel pin, so that the model could be rotated at different orientations relative to the mean wind direction, as mentioned in Section 4.5.2. To avoid adding extra weight and drag area to the model, all electrical cables and wires from the instrumentation were strung horizontally from the sensors on the mast to a vertical support cable that was fixed approximately 50 cm behind the model, stretched tautly from the ceiling to the floor of the wind tunnel on the leeward side of the guyed mast model. The sensor wires were then bundled together and securely fastened to the support cable until they reached the wind tunnel floor (Figure 4.11).

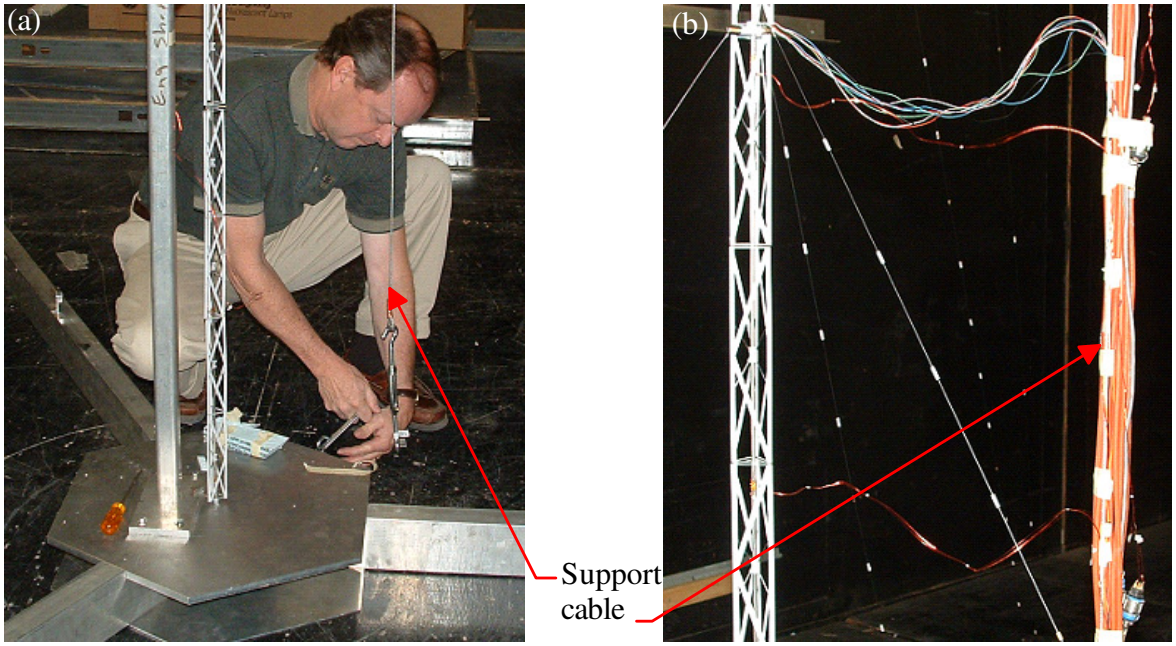

Figure 4.11. Support cable: (a) before instrumentation cabling; (b) after instrumentation setup.

For every test in each of the six test series (Table 4.3), the prescribed wind conditions in the wind tunnel were produced using a computer controlled system. Attempts were made to simulate the turbulent boundary layer flow of the natural wind. In order to simulate the open country exposure characteristics in the wind tunnel, as well as naturally facilitate the rapid growth of a vertical boundary layer over the rough tunnel floor along the test section, a combination of three spires were employed upstream of the test section, along with roughness elements (Figure 4.12 and Figure 4.13) placed on the tunnel floor in patterns known from previous studies to produce the desired boundary layer flow conditions. The over water low turbulence flow conditions, on the other hand, were simulated by removing all spires and roughness elements, creating an unobstructed floor surface.

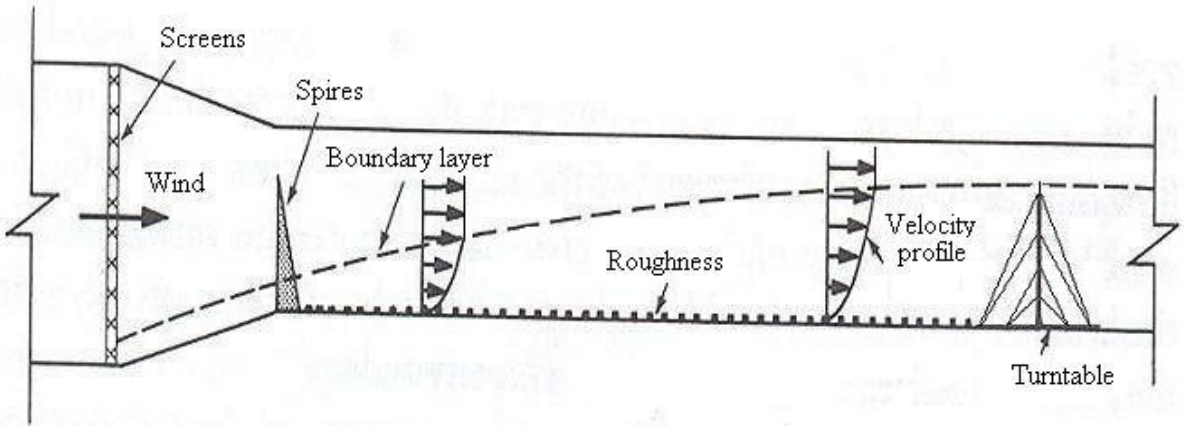

Figure 4.12. Side view of the low-speed test section components in the BLWTL (after Liu 1991).

Figure 4.13. Roughness elements producing the open country exposure.

Along with the Pitot tube and the laser transducer, the fully instrumented 3 m tall guyed mast model installed in the low speed wind tunnel section is shown in Figure 4.14. A photograph of the model test set up for over water conditions is shown in Figure 4.15, in which the model is oriented for the case of a wind azimuth of 30^{o}.

Figure 4.14. Guyed mast model in the wind tunnel, showing the open country condition.

Figure 4.15. Guyed mast model in the wind tunnel, showing the over water condition.

4.5.4 Wind Tunnel Testing Procedures

The wind tunnel test was conducted in two terrain conditions: open country exposure boundary layer flow to investigate the dynamic response to moderate turbulence and over water exposure representing low turbulence to serve as a basis for comparison with the open country exposure, and to establish the aerodynamic stability characteristics of the model. As illustrated in Figure 4.8, three wind azimuths with 0^o, 30^o and 60^o were applied to the model, respectively. For each wind direction, a series of tests were carried out under incrementally increasing wind speeds in the range from 0 m/s to a maximum wind speed up to 5.5 m/s, which corresponds to site wind conditions with a mean wind speed of 55 m/s (198 km/hr) near the top of the full-scale prototype. This maximum wind speed for open country exposure represents a wind storm of approximately equivalent intensity to one that would be required to produce the design mean wind speed of 39 m/s at 10 m above the ground over the smooth terrain assumed in the Canadian Standard CSA-S37-01.

Instantaneous time series data, including bending moments at six locations along the mast, accelerations at four guy levels, displacements at the top guy level and wind speed from the Pitot tubes attached to the pressure transducers, were collected by the BLWTL data acquisition system at a sampling rate of 110 Hz, and stored electronically for subsequent data processing. The sampling frequency for the tests was chosen as 110 Hz due to the frequency range of interest, which lay between 0 and 55 Hz (after processing, the frequency content of the results is limited to ½ of the sampling frequency). The data acquisition system sampled 70,656 readings per sensor at each

wind speed increment with a time increment of 0.009 seconds. Thus, the measurement time was 11 minutes for every wind speed increment in each of the six test series.

All the sensor signals were fed through electronic low-pass filters with a cut-off frequency of approximately 45 Hz to avoid signal contamination from electrical interference. Due to the slow drift fluctuations inherent in the accelerometer output, accelerometer signals were also passed through high-pass electronic filters with a cut-off frequency of 0.1 Hz to attenuate signal drift; however, further digital filtering was also found to be necessary when converting the accelerometer data into dynamic displacements.

Upon the completion of each test series, an initial evaluation of the response trends was carried out. It was found that both the peak and *rms* response levels increased in a smooth and predictable manner with increasing wind speeds. No evidence of excitation due to vortex shedding induced oscillations or other aerodynamic instabilities were observed, which could have manifested themselves as sudden peaks in the response curves at critical wind speeds.

A visual observation of the guyed mast behaviour during wind tunnel tests indicated that the extent of guy vibration depended on the guy location on the structure. When the mast deflected under wind effects, the windward guys constrained the movement and thus became taut and experienced little motion, while the leeward guys became slack and experienced large scale vibration. As expected, the largest degree of sag and vibration amplitudes was noted in the upper guys.

4.6 WIND CONDITIONS IN THE BLWTL

4.6.1 Wind Velocity Profile

Wind modelling plays a key role in wind tunnel testing. To produce realistic response predictions, the wind velocity profile and the wind variance along the height must match those experienced by the prototype.

A detailed study of the flow conditions in the low speed test section was conducted in the BLWTL, using moveable hot wire anemometers to measure flow characteristics at various locations. Figure 4.16 shows the measured mean wind speed profiles normalized by reference mean wind speed at 2.62 m above the tunnel floor and the turbulence intensity (i_u) profiles varying with height for both the open country and over water exposure. In this figure, the measured mean wind speed $\overline{U}$ and the turbulence intensity data are denoted by the blue cross and red solid triangle symbols, respectively, while the corresponding theoretical mean wind profiles assumed for the numerical model are denoted by solid green lines. It should be noted, though, that the mean wind profiles used in the numerical models were fit to the measured data, rather than using established analytical expressions. As expected, the mean wind speed increased with height in a roughly exponential fashion, while turbulence intensities of the mean wind velocity, calculated using Equation 2.11, decreased correspondingly due to the diminishing effects of floor friction and increasing mean wind velocities; as well, turbulence intensity was seen to increase with increasing ground roughness. It is apparent that the longitudinal turbulence intensity in open country is more severe than that in over water while the mean wind speed increased at a slower rate with elevation; also, it is apparent that the wind was highly turbulent near the floor level.

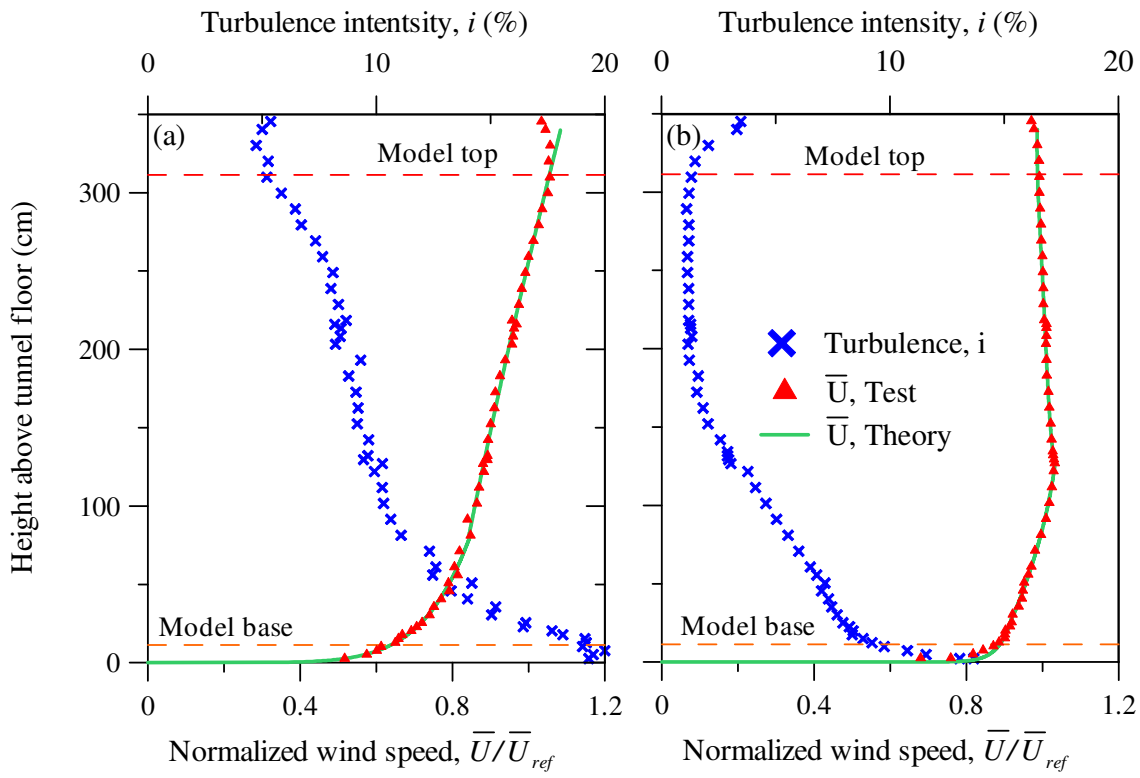

Figure 4.16. Profiles of normalized wind velocity: (a) open country; (b) over water.

4.6.2 Power Spectra of Wind Velocity Turbulence

The power spectral density functions (power spectra), which indicate the distribution of the energy of the wind fluctuations with respect to frequency, of the longitudinal (alongwind) and lateral (crosswind) components of the turbulence under open country and over water exposure are plotted in Figure 4.17; here, the power spectra measured at an elevation of 1 m, 2 m and 3 m above the tunnel floor are represented by red, blue and pink lines, respectively. All power spectra were normalized by the variance (u_{rms}^2) of the wind speed and represented on the more convenient logarithmic scale. Figure 4.17 shows that the energy of turbulence is concentrated in the low frequency range of the spectra (below 2-3 Hz). The spectra measured at three different elevations in Figure 4.17 also indicate that spectral magnitudes did not vary

with height in a consistent way. For open country exposure (Figure 4.17a), the power spectra at the three elevations were very similar; for the over water exposure, though, more energy is concentrated in the low frequency range in the power spectrum measured at 1 m above the floor for both alongwind and crosswind conditions, as shown in Figure 4.17 (b).

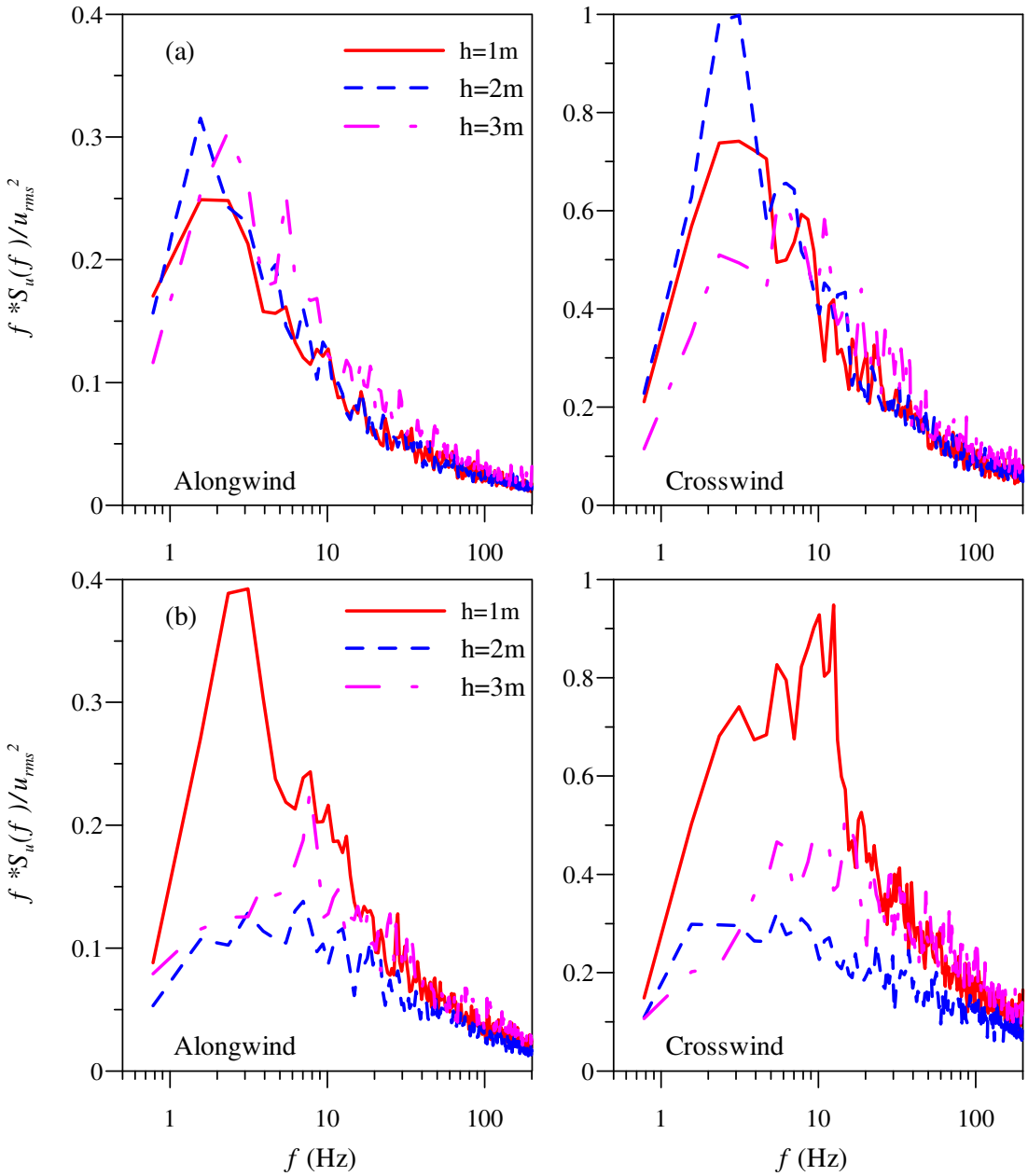

Figure 4.17. Power spectral density of turbulence in the BLWTL : (a) open country; (b) over water.

In Figure 4.18, measured spectra of alongwind velocity fluctuations are compared to two analytical expressions. In addition to the well known Davenport Spectrum (NBCC 1995), a modified version of the Kolmogorov inertial subrange spectrum is also plotted that was used in the numerical model employed in this study. In its original form, the Kolmogorov spectrum can be expressed as (Simiu and Scanlan 1996):

$$\frac{f \cdot S_u(f)}{\tilde{u}^2} = 0.045 \cdot \left(\frac{f \cdot z}{\overline{U}(z)} \right)^{-\frac{2}{3}} \tag{4.1}$$

where $S_u(f)$ is the spectrum of the fluctuating wind speed. Since this form of the spectrum is elevation dependent, while the measured spectra did not appear to be, Equation 4.1 was modified by the factor:

$$k(z) = \left(\frac{z \lambda_f}{L_o} \right)^{\frac{2}{3}} \tag{4.2}$$

in which L_o (m) is a scaling constant selected by manually fitting the modified Kolmogorov spectrum to the measured data (L_o = 2.1 m for open country and 1.3 m for over water, respectively). This modified Kolmogorov spectrum was subsequently incorporated into the numerical analytical model.

4.7 MODE SHAPE AND NATURAL FREQUENCY MEASUREMENTS OF THE GUYED MAST MODEL IN STILL AIR

The guyed mast model was also tested in still air (no wind) conditions to quantify its dynamic characteristics, including its fundamental natural frequencies and mode shapes, as well as its structural damping. Since no external forcing (no wind) was present in this case to excite the necessary vibration, an artificial means of exciting the

model was employed, using impact loads applied to the mast at various points along its height. Attempts were made to select locations for the impact loads that would excite the structure in a variety of vibration modes.

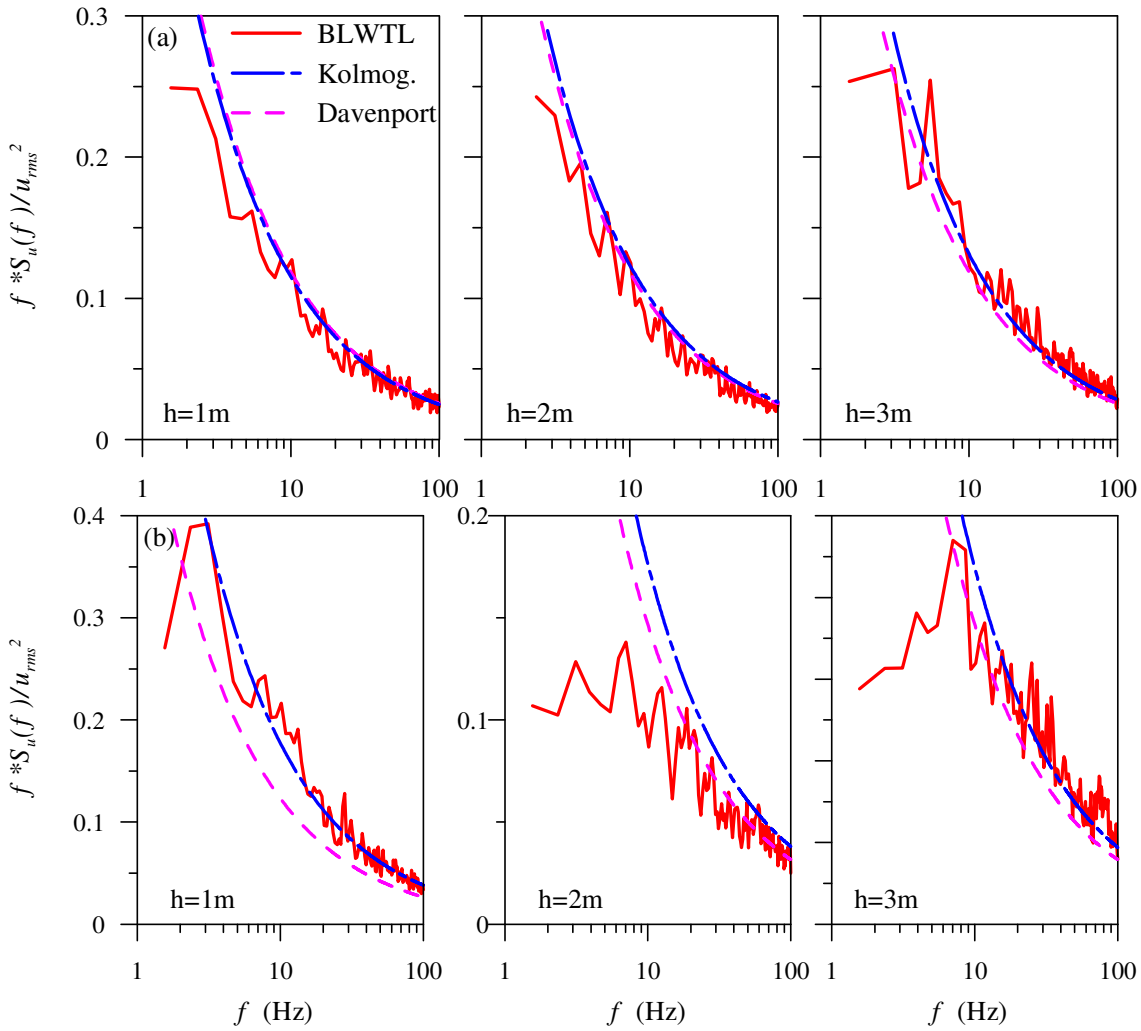

Figure 4.18. Power spectra comparison of alongwind velocity:
(a) open country; (b) over water.

In addition to eight fixed accelerometers that had been mounted at four guy attachment levels at two orthogonal directions for the wind tunnel test, one pair of movable accelerometers was mounted at the mid-span of each panel of mast claddings successively to measure both alongwind (X) and crosswind direction (Y) accelerations

(Figure 4.19). Since there were sixteen panels along the mast, the movable accelerometers were set up 16 times to measure its response at each panel location; the duration of the measurement procedure was approximately five minutes for each setup. The instantaneous acceleration data were captured by the data acquisition system sampling at 110 Hz for each of the ten accelerometers used in every setup.

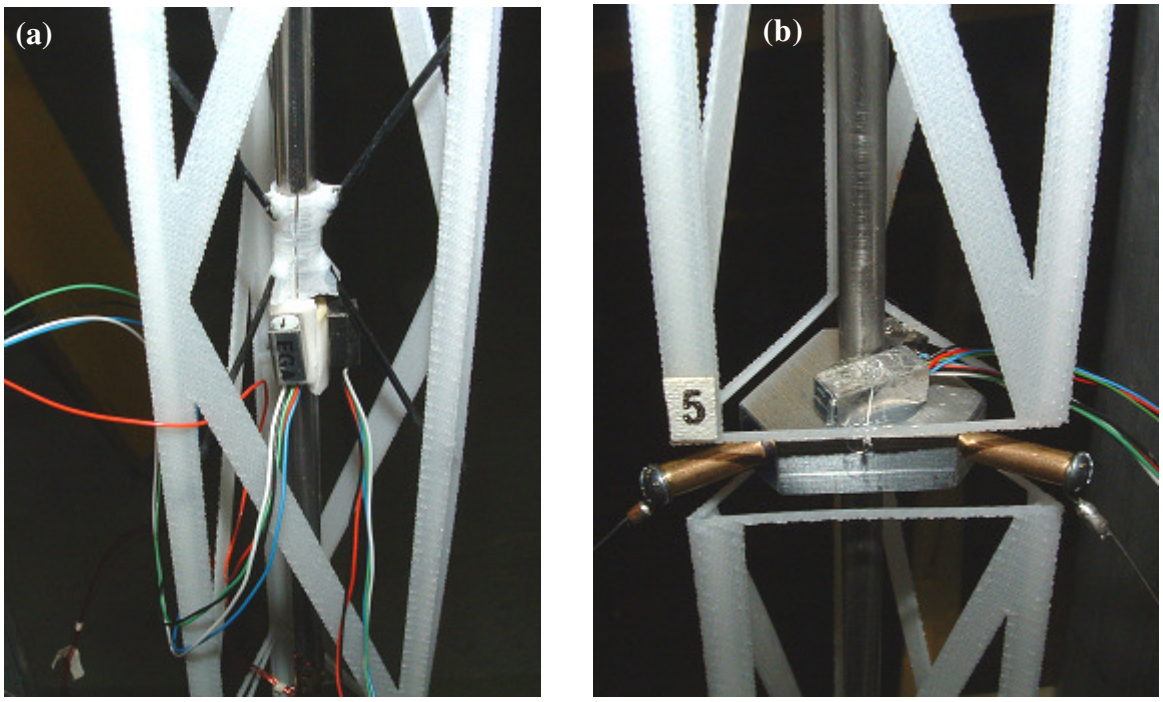

Figure 4.19. Model accelerometers in *X* and *Y* directions: (a) removable accelerometers; (b) fixed accelerometers at the guy level.

The eight fixed accelerometers, mounted at the four guy levels, were chosen as reference accelerometers and used to normalize the results from the various setups so that they could be "pieced" together to form complete mode shapes. A total of twenty points along the mast were thus used as mode shape measurement points, as shown in Figure 4.20. In this figure, sixteen points (denoted as No. 1 to No. 16) located at approximately mid-span of each panel from the bottom to the top along the mast were selected as points monitored by the pair of movable accelerometers; the remaining four

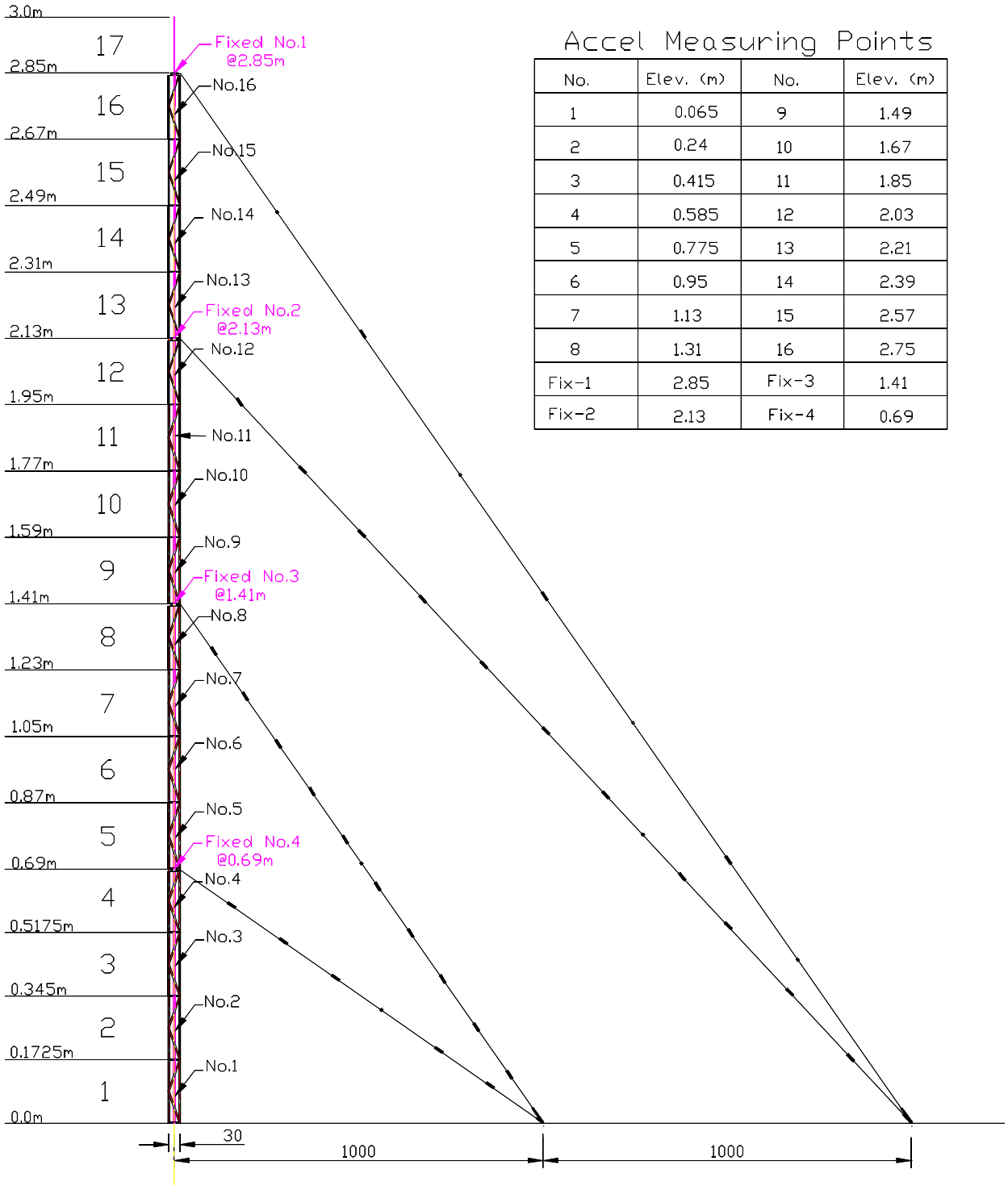

Accel Measuring Points

No.	Elev. (m)	No.	Elev. (m)
1	0.065	9	1.49
2	0.24	10	1.67
3	0.415	11	1.85
4	0.585	12	2.03
5	0.775	13	2.21
6	0.95	14	2.39
7	1.13	15	2.57
8	1.31	16	2.75
Fix-1	2.85	Fix-3	1.41
Fix-2	2.13	Fix-4	0.69

Figure 4.20. Locations of mode shape measurement points.

points were reference points (denoted by Fix-1 to Fix-4 in Figure 4.20). Therefore, the response of the model was measured at the selected 20 points in both alongwind (X) and crosswind (Y) directions using two movable accelerometers and eight reference accelerometers.

4.8 WIND TUNNEL TEST OF THE SECTIONAL MODEL

An aerodynamic test was conducted on a sectional model of the mast in the Wind Tunnel Laboratory at the University of Saskatchewan. The purpose of this test was to study the drag characteristics of the mast and their dependency on Reynolds number, as well as shielding effects on the mast cladding.

The sectional model of the mast, representing a typical panel of the mast cladding and spine, was 179 mm in height and had a face width of 30 mm. The length of the spine was cut to be equal to the overall length of the cladding. The model was mounted on the tunnel floor with one end connected to a rigidly mounted plate (Figure 4.21). The sectional model was tested at fourteen different wind speeds in the range of 10 m/s to 30 m/s and at three different wind azimuths (0^o, 30^o and 60^o). The resulting Reynolds numbers were thus in the range of 23,000 to 70,000, which is subcritical (Figure 3.8). It should be noted that, in order to register sufficiently large readings on the force-balance assembly, the wind speeds used in these tests significantly exceeded those in the full model tests.

The acting force was measured by load cells capable of measuring both lift and drag forces. The results were used to estimate the effective drag area ($C_D A$) and to check shielding effects of the mast cladding on the three mast faces for various

orientations relative to the wind. The dependency of drag forces on Reynolds number was also examined. Results of these tests are presented in Section 5.9.

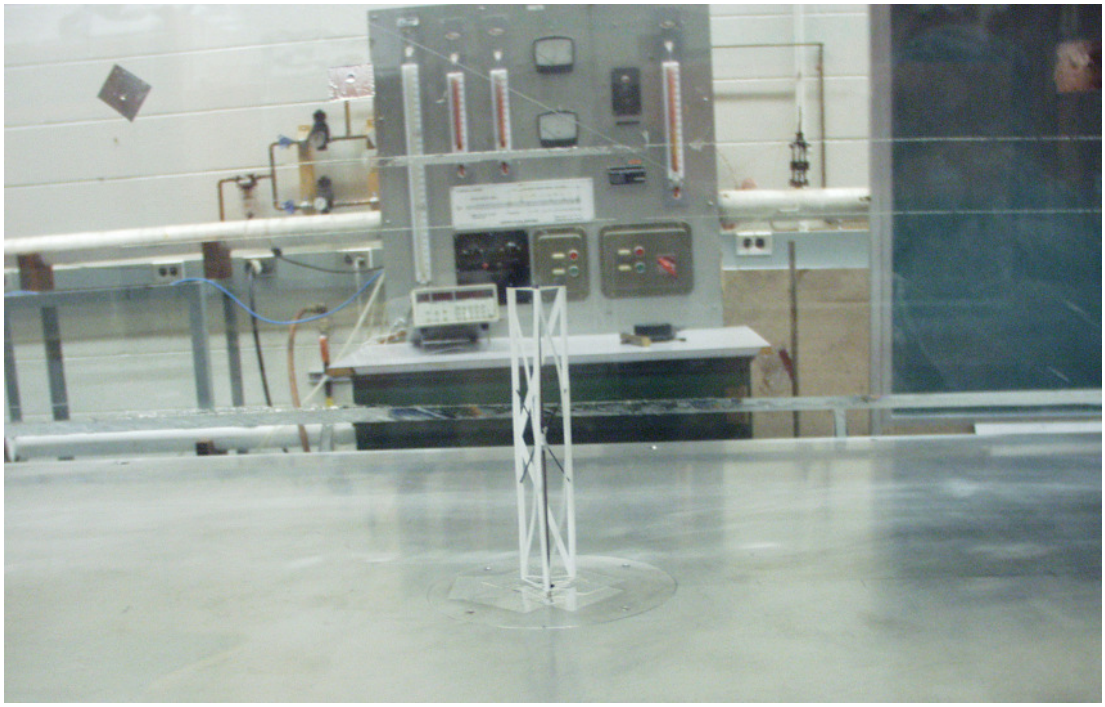

Figure 4.21. Model cladding drag test in the Wind Tunnel Laboratory at the University of Saskatchewan.

An obvious limitation of these tests was the influence of end effects associated with the flow of air over the top of the specimen. These end effects introduced additional flow path around the top of the specimen, resulting in a lower drag coefficient for the body (Holmes 2001). Therefore, the drag characteristics obtained in this manner had to be viewed with some caution.

For the purpose of calculating "effective" drag area of the cladding sections, a mean wind profile following a power law relationship (Equation 2.2) was fitted to mean wind speeds measured at various heights above the tunnel floor. It was determined that a power law exponent of $\alpha = 0.1$ fit the measured wind profile very well (Figure 4.22).

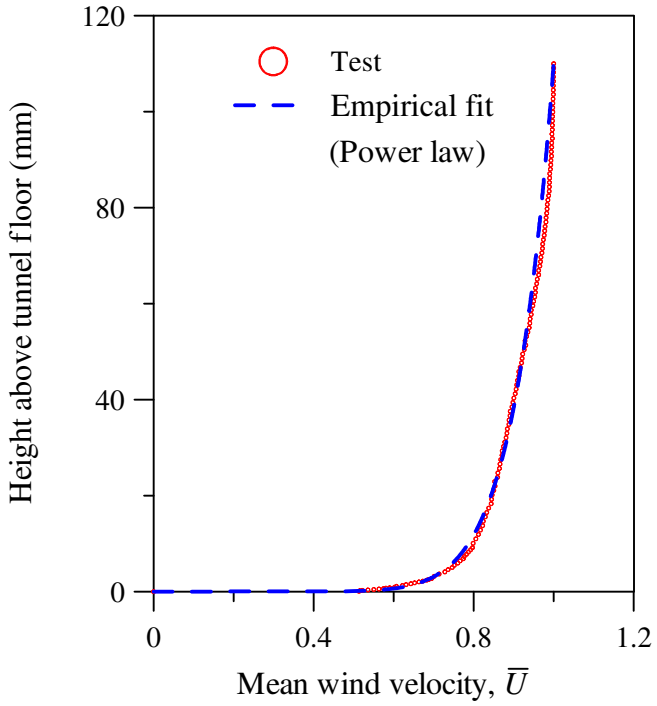

Figure 4.22. Wind velocity profile for Wind Tunnel Laboratory tests at the University of Saskatchewan.

As noted previously, the wind speeds considered in the drag test, however, were higher than those in the test of full aeroelastic model; in addition, the turbulence level was different. As a result, the test results from the drag test could not be used directly as input to the numerical model. Instead, these results were used as a rough indication of the relative drag characteristics for the different wind azimuths.

4.9 SUMMARY

A wind tunnel test of the full aeroelastic model of a 300 m tall guyed mast was carried out in both open country and over water exposure simulating moderate and low turbulence conditions, respectively. Three wind directions were examined in this study. Various wind speeds were considered, up to a maximum of 5.5 m/s at the top of the

model. Dynamic responses measured during the wind tunnel tests included dynamic displacements, bending moments, and accelerations.

The aeroelastic model was also tested in still air conditions to measure its fundamental dynamic characteristics such as natural frequencies, mode shapes and structural damping.

A drag test of a section model of the mast cladding was carried out in the wind tunnel laboratory at the University of Saskatchewan to investigate the drag force characteristics and shielding effects.

All wind tunnel test results are presented in Chapter 5.

5. WIND TUNNEL TEST RESULTS

5.1 INTRODUCTION

The wind tunnel test results of the guyed mast dynamic characteristics measured from the six test series, as described in Chapter 4, are discussed in this chapter. The objective of this experimental program was to investigate the dynamic response characteristics of a 300 m guyed mast subjected to open country (moderate turbulence) and over water (low turbulence) exposure; comparisons were also made with predictions from an existing frequency domain analysis model described in Chapter 2.

In this chapter, the wind tunnel test results of the full aeroelastic model of the guyed mast from the six test series, as well as the experimental results of the dynamic characteristics measured in still air, are presented, along with the drag test results of the sectional model of the guyed mast. Of particular interest was the degree to which the measured dynamic response characteristics agreed with those predicted by an existing numerical frequency domain dynamic analysis model. A frequency domain dynamic analysis model developed by Sparling (1995) specifically to address the buffeting response of guyed masts was used throughout this study.

The dynamic responses presented herein include dynamic displacements, bending moments, the corresponding response spectra and peak factors, as well as model properties such as natural frequencies, mode shapes and structural damping. It

should be noted that, unless specifically noted otherwise, all test results reported in subsequent discussions are based on tests performed at the maximum wind speed in each test series, which was approximately 5.5 m/s at the reference height of h = 2.62 m above the tunnel floor. In addition, comparisons with numerical predictions in subsequent sections are all based on the response in the alongwind direction only, since the crosswind response was not calculated in the numerical model; the measured crosswind response, however, is also described in this chapter. It should be noted that, due to the large amount of data recorded, only typical samples of the results are presented in this chapter; the remaining data are included in Appendix A and B.

The dynamic response of the aeroelastic model can be directly related to that of the full-scale prototype with the use of appropriate scaling parameters (Table 3.2). Since a preliminary study (Section 3.5) demonstrated that the numerically predicted dynamic response of the full-scale prototype and the corresponding scaled model were in excellent agreement, comparisons herein were only made between the direct wind tunnel measurements and the predicted response of the model-scale guy mast.

5.2 DATA PROCESSING

Before meaningful analyses could be undertaken, the raw test data had to be suitably conditioned using various digital signal processing routines. In addition, since the aeroelastic model was rotated through different wind azimuths, the output data had to be transformed to the global (mean wind direction) coordinate system in order to properly identify alongwind and crosswind response components.

The orientation of the unrotated local (model structure) coordinate axes (x' and y' axes) with respect to the global coordinate axes (x and y axes) is illustrated in Figure

5.1, where the global coordinate system is defined by the mean wind direction. When the guyed mast was rotated at an angle of θ, defined as the clockwise angle between the global x (y) axis and the local x' (y') axis, the resulting wind-induced dynamic response components on the mast may be expressed as:

$$r_x = r_x' \cos\theta + r_y' \sin\theta \tag{5.1}$$

$$r_y = -r_x' \sin\theta + r_y' \cos\theta \tag{5.2}$$

where r_x and r_y are the response components in the global coordinate system (x and y axes) in the alongwind (drag) and crosswind (lift) directions, respectively, while r_x' and r_y' are the response components in the local coordinate system (x' and y' axes). The transformation function that relates vectorial response components (r) in the global wind coordinate system to that obtained directly from wind tunnel model tests (r') is thus given by:

$$[r] = [k][r'] \tag{5.3}$$

So that

$$[k] = \begin{bmatrix} \cos\theta & \sin\theta \\ -\sin\theta & \cos\theta \end{bmatrix} \tag{5.4}$$

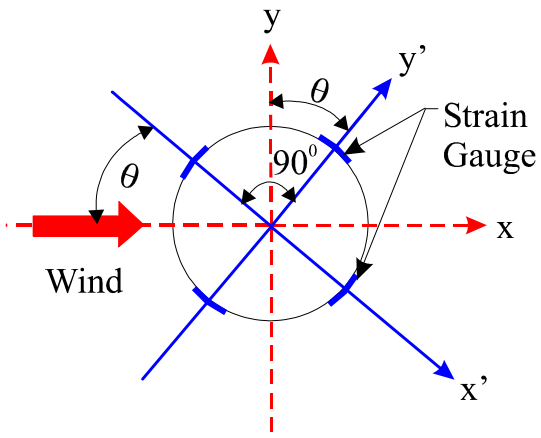

Figure 5.1. Definition of local and global coordinate systems.

The measured bending moments from the wind tunnel test results were thus computed first by applying the calibration factors (Table 4.2), and then by applying the above transformation function. For measured acceleration data, on the other hand, the additional step of applying a digital high pass filter had to be carried out to attenuate the low frequency signal drift, which was found to be important in generating reliable dynamic displacements.

An example time history of the measured acceleration at h = 2.85 m above the model base (representing a prototype height of 285 m above the base) is given in Figure 5.2 for an elapsed period of 60 seconds for the case of open country exposure with the wind at 60°. The wind directions relative to the mast orientation are indicated on this and subsequent plots by a small icon superimposed on the figure, in which $\overline{U}$ denotes the mean wind velocity.

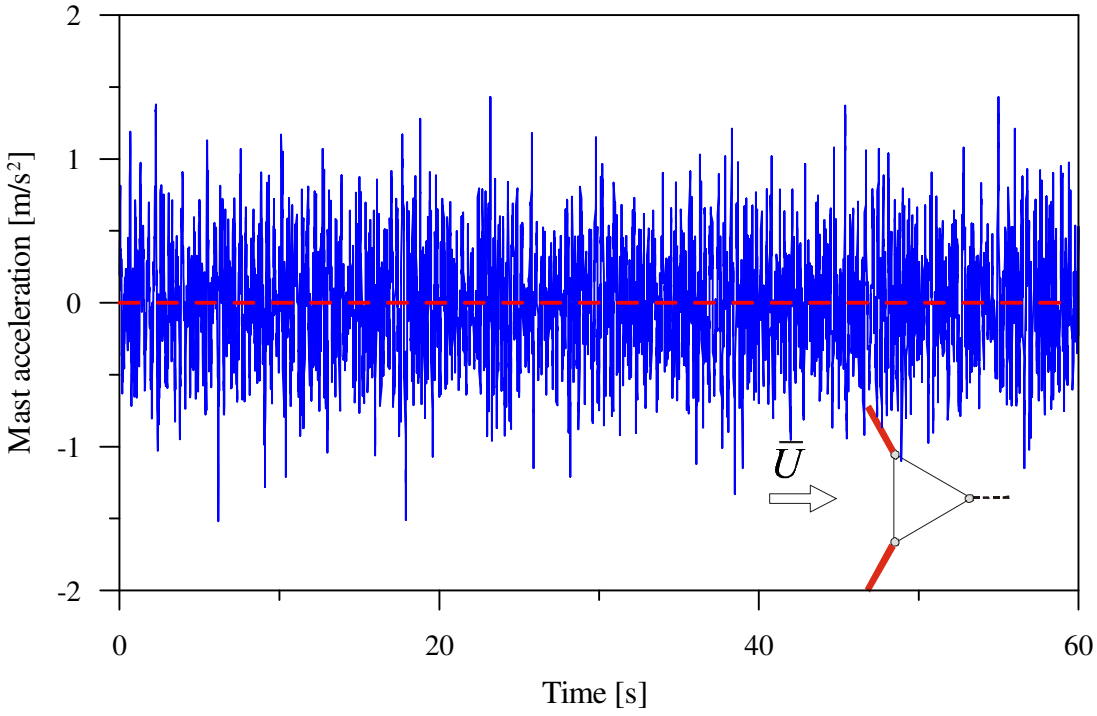

Figure 5.2. Time history of mast acceleration at top guy level (h = 2.85 m) for open country conditions with the wind at 60°.

Corresponding mast displacements at the four guy attachment levels were determined by integrating the measured instantaneous accelerations over the measurement time to yield velocities and displacement time histories consisting of 70,656 points with a time increment of 0.009 s. For the integration process, the trapezoidal approximation method was adopted; additional filtering was applied at each time step using a high pass filter to remove the signal drift; also, linear regression was performed to remove the linear trend in the final displacement time history file. An example displacement time history at the top guy level (h = 2.85 m) produced from the acceleration time history illustrated in Figure 5.2 is presented in Figure 5.3 for an elapsed period of 60 seconds. It is apparent that the time histories of both acceleration and displacement appear to be random dynamic processes. Since the accelerometers could not detect static (time-invariant) displacement components, no mean response of displacement could be extracted from measured accelerations.

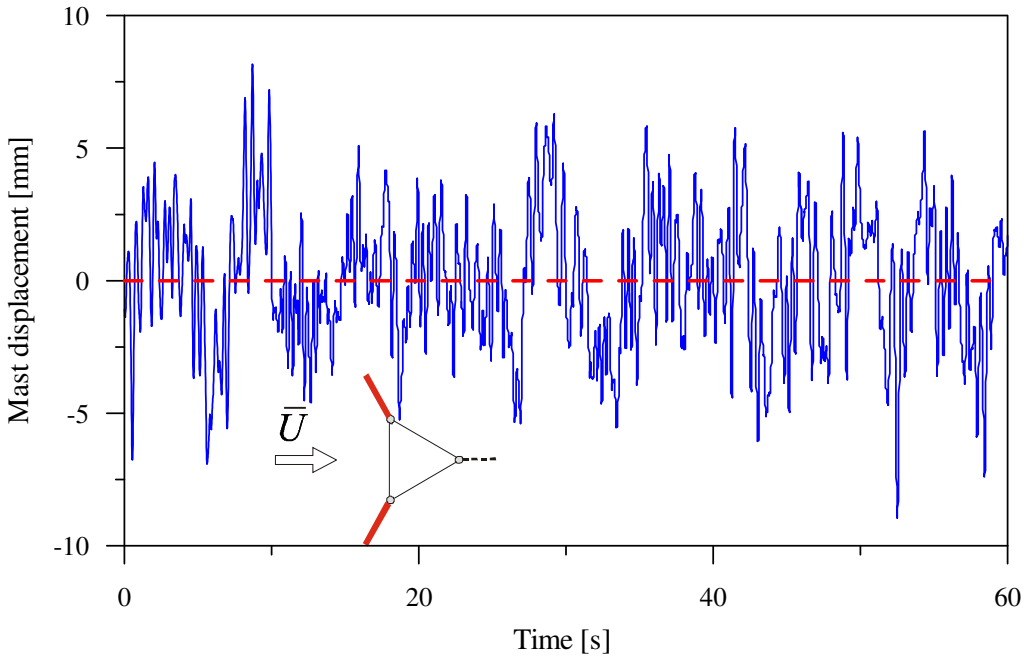

Figure 5.3. Time history of mast displacement at the top guy level (h = 2.85 m) produced from acceleration time history for open country conditions with wind at 60°.

Alongwind dynamic mast displacements were also measured directly with a laser displacement sensor located at the top mast guy support level (h = 2.85 m), in which the mean response could be monitored. A time history of mast displacement measured directly from the laser sensor taken over a 60 second period is shown in Figure 5.4, in which the red dash line represents the mean displacement at the top of the mast.

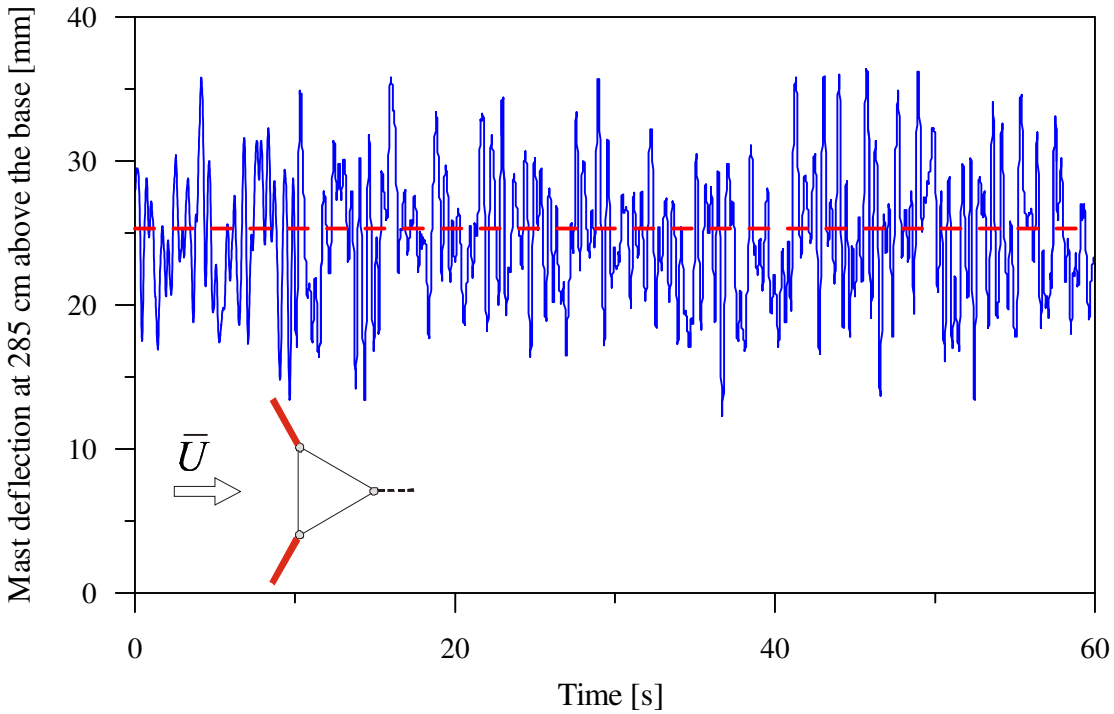

Figure 5.4. Example time history of mast deflections measured by the laser sensor at h = 2.85 m for open country exposure with the wind at 60°.

As with all electronically gathered data, the proper data processing prior to more detailed analyses was of particular importance. A Matlab program specifically written by the author for this purpose was employed to perform the digital signal processing. In this program, a high-pass filter with a cut-off frequency of 0.1 Hz was adopted to remove signal drift. Power spectral density (PSD) functions were then computed using a fast Fourier transform (FFT). Prior to performing the FFT analysis, a Hanning window function, which is equivalent to one period of a cosine-squared function in the time

domain, was applied to each block of data to reduce spectral leakage and produce a smoother PSD function. In addition, to attenuate random variations in the resulting PSD functions, the time history data was subdivided into blocks of 512 time steps; a FFT was then performed on each block individually, and the results were averaged. Furthermore, the data were subdivided such that there was a 50% overlap between successive blocks of data to increase the number of random data sets considered.

PSD functions of mast displacements obtained from a single data block of 512 points, and one using an average of multiple blocks of 512 points with a 50% overlap are compared in Figure 5.5. As shown in Figure 5.5a, the red solid line and blue dashed line represent the spectra of two single cases of 512 point data blocks. It is apparent in Figure 5.5a that there is considerable difference between the two cases, making it difficult to identify meaningful response peaks; thus, averaging was found to be beneficial in reducing the influence of random variations and noise (Figure 5.5b).

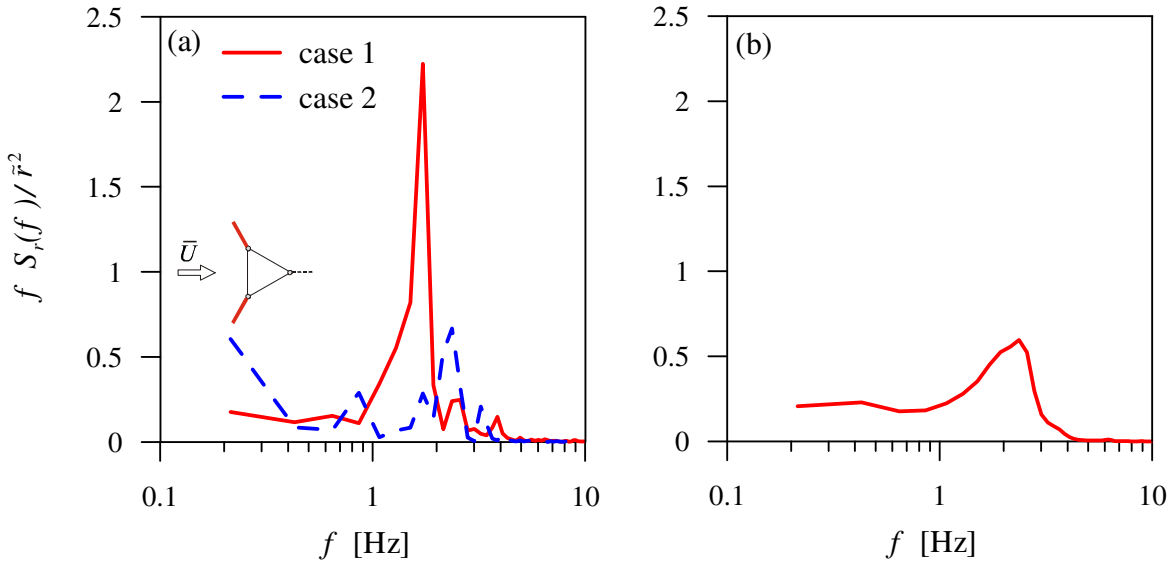

Figure 5.5. Power spectrum density of mast displacement at top guy level (h = 2.85 m) produced from acceleration time history for open country conditions with the wind at 60°: (a) single block of 512 points; (b) averaged points.

5.3 DYNAMIC MAST DISPLACEMENTS

Comparisons between alongwind dynamic mast displacements measured from the wind tunnel tests and those predicted using the frequency domain numerical model for the scaled guyed mast model (3.0 m tall) in both open country and over water exposure are provided in Figure 5.6 and Figure 5.7, respectively, for the three wind directions considered in this study. Here, and in subsequent figures, the measured wind tunnel values are represented by solid circles, while predicted values are denoted by open triangles; $\overline{U}$ represents the mean wind velocity at the reference height.

The measured dynamic displacements presented herein were obtained by integrating the measured dynamic acceleration time series data twice with respect to time. Since static displacement components could not be measured by accelerometers (Section 5.2), only frequency domain predictions for the mean displacements are provided; in addition, to facilitate comparisons between measured and predicted displacements, the peak dynamic displacements shown on the right-most plots in both Figure 5.6 and Figure 5.7 do not include the static mean component.

With the wind at 0° (Figure 5.6a), the frequency domain analysis results underestimate the measured *rms* and peak dynamic displacements by a significant margin. With the wind at 30° (Figure 5.6b), on the other hand, there is good agreement between measured and predicted *rms* and peak dynamic displacements, with the theoretical displacements being marginally higher over the middle third of the mast. Finally, when the wind was at a 60° orientation (Figure 5.6c), the numerical predictions were significantly higher, particularly over the top half of the mast. There are a number of possible explanations for these observed discrepancies, not the least of which may

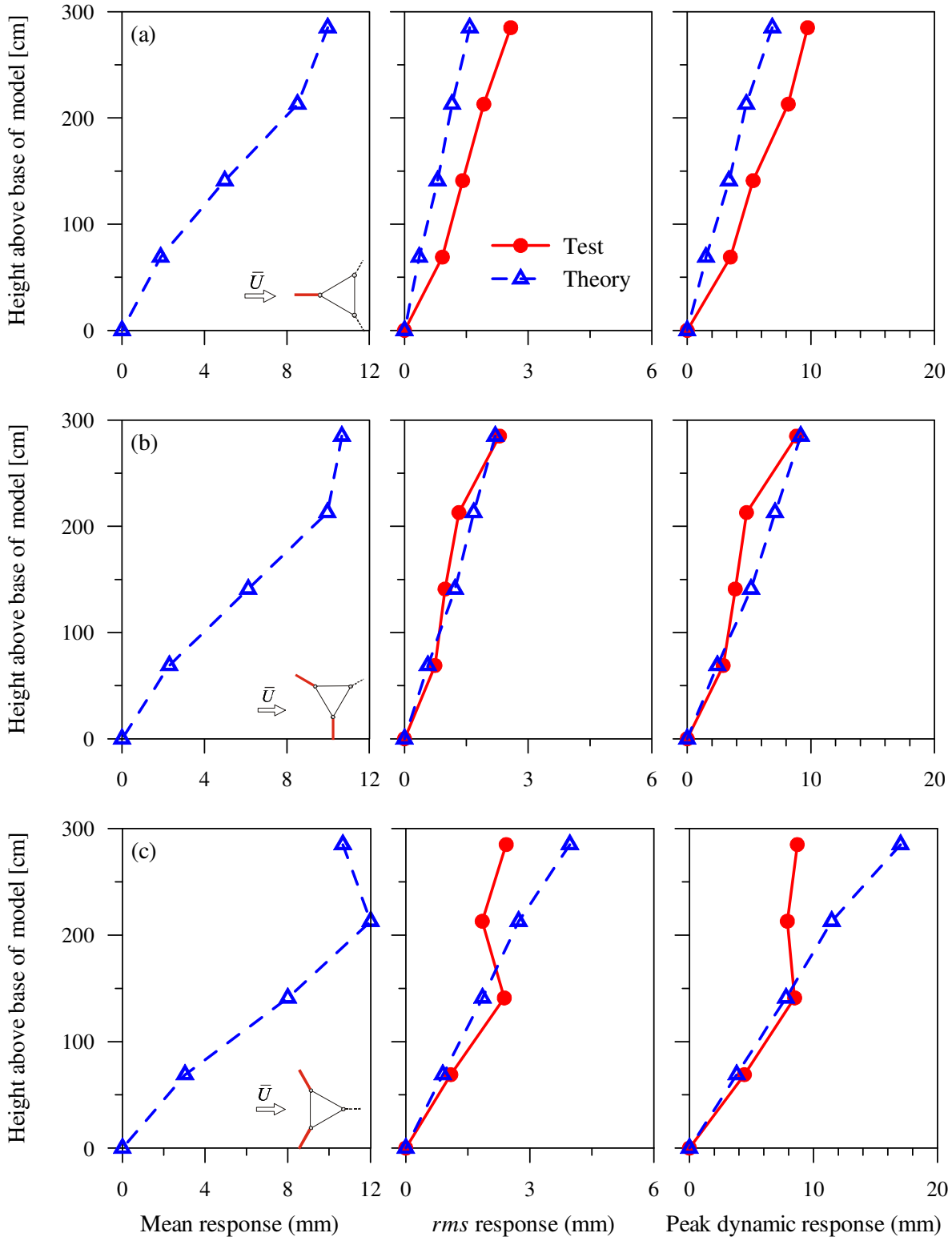

Figure 5.6. Comparison of theoretical and measured alongwind deflections in open country conditions: (a) wind at 0°; (b) wind at 30°; and (c) wind at 60°.

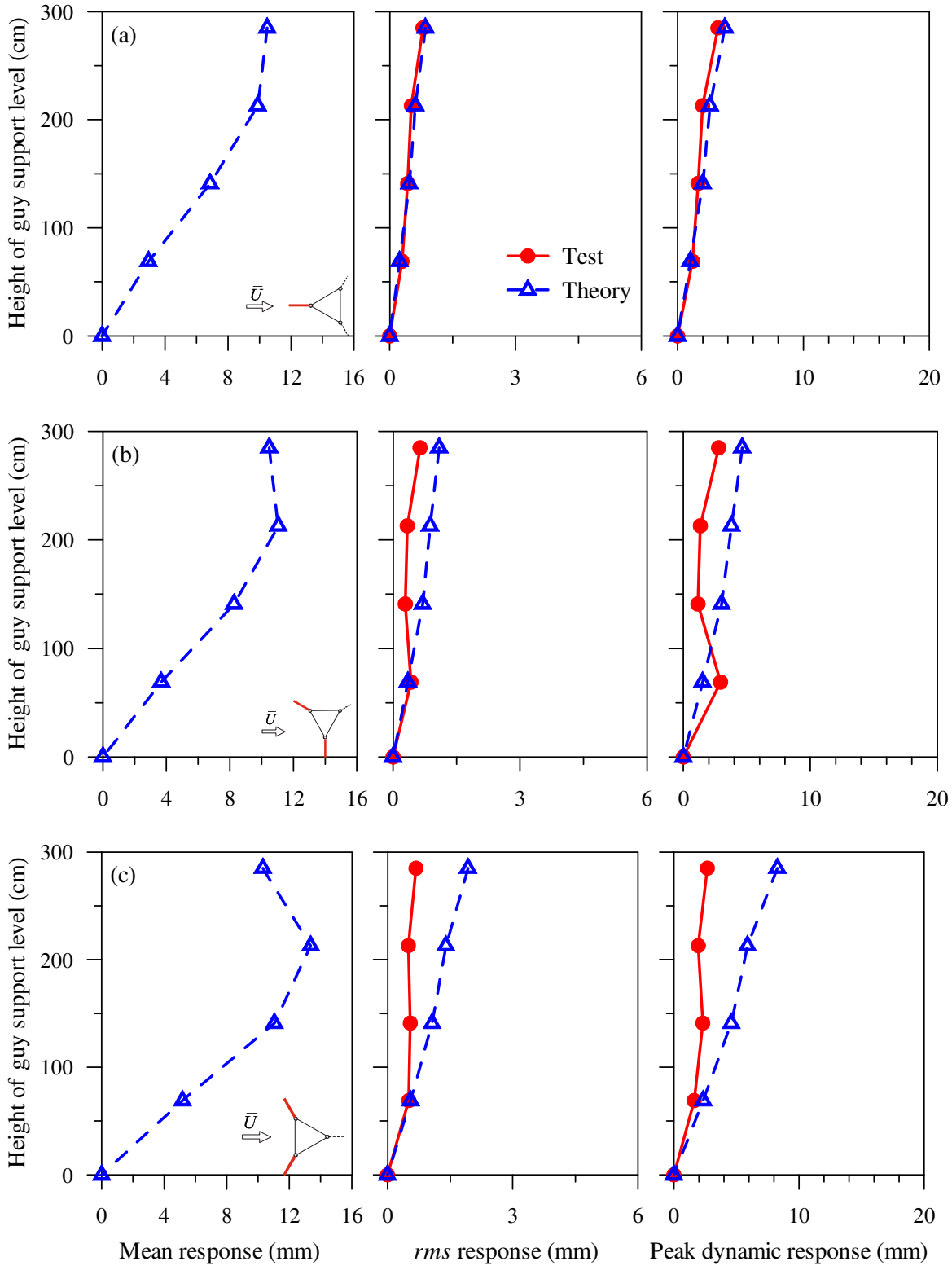

Figure 5.7. Comparison of theoretical and measured alongwind deflections in over-water conditions: (a) wind at 0°; (b) wind at 30°; and (c) wind at 60°.

include possible differences between assumed and actual drag and wind characteristics (turbulence levels and correlation lengths). Differences can also be expected given the fact that the aeroelastic model properties were designed based on still air conditions and may not have precisely captured the nonlinear behaviour of the model under wind loads.

For the over water conditions (Figure 5.7), similar trends were observed except that predicted responses were consistently larger relative to measured values than was seen for open country conditions. With the wind at 0° (Figure 5.7a), there was excellent agreement between measured and predicted *rms* and peak dynamic displacements along the entire height of the mast. At the top guy support level, for example, differences between the *rms* and peak dynamic responses of 7% and 14%, respectively, were observed. For the other two wind directions (Figure 5.7b and Figure 5.7c), on the other hand, the frequency domain analysis results appear to overestimate the measured *rms* and peak dynamic displacements, particularly in the upper half of the mast. While the numerical results predict substantially higher dynamic displacements with the wind at 60° compared to the other wind directions, measured values for all three wind directions were comparable in magnitude.

For the case with the wind at 60°, though, similar discrepancies have also been noted in a previous numerical study (Sparling 2001) comparing linear dynamic frequency domain analysis results with those obtained using a fully nonlinear time domain analysis. This, perhaps, suggests that nonlinear damping effects associated with vibrations of the highly slackened leeward guys on the upper levels of the mast may be beneficial in reducing dynamic mast displacements. The fact that similar reductions were not evident with the wind at 0° in either the wind tunnel test results from the

current study or the nonlinear numerical results from Sparling (2001) may be attributed to the skewed orientation of the leeward guys relative to the mean wind direction, which would have meant that these guys were not slackened to the same extent as the leeward guys for the other wind directions considered.

The measured mast displacements in open country and over water conditions for the three wind directions are summarized in Table 5.1. As expected, corresponding *rms* and peak dynamic displacements are consistently 2.5 - 4 times as large for the open country exposure, as compared to over water exposure.

Comparisons between measured and predicted (numerically calculated) responses are provided in Table 5.2. Here, the difference Δ is defined as:

$$\Delta = \frac{\left| Measured\ \mathrm{Re}sponse - Numerical\ \mathrm{Re}sponse \right|}{Numerical\ \mathrm{Re}sponse} \times 100\,\% \qquad (5.5)$$

As suggested in Figure 5.6, the results in Table 5.2 confirm that the agreement between measured and predicted responses is greatest for the wind at 30^o, as well as at 60^o for the lower guy levels.

One observation that is of interest for design purposes is that the peak dynamic displacements for open country exposure conditions are roughly comparable in magnitude to the predicted mean displacements for all wind directions. This highlights the importance of including an allowance for dynamic response in the evaluation of serviceability requirements for communication structures.

Table 5.1. Summary of measured mast displacements.

Wind Direction	Guy Level	Roughness	*rms* [mm]	Dynamic Peak [mm]
0°	1	Open Country	0.92	3.49
		Over Water	0.29	1.19
	2	Open Country	1.41	5.33
		Over Water	0.43	1.63
	3	Open Country	1.92	8.18
		Over Water	0.52	1.98
	4	Open Country	2.58	9.74
		Over Water	0.79	3.21
	C.O.V. (%) †	Open Country	41.5	41.9
		Over Water	41.5	43.2
30°	1	Open Country	0.74	2.91
		Over Water	0.43	2.92
	2	Open Country	0.98	3.88
		Over Water	0.29	1.14
	3	Open Country	1.32	4.80
		Over Water	0.34	1.34
	4	Open Country	2.30	8.84
		Over Water	0.64	2.77
	C.O.V. (%) †	Open Country	51.4	51
		Over Water	36.7	45.7
60°	1	Open Country	1.09	4.43
		Over Water	0.51	1.62
	2	Open Country	2.38	8.48
		Over Water	0.54	2.32
	3	Open Country	1.85	7.89
		Over Water	0.50	1.95
	4	Open Country	2.43	8.69
		Over Water	0.68	2.68
	C.O.V. (%) †	Open Country	32.2	27
		Over Water	15.2	21.3

C.O.V†**:** Coefficient of variation of response levels.

Table 5.2. Comparisons of measured and predicted mast displacements.

Roughness	Wind Direction	Guy Levels	*rms*			Peak		
			Test	Theory	Δ	Test	Theory	Δ
			[mm]	[mm]	[%]	[mm]	[mm]	[%]
Open Country	0°	1	0.92	0.36	156	3.49	1.52	130
		2	1.41	0.80	76	5.33	3.38	58
		3	1.92	1.15	67	8.17	4.78	71
		4	2.58	1.58	63	9.74	6.88	42
		Average	1.71	0.97	76	6.68	4.14	61
		C.O.V. (%)	41.5	53.5	22	41.9	54.6	23
	30°	1	0.74	0.57	30	2.91	2.43	20
		2	0.98	1.22	20	3.88	5.17	25
		3	1.32	1.68	21	4.80	7.11	32
		4	2.30	2.2	5	8.84	9.18	4
		Average	1.34	1.42	6	5.11	5.97	14
		C.O.V. (%)	51.4	48.9	5	51	48.1	6
	60°	1	1.09	0.9	21	4.43	3.81	16
		2	2.38	1.86	28	8.48	7.78	9
		3	1.85	2.73	32	7.89	11.47	31
		4	2.43	3.97	39	8.69	17.02	49
		Average	1.94	2.36	18	7.37	10.02	26
		C.O.V. (%)	32.2	55.3	42	27	56.1	52
Over Water	0°	1	0.29	0.23	26	1.19	1.00	19
		2	0.43	0.47	9	1.63	2.0	19
		3	0.52	0.61	15	1.98	2.57	23
		4	0.79	0.85	7	3.21	3.75	14
		Average	0.51	0.54	6	2.00	2.33	14
		C.O.V. (%)	41.5	47.91	13	43.2	49.13	12
	30°	1	0.42	0.35	20	2.92	1.51	93
		2	0.29	0.70	59	1.14	3.00	62
		3	0.34	0.88	61	1.34	3.78	65
		4	0.64	1.09	41	2.77	4.63	40
		Average	0.42	0.75	44	2.04	3.23	37
		C.O.V. (%)	36.7	41.37	11	45.7	41.05	11
	60°	1	0.51	0.55	7	1.62	2.35	31
		2	0.54	1.07	50	2.32	4.58	49
		3	0.50	1.40	64	1.95	5.88	67
		4	0.68	1.93	65	2.68	8.27	68
		Average	0.56	1.24	55	2.14	5.27	59
		C.O.V. (%)	15.2	46.87	68	21.3	46.99	55

Example traces of the instantaneous horizontal position of the mast, relative to its mean position, at the penultimate guy support level on the wind tunnel model are provided in Figure 5.8 and Figure 5.9 for open country and over water exposure, respectively. Here, each plot represents a measured time period of approximately 33 s.

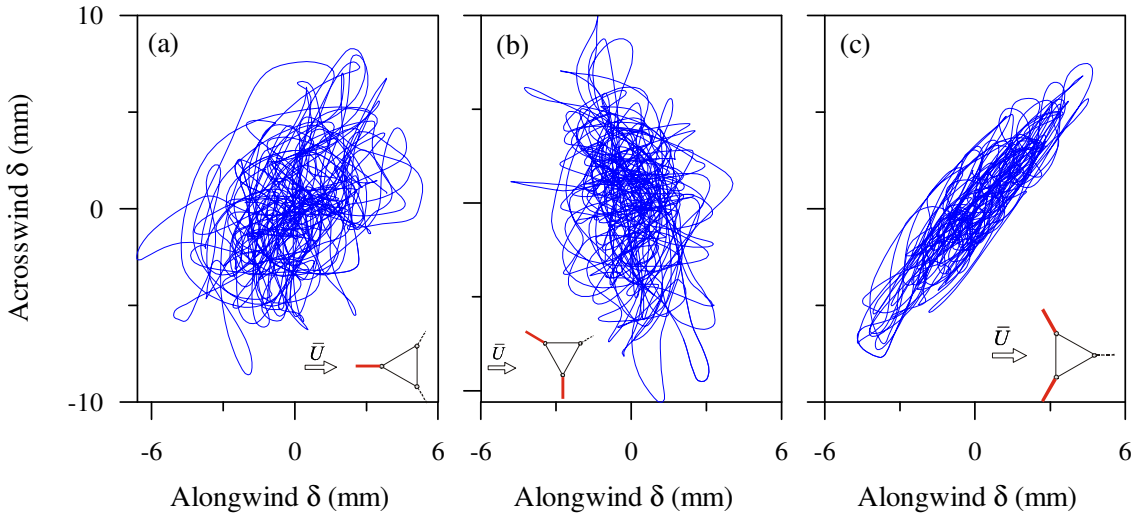

Figure 5.8. Measured horizontal mast displacement (δ) trajectories in open country conditions at the penultimate guy support level for a period of 33 s: (a) wind at 0°; (b) wind at 30°; and (c) wind at 60°.

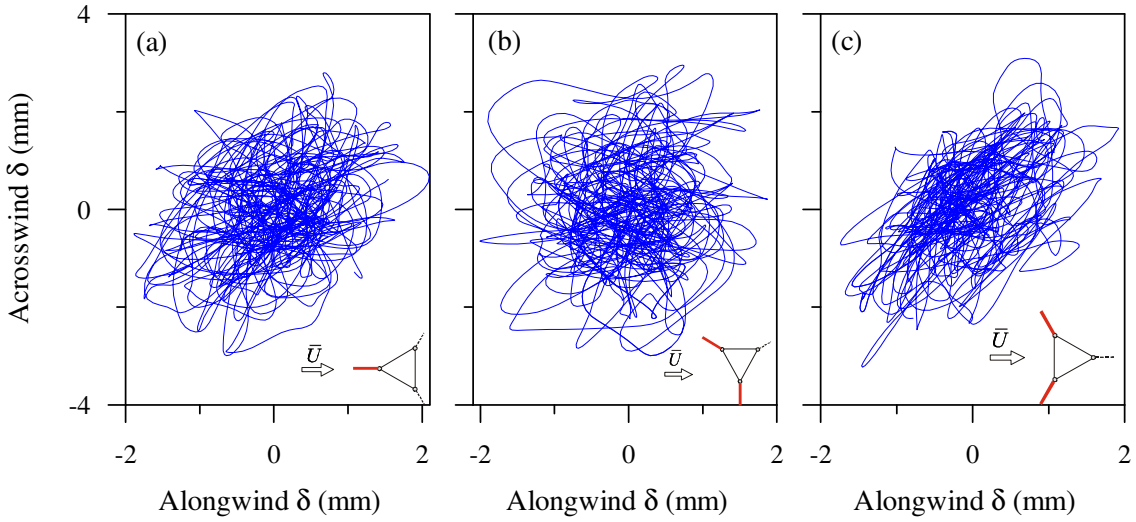

Figure 5.9. Measured horizontal mast displacement (δ) trajectories in over water conditions at the penultimate guy support level for a period of 33 s: (a) wind at 0°; (b) wind at 30°; and (c) wind at 60°.

For wind directions of 0° and 30° (Figure 5.8 a, Figure 5.8 b, Figure 5.9 a, and Figure 5.9 b), crosswind (lateral) dynamic displacement fluctuations are clearly as large or larger, in general, than corresponding alongwind (longitudinal) fluctuations. Similar trends were reported in a previous numerical study of three-dimensional guyed mast behaviour (Sparling and Davenport 1998). Contrary to the response of conventional (unguyed) structures, this relatively large cross-wind response may be attributed to the fact that slackening of the leeward guys significantly reduces the lateral stiffness of the system, particularly for wind at 0° and 30°. Currently, crosswind response is routinely ignored in design standards and in practice (CSA 2001, EIA/TIA 1996 and CEN 1997).

The pronounced skewed directional tendency for dynamic displacements taking place predominantly along an axis oriented at approximately 45° to the mean wind direction when the wind was at 60° (Figure 5.8c and Figure 5.9c) may have resulted from an unintended lack of symmetry in the model construction and / or erection, but cannot be explained adequately at this time.

5.4 BENDING MOMENTS

Comparisons between distributions of measured and predicted mean, *rms* and peak bending moments are shown in Figure 5.10 for open country conditions and in Figure 5.11 for over water conditions. The measured bending moments presented herein were obtained by applying calibration factors introduced in Section 4.4 and the transformation function (Eq. 5.1) for different wind directions to convert measured strains to bending moments. In this case, since the strain gauges were capable of measuring both the static and dynamic bending moments, the measured mean responses were available from the wind tunnel test results and, consequently, have been included

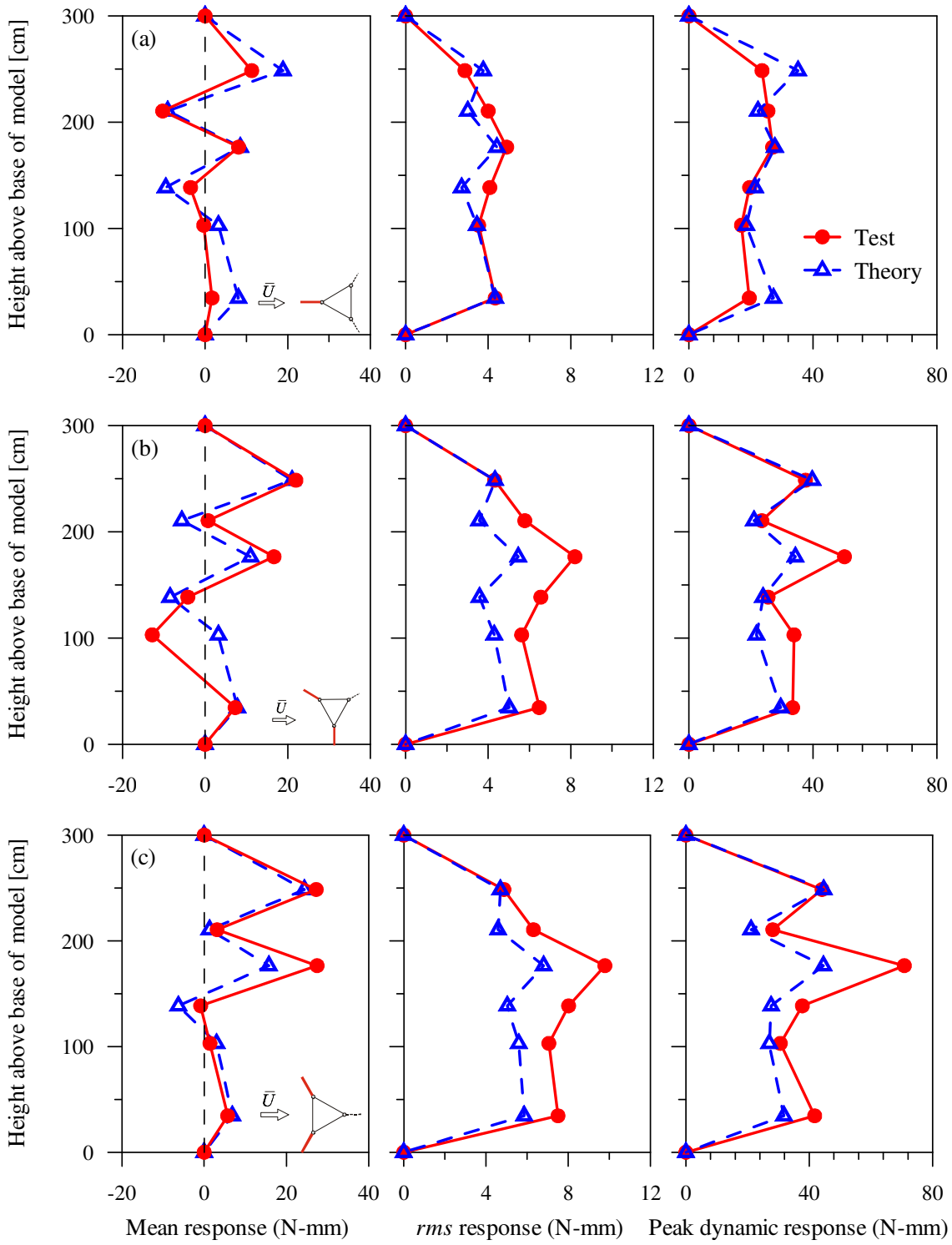

Figure 5.10. Comparison of theoretical and measured alongwind bending moments in open country conditions: (a) wind at 0^{o}; (b) wind at 30^{o}; and (c) wind at 60^{o}.

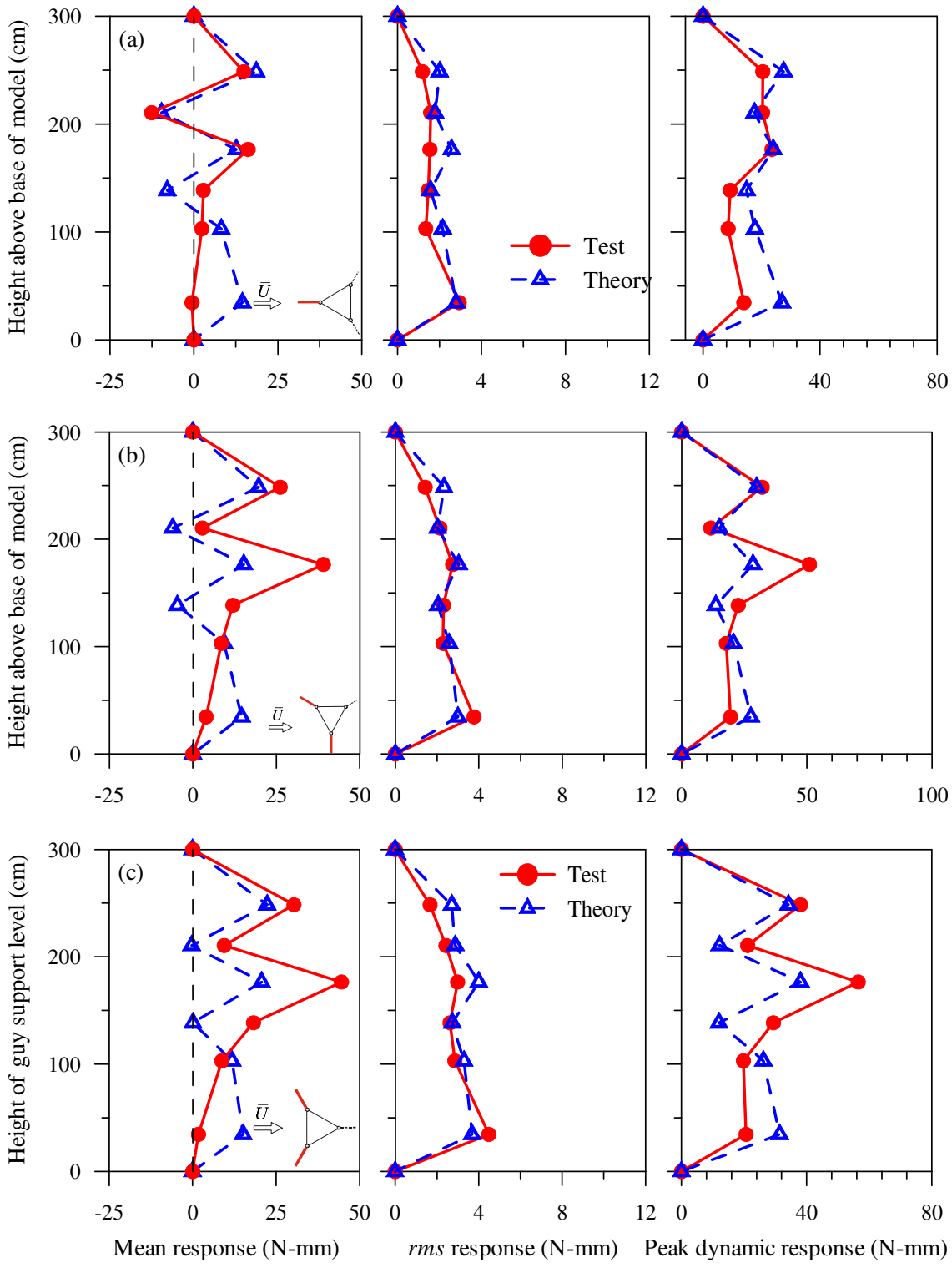

Figure 5.11. Comparison of theoretical and measured alongwind bending moments in over water conditions: (a) wind at 0°; (b) wind at 30°; and (c) wind at 60°.

in the peak (mean plus dynamic) response plots on the right side of Figure 5.10 and Figure 5.11.

The general form of corresponding predicted and measured dynamic bending moments were found to be very similar. In all cases, there was a fairly uniform distribution of measured dynamic (*rms*) bending moments over much of the mast height, a feature also predicted by the numerical model. Equally significant were the distinctly different mean (static) response patterns, which exhibited large variations over the mast height, along with regions of near-zero bending close to points of contraflexure. These notable differences between mean and dynamic bending moments demonstrate the shortcomings of the so-called "gust factor method" employed by the Canadian Standard CSA-S37-01 (CSA 2001), in which the peak response is estimated on the basis the mean wind load increased by a uniform "gust factor".

Given the level of uncertainty in both the numerical and physical model parameters, there is also a satisfactory degree of similarity between the magnitudes of the measured and predicted dynamic bending moments. The somewhat lower numerical *rms* values predicted for winds at 30° and 60° are largely compensated for in the total predicted peak response through the assumption of a conservative peak factor of $g_p = 4.0$ (see Section 5.5).

Comparisons between measured and theoretically predicted bending moments in open country and over water exposure are shown in Figure 5.11. It is evident here that good agreement is generally observed.

Table 5.3 summarizes the wind tunnel measurements of mast bending moments averaged at model midspan and guy levels, respectively, under three wind azimuths in

two different terrains; Table 5.4 gives the comparison of the averaged dynamic response with that based on the numerical model.

In Table 5.3, it is evident that the measured mean response exhibited large variability at all locations, with C.O.V. values ranging between 44.8% and 665%, while the *rms* response was much more consistent, particularly at the guy levels where C.O.V. values for the *rms* response ranged from 0.07% to 5.5%. In addition, the dynamic response in open country exposure was generally observed to exhibit larger variance than corresponding over water terrain when wind was at 30° and 60°.

Based on an examination of Figure 5.10 and Table 5.4, it can be concluded, on the whole, that there is reasonably good agreement between measured and predicted mean bending moments, particularly over the top half of the mast. Predicted dynamic moments tend to be slightly underestimated relative to measured values near the third mid-span region (approximately 2.5 m above the base) except with wind at 0^{o}, in which excellent agreement was achieved. The highest measured mean and dynamic bending moments were seen with the wind at 60°, a condition also predicted by the frequency domain analysis model. This is consistent with the results in open country exposure. The large reported differences between measured and predicted mean bending moment responses seen in Table 5.4, are skewed to some extent by the near-zero response levels predicted for several locations in the lower third of the mast. The resulting large percentage differences, in spite of the more modest absolute differences, were found to have a significant influence on the average difference values summarized in Table 5.4.

Table 5.3. Summary of measured bending moments of the guyed mast.

Roughness	Wind Direction	Location	Mean				*rms*		Peak	
			Min.	Max.	Avg†	C.O.V.	Avg†	C.O.V.	Avg†	C.O.V.
			[N-mm]	[N-mm]	[N-mm]	[%]	[N-mm]	[%]	[N-mm]	[%]
Open Country	0°	Midspan	-0.33	11.3	5.19	104.7	3.91	22.7	21.75	20.4
		Guy Levels	-3.53	-10.3	-6.9	69.0	4.04	0.15	22.53	6.3
	30°	Midspan	7.28	21.98	8.29	184.7	6.15	26.5	38.8	20.2
		Guy Levels	0.73	-4.2	-1.73	200	6.16	0.07	24.5	6.1
	60°	Midspan	1.4	27.46	15.45	89.6	7.3	27.6	46.83	36.4
		Guy Levels	-0.87	3.14	1.14	665	7.16	2.7	32.97	47.4
Over Water	0°	Midspan	-0.57	16.2	8.21	104	1.75	45.9	16.62	40.2
		Guy Levels	2.81	-12.6	-4.89	222	1.52	5.4	14.85	52.6
	30°	Midspan	4.01	36.5	18.81	80.7	2.51	38.5	29.28	47.2
		Guy Levels	2.85	11.86	7.36	86.7	2.2	4.4	16.93	44.7
	60°	Midspan	1.72	44.57	21.33	92.3	3	38.5	33.75	51.4
		Guy Levels	9.45	18.22	13.84	44.8	2.53	5.5	25.26	23

Avg†: Averaged response.

Table 5.4. Comparison of mast bending moments.

Roughness	Wind Direction	Location	Mean			*rms*			Peak		
			Test	Theory	Diff†	Test	Theory	Diff†.	Test	Theory	Diff†.
			[N-mm]	[N-mm]	[%]	[N-mm]	[N-mm]	[%]	[N-mm]	[N-mm]	[%]
Open Country	0°	Midspan	5.19	9.67	-46.4	3.91	3.99	-1.99	21.75	27.2	-20.0
		Guy Levels	-6.9	-9.29	-25.7	4.04	2.86	41.0	22.53	21.78	3.46
	30°	Midspan	8.29	10.77	-23.1	6.15	4.77	28.9	38.8	31.41	23.5
		Guy Levels	-1.73	-7.03	-75.4	6.16	3.57	72.3	24.5	22.45	9.24
	60°	Midspan	15.45	12.49	23.7	7.3	5.74	27.3	46.83	37.03	26.5
		Guy Levels	1.14	-2.49	-119	7.16	4.81	48.8	32.97	24.4	35.1
Over Water	0°	Midspan	8.21	13.47	-39.1	1.75	2.38	-26.4	16.62	24.08	-31.0
		Guy Levels	-4.89	-8.8	-44.5	1.52	1.68	-9.53	14.85	16.23	-8.52
	30°	Midspan	18.81	14.76	27.4	2.51	2.73	-8.2	29.28	26.71	9.63
		Guy Levels	7.36	-5.33	-37.9	2.2	2.03	8.3	16.93	14.32	18.3
	60°	Midspan	21.33	17.47	22.1	3	3.43	-12.4	33.75	32.46	3.96
		Guy Levels	13.84	-0.12	--	2.53	2.81	-10.0	25.26	12.09	-109

Diff†**:** Difference (Equation 5.5), averaged at guyed levels and midspan regions of the mast, respectively.

Some differences between observed and predicted responses are to be expected given the uncertainties associated with the strain gauge calibrations. As reported in Section 4.4, the calibration factors of the middle two gauge levels were obtained using a different procedure from the others, due to difficulties in the calibration process associated with the overall length of the mast. The simply supported beam conditions assumed for these calibrations may not have been achieved exactly due to the negative self weight moments that existed at the two supports, which may have led to an overestimation of the response. One indication that the calibration factors for these locations were suspect was that they were found to be larger than those at other locations, whereas the gauge characteristics themselves were not expected to vary significantly. Furthermore, the measured bending moments near mid-height of the mast tended to be the largest relative to corresponding predicted values.

5.5 DYNAMIC PEAK FACTORS

In the frequency domain analysis method, a statistical peak factor g_p, as defined in Eq. 2.49, was used to scale calculated *rms* response levels to expected peak dynamic values. An equivalent parameter relating to the measured test data can be expressed as follows:

$$\left(g_p\right)_{\text{test}} = \left(\frac{\hat{r} - \bar{r}}{\tilde{r}}\right)_{\text{test}} \tag{5.6}$$

in which $\hat{r}$, $\bar{r}$ and $\tilde{r}$ are the peak, mean and *rms* response values, respectively, determined from wind tunnel test results. For displacement measurements, since the accelerometer readings did not include mean responses, measured peak values represented peak dynamic response ($\hat{r} - \bar{r}$) directly. For bending moments, on the

other hand, mean response values were subtracted from the peak measurements, as suggested in Equation 5.6.

Comparisons of the measured and predicted peak factors for alongwind displacements and bending moments in open country conditions are provided in Figure 5.12 (a) and Figure 5.12 (b), respectively, for each of the three wind angles tested. Similar peak factors for over water conditions are given in Figure 5.13 (a) and Figure 5.13 (b). Averaged peak factors for all wind directions and elevations are summarized in Table 5.5 and Table 5.6. Although measured and predicted values were quite similar, peak factor values predicted by Equation 2.49 in the frequency domain method consistently overestimated measured values by an average of 9.0% for displacements and 3.6% for bending moments in open country exposure.

Due to the dependence of the response cycling rate ν on the natural frequencies f_i of the system, as demonstrated in Equation 2.50, the peak factor g_p will also increase with increasing natural frequencies. Therefore, peak factors at the prototype scale would be lower than those determined for the models as a result of the frequency scaling relationships. Because of this, corresponding prototype peak factors are also provided in Table 5.5 and Table 5.6. For this comparison, frequency domain peak factor estimates at the prototype scale were calculated directly; since comparable prototype values were not available for the measured values, however, approximate prototype-scale peak factors for the measured data were estimated based on the ratio between corresponding predicted prototype and model ratios. It is evident that prototype-scale peak factors are 5 – 21% below the commonly assumed value of 4.0, depending on the response type and wind direction. It should be noted, though, that peak factors are also

dependent on damping levels in the structure, which may differ in practice from those used in this study.

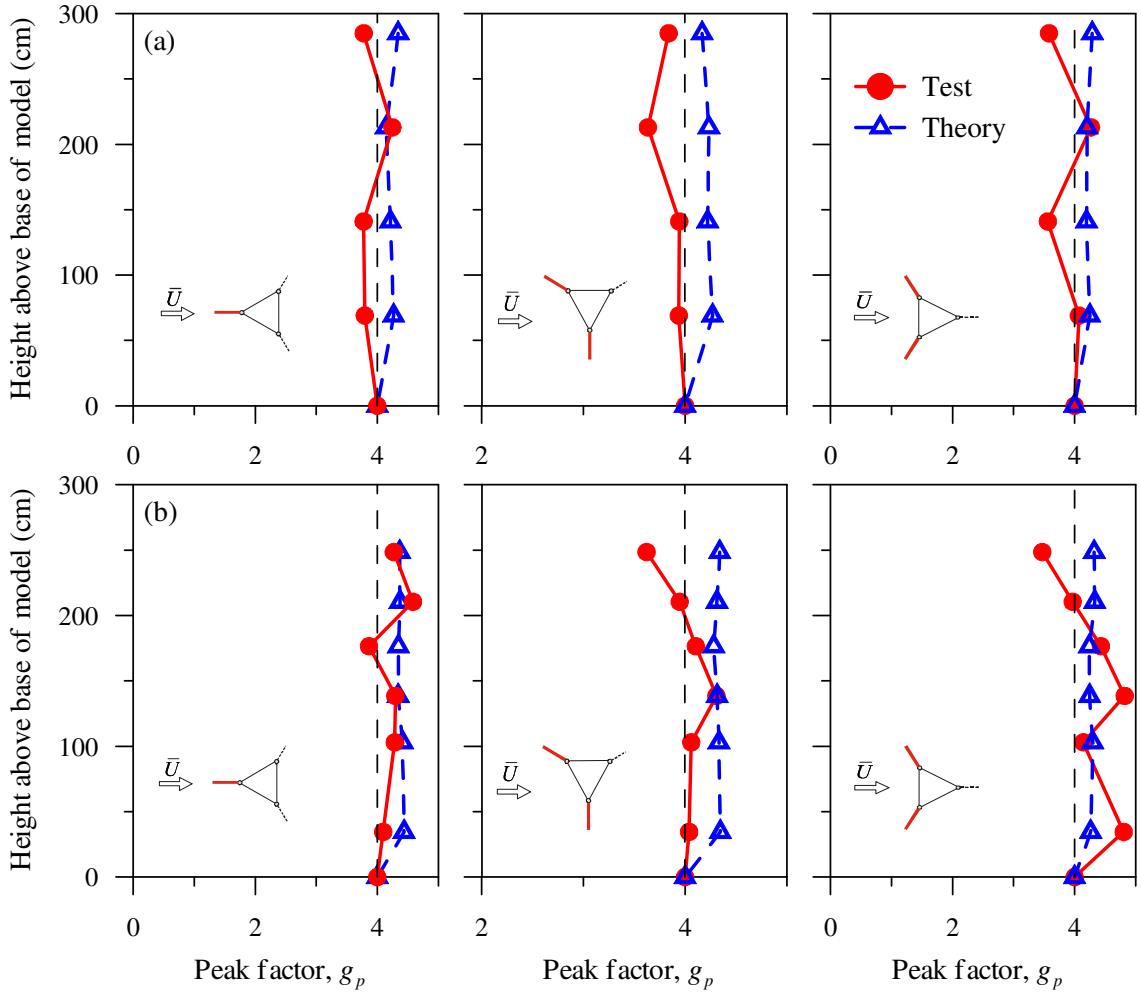

Figure 5.12. Comparison of measured and theoretical peak factors (g_p) in open country conditions: (a) alongwind displacements; and (b) alongwind bending moments.

5.6 POWER SPECTRA

Power spectral density functions (PSD), or power spectra, provide a means of indicating how the energy of a particular response is distributed with frequency. Example power spectra for measured alongwind displacements at the top guy support level and bending moments at the midspan of the penultimate mast span in open country

exposure are shown in Figure 5.14; here, the spectra are plotted in the more convenient $fS_r(f)$ verses $\ln(f)$ form, which enclose the same area as the original spectra. To reduce the uncertainty in the measured spectra, each plot represents the averaged results from PSD functions of 257 equal length time series data segments, each of which was normalized by its respective mean-square value σ^2.

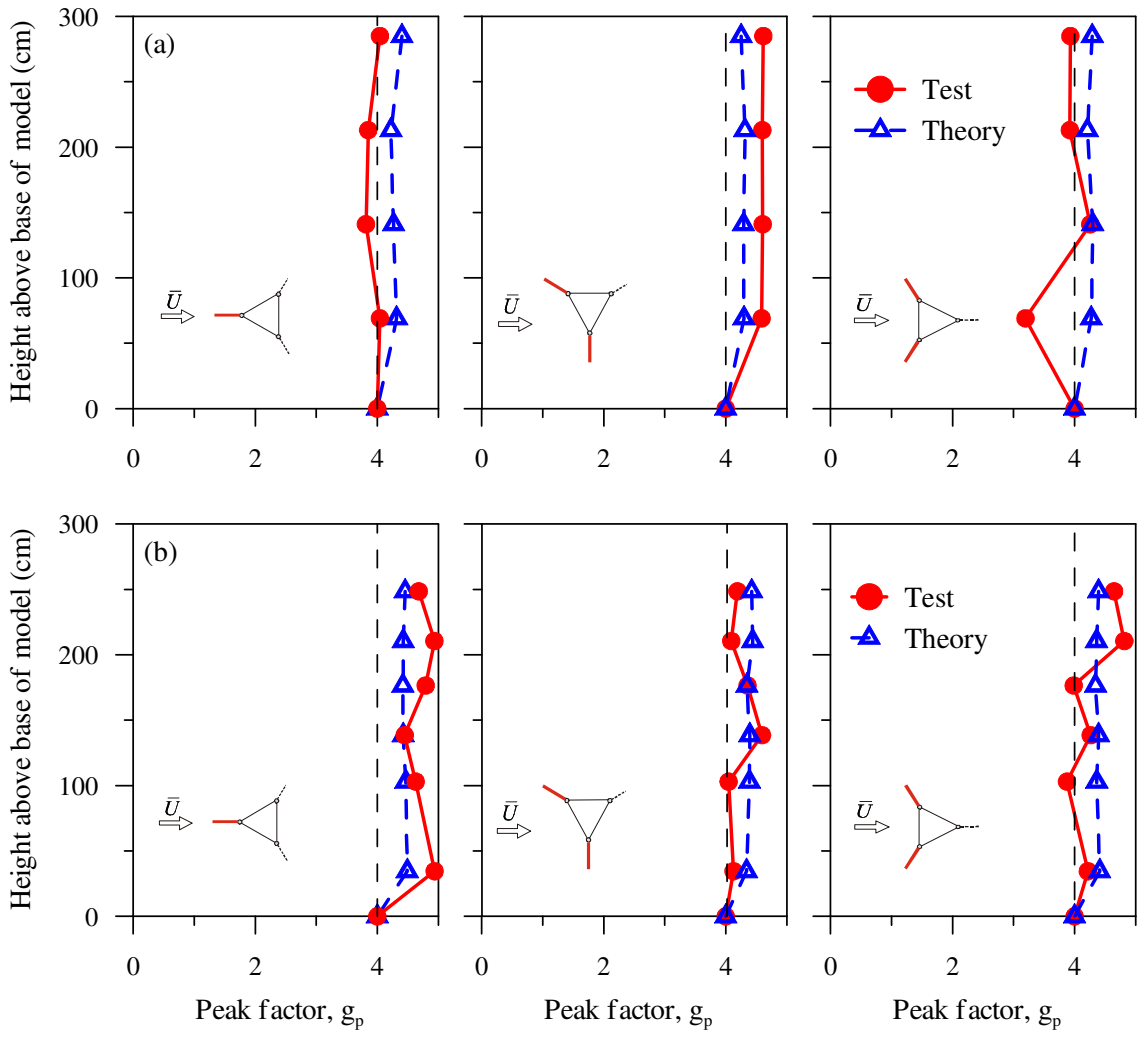

Figure 5.13. Comparison of measured and theoretical peak factors (g_p) in over water conditions: (a) alongwind displacements; and (b) alongwind bending moments.

Table 5.5. Comparison of average peak factors (g_p) at model and prototype scale (open country).

Wind Angle	Peak Factors	Model Scale		Prototype Scale		Average error (%)
		Measured	Predicted	Measured†	Predicted	
0°	Displacement	3.9	4.24	3.36	3.66	5.7
	Bending Moment	4.23	4.38	3.69	3.82	
30°	Displacement	3.84	4.22	3.31	3.64	8.1
	Bending Moment	4.01	4.32	3.48	3.75	
60°	Displacement	3.87	4.23	3.34	3.65	4.3
	Bending Moment	4.27	4.28	3.7	3.71	

†Estimated on the basis of the ratio between predicted prototype to model scale values.

Table 5.6. Comparison of average peak factors (g_p) at model and prototype scale (over water).

Wind Angle	Peak Factors	Model Scale		Prototype Scale		Average error (%)
		Measured	Predicted	Measured†	Predicted	
0°	Displacement	3.938	4.3	3.414	3.731	7.5
	Bending Moment	4.74	4.45	4.16	3.9	
30°	Displacement	4.6	4.29	3.99	3.71	5.6
	Bending Moment	4.23	4.39	3.69	3.83	
60°	Displacement	3.83	4.27	3.31	3.69	6.1
	Bending Moment	4.3	4.38	3.75	3.82	

†Estimated on the basis of the ratio between predicted prototype to model scale values.

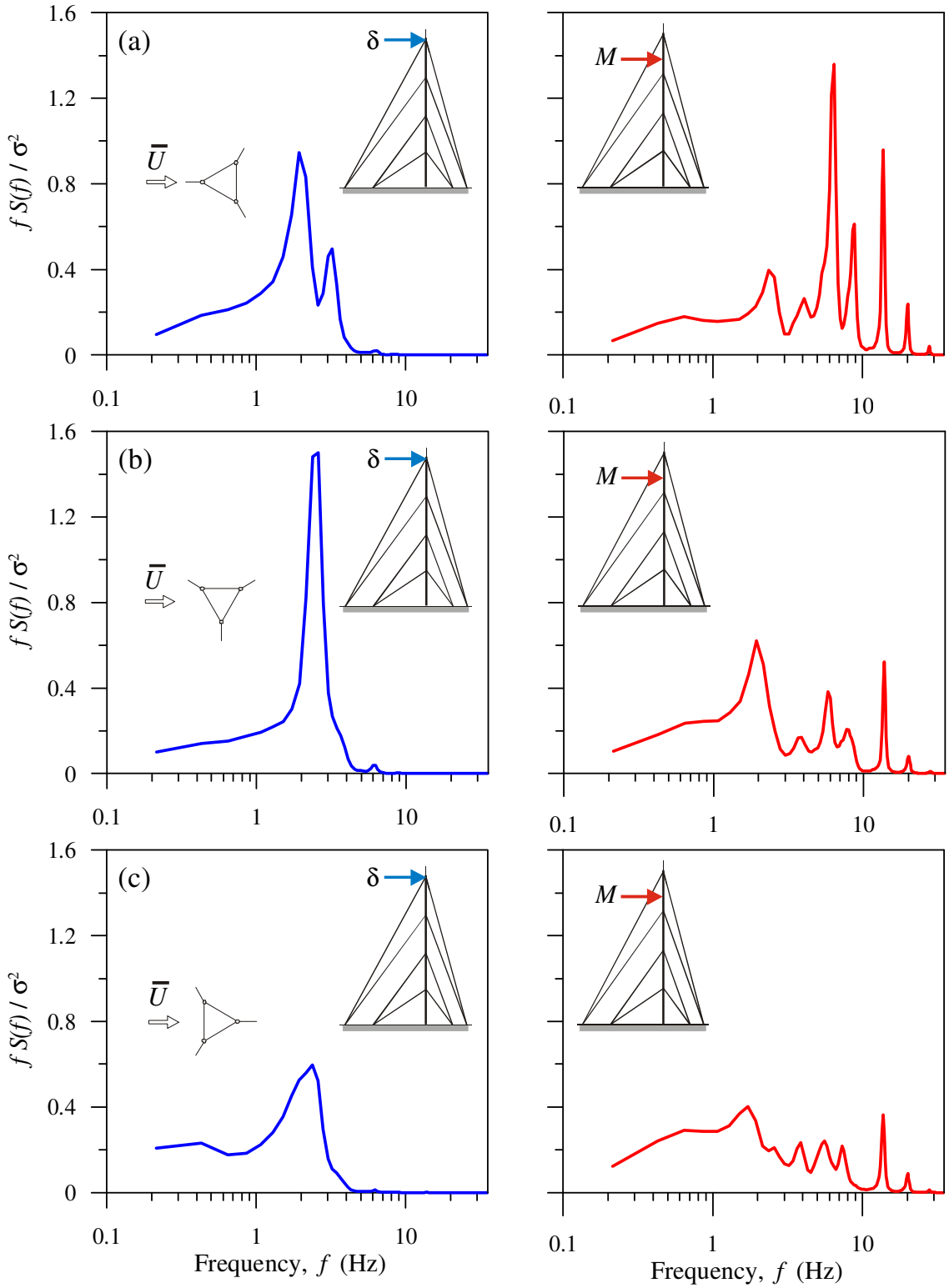

Figure 5.14. Example power spectra in open country exposure for alongwind mast deflection (δ) at the top guy level and midspan bending moment (M) in the penultimate span: (a) wind at 0°; (b) wind at 30°; and (c) wind at 60°.

As expected, dynamic displacements were dominated by the low frequency background response, represented by the wide region below approximately 1.5 Hz, as well as by a relatively few of the lower vibration modes indicated by the peaks in the plots starting at approximate 2 Hz. Spectra for dynamic bending moments, on the other hand, exhibit six or more clearly identifiable resonant peaks in the higher frequency range, indicating the active participation of higher bending modes in the bending response.

These spectral characteristics are consistent with the trends observed in the dynamic peak factors. As illustrated in Table 5.5 and Table 5.6, the peak factors for bending moments are generally larger than those of displacements as a result of the significant contributions provided by the higher modes of vibration for bending moments, while the dynamic response of displacement was principally due to the lowest few modes of vibration (Eq. 5.6). Very similar results were obtained using the frequency domain analysis method.

5.7 STRUCTURAL DYNAMIC CHARACTERISTICS

5.7.1 Overview

The dynamic characteristics of guyed masts such as natural frequencies, mode shapes and structural damping were measured from recorded free vibration acceleration time histories measured in still air (no wind) conditions. The response of the guyed mast model was measured at 20 points along the mast, four of which were at the guy attachment levels, and the remaining 16 points located at each mid-span of the mast cladding sections. Two orthogonal response components were measured at each point.

As introduced in Section 4.7, measured horizontal mast acceleration time histories excited by suddenly applied (impact) forces applied to the mast were recorded for 16 instrumentation setups. Each data set included the acceleration time histories at the four guy attachment points, which were used as stationary reference points, as well as at one location along the midspan regions of the mast measured by a pair of movable accelerometers. Each acceleration time history record consisted of 32768 points recorded at a time increment of 0.009 seconds.

The dynamic characteristics presented herein are based on information from the measurement derived in still air, combined, wherever possible, with properties obtained from the turbulent wind measurements. It should be noted, however, that the collection of experimental data on natural frequencies and mode shapes was particularly difficult since several of the lower modes were not well separated and, therefore, difficult to distinguish.

5.7.2 MACEC SOFTWARE

The commercially available program MACEC (Katholieke University, 1999), specifically intended for modal data analysis, was employed to extract the dynamic properties from the measured acceleration time histories. The stochastic subspace identification (*ssi*) method was used for this purpose, which is based in the time domain method, and tends to provide more accurate results than frequency based methods (MACEC tutorial, 1999). In order to combine the results from all 16 still air measurement set-ups, the results for each data set were normalized by the response at the top guy level, which was used as a common reference for all set ups.

5.7.3 Natural Frequencies

The degree of similarity in model characteristics between the wind tunnel and numerical models was evaluated by comparing corresponding natural frequencies and mode shapes. To determine the natural frequencies, it was necessary to examine the respective power spectral density (PSD) functions of the measured acceleration, which defined the distribution of acceleration with respect to frequency.

Figure 5.15 illustrates an example of the measured free vibration acceleration spectra obtained from one measurement setup involving five measurement points, including four guy attachment points (denoted as a_{1x}, a_{2x}, a_{3x} and a_{4x}) and one location at the mid-span of a cladding section (denoted as a_{mx}) in still air condition. In this approach, the natural frequencies were estimated by locating the highest spectrum values at each pronounced peak. It can be seen from Figure 5.15 that the dominant peaks tend to appear at the same frequency for the various locations on the model, thereby denoting a system natural frequency. The amplitudes at the peak locations were then used to derive the corresponding mode shapes. It is also apparent that several of the higher modes are indicated by clearly defined peaks on the spectra while many of the lower modes, especially with frequencies less than 8 Hz, overlap to some degree and are thus less clearly defined. This demonstrates why the lower modes, dominated by guy vibrations, were more difficult to measure accurately.

Since the model properties were inferred from measured acceleration spectra, only those modes exhibiting significant mast motion could be determined. Also, as mentioned previously, some modes could not be distinguished from one another in the

measured data due to a number of closely spaced modes that were evident in the 0 – 10 Hz range.

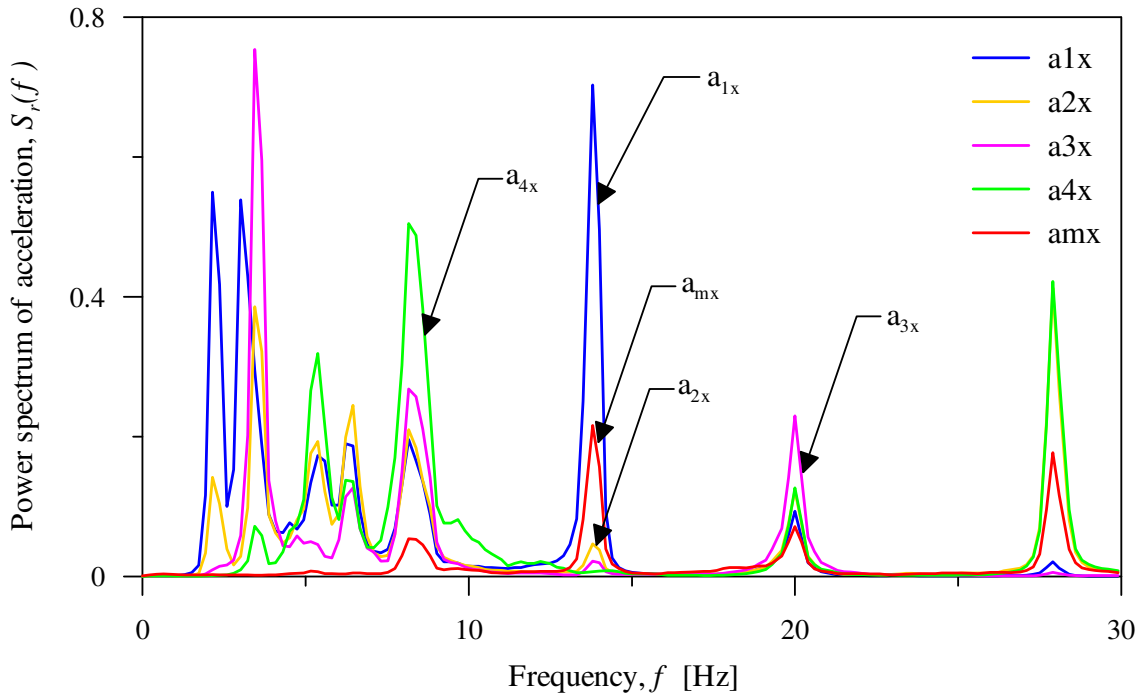

Figure 5.15. Example acceleration spectra at five locations along the mast in still air, free vibration conditions.

A comparison between natural frequencies extracted from measured data and those predicted analytically for the lowest eight detectable vibration modes in still air flow is provided in Table 5.7; a similar comparison for open country exposure at various wind azimuths is summarized in Table 5.8. In general, the agreement between measured and theoretical values was fairly close (with one exception, between 2.3% - 7.9% error), with the numerical model providing slightly higher estimates of natural frequencies, on average. It should be noted, though, as suggested in Figure 5.15, that it was often difficult to determine precisely which of the closely spaced measured modes actually corresponded to specific theoretical modes. Therefore, in Table 5.7, where a

measured frequency fell between two predicted values, the error between the measured values and the average of the two adjacent predicted frequencies is reported.

Table 5.7. Comparison of natural frequencies in still air flow.

Vibration mode	Natural Frequency (Hz)		Error (%)
	Measured	Predicted	
1	2.57	2.50	2.7
2	3.545	2.71 4.22	2.3
3	5.645	5.2	7.9
4	8.366	8.96	7.1
5	13.74	11.62 14.89	3.5
6	19.95	22.82	14.4
7	27.95	29.95	7.1
8	35.82	37.71	5.2

Table 5.8. Comparison of natural frequencies in open country exposure.

Vibration mode	Wind at 0^o		Wind at 30^o		Wind at 60^o	
	Measured (Hz)	Predicted (Hz)	Measured (Hz)	Predicted (Hz)	Measured (Hz)	Predicted (Hz)
1	2.08	2.60	2.64	2.50	2.47	2.60
2	3.11	3.30	-	3.76	3.78	3.45
3	4.13	4.20	-	4.44	-	4.06
4	6.37	6.64	6.15	6.40	6.29	6.65
5	8.79	8.96	8.86	7.23	8.93	9.32
6	13.72	15.00	13.73	13.08	13.80	14.63
7	20.02	22.83	20.01	22.87	20.09	23.00
8	27.92	29.95	28.03	29.96	28.05	29.82
9	35.83	37.71	36.00	37.71	36.01	37.76
10	46.76	48.51	-	48.49	46.45	48.47

5.7.4 Mode Shapes

The measured vibration mode shapes for the mast in still air and computed mode shapes from the frequency domain analytical model are illustrated in Figure 5.16, in which red solid crosses represent the four guy levels. Because the mode shapes are dimensionless, the numerical and measured shapes were all scaled with respect to the top guy level (h = 285 m). While the frequency domain shapes were calculated directly as part of the required eigenvalue analysis, measured mode shapes were inferred from the relative magnitude of resonant peaks on the acceleration spectra at various elevations on the mast.

In addition, example vibration mode shapes determined on the basis of wind tunnel measurements and frequency domain analysis results are also presented in Figure 5.17. For the wind tunnel measurements, only four measurement points (i.e. the accelerometers at the four guy support levels) were obtained. It should be noted that the data presented here were taken from tests performed under open country exposure at the maximum wind speeds considered for each wind direction; due to the nonlinear structural properties of the guys, therefore, it is expected that these dynamic properties may differ from those under still air conditions.

As can be seen in Figure 5.16 and Figure 5.17, the selected measured and predicted mode shapes are generally in good agreement, exhibiting, in most cases, the same basic pattern and number of node (zero) points, if not always similar magnitudes at all elevations. This was not true, however, for all modes that were investigated. In many cases, the experimental mode shapes could not be adequately defined due to difficulties in distinguishing between closely spaced modal peaks in the lower

frequency range (0-10 Hz), although a number of peaks were obvious in the acceleration spectra.

Several features of the vibration modes were noted. First of all, as expected, the curvature of the deflected mast shape increased with increasing natural frequency. The numerical model clearly showed that the lower modes were dominated by large amplitude guy vibrations, starting with those at the top support level for the fundamental mode and moving downward to lower guy levels for successive modes.

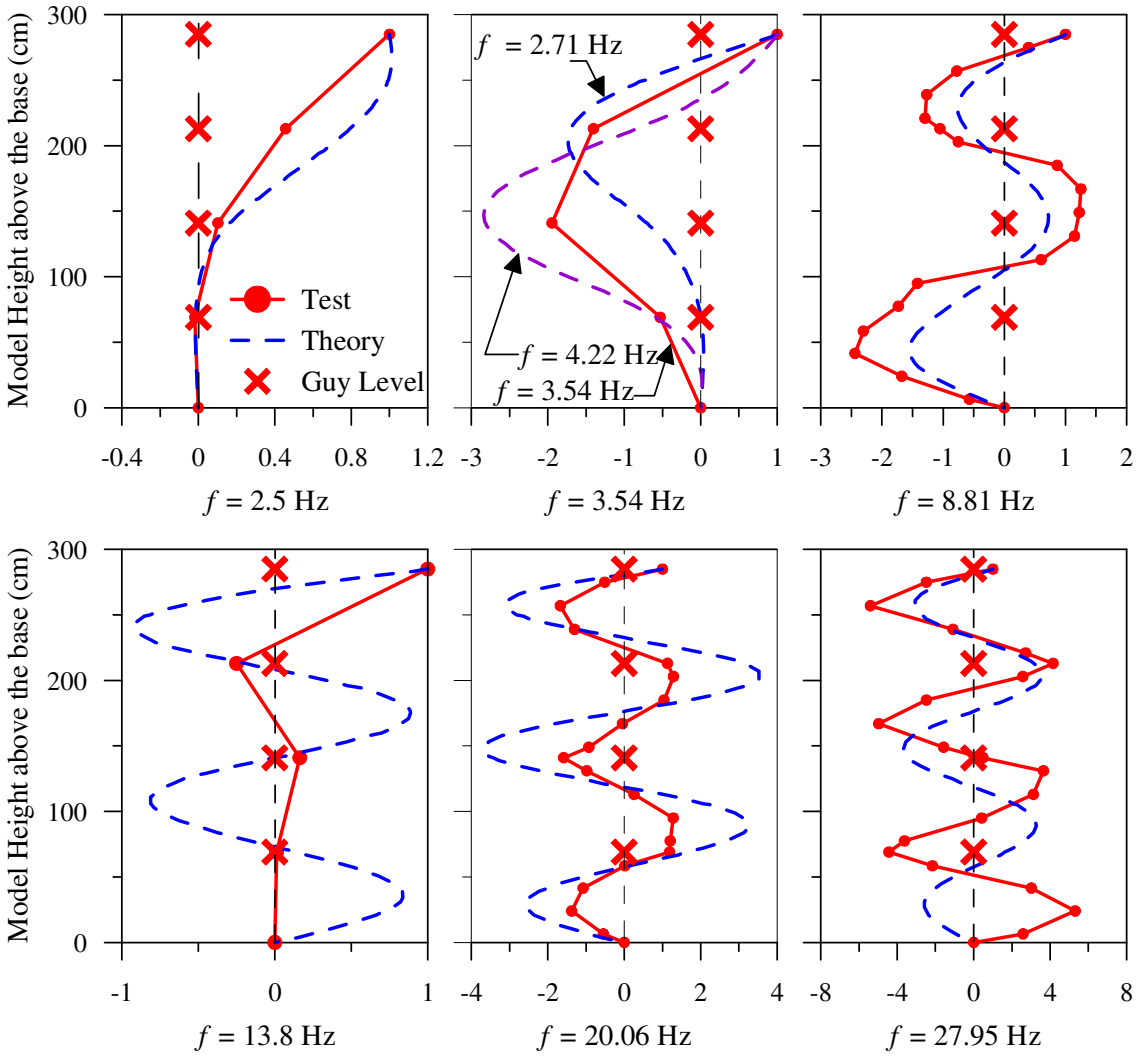

Figure 5.16. Comparison of measured and predicted vibration mode shapes in still air conditions.

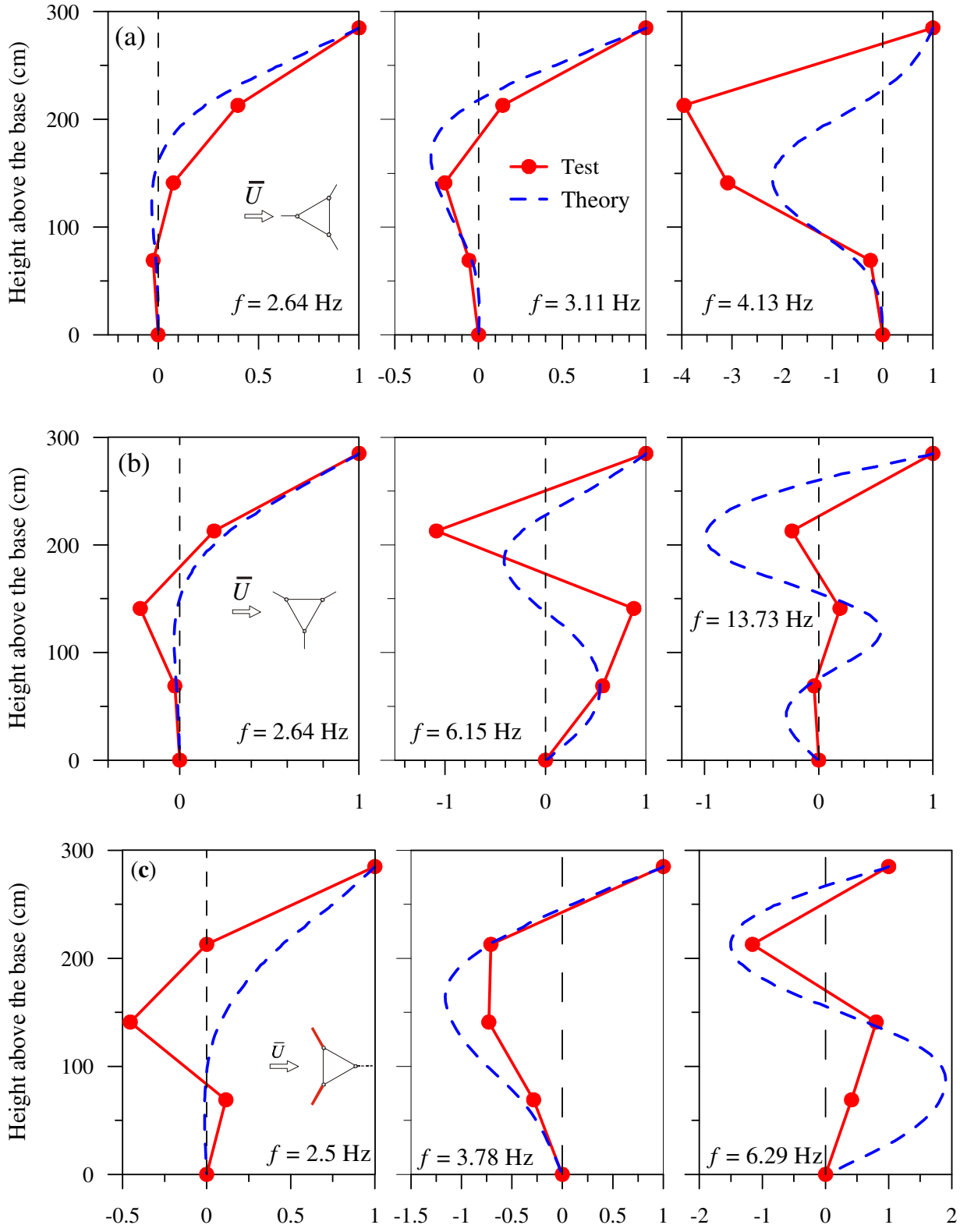

Figure 5.17. Comparison of measured and predicted vibration mode shapes found under open country exposure: (a) wind at 0°; (b) wind at 30°; and (c) wind at 60°.

Higher modes, on the other hand, were characterized mainly by mast motion, with little guy vibration.

Secondly, a number of complex modes (in which each part of the structure has not only its own amplitude of vibration, but also its own temporal phase angle) were indicated by the *ssi* analysis. In part, these complex modes may be due to the nonlinear guy response, as this is a characteristic of nonlinear systems. On the other hand, the complex modes may be an artifact of the modal extraction analysis, related to the difficulty in distinguishing between closely spaced modes. Therefore, when the structure was excited at a frequency between two closely spaced natural frequencies, the apparent measured mode shapes may have resulted from a combination of two pure mode shapes, as demonstrated in Figure 5.16 for $f = 3.54$ Hz.

It can be concluded, though, that experimental results generally supported theoretically derived mode shapes in cases where reliable comparisons were feasible.

5.7.5 Structural Damping

Structural damping measurements for the guyed mast model were carried out in still wind conditions by means of impact-induced excitation (Section 4.7). Because of the still air conditions for these tests, it was assumed that energy dissipation due to air viscosity was negligible. Therefore, all observed damping was attributed to the structure.

An example recorded acceleration time history over 50 seconds at a mast midspan location under repeated impact load, is provided in Figure 5.18. Here, the damping is readily apparent in the exponentially decaying response amplitudes over time.

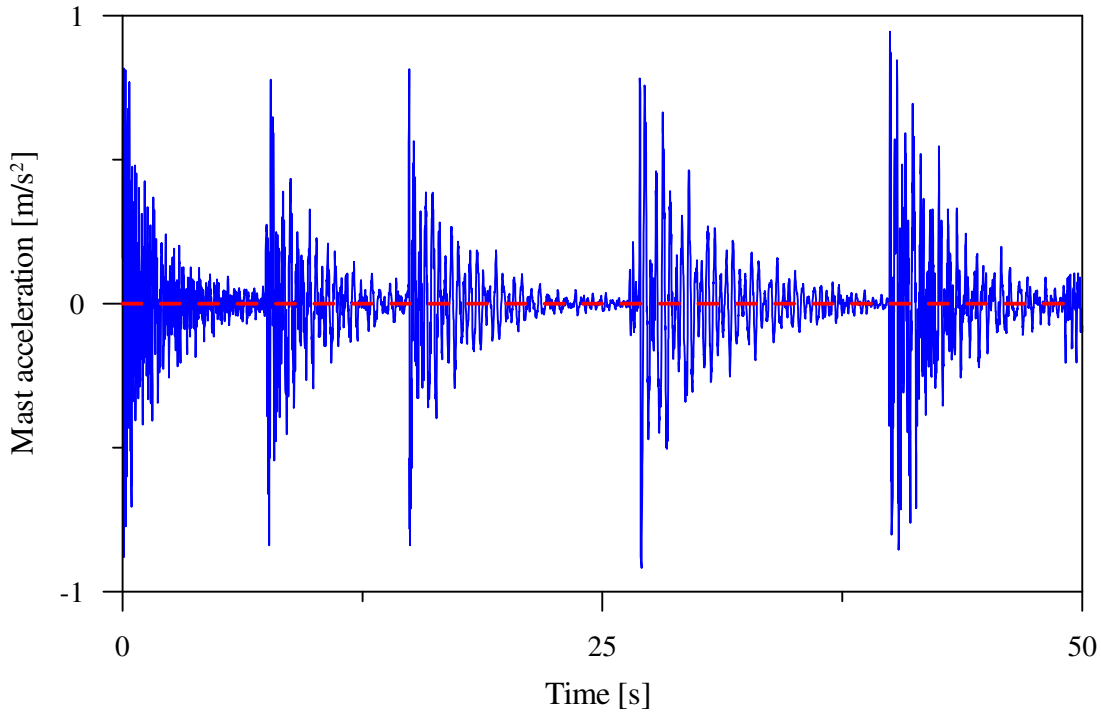

Figure 5.18. Time history of mast acceleration in forced vibration in 50 seconds.

The computer program MACEC (see Section 5.7.2) was also employed to analyse the traces and, thus, to determine the structural damping using the *ssi* time domain method. The average computed structural damping ratios for twelve modes are tabulated in Table 5.9. These results suggest structural damping ratios of the model varying from 0.5% to 5% of the critical damping, with higher damping ratios generally observed for the lower modes dominated by vibration of the guys.

Table 5.9. The averaged measured structural damping ratio of model in different modes.

Mode	1	2	3	4	5	6	7	8	9	10	11	12
Frequency (Hz)	2.22	3.48	5.39	6.37	8.29	13.8	19.9	27.8	35.68	41.6	47.2	53.9
Damping ζ (%)	2.54	1.60	5.89	3.14	3.08	0.69	1.26	0.64	0.6	0.65	0.67	0.51

It should be noted that, due to the complex dynamic behavior of guyed masts caused by the interaction of the mast and the nonlinear guys, the structural damping was very difficult to capture accurately. The structural damping ratio adopted for use in the frequency domain analysis model in this study was taken as 0.5% of critical for all modes; therefore, on the basis of the measured structural damping ratios, it may be expected that predicted dynamic responses in the lower modes would be overestimated slightly due to the higher observed damping in these modes.

Approximate structural damping ratios representing the composite behaviour of all active vibration modes were also estimated based on the decaying characteristics of the free vibration response envelopes, such as those shown in Figure 5.18 (Clough and Penzien, 1975). These composite damping ratios were found to range from 0.2% to 0.6% for all the data sets considered.

5.8 DYNAMIC CHARACTERISTICS AT DIFFERENT WIND SPEEDS

5.8.1 Introduction

A number of assumptions were made in the design of the scaled model. First, it was assumed that drag properties were Reynolds number independent. Secondly, aerodynamic instabilities, including vortex shedding, were ignored. Finally, the scaled model properties were defined for still air conditions, assuming that nonlinear effects associated with changes in cable sag under wind loads would also be adequately represented by the scaling laws.

A series of wind tunnel tests were therefore conducted under different wind velocities to investigate the factors mentioned above. In these tests, the mean wind speed was continuously increased in constant increments from 0.58 m/s to 5.5 m/s (5.8

m/s to 55 m/s at full scale), measured at the reference height of h = 2.62 m above the floor. The corresponding dynamic characteristics, including bending moments, displacements and the power spectra, are presented herein. Trends in the dynamic response characteristics were then used to assess the influence of Reynolds number and other wind speed related effects.

5.8.2 Bending Moments

As presented in Chapter 3, the wind drag force on structures may be dependent upon Reynolds number (Fig. 3.8) which, in turn, is determined by the wind speed (Eq. 3.19). Therefore, in order to study Reynolds number effects on the guyed mast model, the dynamic response at several wind speeds are presented and compared, including the mean response, *rms* amplitude and peak response, all in the alongwind direction.

The overall variation of bending moments of the guyed mast at three different wind angles is shown in Figure 5.19 for open country conditions. Each graph within this figure includes a series of six typical response patterns for wind velocities varying from 1.08 m/s to 5.56 m/s. Similar dynamic response comparisons in over water conditions are shown in Figure 5.20, including a series of seven typical response patterns at different wind speeds varying from 0.95 m/s to 5.56 m/s.

Since the wind drag force is proportional to the second power of the wind velocity, the amplitude of the dynamic response (bending moments and displacements) in these and subsequent plots are normalized by the square of the reference wind speed:

$$r_n = \frac{r\,\overline{U}_{ref}^{\,2}}{\overline{U}^{\,2}} \tag{5.7}$$

where r_n is normalized response, r is the measured dynamic response under mean

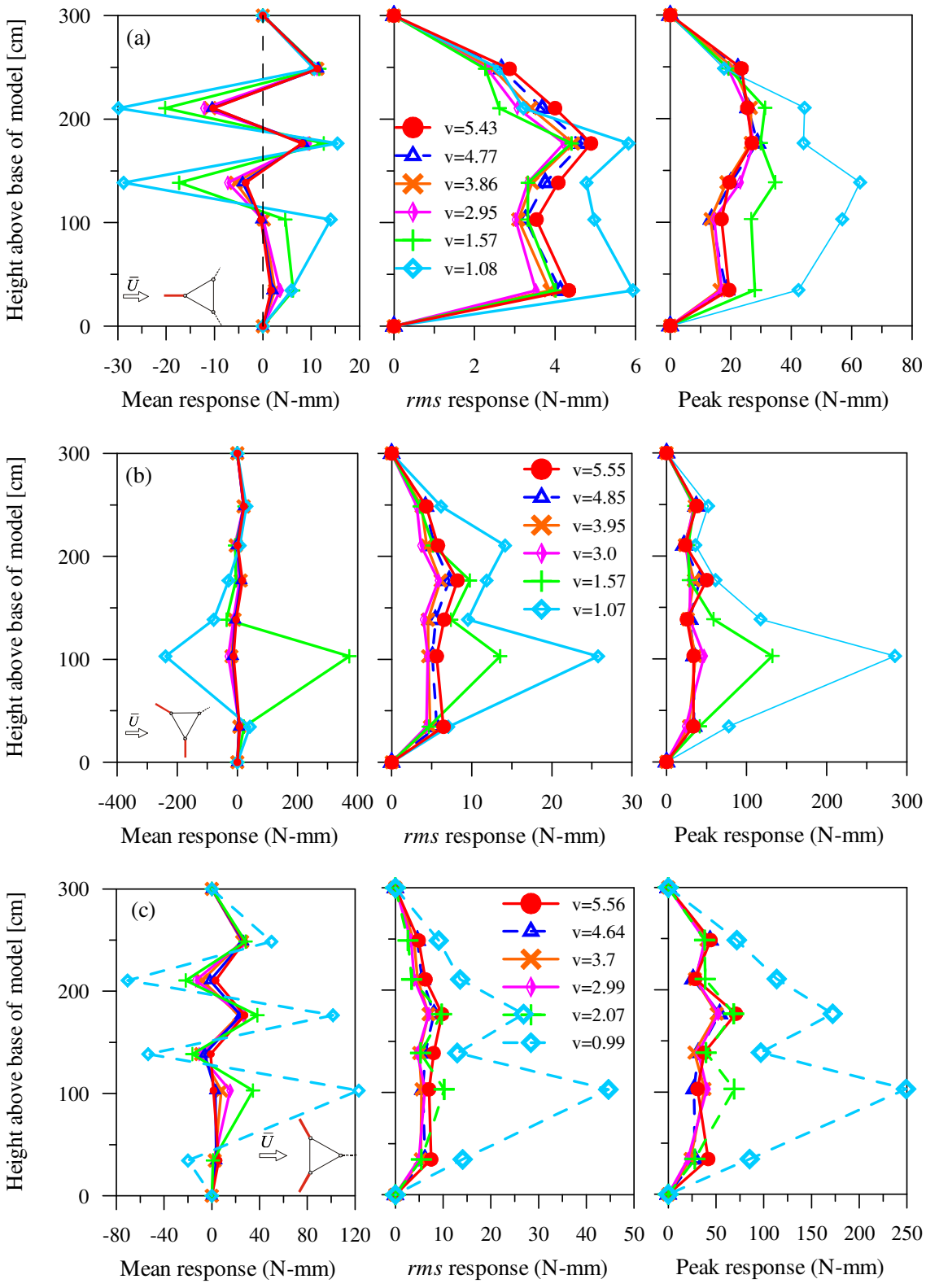

Figure 5.19. Measured normalized alongwind bending moments in open country conditions at various wind speeds (m/s): (a) wind at 0°; (b) wind at 30°; and (c) wind at 60°.

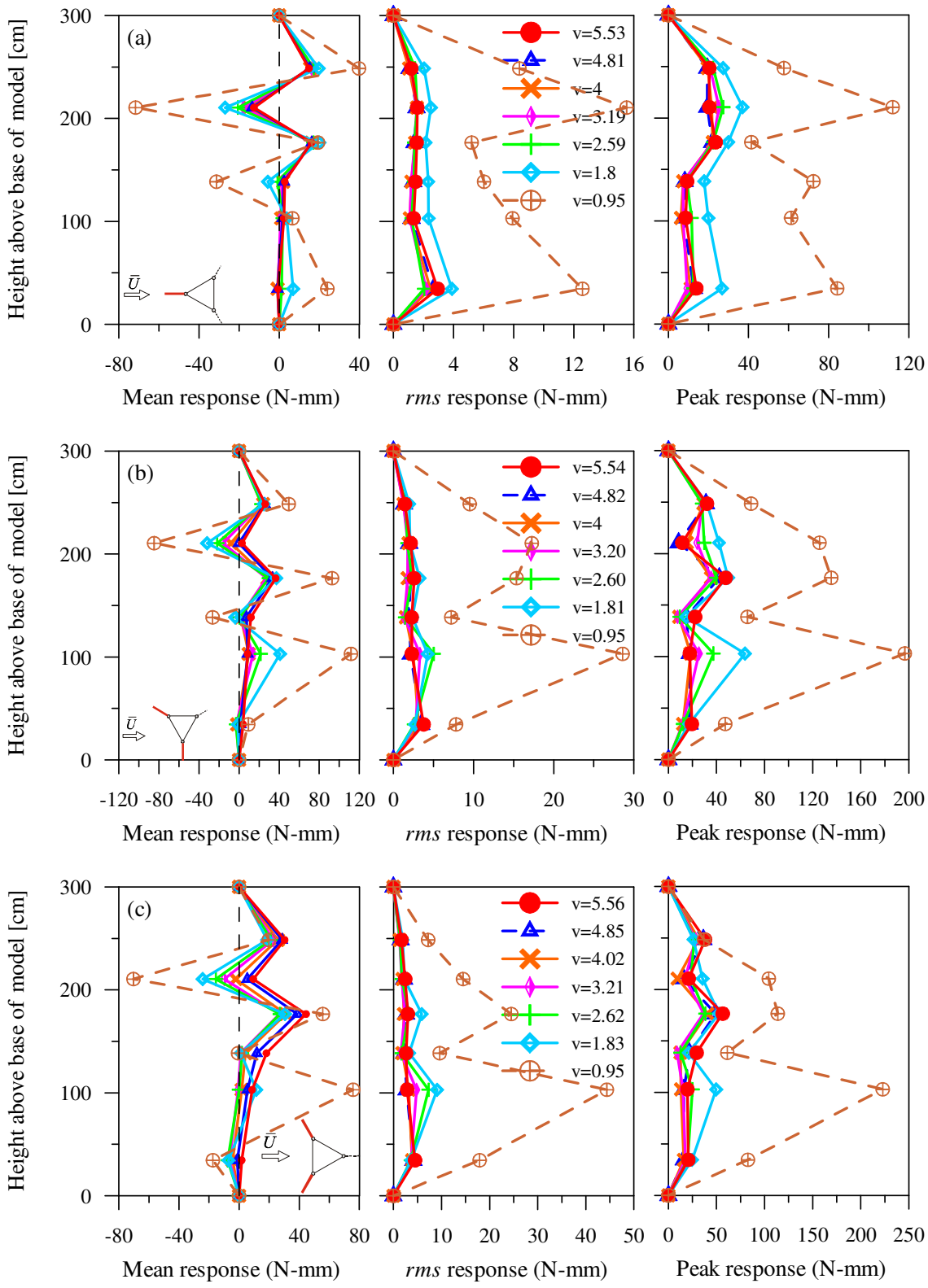

Figure 5.20. Measured normalized alongwind bending moments in over water conditions at various wind speeds (m/s): (a) wind at 0°; (b) wind at 30°; and (c) wind at 60°.

wind speed $\overline{U}$ and $\overline{U}_{ref}$ is the reference mean wind speed, which was chosen as the maximum wind speed in the relevant test series. Here, all wind speeds refer to the mean measured value at the reference Pitot tube, located 2.62 m above the tunnel floor.

In general, the normalized bending moment response for a given wind condition was similar for all wind speeds with all plots falling within a relatively narrow band. The striking exceptions to this occurred at the lowest wind speeds in each series (approximately 1.0 m/s), for which the normalized response increased significantly relative to other wind speeds. In part, this larger relative response at low wind speeds may reflect a sudden, large increase in the drag resistance of the cylindrical components at very low Reynolds numbers (less than 10^4), as previously suggested by Simiu and Scanlan (1996). A rapid increase in the stiffness of the windward guys as the mast begins to deflect from its still air position (Sparling 1995) may also contribute to the observed response differences at low wind speeds.

To facilitate comparisons at the higher wind speeds that are of most interest, the data from Figure 5.19 have been plotted in Figure 5.21 for wind speeds in the range of about 2.95 m/s to 5.56 m/s. As seen, with wind at 0^o, the normalized mean, *rms* and peak response at the four different wind speeds in this higher range are all in excellent agreement; for wind at 30^o and 60^o, the distributions are all very similar as well. The lack of any significant trend in the mean normalized response (the left most plots on Figure 5.19 to Figure 5.21) for all three wind directions at wind speeds above 3 m/s suggests that drag characteristics were relatively insensitive to wind speed over that range. Also, the predictable normalized peak response in both the along-wind and across-wind directions at all wind speeds tested provided no evidence of any tendency

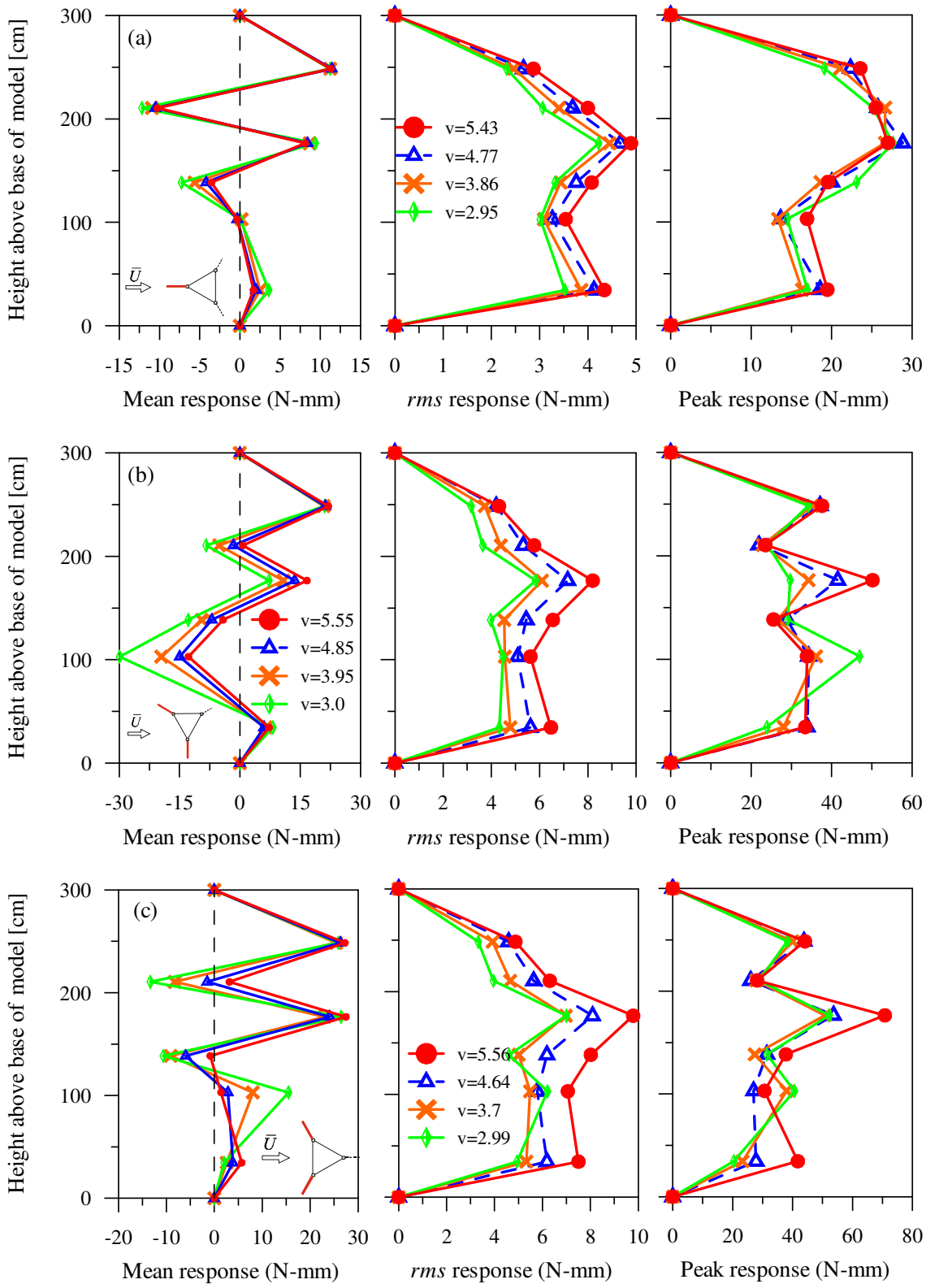

Figure 5.21. Measured normalized alongwind bending moments in open country conditions at wind speeds between 2.95 m/s to 5.56 m/s: (a) wind at 0°; (b) wind at 30°; and (c) wind at 60°.

toward the development of aerodynamic instabilities, including vortex shedding, which would have manifested themselves by a sudden increase in the relative response levels at particular wind speeds. Although there appears to be a slight slow, consistent increase in the level of the normalized *rms* response (the middle plots on Figure 5.21) with increasing wind speeds, this may simply reflect the expected shift in the turbulent power spectrum toward the higher frequency range that contributes heavily to the resonant bending moment response.

5.8.3 Displacement

Similarly, the variation of mast displacements at the four guy support levels at seven wind speed increments in open country exposure are presented in Figure 5.22. As was done for the bending moment response, the displacement amplitudes presented here have been normalized by the square of the wind speed (Eq 5.7). The trends observed in the normalized displacements are generally similar with those discussed previously for bending moments. As illustrated, with wind speed of 2 m/s or lower, a marked increase is evident in the normalized displacement response, likely due to higher cylindrical drag characteristics at low Reynolds numbers, as discussed in the previous section.

The normalized displacement data are replotted for wind speeds in the range of 2.95 m/s to 5.56 m/s in Figure 5.23. In general, the mean and peak dynamic normalized responses were very similar for these stronger wind conditions. Unlike bending moments, there was no evidence of a trend of increasing normalized dynamic response at higher wind speeds since the lower modes that dominate displacement response would be influenced to a lesser degree by the shift to increasing frequencies in the turbulence.

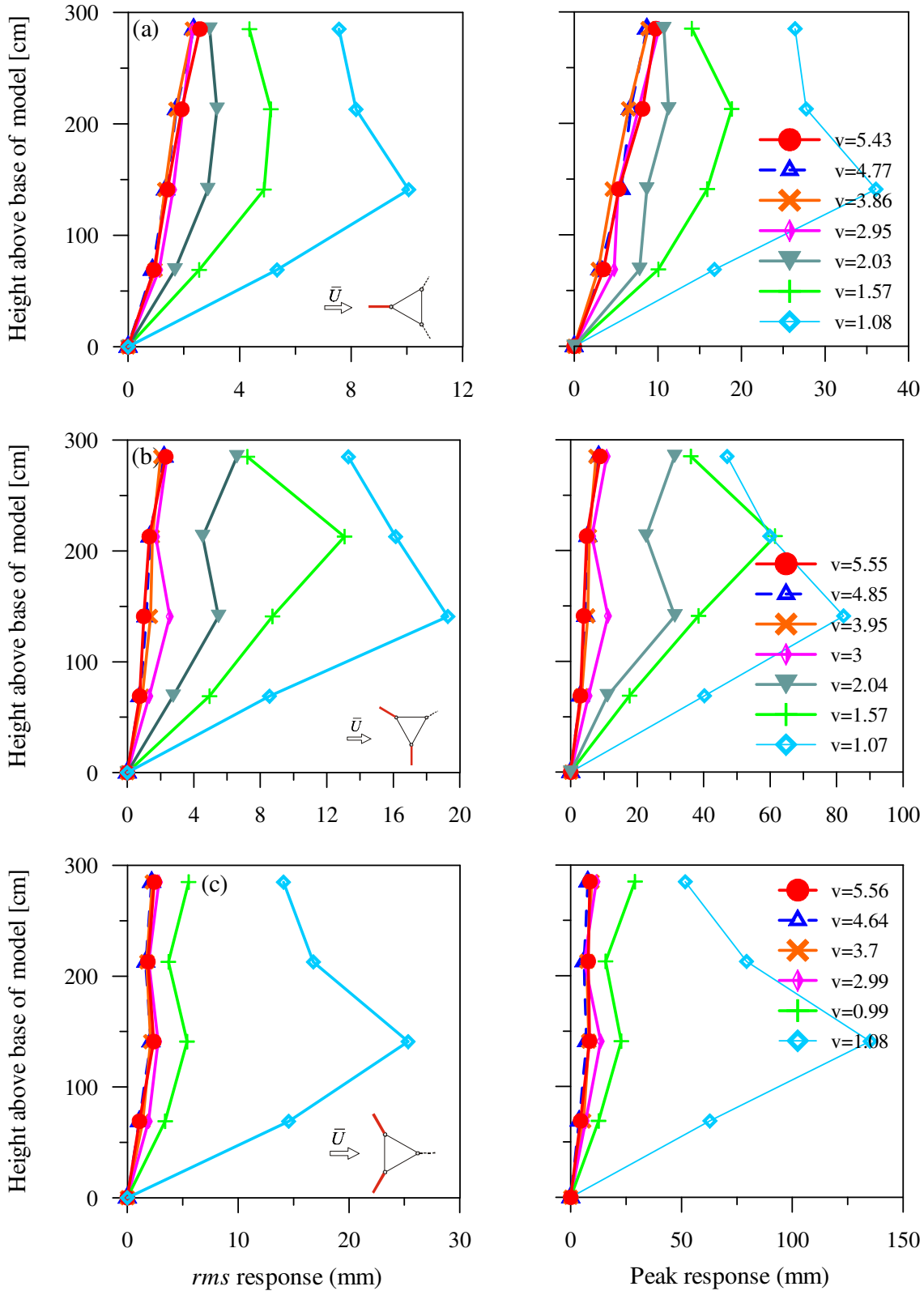

Figure 5.22. Measured normalized alongwind mast displacements at various wind speeds in open country conditions: (a) wind at 0°; (b) wind at 30°; and (c) wind at 60°.

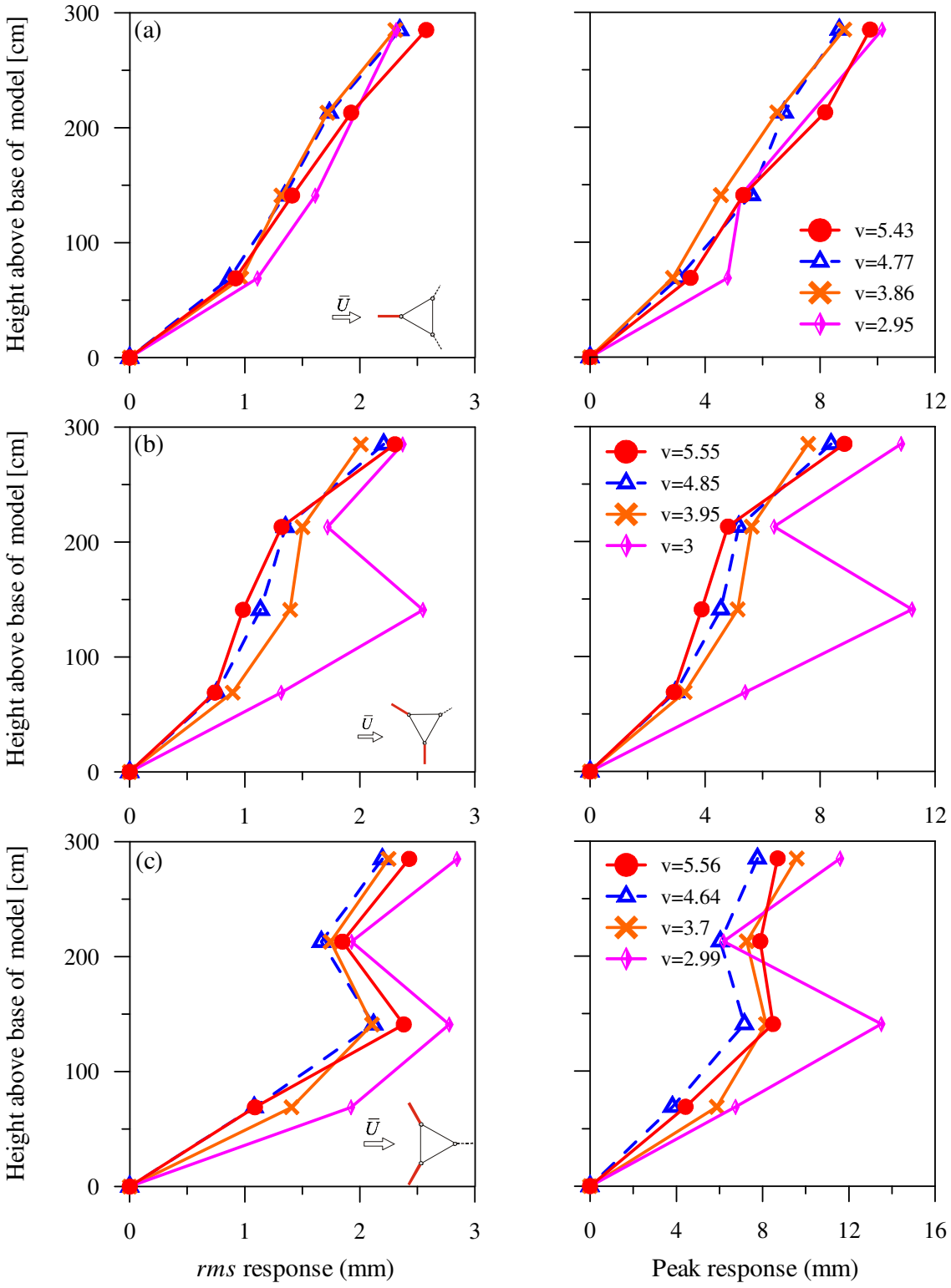

Figure 5.23. Measured normalized alongwind mast displacements for wind speeds between 2.95 m/s and 5.56 m/s in open country conditions: (a) wind at 0°; (b) wind at 30°; and (c) wind at 60°.

The rather significant discrepancies in mean normalized displacement noted at wind speeds near 3 m/s for wind at 30^o and 60^o, may be indicative that nonlinear effects associated with guy sag were still evident at these wind speeds, but became less prominent as the wind speed increased further.

Overall, then, the results of these tests suggest that the Reynolds number dependency of the drag forces in this model study were relatively weak for stronger winds with speeds higher than 3 m/s. Furthermore, no evidence of aerodynamic instability was detected over the range of wind speeds investigated.

5.8.4 Power Spectra of Mast Displacement Based on Laser Transducer Measurements

The guyed mast displacement at the top guy level (285 m at full scale height) in the alongwind direction was also measured by a non-contacting type of laser displacement transducer (see Fig. 4.9) mounted on the roof of the wind tunnel. The instantaneous displacements were recorded at scaled wind speeds varying from 0.046 m/s to 5.5 m/s for three different wind directions in both open country and over water exposure. The normalized power spectra of the displacement at eight different wind speeds are plotted in Figure 5.24, showing the spectral variation with increasing wind speeds. Here, smoothed spectra obtained by averaging results from multiple segments have been normalized by the mean-square value $\tilde{r}^2$ of the measured response for each test; again, the spectra have been plotted in the form of $f\,S_r(f)$ vs. $\ln(f)$ to facilitate comparisons over wider frequency ranges.

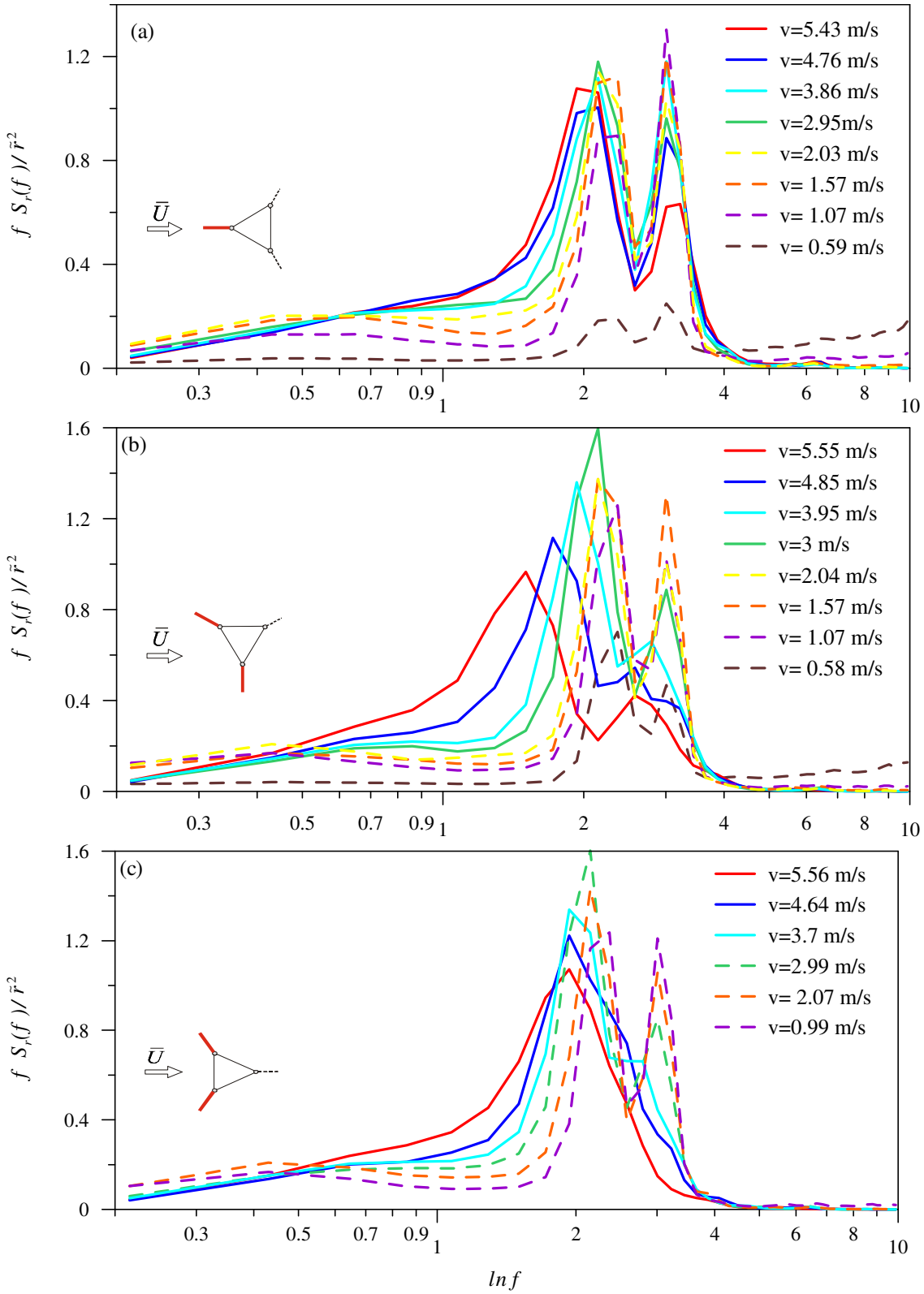

Figure 5.24. Power spectra of displacement at the top of the mast in open country exposure at varying wind speed, measured by a laser transducer: (a) wind at 0°; (b) wind at 30°; and (c) wind at 60°.

From Figure 5.24 (a), (b) and (c), it can be seen that the spectral distributions in various wind conditions are fairly similar. In all cases, it is evident that the resonant components of the displacements at the top of the mast are dominated by the first and second modes (approximately 2.5 and 3.2 Hz, respectively, as discussed in Section 5.7.3). In addition, significant response is also apparent in the wide, low frequency range associated with the quasi-static background response. This finding is consistent with results from the numerical model, which suggested that mast displacements were generally contributed by lower modes, which are dominated by the slack upper guy cables. It is also shown in Figure 5.24 that, with the increasing wind speeds, the background portion of the response increases relative to the resonant component. Furthermore, the energy distribution is seen to shift gradually to accentuate the first mode response (approximately 2.5 Hz) at the expense of the second mode with the increasing wind speeds. As an example, when wind speed was 0.59 m/s, both first and second modes contribute almost same portion to the total response; for a wind speed of 5.5 m/s, on the other hand, the first mode dominates the mast motion with much less contributed from the second mode on a relative basis. This feature is particularly evident when wind at 60^{o}, for which the first mode accounts for almost all of the resonant displacement response at the top guy level at the higher wind speeds.

5.9 DRAG TEST RESULTS

As described in Section 4.8, a series of section tests were conducted at the University of Saskatchewan to measure the drag characteristics of a typical mast section. The measured effective drag areas ($C_D A$) of the mast section obtained from the drag tests with wind at 0^{o}, 30^{o} and 60^{o} are presented in Figure 5.25. The primary focus

of these tests was to investigate the Reynolds number (R_e) dependency of the drag force, as well as to determine the influence of wind direction on drag force. It is notable from Figure 5.25 that the effective drag area generally does not vary with Reynolds number for wind at 0^o and 60^o; hence, it may be concluded that the drag coefficient of the mast cladding is not dependent on Reynolds number for these directions, which was expected due to the fact that the mast is primarily composed of cladding sections with sharp corners, causing immediate flow separation. For wind at 30 degree, on the other hand, the drag coefficient at the lower wind speeds appears to be somewhat dependant on Reynolds number.

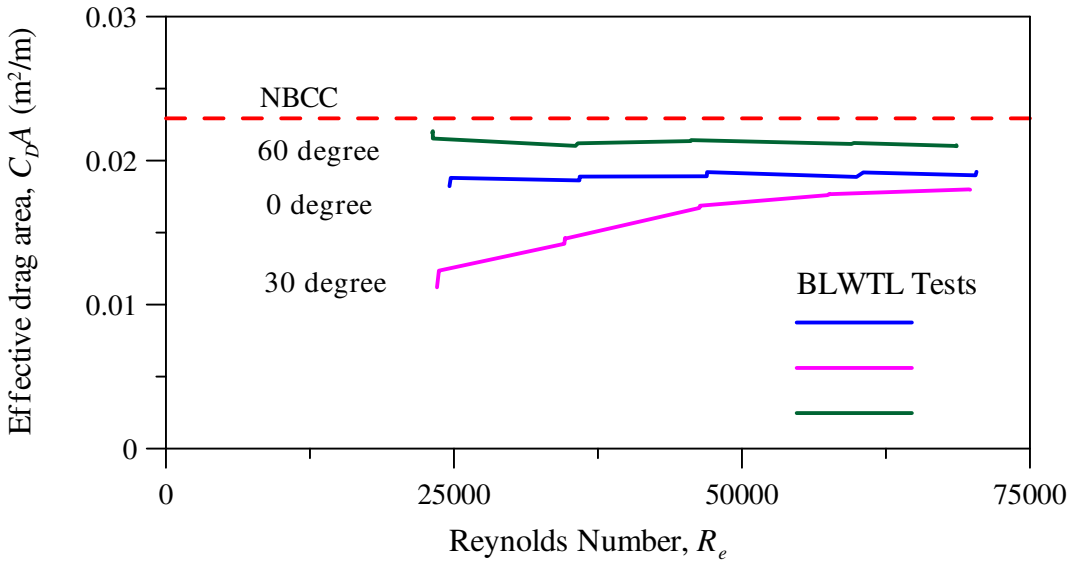

Figure 5.25. Comparison of effective drag area of the cladding for different wind directions based on section tests at the University of Saskatchewan.

A comparison of the measured effective drag areas with the computed theoretical value according to National Building Code (NBCC 1995), which is based on global shielding factors and was adopted for the numerical analytical model, is also presented in Figure 5.25. As seen in this figure, the theoretical drag area for the mast cladding

according to the NBCC (represented by the dashed red line) appears to provide a conservative estimate of the effective shielding factor. In addition, while no directional difference is implied in the NBCC method, measured effective drag area for the cladding was lowest when wind at 30^{o}, while highest drag area was found with the wind at 60^{o}. The section drag test results therefore indicate that the assumptions used in the analytical model for drag areas were highly conservative.

Due to limitations in the drag tests, however, the results presented herein must be viewed with caution. First, due to the limited height of the section model, tip vortices (end flow at the top) may have resulted in artificially low drag readings. Secondly, the drag test was conducted only in smooth flow, which may not provide an accurate representation of turbulent conditions. Finally, the wind speeds used for the section tests varied from 10 m/s to 30 m/s during the drag test, compared to speeds of 0 m/s to 5.5 m/s in the BLWTL wind tunnel tests. While these factors made it impossible to apply the findings of the section drag rests in a quantitative manner, they were useful in aiding in the qualitative interpretation of the model wind tunnel test results.

5.10 SUMMARY

The dynamic characteristics of a 300 m guyed mast were experimentally measured using wind tunnel tests on an aeroelastically scaled model, and the measured responses were compared with those obtained from a frequency domain analytical model. Comparisons of the results between the numerical model and the wind tunnel model were presented in terms of displacements, bending moments, peak factors, natural frequencies, mode shapes and structural damping. In addition, the bending moments,

displacements and the relative power spectra under different wind speeds varying from 0 m/s to 5.5 m/s were presented.

It is clear from the results that, considering the level of uncertainty involved, good agreement was observed between the experimental measurements and the theoretical dynamic response, especially for mast bending moments, as well as the relevant peak factors, with the numerical model results being somewhat conservative on average. In addition, the measured structural dynamic properties, such as natural frequencies, mode shapes and structural damping, were found to be satisfactorily similar to those predicted by the analytical model.

A detailed summary and listing of conclusions are reported in Chapter 6.

6. SUMMARY AND CONCLUSIONS

6.1 SUMMARY

A wind tunnel study was undertaken on a full aeroelastic model of a 300 m tall guyed mast in both open country (moderate turbulence) and over water (low turbulence) exposure to investigate the dynamic response characteristics of guys and guyed masts subjected to various wind conditions.

The primary objective of this study was to use wind tunnel testing to obtain reliable measurement data representing the dynamic response of a full-scale 300 m tall guyed mast under both open country and over water conditions. Although the dynamic response of telecommunication guyed masts subjected to wind loads has been routinely analyzed using a number of numerical models, typically in the frequency domain, insufficient experimental data are available to adequately validate the proposed analytical methods. Thus, the need for experiments to examine the dynamic response remains.

In this investigation, a representative 300 m tall guyed mast, designed in conformance with the Canadian design standard CSA-S37-01 (CSA 2001), was used as the prototype for the wind tunnel study. Representative properties for the prototype were selected on the basis of a parametric study of 41 existing masts of various sizes. The design wind speed was intended to represent a strong wind condition based on a survey of climatic data from 640 sites across Canada (NBCC 1995). A full aeroelastic

1:100 scale guyed mast model was designed and constructed, simulating the exterior geometry and the shape of the prototype as well as the stiffness, mass and drag characteristics according to Froude number scaling.

The wind tunnel test of the aeroelastic guyed mast model was carried out in both open country and over water exposure in the BLWTL to determine the nonlinear, wind-induced dynamic response of masts subjected to moderate and low turbulence flows. Three different wind azimuths (0^o, 30^o and 60^o) were examined to define the critical peak response.

Dynamic responses measured during the wind tunnel tests including dynamic displacements, bending moments, the corresponding response spectra and peak factors, as well as model properties such as natural frequencies, mode shapes and structural damping. Comparisons were made with predictions obtained from an existing frequency domain analysis model. It was found that good agreement was generally achieved between the frequency domain analytical model and the wind tunnel model.

6.2 CONCLUSIONS

The experimental results of the guyed mast dynamic response were compared with those from the frequency domain analysis model. The following conclusions can be drawn from this experimental investigation on a 300 m guyed mast:

1. Generally, the agreement of dynamic response characteristics between the measurement from the wind tunnel tests and the numerical model was satisfactory.
2. The degree of agreement between predicted and measured dynamic displacements depended on the direction of the wind relative to the mast and wind conditions. In open country exposure, with the wind parallel to the windward guy lane (wind at

0^o), the frequency domain analysis results underestimated the *rms* and peak dynamic displacements by a significant margin, while for other wind directions, the predicted displacements were similar to or greater than measured values. The numerical predictions were significantly higher over the top half of the mast, particularly with the wind at 60^o. There was some evidence to suggest that the nonlinear behaviour of slackened leeward guys helped reduce dynamic displacements, particularly near the top of the mast. In over water conditions, on the other hand, good agreement was observed between the measured and predicted dynamic displacements when the wind was blowing in the plane of the windward guy lane (wind at 0^o). For other directions, dynamic displacements tended to be overestimated by the frequency domain analysis, particularly in the upper half of the mast. Once again, the lower measured response was possibly due to nonlinear damping effects associated with vibrations of the highly slackened leeward guys on the upper levels of the mast, which may be beneficial in reducing dynamic mast displacements.

3. The magnitude and distribution of measured and predicted dynamic bending moments were acceptably similar all along the mast for the three wind directions considered in this study. As predicted by the frequency domain numerical analysis, measured dynamic (*rms*) bending moments were found to be distributed in a fairly uniform manner over much of the mast height. Mean (static) bending moments, on the other hand, were found to exhibit large variations over the mast height, along with near-zero response zones at points of contraflexure. These notable differences demonstrate the shortcomings of the "gust factor method"

employed by the Canadian Standard CSA-S37-01 (CSA 2001). The measured and predicted peak bending moments were found to be comparable in magnitude. The discrepancies, where they existed, could probably be attributed to either to uncertainty in model calibration factors, or to required assumptions in the numerical model, such as structural damping levels and effective drag coefficients.

4. Measured dynamic peak factors (the ratio of peak dynamic response to *rms* response) appeared to be slightly lower (9.3% for displacements and 3.6% for bending moments in open country exposure, 3.77% for displacements and 0.38% for bending moments in over water exposure) than the assumed value (4.0) adopted for the frequency domain model. Estimated full-scale peak factors based on the wind tunnel test results (3.33 for displacements and 3.62 for bending moments in open country exposure, as well as 3.57 for displacements and 3.86 for bending moments in over water exposure) were well within expected ranges and slightly lower than the commonly assumed design value of $g_p = 4.0$.

5. Where it was possible to clearly distinguish resonant peaks in the response spectra, the experimental results of natural frequencies and mode shapes of vibration agreed well with predicted values from the analytical model. However, the presence of closely spaced modes made it difficult to confidently identify all modes based on the measured time series results, in part due to coupling effects which could have contributed to the detection of apparently complex modes.

6. The vibration modes obtained from both the measurements and theory indicate that lowest modes were dominated by large guy movements at the top guy level

and small mast movements; the middle modes were characterized by coupled effects between the guyed cables and mast, and thus involved moderate movements in both the guys and mast; meanwhile, the highest modes involved significant mast movements with little guy vibration. The spectra of bending moments and displacements also indicated that the lower modes typically accounted for most of the mast displacements, while higher modes typically dominated the dynamic bending moments.

7. The structural damping ratio of guyed mast measured in free vibration and still air conditions was found to be approximately 0.5%-6% of critical damping for most modes, which compared well with that assumed for the analytical model, which was taken as 0.5% of critical for all modes. However, there was considerable variability in the measured values.

8. The observed discrepancies of dynamic response between the aeroelastic model and the numerical model can be attributed to a number of factors: (a) the aeroelastic model properties were based on still air conditions, so that the numerical model may not have precisely captured the nonlinear behaviour of the model under wind loads; (b) the structural damping levels assumed in the numerical model may have differed from those of the aeroelastic model; (c) the calibration factors used to calculate measured bending moments were somewhat uncertain; (d) the air density may have differed from that assumed in the open country and over water conditions; (e) effective drag areas may have been different than that assumed, and (f) scaling effects on the model as well as the

nonlinear variation of guy tension may not be reproduced exactly in numerical model.

9. It is evident that displacement at the top of the mast was dominated by the lowest two observable modes. In addition, the resonant portion of this response decreased relative to the background component with the increasing wind speeds.
10. Comparison of the drag response of the sectional model of cladding to theoretical predictions from NBCC (NBCC 1995) indicates that theoretical predictions were fairly high relative to measured values. In addition, the maximum drag force was found to occur with wind at 60 degrees to the mast, while relatively small drag forces were measured with wind at 30 degrees. This suggests that special attention should be paid to wind at 60 degrees when designing a guy mast; however, the applicability of these results is questionable due to limitations in the test set-up.
11. Dynamic response in open country exposure was much more severe than that in over water exposure. In addition, the measured dynamic response with wind at 60 degrees was consistently higher than the other two wind directions.

6.3 RECOMMENDATIONS FOR FUTURE WORK

Recommendations for further research work based on results from the present study are presented below.

1. A wind tunnel test of the dynamic response of the guyed mast model combining ice and wind loads is recommended. It would be useful to obtain a direct measurement of the axial forces, in addition to bending moments.
2. For the guyed mast considered in this study, significant crosswind response has been observed. A more comprehensive investigation using a suitable numerical

model may be carried out to examine the dynamic response in crosswind direction in more detail.

3. The measured dynamic response was compared with a numerical model based on the frequency domain method. A similar comparison with the other commonly used type of numerical dynamic model, namely a time domain analysis model, would be useful to explore more complex, nonlinear behaviours of guyed masts.
4. There is a need to measure the guy tension in order to better study the nonlinear effects of guy cable stiffness, as well as the effect of wind loads acting on the cables.

REFERENCES

Allsop, A.C. 1983. Dynamic Analysis of Guyed Masts: Simplified Methods. M.Sc. Thesis, University of Western Ontario, London, Ontario, 141 pp.

ANSI. 1982. American National Standard A 58.1-1982, Minimum Design Loads for Buildings and Other Structures. American National Standards Institute, Inc.

ASCE. 1997. Manual of Practice for Wind Tunnel Studies of Buildings and Structures. American Society of Civil Engineers, 177 pp.

ASCE. 2002. Dynamic Response of Lattice Towers and Guyed Masts, ASCE Task Committee on the Dynamic Response of Lattice Towers, American Society of Civil Engineers, Reston, VA, 266 pp.

Barlow, J.B., Rae, W.H., JR and Pope, A. 1999. Low-Speed Wind Tunnel Testing. John Wiley & Sons, Inc, 713 pp.

Beitin, K.I. 1969. Dynamic Response of Guyed Towers to Wind Loading. Preprint 1032, ASCE Annual and Environmental Meeting, Chicago, Oct. 13-17, 27 pp.

Ben Kahla, N. 1993. Static and Dynamic Analysis of Guyed Towers. Ph.D. Thesis, University of Wisconsin-Madison, 176 pp.

BSI. 1995. British Standard BS 8100 Part 4-- Lattice towers and masts. Code of Practice for Loading of Guyed Masts, British Standard Institute, London, UK.

Buchholdt, H.A., Moossavinejad, S., and Iannuzzi, A. 1986. Non-linear Dynamic Analysis of Guyed Masts Subjected to Wind and Guy Ruptures. Proceedings, Institute of Civil Engineers (England), Vol. 81, Part 2, Paper 9015, pp. 353-395.

CEN. 1997. Eurocode 3. Design of Steel Structures: Towers, Masts and Chimneys-Towers and Masts. CEN, European Committee for Standardisation, Brussels, Belgium.

Clough, R.W. and Penzien, J. 1975. Dynamics of Structures, 2nd Edition. McGraw-Hill,

New York, 738 pp.

Cohen, E., and Perrin, H. 1957. Design of Multi-level Guyed Towers: Structural Analysis. ASCE Journal of the Structural Division, Vol. 83, No. ST5, Paper 1356, 29 pp.

CSA. 2001. CSA Standard S37-01. Antennas, Towers, and Antenna-Supporting Structures. Canadian Standards Association, Rexdale, Ontario, 118 pp.

Davenport, A.G. 1959. The Wind Induced Vibration of Guyed and Self Supporting Cylindrical Columns. Transactions, Engineering Institute of Canada, Vol. 3, pp. 119-141.

Davenport, A.G. 1961. Application of Statistical Concepts of Wind Loading of Structures. Proceedings, Institute of Civil Engineers (England), Vol. 19, Paper 6480, pp. 449-472.

Davenport, A.G. 1964. Note on the Distribution of the Largest Value of a Random Function with Application to Gust Loading. Proceedings, Institute of Civil Engineers (England), Vol. 28, Paper 6739, pp. 187-196.

Davenport, A.G. 1965. The Relationship of Wind Structure to Wind Loading. Proceedings of the Symposium on Wind Effects on Buildings and Structures, Vol. 1.pp. 53-102.

Davenport A.G. 1977. The Prediction of Response to Gusty Wind. International Research Seminar Safety of Structures under Dynamic Loading, Trondlheim, Norway, June (Published by Tapir 1978).

Davenport, A.G., and Steels, G.N. 1965. Dynamic Behavior of Massive Guy-Cables. ASCE Journal of the Structural Division, Vol. 91, No. ST2, 1965, pp. 43-70.

Davenport, A.G., and Vickery, B.J. 1968. The Response of the Savannah River Guyed Stack under Wind and Earthquake Action, University of Western Ontario, 50 pp.

Davenport, A.G., and Loh, P. 1986. Analysis of the Dynamic and Static Response of a Very Tall Guyed Mast to Wind. Research Report BLWT-SS24-1986, Boundary Layer Wind Tunnel Laboratory, University of Western Ontario, London, Ontario, 44 pp.

Davenport, A.G. 1987. The Response of Slender Structures to Wind. Presented as part of a short course on “The Application of Wind Engineering Principles to the Design of Structures”, Lausanne, Switzerland, Feb. 23-27.

Dean, D.L. 1961. Static and Dynamic Analysis of Guy Cables. ASCE Journal of the Structural Division. Vol. 87, No. ST1, pp. 1-21.

Davenport A.G. and Sparling, B.F. 1992. Dynamic Gust Response Factors for Guyed Towers. Journal of Wind Engineering and Industrial Aerodynamics, 44: 2237-2248.

EIA/TIA. 1996. EIA/TIA Standard EIA/TIA-222-E. Structural Standards for Steel Antenna, Towers and Antenna Supporting Structures. Washington, D.C., 107 pp.

Ewins D.J. 2000. Modal Testing: Theory, Practice and Application, Second Edition. Research Studies Press Ltd., pp.113-117.

Fahleson, C. 1995. Ice and Wind Loads on Guyed Masts. Ph.D. Thesis. Luleå University of Technology, Luleå, Sweden.

Hartmann, A.J. and Davenport A.G. 1966. CFPL Television Tower. University of Western Ontario, 60 pp.

Hirsch, G.H. 1994. Damping Measures to Control Wind-induced Vibrations. Wind-excited Vibrations of Structures. pp. 1-48.

Holmes, J.D. 2001. Wind Loading of Structures. Spon Press. New York. pp76-86.

Iannuzzi, A., and Spinelli, P. 1989. Response of a Guyed Mast to Real and Simulated Wind. IASS Bulletin, No. 99, pp. 38-45.

IASS. 1981. Recommendations for Guyed Masts. International Association of Shell and Space Structures, Madrid.

Irvine, H.M. 1978. Free Vibrations of Inclined Cables. ASCE Journal of the Structural Division, Vol. 104, No. ST2, pp. 343-347.

Irvine, H.M. 1981. Cable Structures. The MIT Press, Cambridge, Mass.

Kärnä, T. 1984. Dynamic and Aeroelastic Action of Guy Cables. Publication 18, Technical Research Centre of Finland, 91 pp.

Kolousek, V. 1947. Solution Statique et Dynamique des Pylones D'antennae Haubanes. Publication of the International Association of Bridge and Structural Engineers, Vol. 8.

Liu, Henry. 1991. Wind Engineering- A Handbook For Structural Engineers. Prentice Hall, New Jersey. pp. 147-172.

MACEC Tutorial. Katholieke University, 1999. Introduction to MACEC, Modal Analysis on Civil Engineering Constructions, 51 pp.

McCaffrey, R.J. and Hartmann, A. J. 1972. Dynamics of Guyed Towers. ASCE Journal of the Structural Division, Vol. 98, No. ST6, pp. 1309-1322.

Meshmesha, A., Sennah, K. and Kennedy J.B. 2003. Beam-Column Analysis of Guyed Masts. Proceedings of CSCE 2003. 7 pp.

Madugula, M.K.S., Wahba, Y.M.F. and Monforton, G.R. 1998. Dynamic Response of Guyed Masts. Engineering Structures. Vol. 20, No. 12, pp. 1097-1101.

Nakamoto, R.T. and Chiu, A.N.L. 1985. Investigation of Wind Effects on Tall Guyed Tower. Journal of Structural Engineering, Vol. 111, No. 11. pp. 2320- 2331.

NBCC. 1995. National Building Code of Canada, National Research Council of Canada, Ottawa, Canada.

Nielson, M.G. 1991. Simplified Dynamic Analysis of Guyed Masts. IASS Meeting of the Working Group for Masts and Towers, Stockholm, Sept., 19 pp.

Peil, U. and Nölle, H. 1992. Guyed Masts under Wind Load. Journal of Wind Engineering and Industrial Aerodynamics, Vol. 44, pp. 2129-2140.

Shears, M. 1968. Static and Dynamic Behavoiur of Guyed Masts. Report No. 68-6, Structural Engineering Laboratory, University of California, Berkeley, 167 pp.

Simiu, E. and Scanlan, R. H. 1996. Wind Effects on Structures, Third Edition. John Wiley & Sons, Inc. 589 pp.

Sparling, B.F. 1995. The Dynamic Behavior of Guys and Guyed Masts in Turbulent Winds. Ph.D. Thesis, University of Western Ontario, London, Ontario, 433 pp.

Sparling, B.F., Smith, B.W., and Davenport, A.G. 1996. "Simplified Dynamic Analysis Methods for Guyed Masts in Turbulent Winds". Journal of the International Association of Shell and Space Structures, Vol. 37, No. 2, pp. 89-106.

Sparling, B.F. and Davenport, A.G. 1998. Three-dimensional Dynamic Response of Guyed Towers to Wind Turbulence. Canadian Journal of Civil Engineering, Vol. 25. pp 512-pp 525.

Sparling, B.F. and Gress M. 1997. The Development of a Simpler Dynamic Analysis Method for Guyed Masts: A Progress Report. International Association of Shell and Space Structures – Meeting of Working Group 4 on Masts and Towers, Chicago, Sept. 14-18, 19 pp.

Sparling, B. F. 2001. Comparison of Frequency and Time Domain Analyses for Guyed Masts in Turbulent Winds. International Association of Shell and Space Structures – Meeting of Working Group 4 on Masts and Towers, 21 pp.

Sparling, B. F. and Davenport, A.G. 2001. Nonlinear Dynamic Behavior of Guy Cables in Turbulent Winds. Canadian Journal of Civil Engineering, 25. pp. 98- 109.

Sparling, B. F. and Davenport, A.G. 2002. Evaluation of Simplified Guy Models in the Dynamic Analysis of Guyed Masts. Journal of the International Association for Shell and Spatial Structures.

Vellozzi, J. W. 1975. Tall Guyed Tower Response to Wind Loading. Proceedings, 4th International Conference on Wind Effects in Buildings and Structures, London, UK, pp. 735- 743.

Wahba, Y., Madugula, M.K.S. and Monforton, G.R. 1998. Evaluation of Non-Linear Analysis of Guyed Antenna Towers. Computers and Structures 68. pp 207- 212.

Wahba, Y. 1999. Static and Dynamic Analyses of Guyed Antenna Towers. Ph.D. Thesis, University of Windsor, Ontario, 310 pp.

Wang, Z., Deng, H. and Wang, Z. 2003. Experimental Study of the Dynamic Behavior of Guyed Masts in Wind Tunnel. Engineering Mechanics.

Zhu, N., Sparling, B. F. and King, J. P. C. 2005. Wind Tunnel Test of a 300m Guyed Mast. International Association of Shell and Space Structures – Meeting of Working Group 4 on Masts and Towers Meeting of the IASS Working Group on

Masts and Towers, 23 pp.

Zhu, N., Sparling, B. F. and King, J. P. C. 2006. Wind Tunnel Test for Dynamic Response of a 300m Guyed Mast. Proceedings, 1st International Structural Specialty Conference, Calgary, Canada, 10 pp.

APPENDIX A --- DYNAMIC RESPONSE IN CROSSWIND

A.1. BENDING MOMENTS

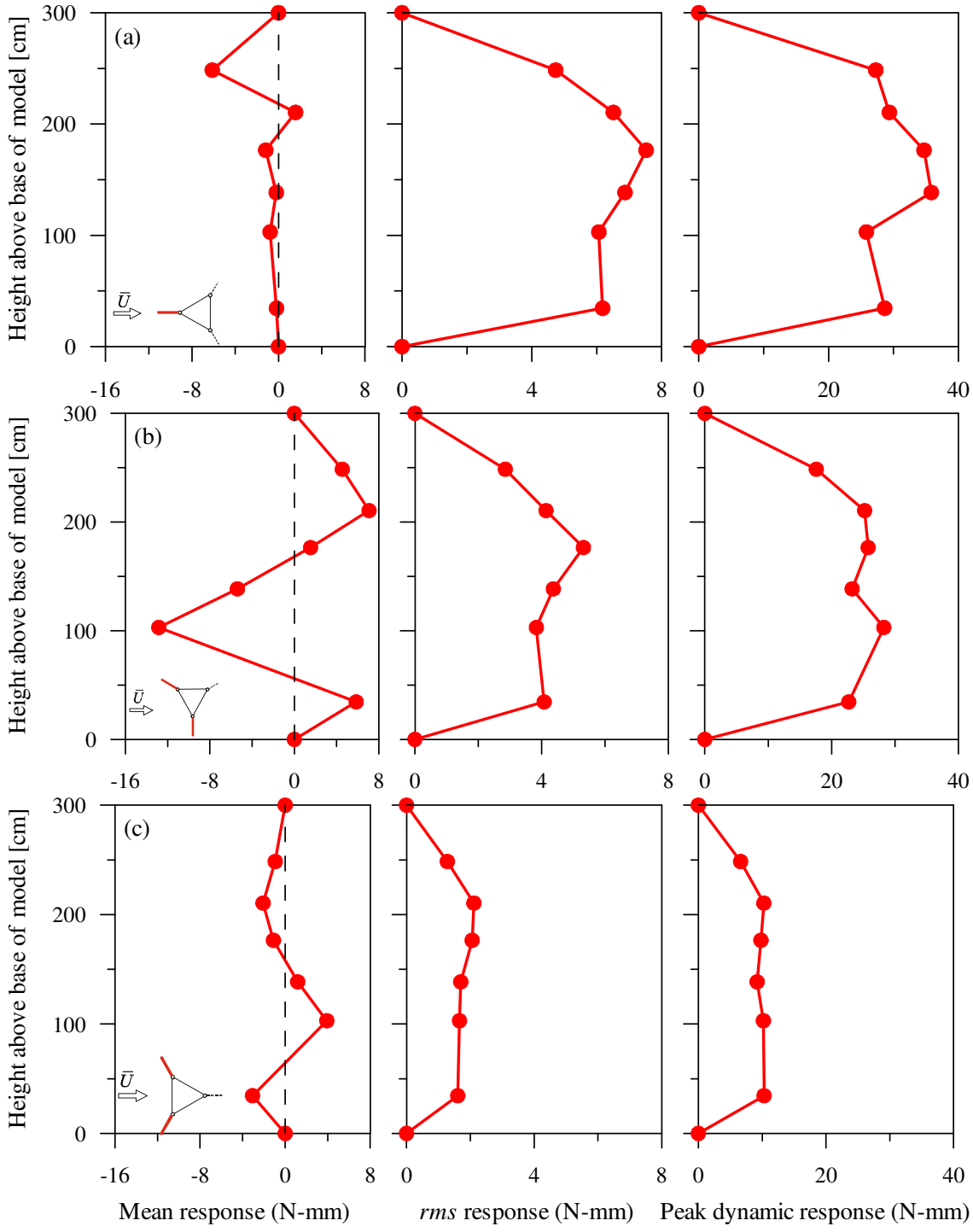

Figure A.1. The measured crosswind bending moments in open country conditions: (a) wind at 0°; (b) wind at 30°; and (c) wind at 60°.

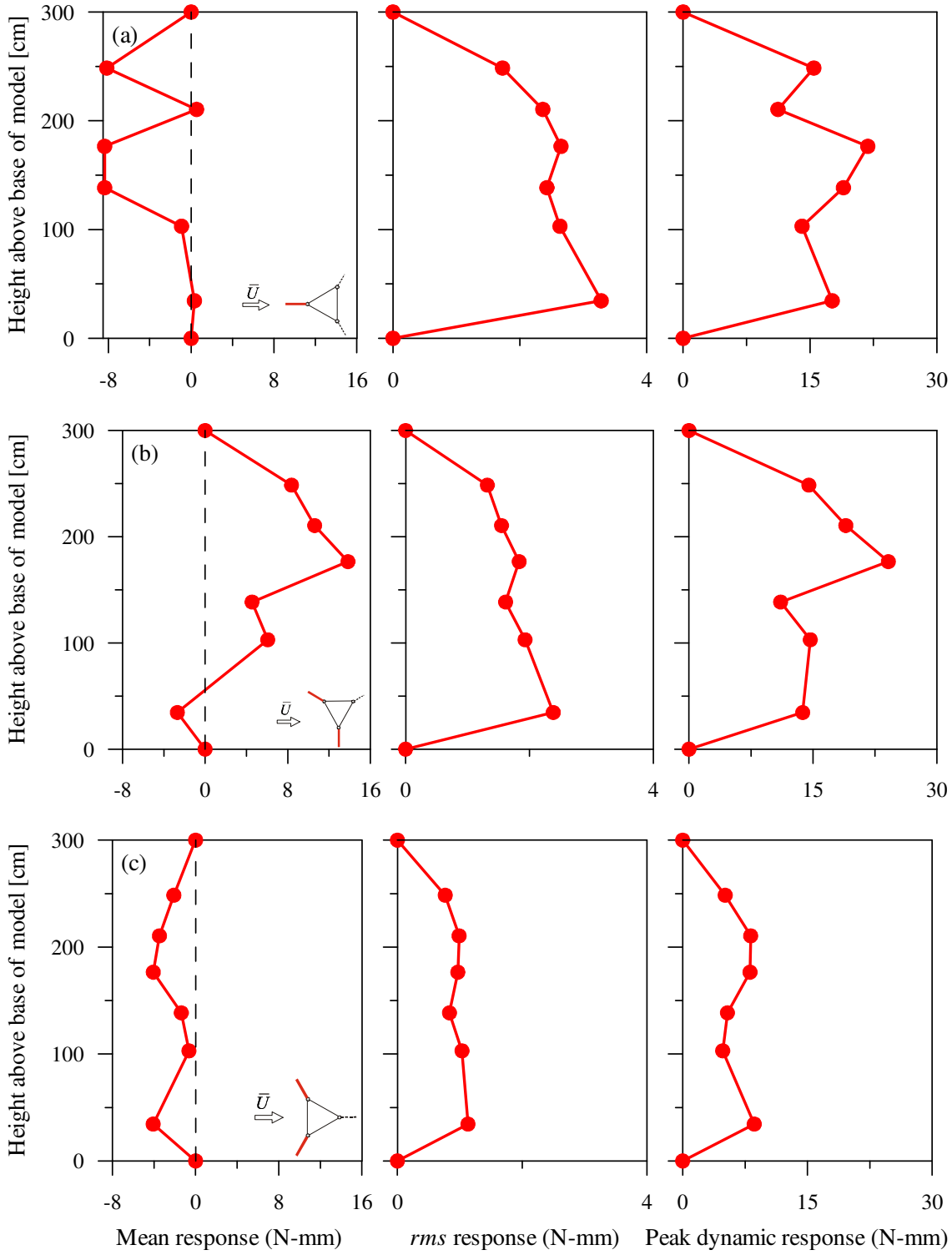

Figure A.2. The measured crosswind bending moment in over water conditions: (a) wind at 0°; (b) wind at 30°; and (c) wind at 60°.

A.2. DYNAMIC MAST DISPLACEMENTS

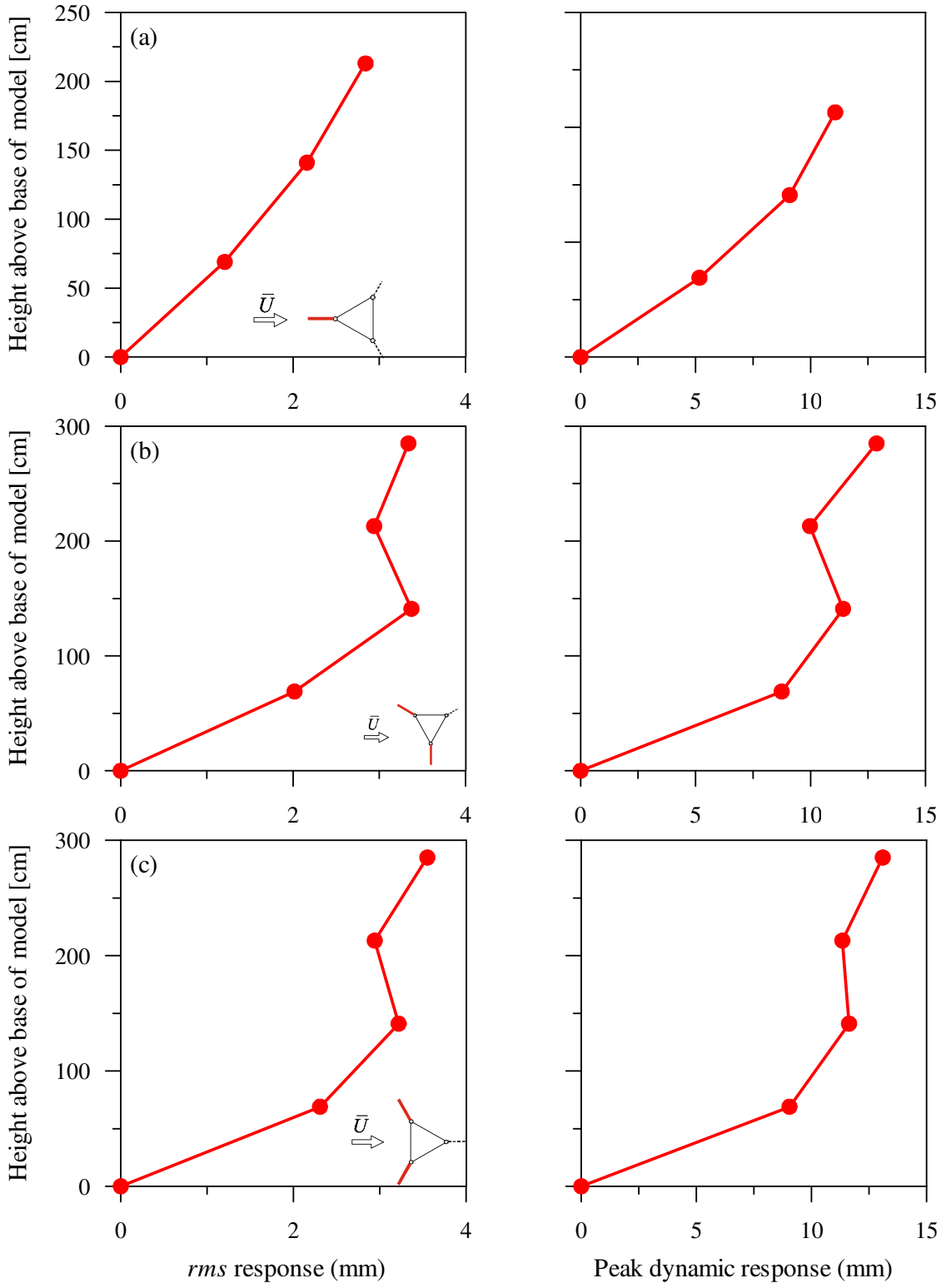

Figure A.3. The measured crosswind mast deflections in open country conditions: (a) wind at 0°; (b) wind at 30°; and (c) wind at 60°.

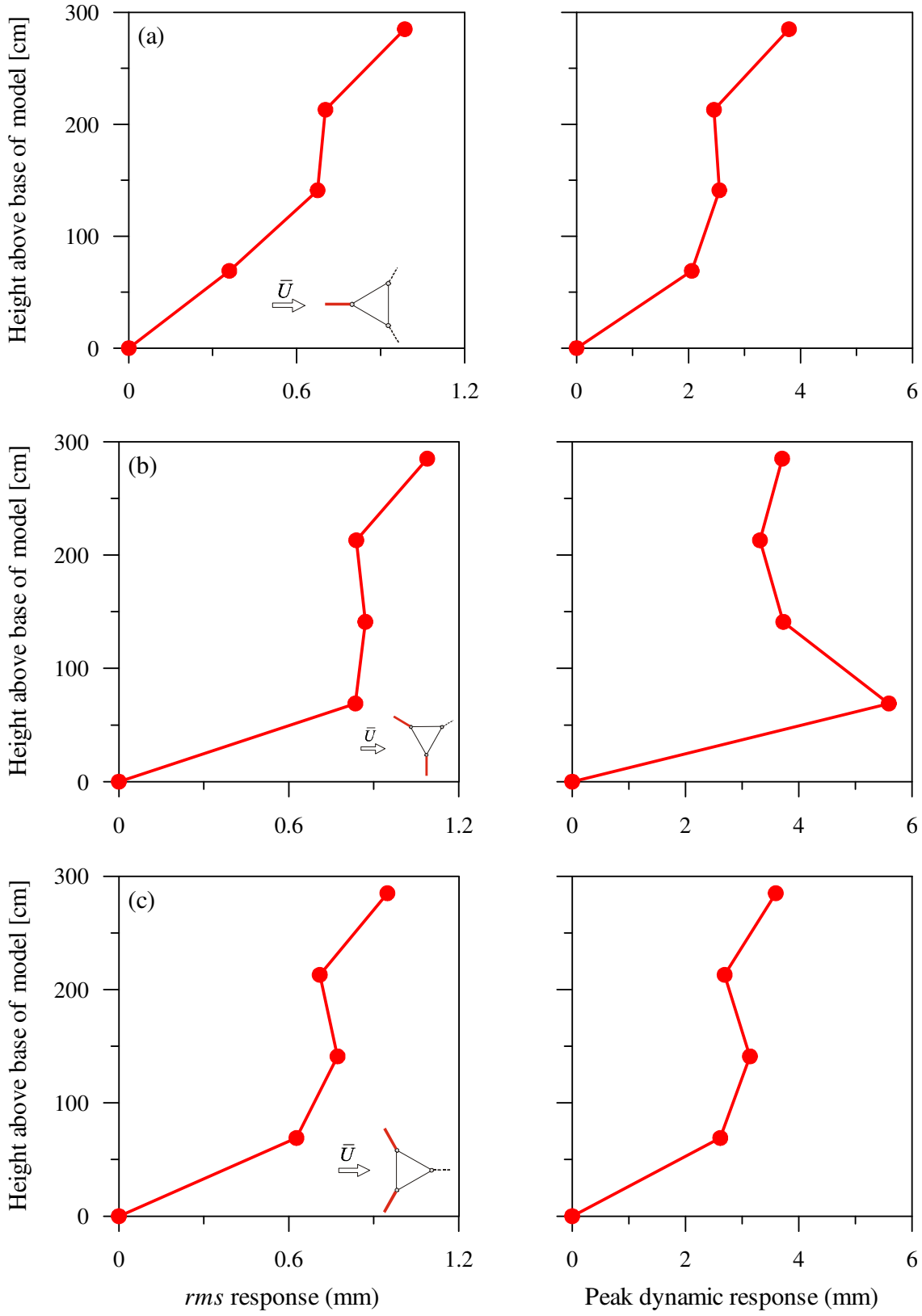

Figure A.4. The measured crosswind mast deflections in over water conditions: (a) wind at 0°; (b) wind at 30°; and (c) wind at 60°.

APPENDIX B --- TIME HISTORY OF MEASURED DYNAMIC RESPONSE

B.1. MAST DISPLACEMENTS IN OPEN COUNTRY CONDITIONS

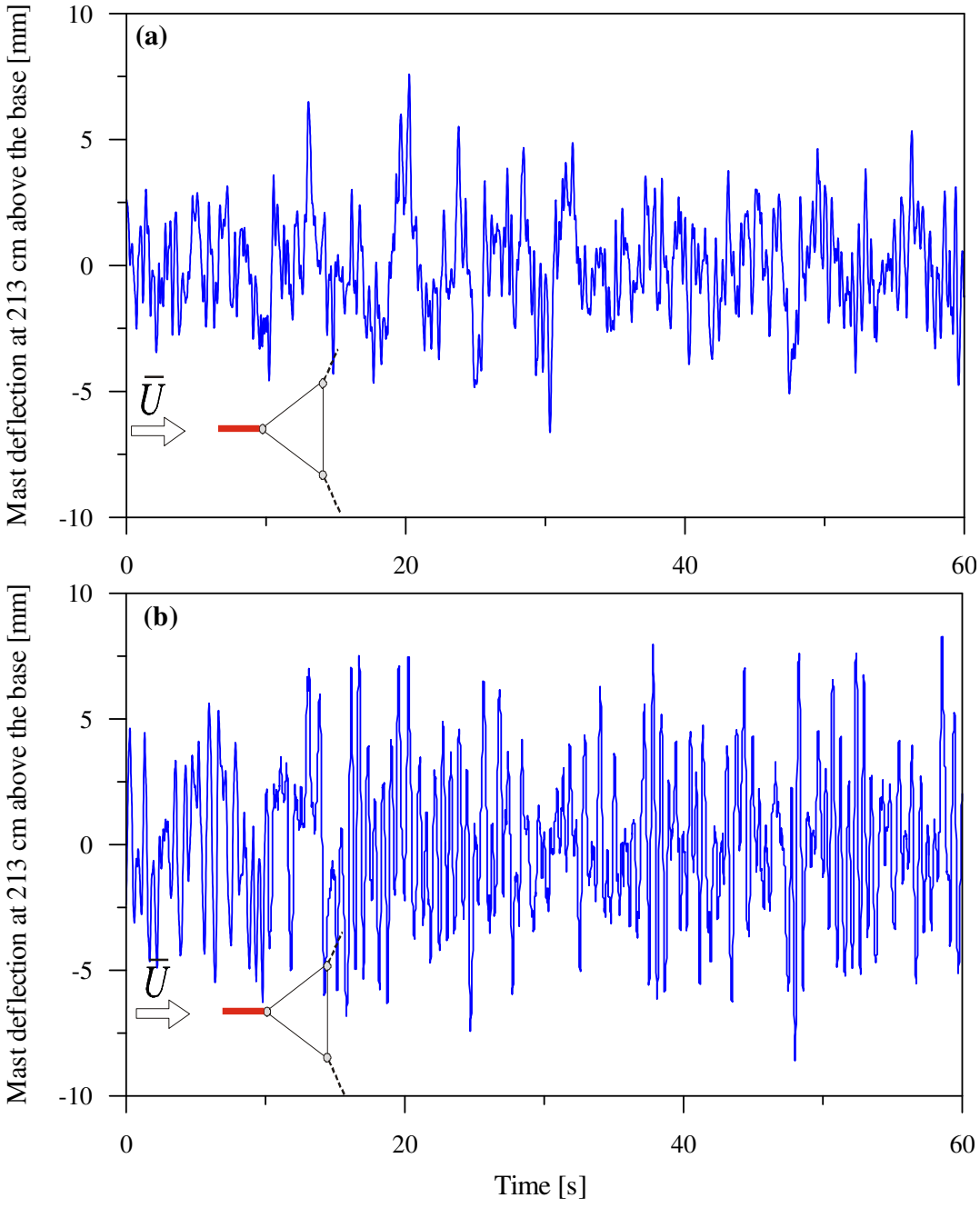

Figure B.1. Time history of mast displacement at 213 cm above the base produced from acceleration time history for open country conditions with wind at 0^{o}:
(a) alongwind direction; (b) crosswind direction.

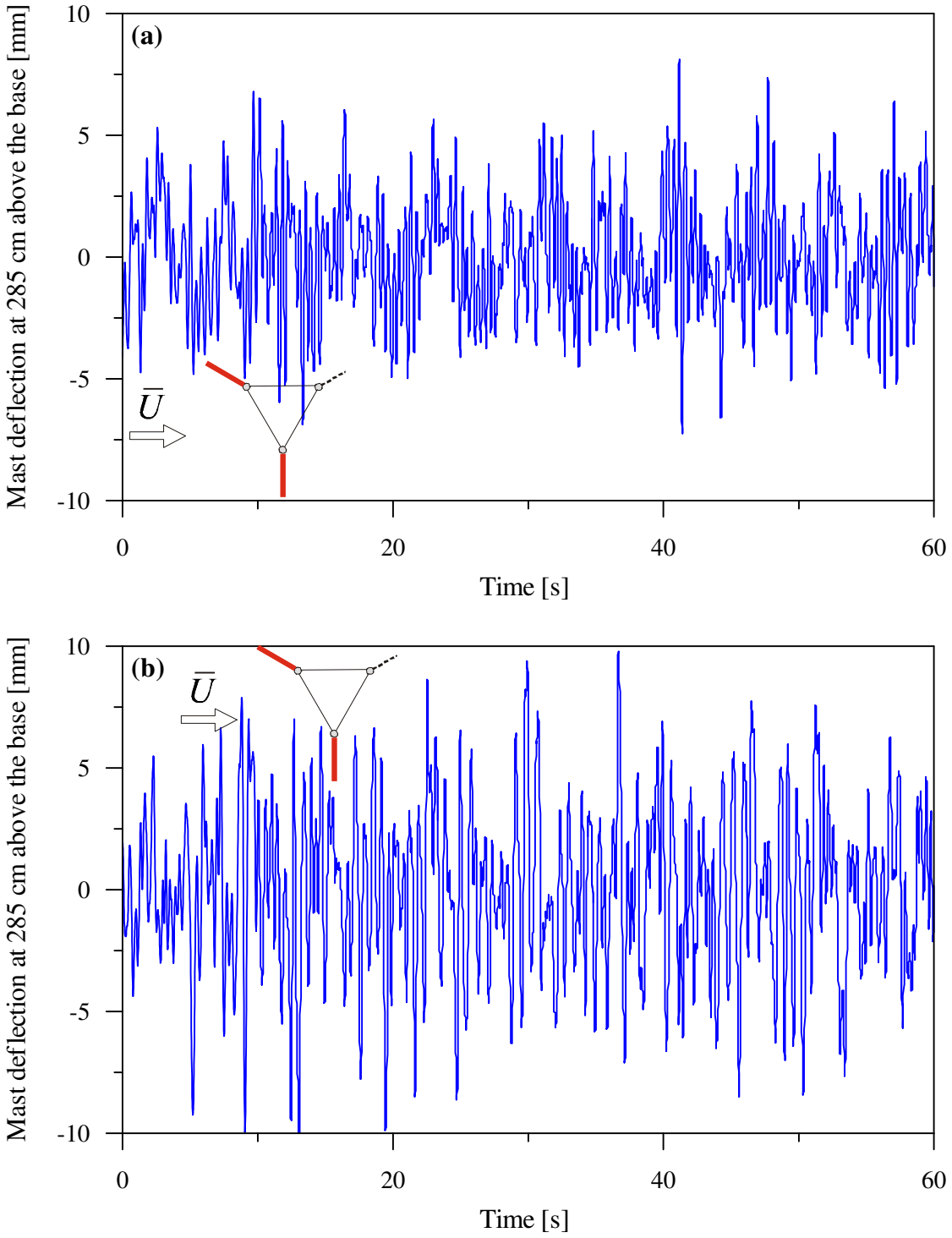

Figure B.2. Time history of mast displacement at the top guy level (h = 285 cm) produced from acceleration time history for open country conditions with wind at 30°: (a) alongwind direction; (b) crosswind direction.

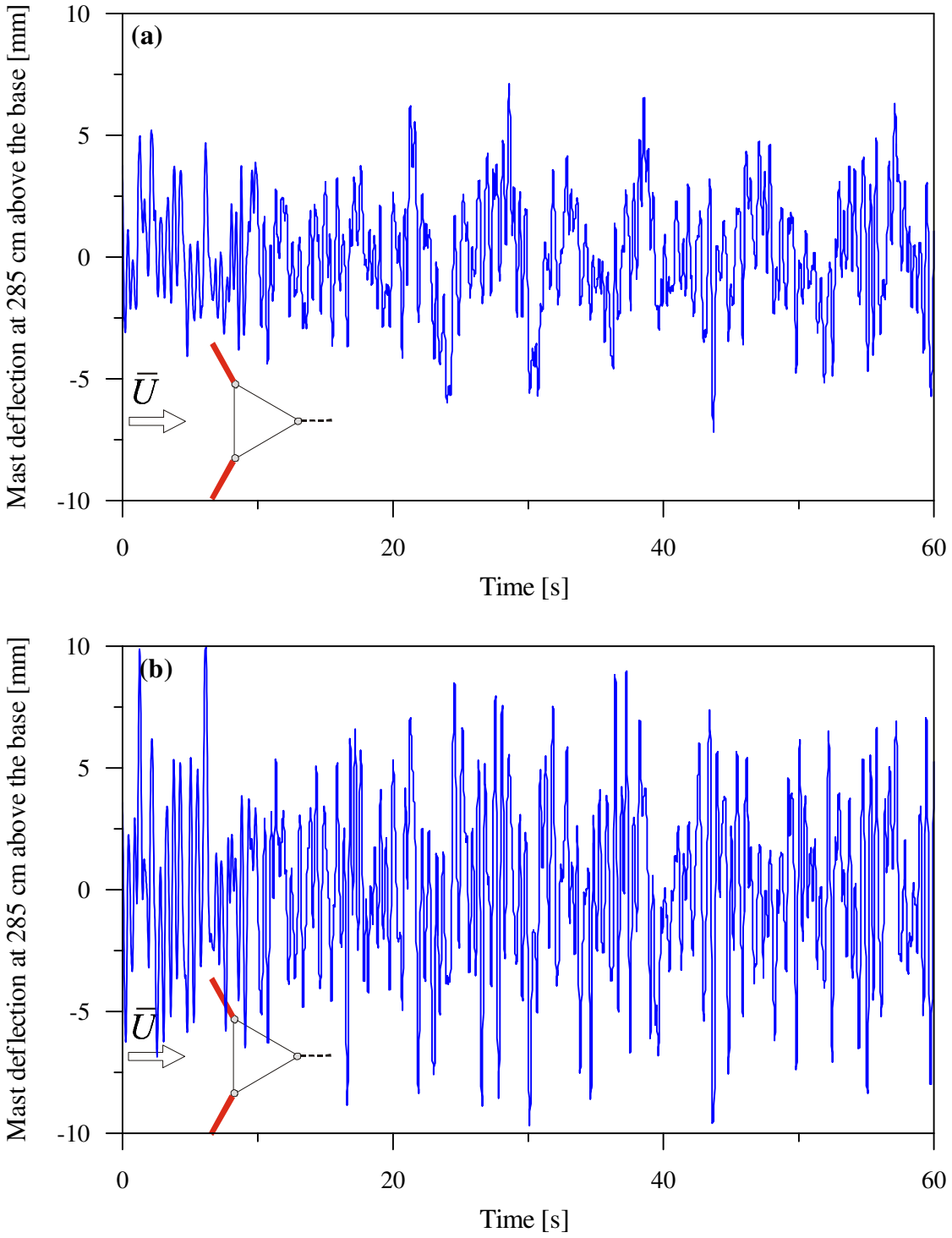

Figure B.3. Time history of mast displacement at the top guy level (h = 285 cm) produced from acceleration time history for open country conditions with wind at 60°: (a) alongwind direction; (b) crosswind direction.

B.2. MAST DISPLACEMENTS IN OVER WATER CONDITIONS

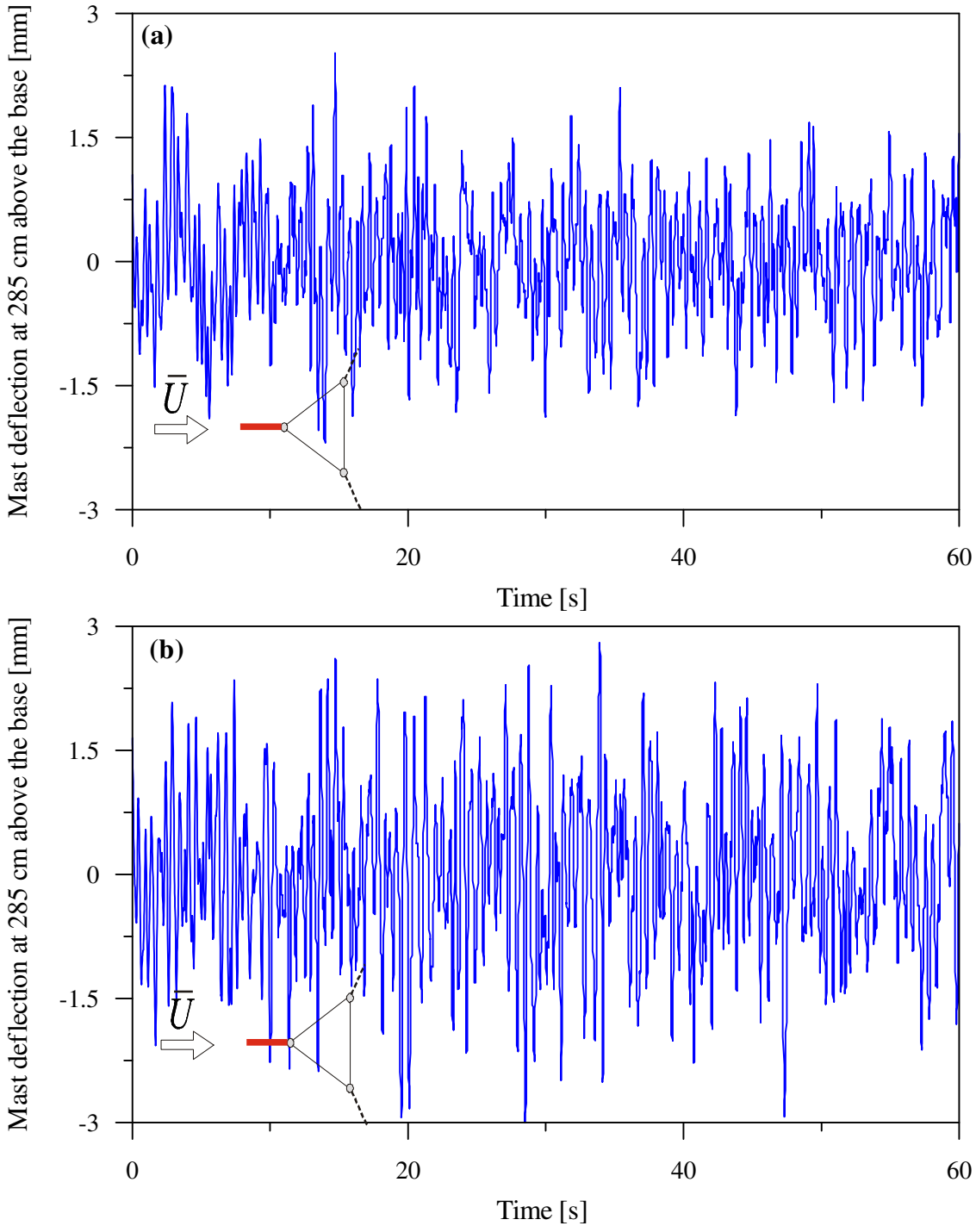

Figure B.4. Time history of mast displacement at the top guy level (h = 285 cm) produced from acceleration time history for over water conditions with wind at 0°: (a) alongwind direction; (b) crosswind direction.

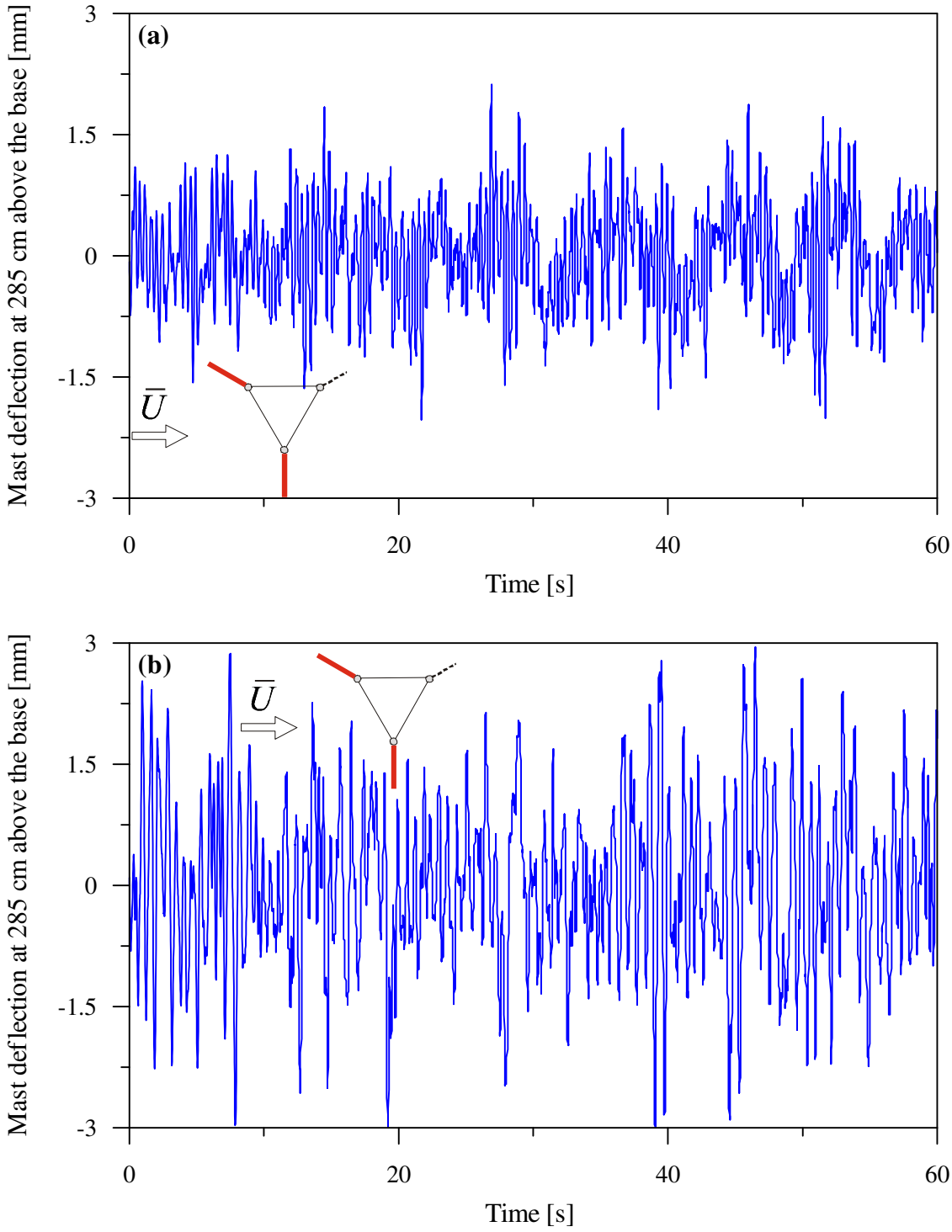

Figure B.5. Time history of mast displacement at the top guy level (h = 285 cm) produced from acceleration time history for over water conditions with wind at 30°: (a) alongwind direction; (b) crosswind direction.

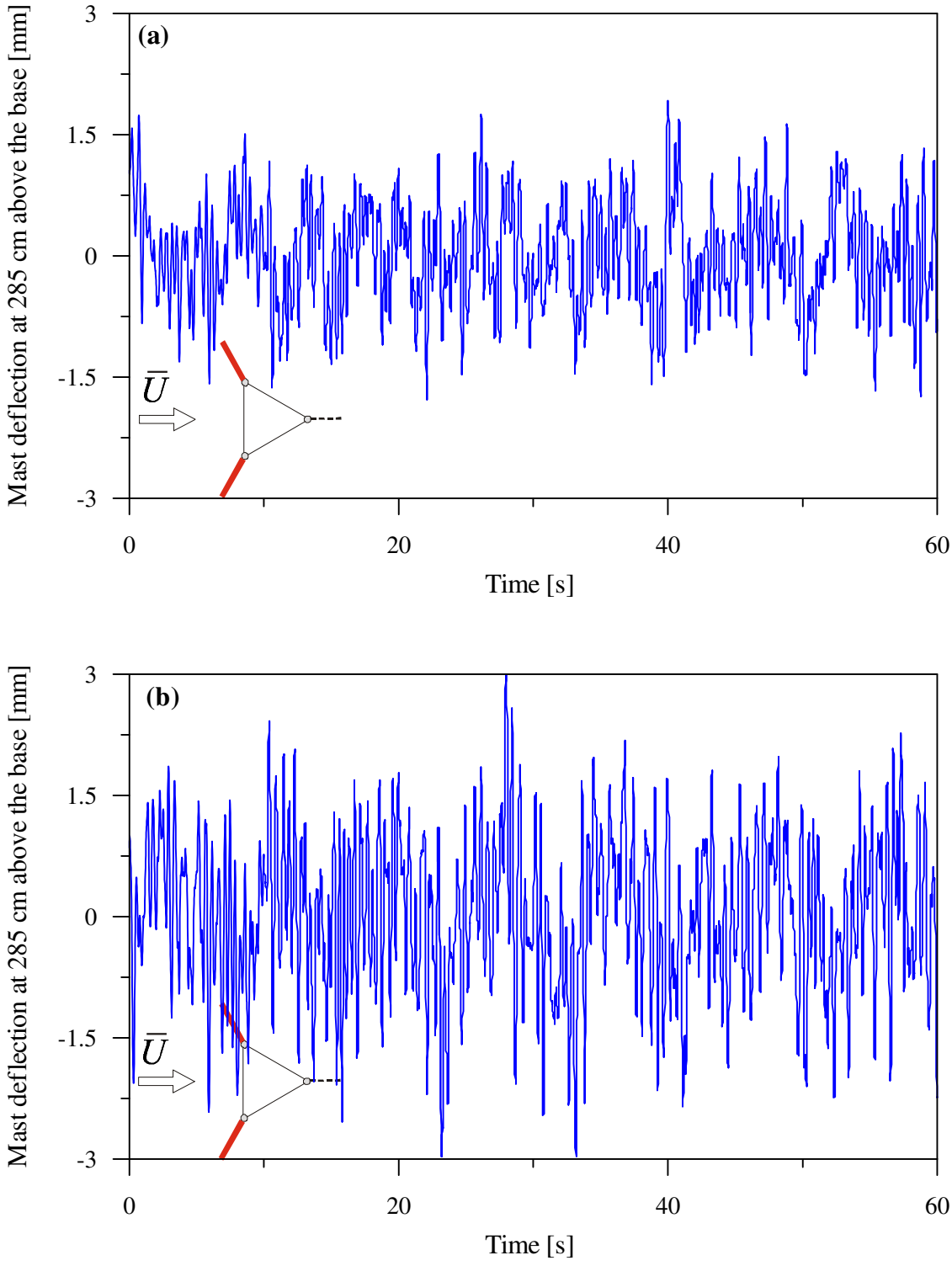

Figure B.6. Time history of mast displacement at the top guy level (h = 285 cm) produced from acceleration time history for over water conditions with wind at 60°: (a) alongwind direction; (b) crosswind direction.

B.3. MAST BENDING MOMENTS IN OPEN COUNTRY CONDITIONS

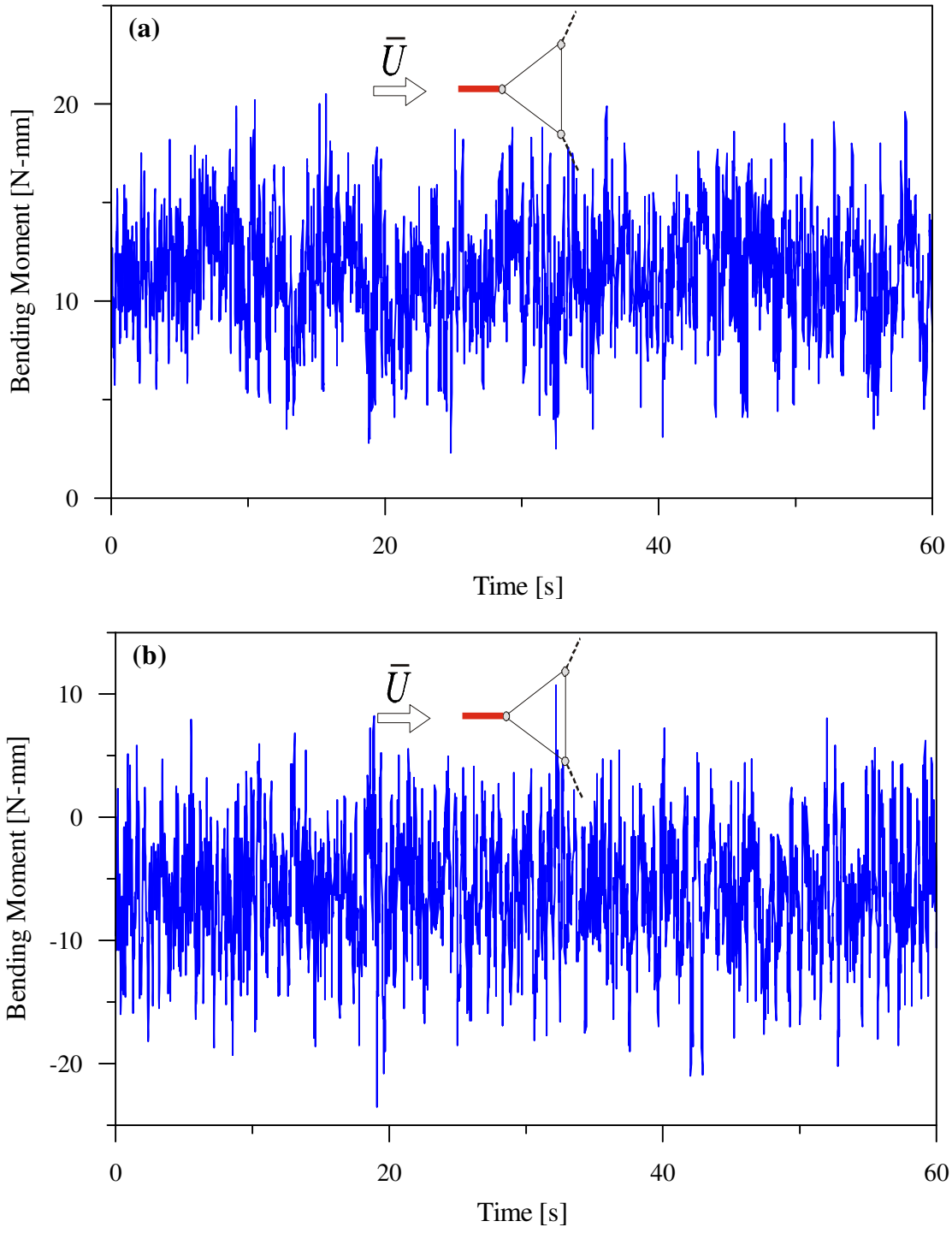

Figure B.7. Time history of measured mast bending moment at the top midspan (h = 248 cm) for open country conditions with the wind at 0^{o}: (a) alongwind direction; (b) crosswind direction.

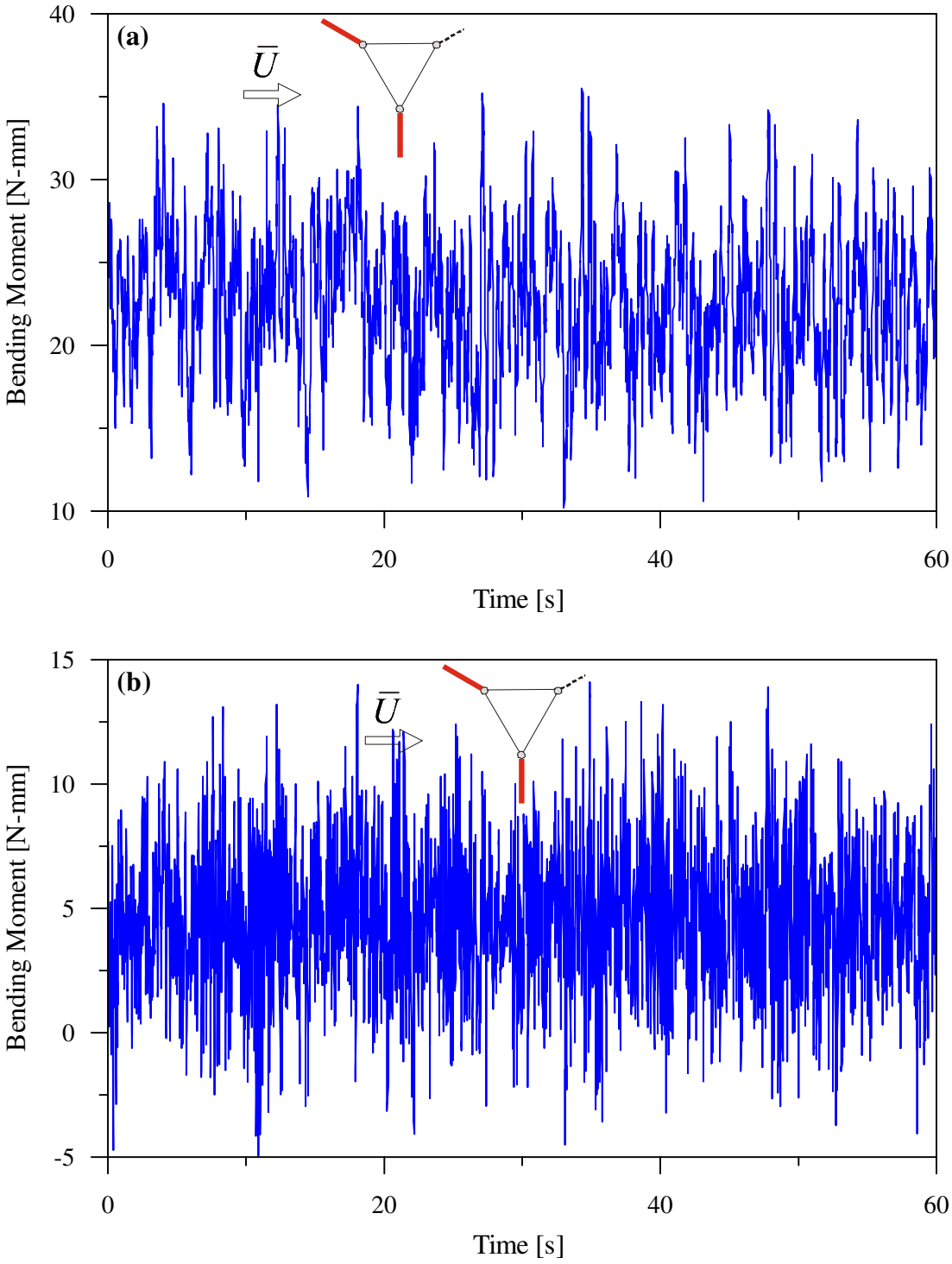

Figure B.8. Time history of measured mast bending moment at the top midspan (h = 248 cm) for open country conditions with the wind at 30°:
(a) alongwind direction; (b) crosswind direction.

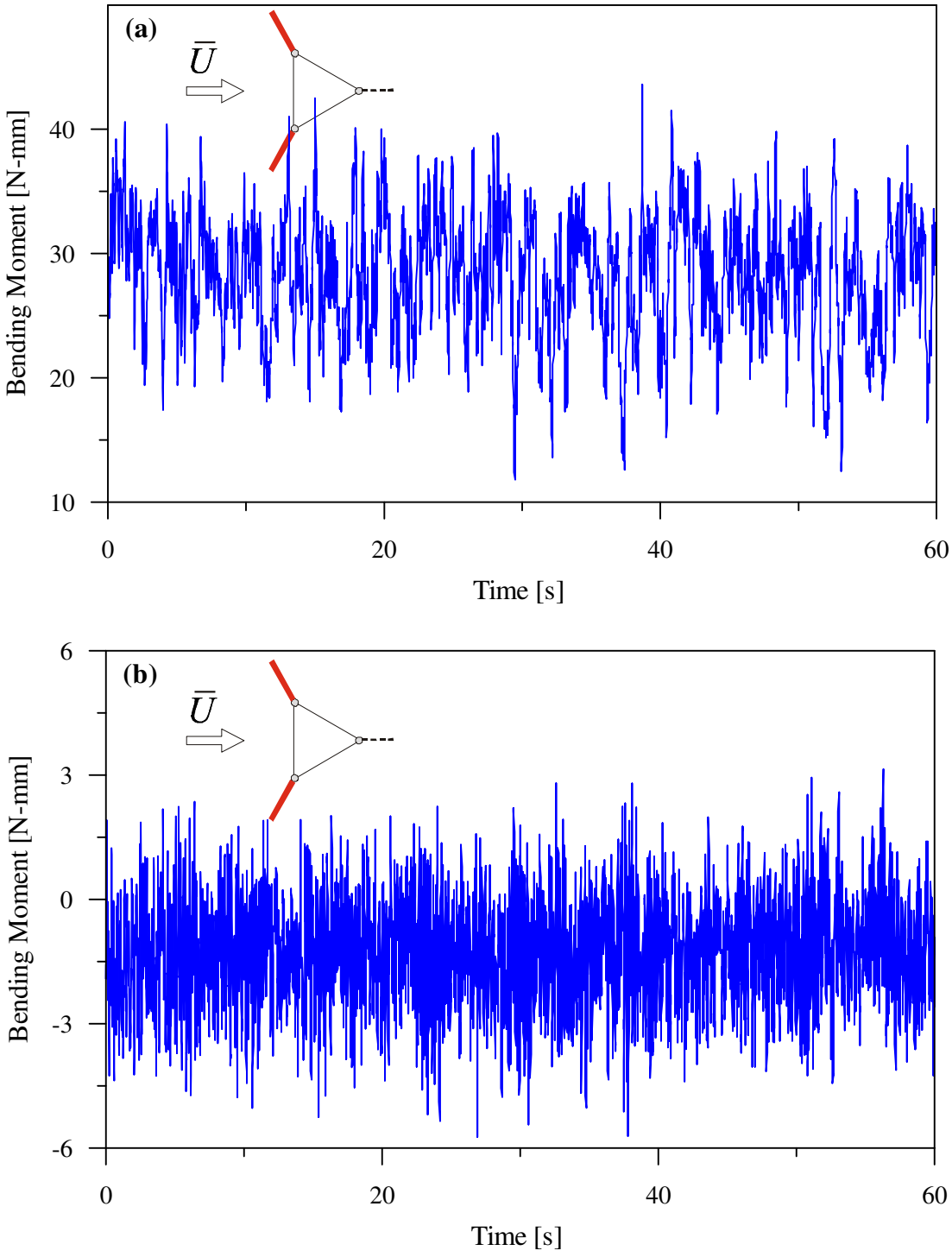

Figure B.9. Time history of measured mast bending moment at the top midspan (h = 248 cm) for open country conditions with the wind at 60°:
(a) alongwind direction; (b) crosswind direction.

B.4. MAST BENDING MOMENTS IN OVER WATER CONDITIONS

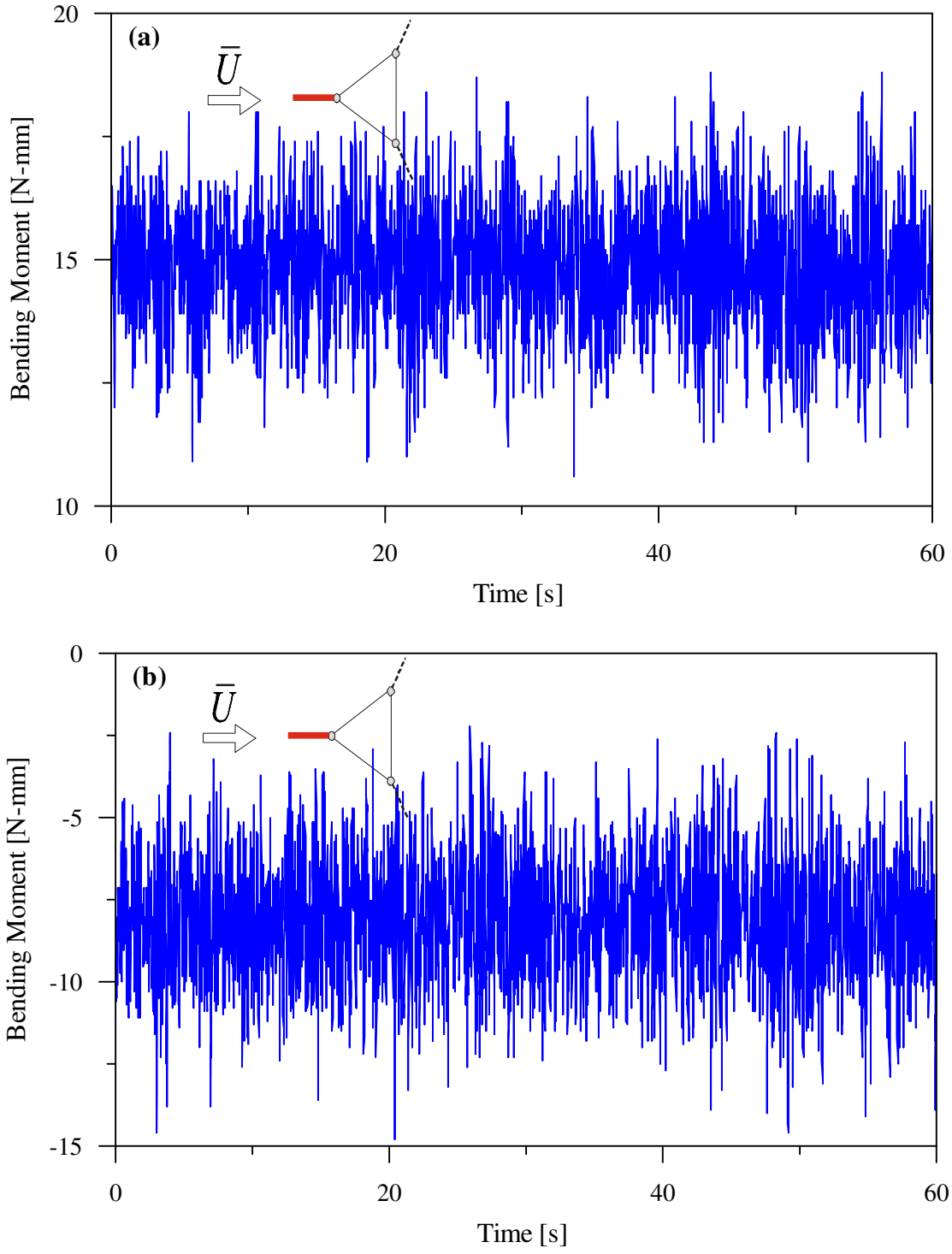

Figure B.10. Time history of measured mast bending moment at the top midspan (h = 248 cm) for over water conditions with the wind at 0°:
(a) alongwind direction; (b) crosswind direction.

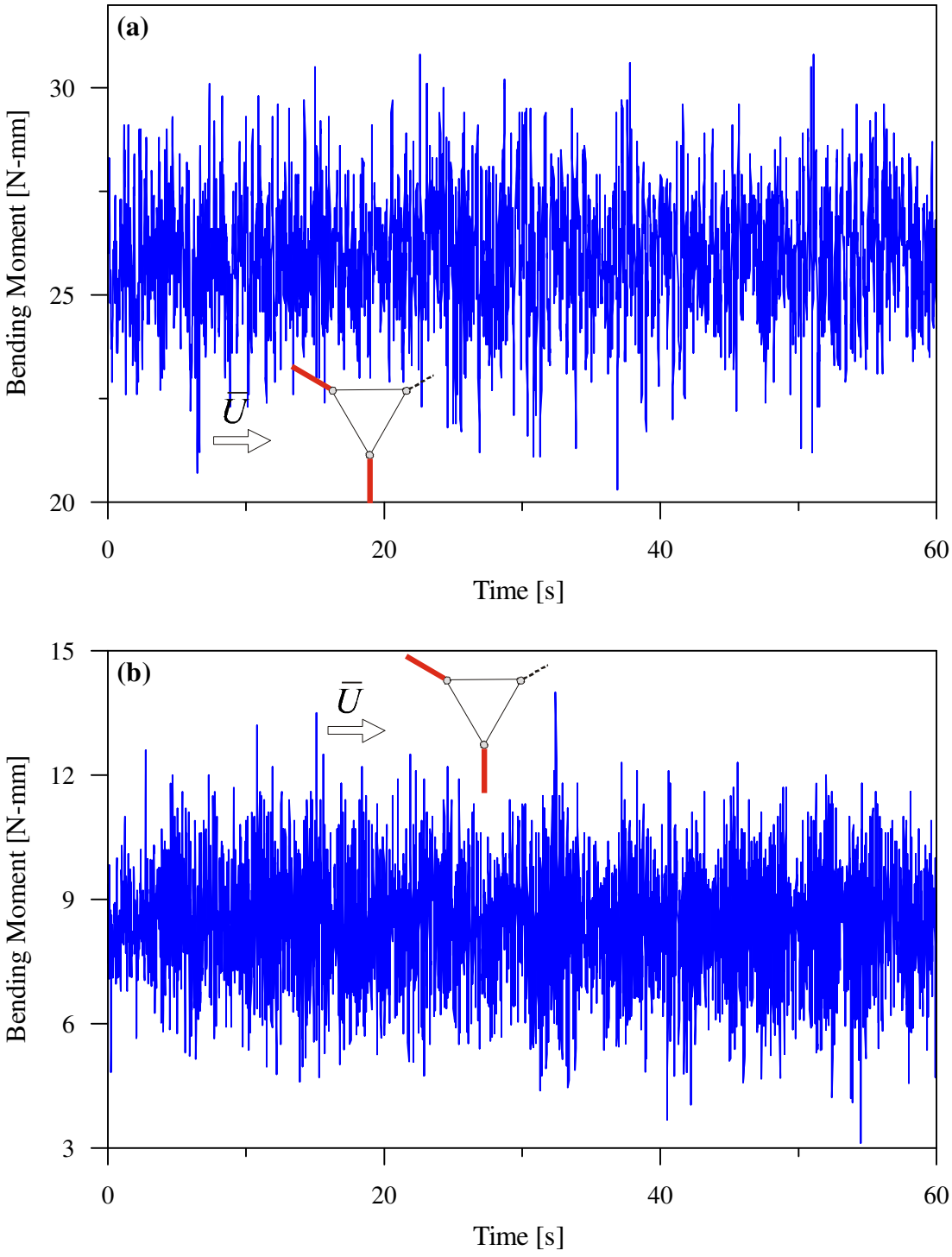

Figure B.11. Time history of measured mast bending moment at the top midspan (h = 248 cm) for over water conditions with the wind at 30°:
(a) alongwind direction; (b) crosswind direction.

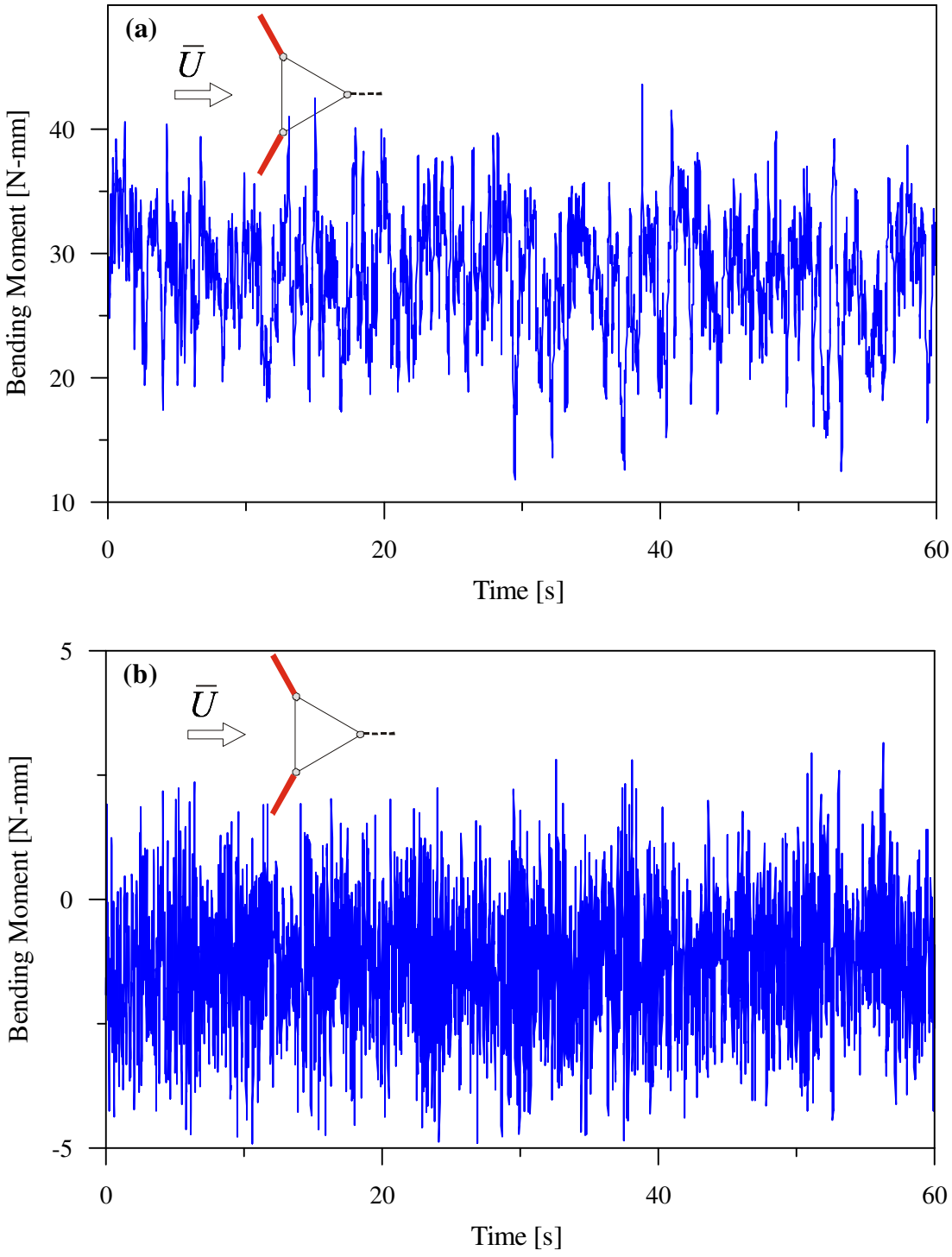

Figure B.12. Time history of measured mast bending moment at the top midspan (h = 248 cm) for over water conditions with the wind at 60°:
(a) alongwind direction; (b) crosswind direction.